ENERGY

CONSERVATION

ORNL/Sub/80-61618/1

Free-Piston Stirling Engine Diaphragm-Coupled Heat-Actuated Heat Pump Component Technology Program

Phase I/IA Final Report

Report Prepared by

MECHANICAL TECHNOLOGY, INC.
968 Albany-Shaker Road
Latham, New York 12110

for

CONSOLIDATED NATURAL GAS RESEARCH COMPANY
11001 Cedar Avenue
Cleveland, Ohio 44106

under
Subcontract 86X-61618C

for

OAK RIDGE NATIONAL LABORATORY
operated by
MARTIN MARIETTA ENERGY SYSTEMS, INC.
for the

U.S. DEPARTMENT OF ENERGY

OFFICE OF BUILDINGS ENERGY
RESEARCH AND DEVELOPMENT

Printed in the United States of America. Available from
National Technical Information Service
U.S. Department of Commerce
5285 Port Royal Road, Springfield, Virginia 22161
NTIS price codes—Printed Copy: Microfiche A01

This report was prepared as an account of work sponsored by an agency of the United States Government. Neither the United States Government nor any agency thereof, nor any of their employees, makes any warranty, express or implied, or assumes any legal liability or responsibility for the accuracy, completeness, or usefulness of any information, apparatus, product, or process disclosed, or represents that its use would not infringe privately owned rights. Reference herein to any specific commercial product, process, or service by trade name, trademark, manufacturer, or otherwise, does not necessarily constitute or imply its endorsement, recommendation, or favoring by the United States Government or any agency thereof. The views and opinions of authors expressed herein do not necessarily state or reflect those of the United States Government or any agency thereof.

ORNL/Sub/80-61618/1
Dist. Category UC-95d

FREE-PISTON STIRLING ENGINE DIAPHRAGM-COUPLED HEAT-ACTUATED HEAT PUMP COMPONENT TECHNOLOGY PROGRAM

PHASE I/IA FINAL REPORT

Date Published—June 1985

Report Prepared by

MECHANICAL TECHNOLOGY, INC.
968 Albany-Shaker Road
Latham, New York 12110

for

CONSOLIDATED NATURAL GAS RESEARCH COMPANY
11001 Cedar Avenue
Cleveland, Ohio 44106

under
Subcontract 86X-61618C

for

OAK RIDGE NATIONAL LABORATORY

Oak Ridge, Tennessee 37831
operated by
MARTIN MARIETTA ENERGY SYSTEMS, INC.
for the
U.S. DEPARTMENT OF ENERGY
under Contract DE-AC05-84OR21400

ABSTRACT

This report presents the results of an effort to develop and demonstrate the technical feasibility of a residential size Stirling engine driven, diaphragm coupled compressor for a heat pump application. The module was to consist of a free piston resonant engine capable of producing 3 kW of useable power, a low loss hydraulic transmission and a nominal 3 ton refrigerant-22 reciprocating compressor. Presented are details of analysis predicted performance goals, design, development of hardware, component testing, and engine/compressor breadboard testing. The test results demonstrated the mechanical feasibility and operational stability of the design concept. The assembly did not stroke out to achieve the full capacity levels predicted, however, and a follow on phase IA was initiated in which the reasons for the short fall will be determined. Details of phase IA are included in the appendix. In general, it was concluded that losses in the hydraulic transmission were excessive to the point where insufficient power was available to the compressor to satisfy its driving requirements at the design point conditions. Future work is recommended to reduce the transmission losses so that full capacity can be achieved.

TABLE OF CONTENTS

Section		Page
	EXECUTIVE SUMMARY	x
1.0	INTRODUCTION	1-1
2.0	SYSTEM DESCRIPTION	2-1
	2.1 Component Description	2-3
	2.1.1 Engine Components	2-3
	2.1.1.1 Combustor	2-3
	2.1.1.2 Displacer Drive System	2-3
	2.1.1.3 Heater Head and Thermal Regenerator	2-6
	2.1.1.4 Cooler	2-8
	2.1.2 Rankine Refrigerant Compressor	2-8
	2.1.3 Hydraulic Coupling (Transmission)	2-8
3.0	TECHNICAL DISCUSSION	3-1
	3.1 Program Objectives and Task Description	3-1
	3.2 Breadboard Design Studies and Performance Analysis	3-1
	3.2.1 Steady-State Matching Analysis	3-2
	3.2.1.1 Compressor Characterization	3-2
	3.2.1.2 Engine/Compressor Matching	3-7
	3.2.1.3 Gas Spring Sizing	3-13
	3.2.1.4 Compressor Component Mass	3-13
	3.2.1.5 Transition Section Design	3-13
	3.2.2 HAHP Stability Analysis	3-13
	3.2.2.1 Linear Stability Analysis (Computer Code)	3-13
	3.2.2.2 Nonlinear Stability Analysis	3-14
	3.3 Component Development and Breadboard Demonstration	3-15
	3.3.1 Heater Head Analysis	3-17
	3.3.2 Interim Engineering Model Engine Verification Test	3-17
	3.3.3 Compressor Development	3-20
	3.3.3.1 Valve Design and Analysis	3-20
	3.3.3.2 Compressor Seal Development	3-24
	3.3.3.3 Cylinder Head Thermal and Structural Analysis	3-28
	3.3.4 Hydraulic Transmission Development	3-31
	3.3.4.1 Diaphragm Life Testing	3-33
	3.3.4.2 Hydraulic Transmission Losses	3-35
	3.3.4.3 Effect of Refrigerant (R-22) Solubility in Oil	3-43
	3.3.4.4 Oil Management System	3-44
	3.3.4.5 Compressor Oil Management System	3-46
4.0	SYSTEM PERFORMANCE	4-1
	4.1 Breadboard Performance	4-1
	4.2 Advanced Prototype System Performance	4-1
5.0	EM 1 AND EM 4 VERIFICATION TESTS	5-1
	5.1 Test Objectives	5-1
	5.1.1 HAHP Verification Acceptance Criteria	5-1
	5.2 Test Procedures	5-2
	5.2.1 Rod Area	5-2
	5.2.2 Transient Plate	5-4
	5.2.3 Load	5-4
	5.2.4 Variable-Piston Gas Spring Volume	5-4

TABLE OF CONTENTS (Cont'd)

Section		Page
	5.3 EM 1 Mapping Procedures and Test Results	5-6
	5.4 EM 4 Verification Test Procedures	5-15
	5.5 EM 4 Test Results	5-15
	5.6 EM 1 and EM 4 Verification Test Conclusions	5-23
6.0	BREADBOARD SYSTEM	6-1
	6.1 System Description	6-1
	6.1.1 Engine Characteristics	6-1
	6.1.2 Compressor Description	6-6
	6.1.3 Refrigerant Loop and Compressor Loading Control	6-6
	6.1.4 HAHP Breadboard System Instrumentation	6-10
	6.2 HAHP Breadboard System Test Plan	6-10
	6.2.1 Introduction	6-10
	6.2.2 Test Procedures	6-19
	6.2.2.1 Displacer Gas Spring Characterization	6-19
	6.2.3 Engine Tuning Sensitivity and Control	6-25
	6.2.4 Design Point Piston Stroke	6-26
	6.2.5 Design Point Condenser/Evaporator Conditions at Intermediate Piston Strokes	6-26
	6.2.6 Establishing the Four ARI Operating Points	6-27
7.0	COMPRESSOR DEVELOPMENT	7-1
	7.1 Compressor Description	7-1
	7.2 Compressor Development Objectives	7-1
	7.3 Test Objectives	7-5
	7.4 Test Plan Procedures	7-5
	7.4.1 Establish Tuning of the System	7-5
	7.4.2 Reinjection of Hydraulic Fluid	7-6
	7.4.3 Evaluation of Clearance Seals and Mid-Stroke Ports	7-6
	7.4.4 Quantify Parasitic Losses	7-7
	7.4.5 Optimize Compressor Valve Performance	7-8
	7.4.6 Mapping of Compressor Performance	7-9
	7.5 Test Results	7-9
	7.5.1 Hydraulic Simulator Tests	7-9
	7.5.2 Oil Management System Testing	7-11
	7.5.3 Compressor Testing	7-13
	7.5.3.1 Early Testing	7-13
	7.5.3.2 Testing With Freon Load	7-14
8.0	BREADBOARD SYSTEM TESTING	8-1
	8.1 Shakedown Testing	8-1
	8.2 Breadboard System Performance	8-5
	8.2.1 System Modifications	8-5
	8.2.2 Preliminary System Performance	8-5
	8.3 Future Development	8-10
	Appendix - The Phase IA Program	

LIST OF FIGURES

Number		Page
1	Engineering Model FPSE-Driven Heat-Actuated Heat Pump	ix
1-1	HAHP Master Schedule	1-2
1-2	Detailed HAHP Master Schedule	1-3
1-3	Detailed HAHP Master Schedule	1-4
2-1	Breadboard HAHP Power Module and Compressor Assembly	2-2
2-2	Engineering Model Combustor Schematic	2-4
2-3	Engineering Model External Heat System	2-5
2-4	Displacer Rod Dynamics	2-7
2-5	Monolithic Heater Head Configuration for Engineering Model Engine	2-9
2-6a	Compressor and Hydraulic Transmission Layout	2-10
2-6b	Compressor Housing (Side View/Top View)	2-11
2-7	Compressor Schematic	2-13
3-1	Bendix Diaphragm Stiffness Versus Counterweight Amplitude	3-4
3-2	Calculation of Compressor Oil Temperature	3-6
3-3	Engine/Compressor Power Versus Piston Stroke (95°F)	3-16
3-4	Engine/Compressor Power Versus Piston Stroke (47°F)	3-16
3-5	HAHP Verification Test Power Versus Piston Stroke	3-19
3-6	HAHP Verification Test Dynamic Response Versus Piston Stroke	3-19
3-7	Suction/Discharge Valve Plate Assembly	3-25
3-8	Pumping Ring Seal Layout	3-25
3-9	Flow and Pressure Relation	3-26
3-10	Compressor Cylinder Head	3-29
3-11	Diaphragm-Type Hydraulic Simulator Rig	3-32
3-12	Contoured Engine and Gas Spring Diaphragm	3-34
3-13	Compressor Schematic - HAHP	3-37
3-14	Comparison of Predicted and Measured Losses (Results of Testing on Hydraulic Simulator)	3-39
3-15	Compressor Energy Balance for 95°F Ambient	3-39
3-16	Comparison of Predicted and Measured Gas Spring Thermal Hysteresis Losses for Nitrogen and Helium on the Hydraulic Simulator	3-42
3-17	Effect of R-22 Solubility in Suniso 3GS Refrigeration Oil on Hydraulic Transmission Losses and Diaphragm Stroke for 10-mm Piston Stroke and 60 Hz	3-45
3-18	Viscosity of Solutions of R-12 in Suniso 3GS Refrigeration Oil at 100°F	3-45
3-19	Hydraulic Flow Diagram	3-47
3-20	Preliminary Compressor Oil Management Circuit Concept	3-49
4-1	HAHP Power Flow Diagram (Advanced Prototype)	4-2
5-1	Comparison Between the EM Engine/Alternator Configuration and the EM Engine/Compressor	5-5
5-2	Engine Operating Characteristics for the HAHP Engine Configuration	5-7
5-3	Engine Operating Characteristics for the Engineering Model (EM 1) Engine Configuration	5-7
5-4	EM 1 Load Map (Piston P-V Power Versus Piston Stroke)	5-10
5-5	T/C Reading Versus Heater Head Axial Location	5-12
5-6	Displacer Stroke Versus Piston Stroke for EM 1	5-13
5-7	P-V Power Versus Piston Stroke for EM 1	5-13
5-8	Engine-to-Engine Repeatability Data (EM 1 Versus EM 4)	5-16
5-9	P-V Power/Efficiency Versus Piston Stroke	5-18
5-10	Displacer Motor Current Versus Piston Stroke	5-18
5-11	EM Load Map - Displacer Stroke Versus Piston Stroke	5-19

LIST OF FIGURES

Number		Page
5-12	EM Load Map - P-V Power Versus Piston Stroke	5-19
5-13	P-V Power Versus Load Resistance	5-21
5-14	P-V Power Versus Load Resistance	5-21
5-15	Displacer Gas Spring #2 Loss Versus Displacer Stroke	5-24
6-1	HAHP Engine/Compressor Layout	6-2
6-2	Displacer Bearing Supply	6-3
6-3a	HAHP Compressor and Hydraulic-Drive Hardware	6-4
6-3b	Compressor and Hydraulic Transmission Hardware	6-5
6-4	Calorimeter System Schematic	6-7
6-5	HAHP Instrumentation Schematic	6-12
6-6	HAHP Displacer Gas Spring Volumes	6-22
6-7	Calculated Displacer Gas Spring Losses Versus Displacer Stroke	6-24
7-1	HAHP Compressor Assembly	7-2
7-2	Hydraulic Simulator Test Rig	7-10
7-3	Hydraulic Simulator, 3.250" ϕ Pistons - Predicted Losses	7-10
7-4	HAHP Hydraulic Simulator - Parasitic Losses Versus Pressure Amplitude	7-12
7-5	Oil Management System with Hydraulic Simulator	7-12
7-6	HAHP Hydraulic Simulator - Parasitic Losses Versus Pressure Amplitude	7-15
7-7	HAHP Hydraulic Simulator - Predicted and Experimental Parasitic Losses	7-15
8-1	Displacer/Piston Stroke Ratio Versus Piston Stroke for the Breadboard System	8-2
8-2	P-V Power Versus Piston Stroke for the Breadboard System	8-4
8-3	Engine Operating Characteristics for the HAHP Engine Configuration	8-4
8-4	P-V Power Versus Piston Stroke for the Breadboard System With and Without the Counterweight	8-6
8-5	P-V Power Versus Piston Stroke for the Breadboard System for Two Different Drive Piston Diameters (No Counterweight)	8-6
8-6	Breadboard System Preliminary Heating and Cooling Capacity for the Westinghouse Test Points	8-8

LIST OF TABLES

Number		Page
1-1	Critical Milestones	1-5
3-1	HAHP Operating Points	3-2
3-2	Compressor Power and Efficiency	3-4
3-3	Compressor Seal Losses	3-8
3-4	Matching Analysis Results for Preliminary Control Scheme	3-11
3-5	Matching Analysis Results for Preliminary Control Scheme	3-12
3-6	Matching Analysis Results for Preliminary Control Scheme	3-13
3-7	Matching Analysis Results for Preliminary Control Scheme	3-14
3-8	Stability Analysis Results	3-17
3-9	HAHP Verification Test Points (Nominal Design Points)	3-22
3-10	Breadboard Compressor Specifications	3-26
3-11	Variables Examined for Parametric Analyses for HAHP Compressor Valves	3-28
3-12	HAHP Compressor Valve Design Tradeoffs at Conditions Representing Heat Pump Ambients (°F)	3-29
3-13	Calculated Chevron Seal Performance - Summary	3-34
3-14	Calculated Pumping Ring Seal Performance - Summary	3-35
3-15	Diaphragm Life Test Results	3-43
3-16	Compressor Operating Characteristics	3-45
3-17	HAHP Compressor Drive Hydraulic Efficiency Summary	3-48
3-18	Measured Gas Spring Results	3-51
3-19	Engine/Compressor Power and Efficiency Summary	3-52
4-1	Steady-State C.O.P. Calculation for the Breadboard Power Module (Laboratory Testing)	4-2
4-2	Estimated HAHP External Power Requirements	4-4
4-3	Advanced Diaphragm-Coupled HAHP (Site Steady-State Calculation)	4-6
5-1	Dissimilar Characteristics Between the EM 1 and HAHP Engines	5-3
5-2	Comparison of EM 1 and HAHP Engine Design Specifications	5-4
5-3	HAHP Verification Test Data	5-12
5-4	HAHP Verification Test Data	5-17
5-5	HAHP Verification Test Data	5-32
5-6	Comparison Between EM 4 and a Rerun of the EM 1 Point	5-34
6-1	HAHP System Measurement Points (Time-Dependent Measurements)	6-11
6-2	HAHP System Measurement Points (Steady-State Measurements)	6-11
6-3	HAHP Data Reduction Parameters	6-13
6-4	Definition of Terms	6-15
6-5	Predicted HAHP Engine Operating Conditions	6-20
6-6	Predicted HAHP Engine Operating Conditions	6-20
6-7	Predicted HAHP Engine Operating Conditions	6-21
6-8	Predicted HAHP Engine Operating Conditions	6-21
6-9	Compressor Power and Efficiency (Predicted or Calculated)	6-28
6-10	Compressor Seal Loss - Predicted	6-28
7-1	HAHP Operating Points	7-3
7-2	Compressor Design Specifications	7-3
7-3	Compressor Power and Efficiency	7-4
7-4	Compressor Seal Loss	7-4
7-5	Initial Compressor Test Data	7-16
8-1	Breadboard System Shakedown Test Results	8-3
8-2	Oak Ridge National Laboratory High-Efficiency Heat Pump Test	8-7
8-3	HAHP Breadboard System Data	8-9

EXECUTIVE SUMMARY

This report covers the effort performed for Consolidated Natural Gas (CNG) Research Company under subcontract 86X-61618C for Martin Marietta Energy Systems, Inc., for the period June 1, 1981 through February 28, 1984. The objective of this project was to demonstrate the technical feasibility of a free-piston Stirling engine (FPSE) driven heat pump for residential space conditioning applications. A breadboard unit that consists of a natural gas combustor, engine, transmission, and refrigerant compressor was designed, fabricated, assembled, and tested. A photograph of the breadboard unit mounted on its test stand is shown in Figure 1 with the combustor and engine located above the support plate and the transmission and compressor located below.

A diaphragm-actuated hydraulic transmission was selected to couple the FPSE to the refrigerant compressor. The Stirling engine was based on an existing free-piston design called the Engineering Model (EM) that was developed jointly by CNG Research Company and Mechanical Technology Incorporated (MTI). The EM engine burns natural gas and uses an electric displacer motor to control the output of the machine. The hydraulic transmission and compressor are contained between two diaphragms that hermetically seal the helium gas in the engine from the transmission fluid. The refrigerant compressor is a linear, double-acting design with a hydraulically-coupled counterweight to eliminate vibrations. The compressor is positioned transversely in the machine which allows the use of conventional compressor piston and valve assemblies and allows for easy access to the compressor components for maintenance. The breadboard unit was designed to product 3 tons of refrigerant at 95°F ambient conditions and 38,000 Btu/hr of heating at 17°F ambient conditions.

The initial experiments during Phase I of the project consisted of testing of the EM engine with an alternator load to ensure that the engine could produce enough power to drive the compressor load. Results indicated that the EM engine could produce the design power of 2900 W at the 95°F ambient conditions. Phase I testing of the complete breadboard unit demonstrated the stable operation of a refrigerant compressor coupled to a FPSE, the mechanical feasibility of the diaphragm-coupled hydraulic transmission concept, and the ability of the displacer motor to control the output to the machine. The major deficiency of

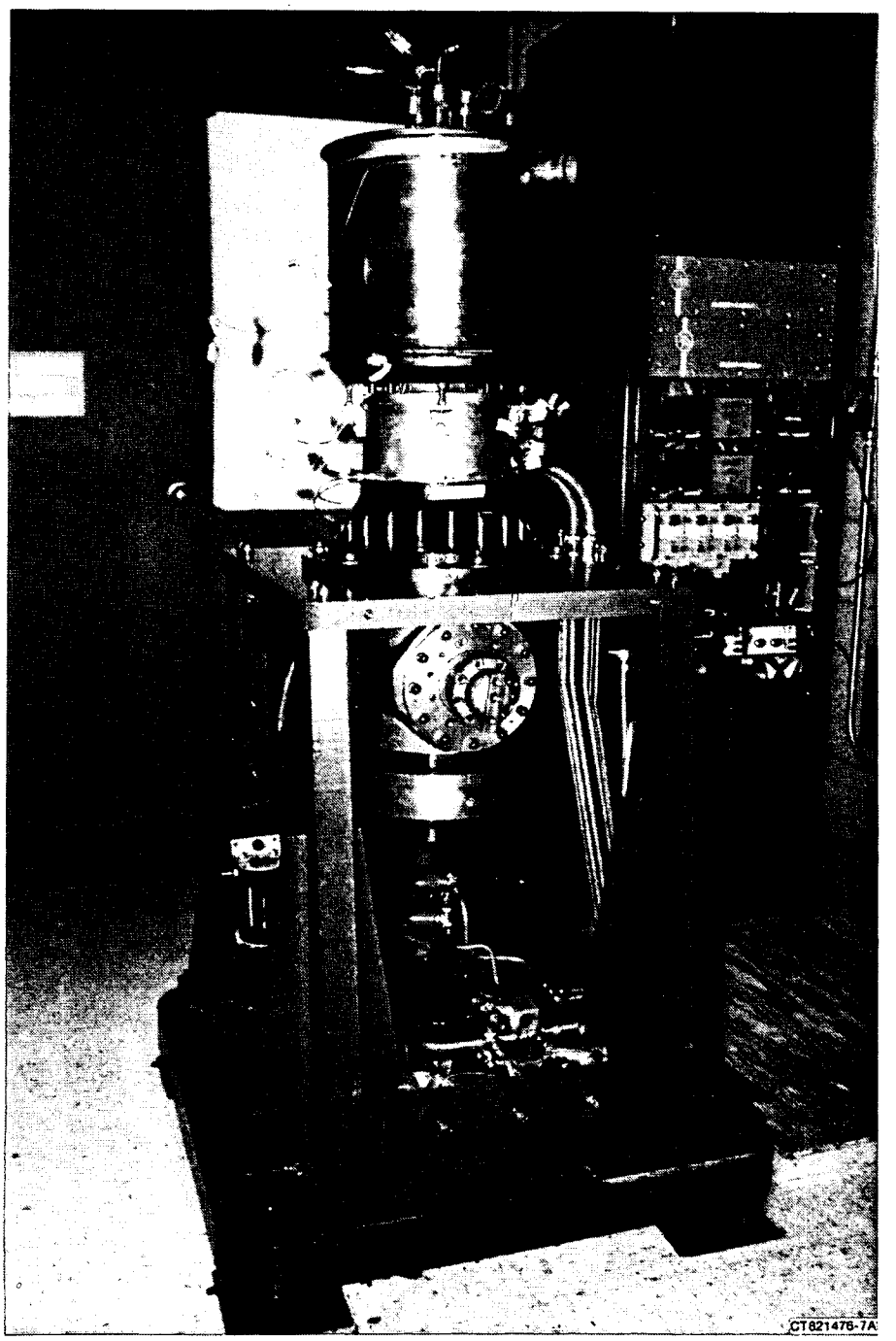

Figure 1 Engineering Model FPSE-Driven Heat Actuated Heat Pump

V5-81

the breadboard unit at the end of Phase I was that it achieved only 1.4 tons of refrigeration at the 95°F ambient conditions, which is less than half of the design capacity.

The Phase IA effort was initiated to determine analytically and experimentally the reasons for the refrigeration capacity deficiency in the breadboard unit. Since the EM engine could produce its design power output when it was tested separately, excessive hydraulic transmission and compressor losses were investigated as the cause of low cooling capacity. Comparison of Phase IA test data with computer model predictions confirmed that these losses were signicantly larger than design values. Additional development work is recommended to reduce losses such as oil leakage past transmission seals, refrigerant leakage past compressor piston seals, seal friction, viscous dissipation, and gas spring hysteresis.

1.0 INTRODUCTION

The HAHP is a Stirling-engine, Rankine-cycle compressor system that provides heating and cooling for space conditioning from a natural-gas source. The system, rated to produce three tons of refrigeration at a 95°F ambient outdoor temperature, and 38,000 Btu/hr of heating at a 17°F ambient temperature, consists of:

- a Stirling-engine driver;
- a Rankine refrigerant compressor; and,
- a diaphragm-isolated hydraulic-engine-to-compressor coupling.

The following paragraphs describe the system and define the technical progress made during the program period of June 1, 1981 through September 30, 1983. The program schedules defining the relationship of the individual tasks are shown in Figures 1-1 through 1-3. As stated, the program objective was to develop a breadboard heat-powered engine-compressor system that demonstrated the potential of a Stirling-engine-driven heat pump. To achieve this in the most cost-efficient manner, the system was designed to use an existing MTI Stirling-engine driver (the EM FPSE developed under a privately-funded program with CNG) mated with a hydraulically-driven refrigerant compressor. The compressor and hydraulic drive were fabricated and tested separately under Task 4.1, Component Development, and then mated to the Stirling-engine driver. System testing was performed under Task 4.3. Prior to integrating the engine and compressor, the performance of the engine was verified over the entire heat pump operating range by measuring its performance with an electric alternator load. The results of the engine verification, compressor characterization, and breadboard system testing are presented in this report. A description of the critical milestones is given in Table 1-1.

As of the completion of this program in September, 1983, a breadboard engine, compressor, and hydraulic transmission power module were designed, fabricated, and tested at four operating points (95, 80, 47, and 17°F ambient temperatures). The details of this work follows; however, in summary, the important accomplishments were:

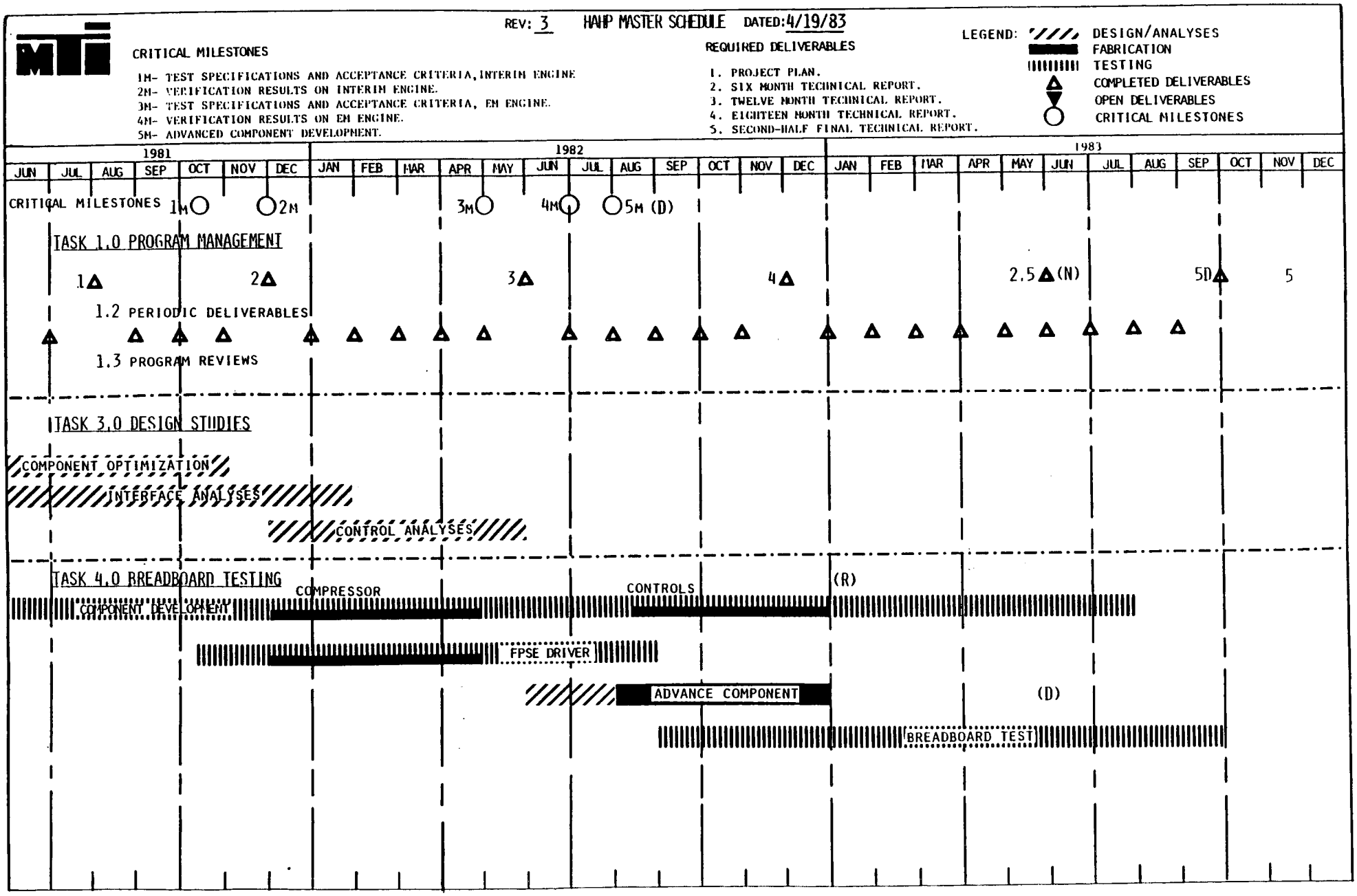

Figure 1-1 HAHP Master Schedule

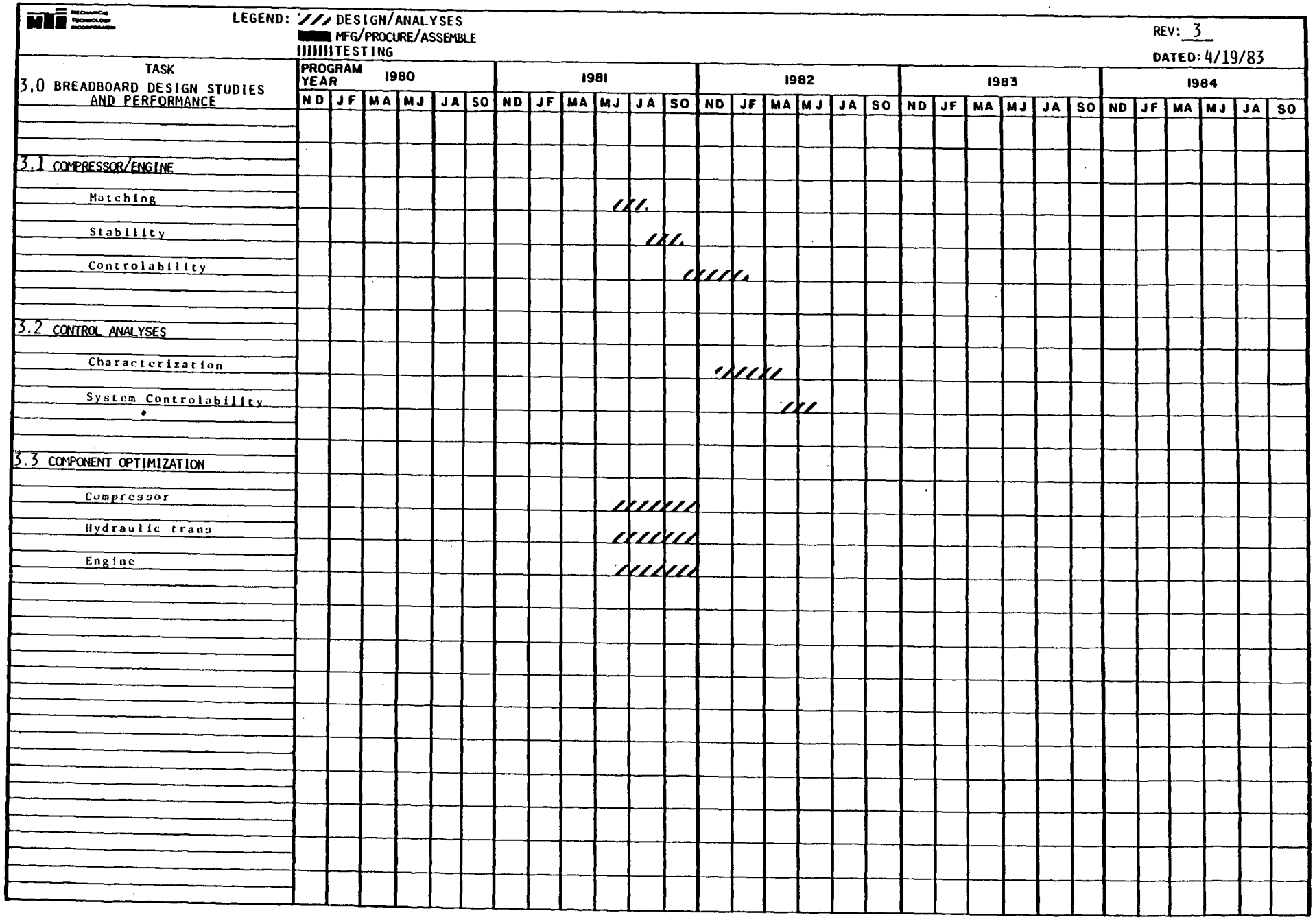

Figure 1-2 Detailed HAHP Master Schedule

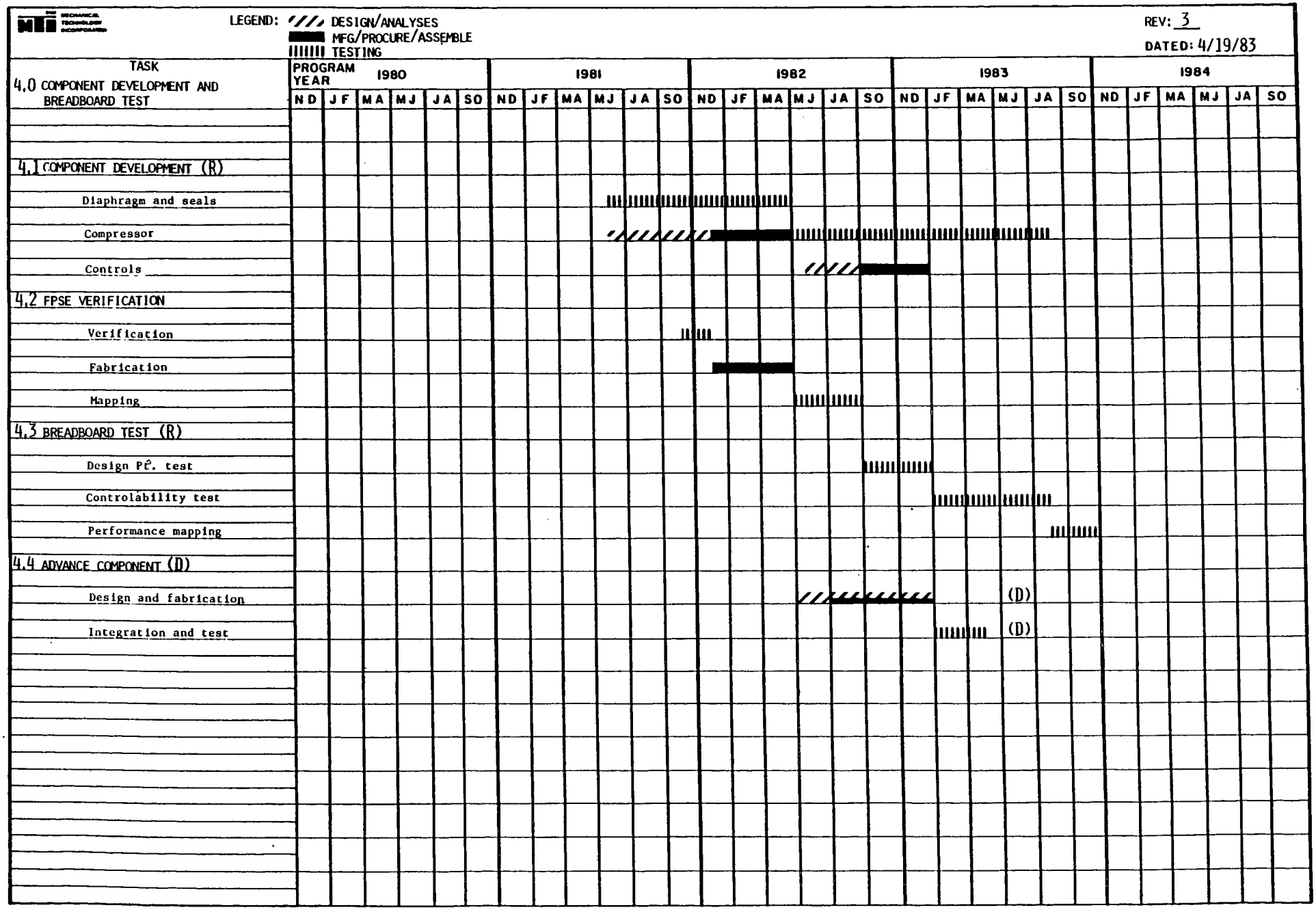

Figure 1-3 Detailed HAHP Master Schedule

TABLE 1-1
CRITICAL MILESTONES

No.	Description	Dependent Subtask
1M	TPM approval of test specifications and acceptance criteria for iterim engine.	4.2.1
2M	TPM acceptance of verification results on iterim engine and authorization of EM engine fabrication.	4.2.2
3M	TPM approval of test specifications and acceptance criteria for EM engine.	4.2.3
4M	TPM acceptance of verification results from EM engine mapping tests and of the breadboard test plan.	4.3
5M	TPM approval of proposed advanced component development.	4.4

- demonstration of the stable operation of an FPSE and vapor-compression refrigerant compressor at the four designated operating points;

- demonstration of the mechanical integrity of the breadboard unit and the longevity of the metallic diaphragms;

- demonstration of the workability of the hydraulic transmission and its potential as an efficient coupling between the engine and compressor; and,

- the successful completion of two engine verification milestones*. Upon successful completion of these two milestones, the breadboard hardware fabrication was started in March, 1982, and testing began in February, 1983 (a delay was encountered in starting the fabrication and testing due to funding constraints imposed by the Contractor (UCC-ND)).

The major shortfall of the breadboard system is that it has not achieved the three tons of refrigeration at the 95°F ambient conditions for which it was designed. A follow-on program (Phase IA) was initiated in November, 1983 to determine the reasons for the shortfall.

---

*These milestones were significant because they involved verification testing of an interim EM FPSE and the heat pump engine (EM 4) to verify performance from engine build to engine build, and the accuracy of the MTI computer design codes.

2.0 SYSTEM DESCRIPTION

Figure 2-1 is a layout drawing of the breadboard heat pump power module and compressor assembly. The power unit, located above the aft gas spring, is based on the Engineering Model Free-Piston Stirling Engine (EM FPSE) being developed at MTI in cooperation with CNG for use as a general-purpose Stirling-engine driver for electric generator and heat pump systems. The EM engine consists of:

- a natural-gas combustor;
- a displacer drive subsystem;
- a heater head and thermal regenerator; and,
- a cooler.

The lower end of the unit consists of a hydraulic coupler that efficiently transfers engine power to the refrigerant compressor. These subassemblies, along with the gas springs in the power module, form a coupled resonant system that effectively functions with the Stirling engine. In the engine, the displacer shuttles the engine working fluid (Helium) between the hot and cold spaces, generating the driving pressure wave for the system. The pistons (refrigerant compressor) extract work from the gas to power the load (refrigerant circuit); hence, in this system, power is extracted from the engine and delivered to the compressor through the hydraulic fluid, providing a force/displacement transfer path between the engine and compressor. This coupling also applies the proper dynamics to the engine, providing resonant characteristics and volumetric phase relationships.

Hermetic separation between the engine working fluid and refrigerant is achieved by employing a flexible metal diaphragm between the engine and hydraulic system. Engine power is transferred to the compressor through the volumetric displacements of the diaphragm, and corresponding displacement of oil in the hydraulic transmission induced by the pressure wave in the engine. Benefits to be derived from this HAHP system are:

- the use of the power-transfer diaphragm reduces the system from a three-degree-of-freedom to a two-degree-of-freedom resonant system, improving its operating control and stability;

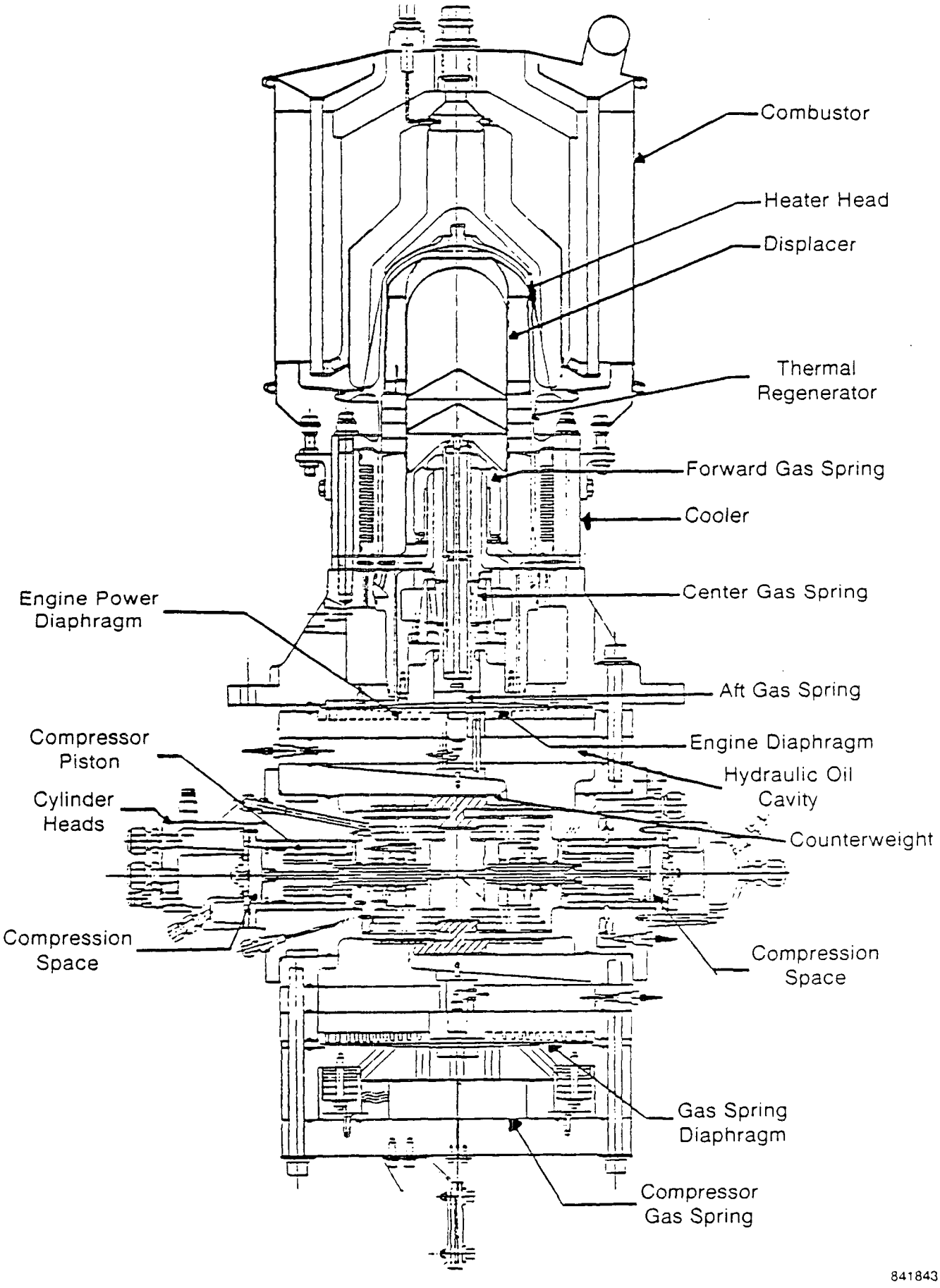

Figure 2-1 Breadboard HAHP Power Module and Compressor Assembly

- hermetic separation of the working fluids thermally isolates the refrigerant suction flow into the compressor, minimizing the superheating of the suction vapor and the associated penalties in compressor performance; and,

- the compressor closely resembles a conventional heat pump refrigerant compressor, allowing for the design and use of some standard heat pump compressor parts.

2.1 Component Description

This section describes the individual components of the breadboard power module; however, since engine development is not being conducted under this program, and the program objective is to provide a breadboard demonstration with an existing MTI Stirling engine, description of the engine will be confined to defining its characteristics for heat pump application.

2.1.1 Engine Components

2.1.1.1 Combustor - The combustor consists of a natural-gas turbulent burner and a preheater. Figure 2-2 is a schematic diagram of the combustor shown in Figure 2-1. During operation at the 95°F ambient operating point, air enters the preheater at 95°F and is warmed to 1467°F by the exhaust gases. The preheated air is mixed with fuel in the burner and ignited, raising its temperature to 3550°F. The hot gas is then passed over the heater head, providing heat input to the engine. The gas from the head enters the preheater at 1550°F, and is further cooled by transferring heat to the air intake stream. Combustor efficiency is predicted at 86% for the 95°F operating point, based on the lower heating value for natural gas. Initial testing of the combustor on the EM engine has indicated that the combustor will achieve this efficiency.

A drawing of the EM external heat system, consisting of the combustor and heater head, is shown in Figure 2-3.

2.1.1.2 Displacer Drive System - The displacer drive system consists of the displacer, displacer rod, gas bearing support, gas spring pistons and cylinders,

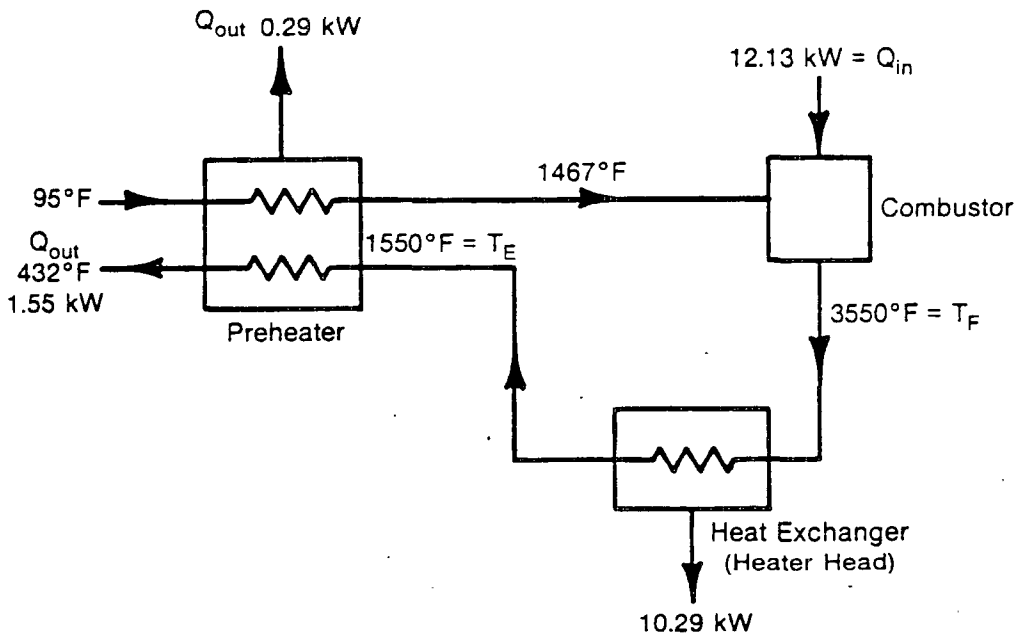

Predicted Efficiency Preheater:	≈0.94
Predicted Efficiency Combustion:	≈1.00
Predicted Efficiency Combustor:	≈0.86 (LHV)
Measured Efficiency Combustor:	0.92 (LHV)
Combustion Temperature:	3550°F
Air Preheater Temperature:	1467°F
A/F:	16.18
QA:	623 $SCFH_{32}$
QF:	38.5 $SCFH_{32}$
Radiation Losses:	2.4%
Heater Head Efficiency:	$0.93 = \frac{T_F - T_E}{T_F - T_H} = \frac{3550 - 1555}{3550 - 1400}$

$$\frac{Q_{in} - Q_{out}}{Q_{in}} = \frac{Q_{heat}}{Q_{in}}$$

Nomenclature:

T_H = Heater Head Temperature
Q_{in} = Heat into the System from Fuel
Q_{out} = Heat Lost from the Preheater
A/F = Air/Fuel Ratio
QA = Airflow
QF = Fuel Flow

Figure 2-2 Engineering Model Combustor Schematic

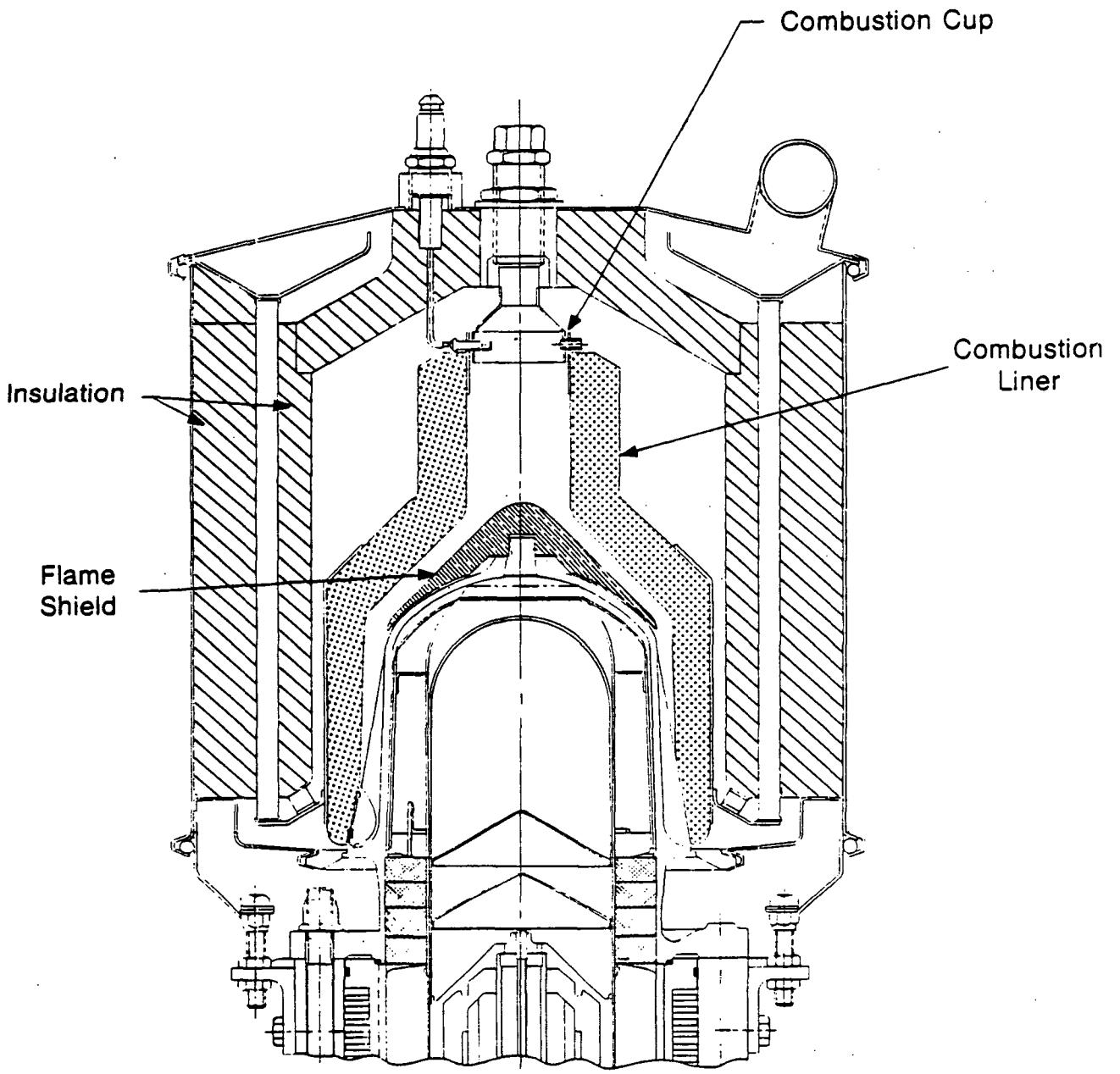

Figure 2-3 Engineering Model External Heat System

822159

and displacer control. The dynamic arrangement for the displacer drive system is shown in Figure 2-4. As depicted, the displacer is a free member radially supported by gas bearings on the rod, and axially balanced by the dynamic forces. The function of each component in this system is as follows:

Displacer - The displacer is used to shuttle the engine working fluid through the heat exchanger components in the engine to the hot expansion and cool compression volumes.

Displacer Rod - The displacer rod serves two functions: 1) it transmits radial support for the displacer; and, 2) it provides the thermodynamic power required to move the displacer against the losses from the heat exchanger pressure drop, gas spring thermal hysteresis, and gas spring leakage pumping loss.

Gas Bearing Support - Hydrostatic gas bearings are used to provide radial support for the displacer. The gas bearings are located along the displacer rod and are designed to be internally fed by bleeding gas out of the working volumes (compression space) during the high-pressure portion of the cycle.

Gas Spring Piston and Cylinders - Gas springs are employed to provide a restoring force to the displacer, providing its resonant characteristics. As shown in Figure 2-1, the displacer gas springs are the "Forward Gas Spring" located in the bottom end (cool end) of the displacer, the "Aft Gas Spring" located at the base of the displacer rod, and the "Center Gas Spring" located along the displacer rod.

Displacer Control - The displacer control allows external control of the displacer for stroke modulation, providing primary engine control to the system for load matching at different ambient operating conditions. Displacer control is achieved by applying a forcing function, F_c (Figure 2-4), to the displacer to control stroke.

2.1.1.3 Heater Head and Thermal Regenerator - The heater head design for the EM engine is based on a monolithic heater head concept that has been under development for the past several years. The monolithic heater head design has the potential of being more reliable and less costly because it eliminates the fitting and brazing of the tubes required in a tubular design. The concept of

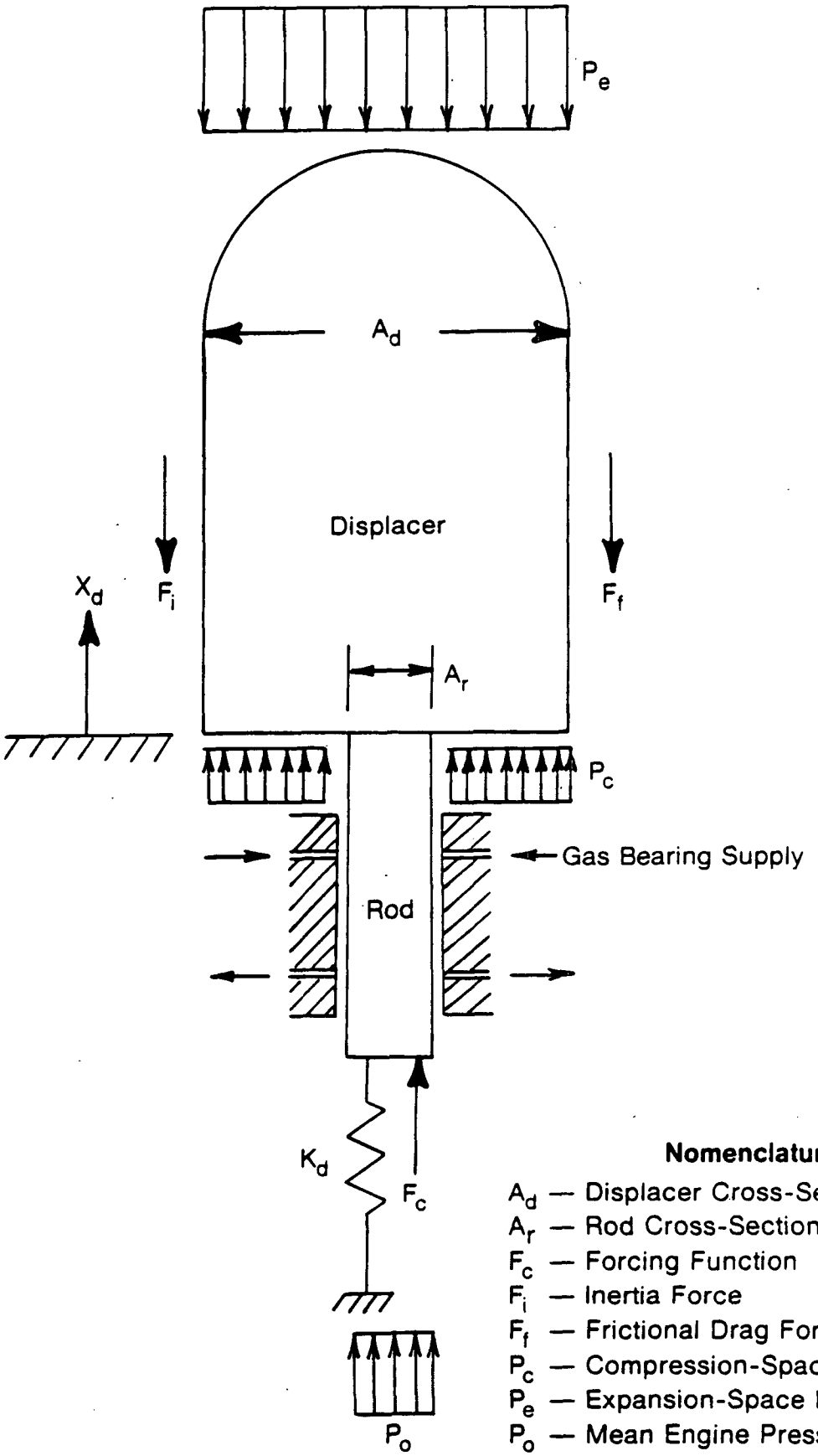

Nomenclature

A_d — Displacer Cross-Sectional Area
A_r — Rod Cross-Sectional Area
F_c — Forcing Function
F_i — Inertia Force
F_f — Frictional Drag Force
P_c — Compression-Space Pressure
P_e — Expansion-Space Pressure
P_o — Mean Engine Pressure
X_d — Displacer Motion
K_d — Gas Spring Stiffness

Figure 2-4 Displacer Rod Dynamics

the head is to use a one-piece head construction with fins on the inner and outer sides of the head to transfer the heat from the combusted gases in the combustor to the working fluid of the engine. The monolithic head configuration with external fins is shown in Figure 2-5. The lower portion of the head houses an annular thermal regenerator. The regenerator serves to periodically exchange heat in the gas streams being shuttled between the cooler and heater head. This heat exchanger provides the internal storage of heat necessary to approach the ideal potential of Carnot efficiency. Standard, fine wire-mesh materials are used in the regenerator.

2.1.1.4 Cooler - The EM cooler is designed for water cooling with material and external fins to enhance its heat transfer characteristics. The function of the cooler is to reject heat from the working fluid.

2.1.2 Rankine Refrigerant Compressor

The heat pump compressor is a resonant-piston compressor sinusoidally driven by the pressure wave in the engine. In the design for the compressor and hydraulic coupling (shown in Figure 2-6a), the compressor was positioned horizontally in order to allow the use of pistons, piston cylinders, cylinder heads, and valve assemblies similar to those commonly used in electrically-driven, residential-size heat pump compressors. The operation of the compressor, closely linked to the operation of the hydraulic transmission, will be described in the following section.

2.1.3 Hydraulic Coupling (Transmission)

The hydraulic transmission (provides the force displacement link between the engine and compressor) which consists of the engine power diaphragm, gas spring diaphragm, lateral vibration counterweight, hydraulic oil, and compressor gas spring, transfers power from the engine to the compressor through deflections of the engine power diaphragm, creating a force unbalance across the counterweight (Figure 2-6a), forcing it to move. Because of the incompressibility of the oil, the compressor piston is also acted upon, but in the opposite direction to the counterweight. Compression spaces on either side of the piston compress the refrigerant. The lower gas spring diaphragm and compressor gas spring provide the restoring force for the compressor piston. Descriptively, the compressor

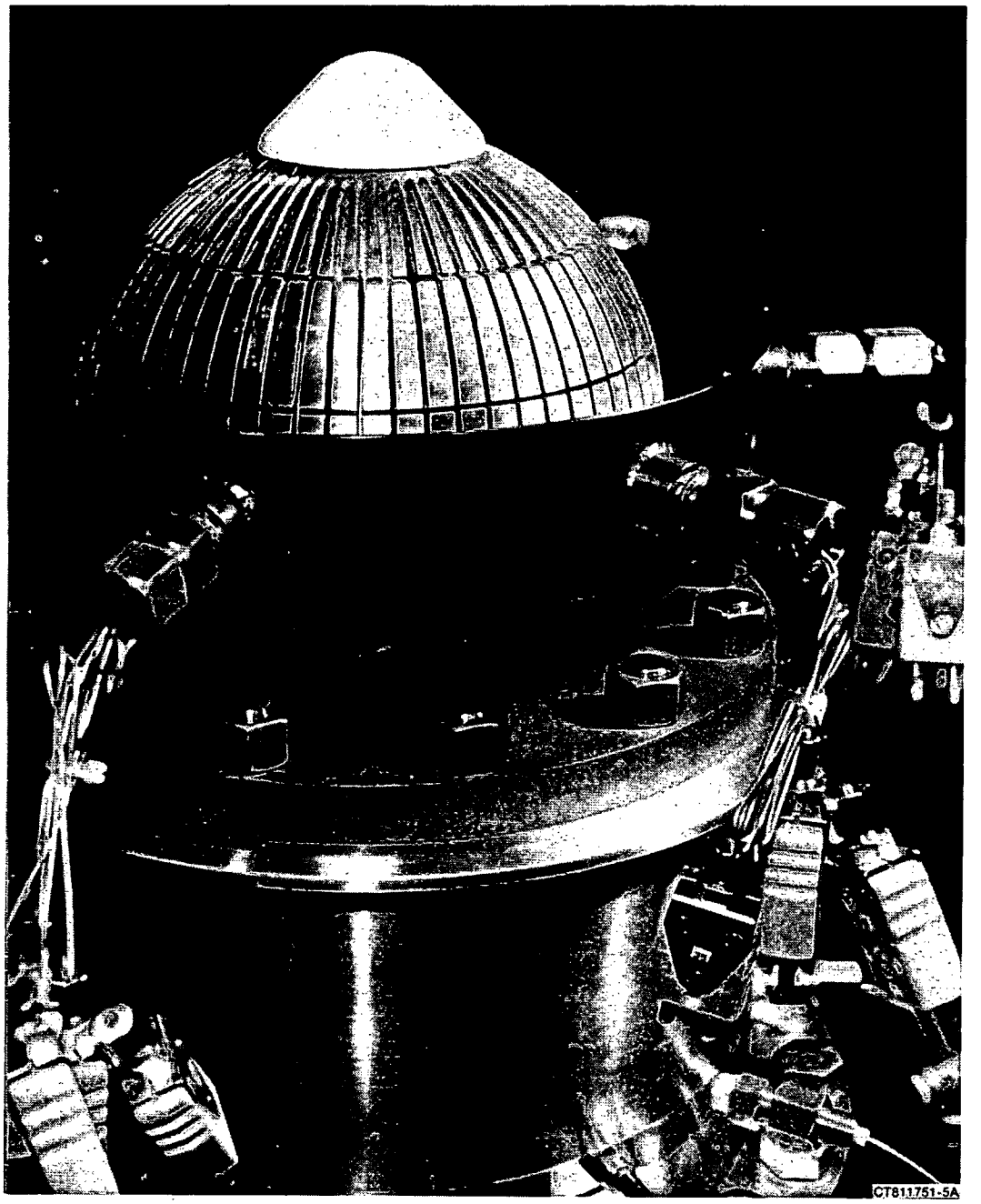

Figure 2-5 Monolithic Heater Head Configuration for Engineering Model Engine

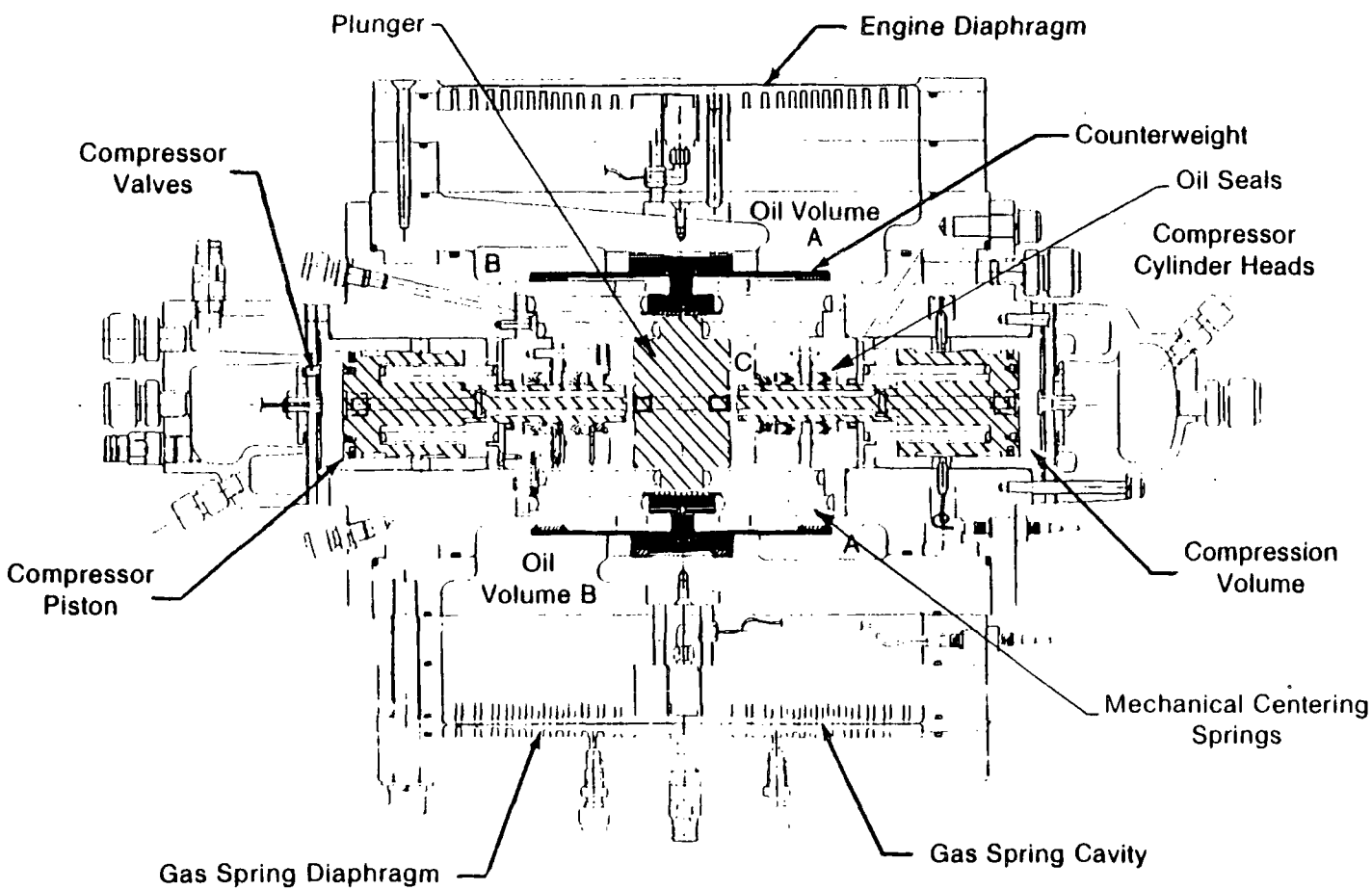

Figure 2-6a Compressor and Hydraulic Transmission Layout

Side View

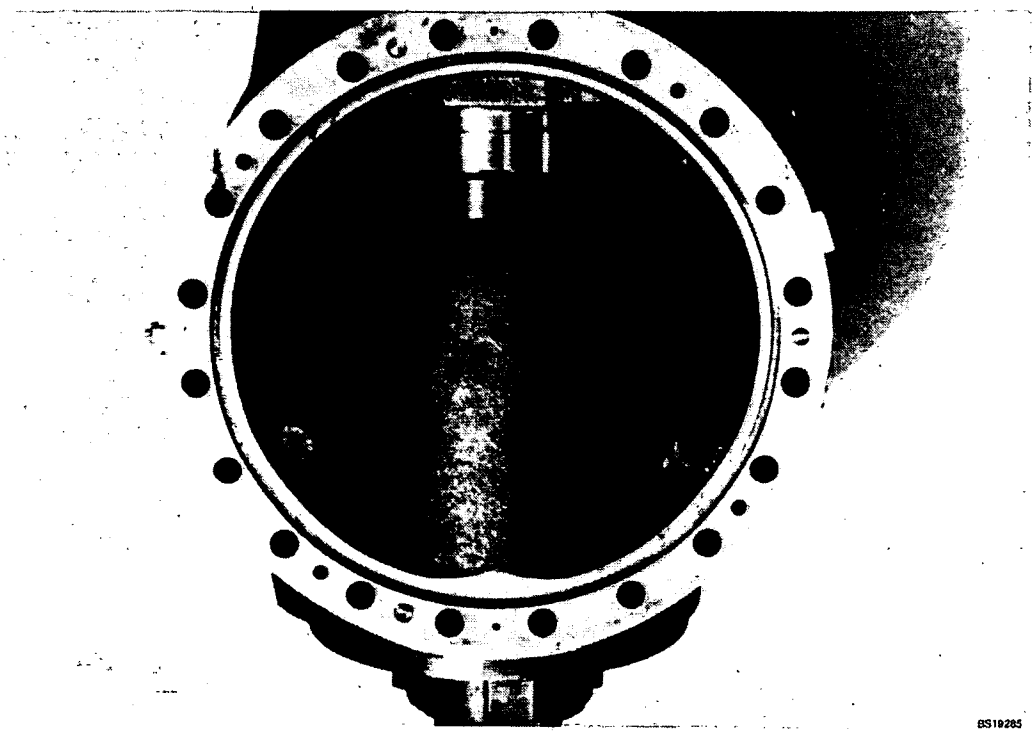

Top View

Figure 2-6b Compressor Housing

operation can be seen more clearly in Figure 2-7, which defines each of the oil volumes and the interaction between the counterweight and compressor piston. Starting with motion of the counterweight from right to left, as the engine power diaphragm deflects downward, the pressure increases in volume A, producing movement of the counterweight to the left. This motion produces two resultant effects: 1) the oil in volume B acts on the compressor gas spring diaphragm (located at the bottom) causing it to deflect, thus creating a restoring force on the counterweight; and, 2) as the counterweight moves to the left, volume C increases relative to volume D. Because the oil is incompressible, and the quantity of oil in volumes C and D is fixed, the compression piston must move to the right to maintain volumes C and D constant. The movement of the compressor piston to the right produces the compression stroke in the right compression volume, and the intake stroke in the left compression volume. The compressor gas spring provides the restoring force to return the piston to the left, and counterweight to the right.

The compressor and hydraulic transmission designs were selected for the following important features:

- engine/compressor fluids are hermetically sealed from one another;

- the horizontal design makes the compressor cylinder heads accessible from outside the machine; thus, repairs can be easily made to the compressor valve assemblies without having to disassemble the entire machine, and the suction manifolds can be insulated to minimize superheating of the suction refrigerant vapor;

- use of diaphragms eliminates the power piston from Stirling engines, reducing the system from a three-degree to a two degree-of-freedom system, thus improving the system's operating control.

A detailed description of the design of these components is presented in the following sections.

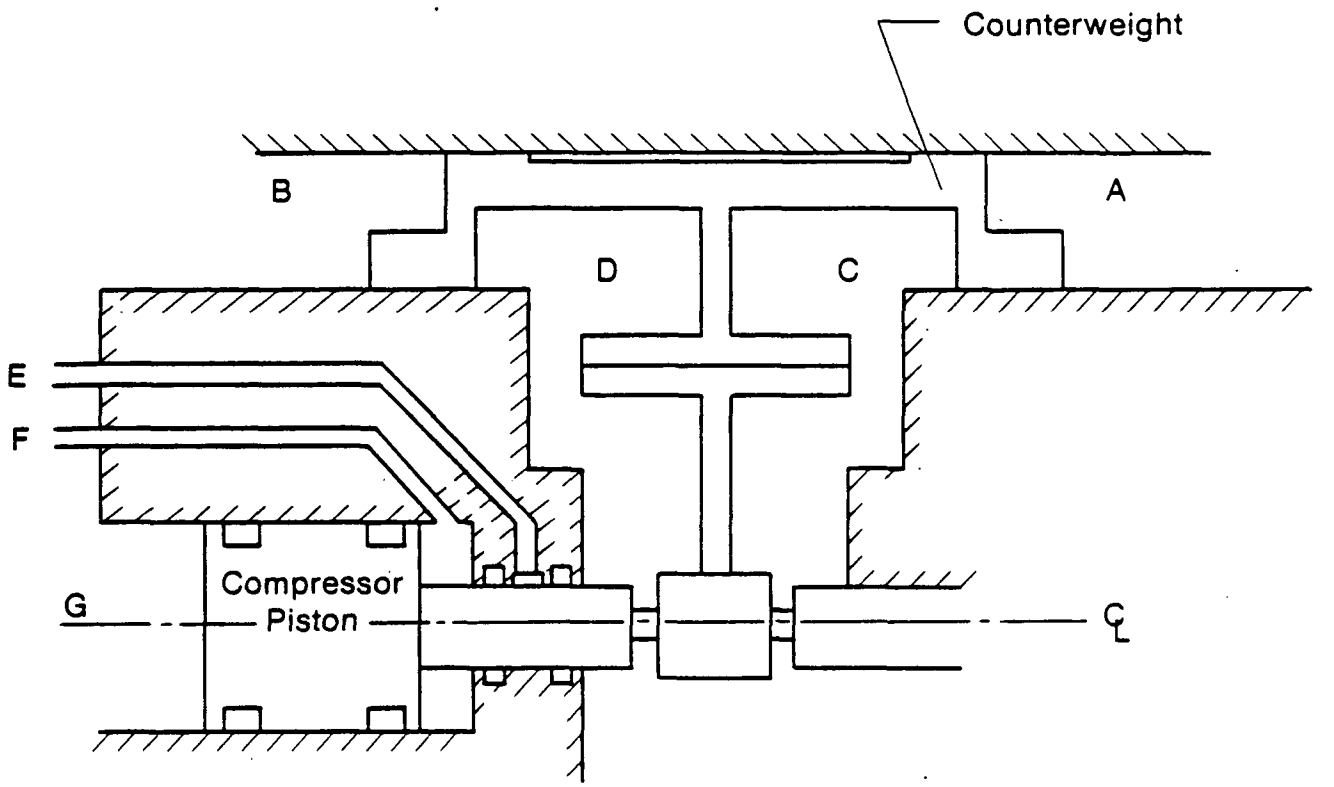

Pressure Levels

High Pressure (Oil)	$P_A = P_B = P_C = P_D$	(Harmonic)
Intermediate Pressure (Oil)	P_E	(Constant)
Suction/Discharge (Refrig.)	P_F	(Constant)
Compression Space (Refrig.)	P_G	(Harmonic)

Figure 2-7 Compressor Schematic

3.0 TECHNICAL DISCUSSION

3.1 Program Objectives and Task Description

The objectives of the HAHP program are to design, fabricate, and test a breadboard FPSE diaphragm-coupled HAHP system. The work plan states that the breadboard system will use an existing MTI Stirling engine which will be tested independently to verify that it will operate over the entire HAHP operating range. To accomplish the technical objectives, the major tasks and appropriate subtasks being worked on are:

Task 3.0 Breadboard Design Studies and Performance Analyses

Task 4.0 Component Development and Breadboard Demonstration

- Compressor/Hydraulic Transmission Component Development
- Fabrication/Verification Testing of an Existing EM Engine
- Breadboard Engine/Compressor Testing

Each of these tasks has been completed. A discussion of the analyses, design criteria, and results follows.

3.2 Breadboard Design Studies and Performance Analysis

To match an existing FPSE to a resonant compressor, matching of the engine/compressor dynamic operation conditions is necessary to ensure that the power and strokes of the engine and compressor are correct, and that the system will operate stably over the intended operating range. The four ARI rating points (95°, 80°, 47°, and 17°F ambient temperatures) were taken as representative of the operating range, and heating/cooling capacity was based on a three-ton rated cooling capacity at 95°F and the DOE heating/cooling load lines. Table 3-1 defines the operating specifications for the heat pump at the four operating points. The matching analyses included characterization of the dynamic/thermodynamic conditions of the hydraulic transmission and compressor, steady-state matching analysis, and transient stability analysis.

TABLE 3-1

SELECTED HAHP BREADBOARD SYSTEM OPERATING POINTS

Outdoor Temperature (°F)	95	80	47	17
Heating/Cooling Load (Btu/hr)	-36,000	-18,000	+14,000	+38,000
Suction Pressure (psia)	90.7	111.3	83.4	42.2
Discharge Pressure (psia)	277.4	193.6	188.8	264.4
Evaporator Temperature (°F)	45.0	57.3	40.1	4.2
Condenser Temperature (°F)	120.8	93.9	92.2	117.0
Freon Flow Rate (lbm/hr)	570.0	230.6	110.4	290.6

3.2.1 Steady-State Matching Analysis

This section describes the results of the matching analysis for the HAHP EM/Resonant Compressor System, which was performed at the four operating points (2 heating, 2 cooling) shown in Table 3-1. Note that these conditions assume zero degrees superheat at the compressor suction inlet. The following sections describe the details of the matching procedure.

3.2.1.1 Compressor Characterization - To perform the matching of compressor to engine, it was necessary to characterize the compressor in terms of effective mass, stiffness, and damping for a given geometry over the range of strokes, suction/discharge pressures, and mass flow rates to which the compressor was subjected. The compressor was designed for a .75-inch stroke at the 95°F design point in order to minimize bearing losses and provide an overall "bottom-end" stiffness that required a reasonable aft gas spring size and compressor mass for proper system tuning. The valves were designed using MTI's valve dynamics code.

To calculate effective compressor damping, adiabatic compressor efficiency was calculated in two steps: 1) the ratio of adiabatic work with suction/discharge valve and plenum pressure drops to adiabatic work without these pressure drops; and, 2) this efficiency was then multiplied by 94% to account for irreversibilities (2%) and leakage power loss (4%) to arrive at overall compressor efficiency. Actual compressor power was calculated by dividing adiabatic power (based on suction discharge line conditions) by overall compressor efficiency (results shown in Table 3-2). Compressor stiffness (shown in Table 3-2) was

calculated by determining the slope of a least-squares fit line through a plot of external net gas force on the double-acting compressor versus position.

TABLE 3-2

PREDICTED COMPRESSOR POWER AND EFFICIENCY

Suniso Refrigerant Oil 3GS (150 SUS/100°F)

Outdoor Temperature	(°F)	95	80	47	17
Frequency	(Hz)	60	60	60	60
Suction Line Pressure	(psia)	90.70	111.3	83.4	42.2
Suction ΔP	(psi)	7.5	4.3	2.7	4.8
Suction Pressure	(psia)	83.2	107.0	80.7	37.4
Discharge Line Pressure	(psia)	277.4	193.6	188.8	264.4
Discharge ΔP	(psi)	13.1	6.5	3.8	10.2
Discharge Pressure	(psia)	290.5	200.1	192.6	274.6
Work w/o ΔP/Work w/ΔP		.885	.880	.936	.90
Compressor η	(.94xabove)	.832	.827	.880	.854
Adiabatic Power	(watts)	2001	391	280	1725
Actual Power	(watts)	2405	473	318	2020
Compressor Damping	(lb_f-s/in)	2.13	1.45	0.77	1.25
	(N-S/m)	(373.0)	(254.1)	(135.2)	219.5
Compressor Stiffness	(lb_f/in)	1.86×10^3	1.79×10^3	1.84×10^3	1.47×10^3
	(N/m)	(3.256×10^5)	(3.133×10^5)	(3.226×10^5)	(2.577×10^5)

Transmission Characterization - The hydraulic transmission components (counterweight, oil, seals, bearings, piston rings, diaphragms) provide additional mass, stiffness, and damping to the "bottom end." For this analysis, the following assumptions were made:

- hydraulic oil incompressible ($K = \infty$); and,
- diaphragm mass and damping negligible.

A. Diaphragm - As noted above, the diaphragm mass and damping were assumed negligible. The stiffness versus counterweight amplitude (for a 12-in.^{2} counterweight area) is shown in Figure 3-1.

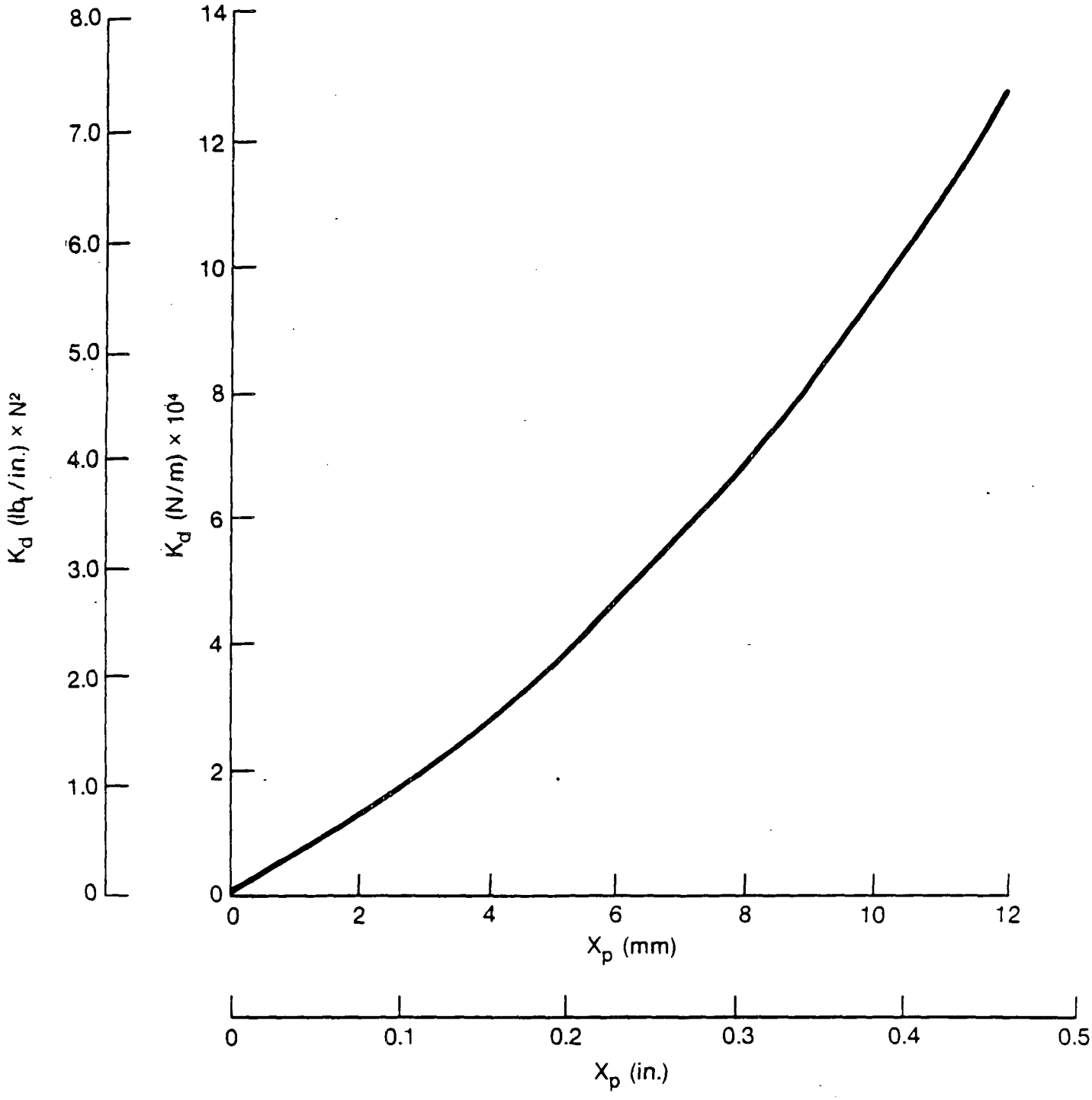

Figure 3-1 Bendix Diaphragm Stiffness Versus Counterweight Amplitude (½ Stroke) (12-in^2 Counterweight Area)

822413-

B. Oil - Effective dynamic mass of the oil was calculated from the compressor housing drawings to be 4.33 lb_m (1.97 kg). The viscous loss was assumed to be equal to that measured for the hydraulic simulator. (A description of the hydraulic simulator and the testing performed with this rig is presented in Section 3.3.4.) This assumption is adequate since the viscous oil loss for such systems is on the order of a few watts.

C. Seal Losses - Compressor seal loss is a function of oil viscosity which is, in turn, a function of oil temperature. Oil temperature was estimated in the following manner: heat generated in the oil is assumed to be transferred to the cooler via conduction through the compressor housing and transferred to the ambient via natural convection/radiation from the compressor surface. Figure 3-2 shows the total heat rejected (to cooler and ambient) for oil temperatures ranging from 80-180°F. The amount of heat generated in the oil is assumed to be equal to the seal losses, including balance drive seal, balance/piston seal, balance/sleeve seal, pumping ring seal, discharge/suction seal, and the piston ring for one cylinder. Power loss for the other piston ring is assumed to be conducted into the refrigerant gas, as opposed to the oil. These losses are shown for various oil temperatures in Figure 3-2 for the four operating points. The intersection points of these curves with the heat rejection line determine the oil temperatures at the operating points; results are shown in Table 3-3.

TABLE 3-3

ESTIMATED COMPRESSOR SEAL LOSSES

Outdoor Temperature (°F)	95	80	47	17
Frequency (Hz)	60	60	60	60
Oil Temperature (°F)	100	80	80	117
Itemized Losses (watts - approx.)				
Balance Drive Seal (2)	42	11	14	72
Balance Piston Seal	32	7.7	9.8	59
Balance Sleeve Seal (2)	46	13	17	76
Pumping Ring (2)	70	38	42	84
Compressor Piston Bearing (2)	3.8	2.0	2.4	4.4
Oil Viscous Loss	2.2	0.5	0.7	3.2
Piston Rings (2)	234	56	76	320
Total Seal Losses (watts - approx.)	427	129	162	585

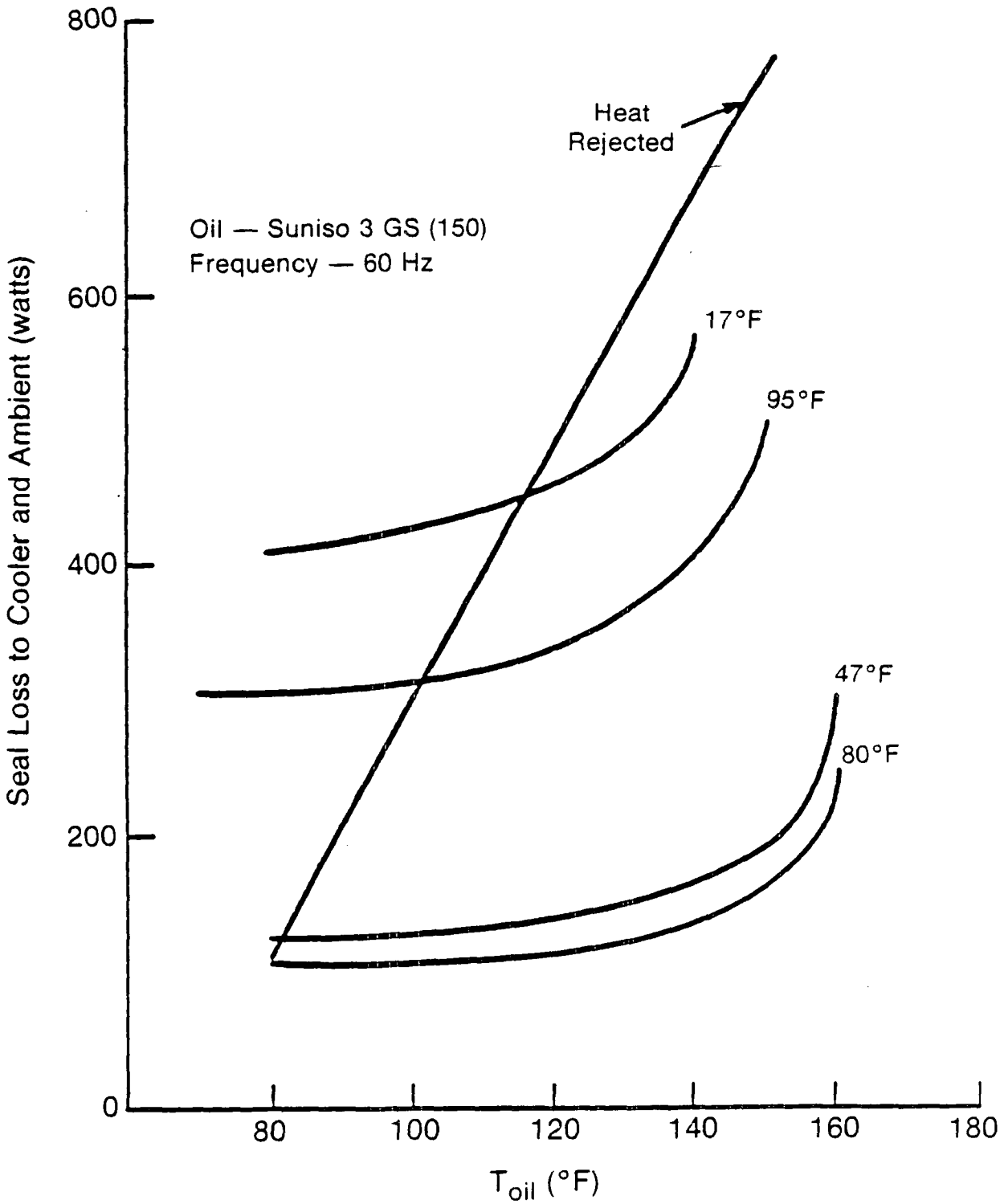

Figure 3-2 Calculation of Compressor Oil Temperature

D. Centering Springs - Piston centering springs are assumed to have a total stiffness of 228 lbf/in. (4×10^4 N/m), while counterweight springs are assumed to have a stiffness of 272 lbf/in. (4.76×10^4 N/m), for a total of 500 lbf/in.

E. Gas Spring Stiffness and Power Loss - The aft gas spring was sized so that at the design point the pressure amplitude in the spring would equal the compression-space amplitude, thus minimizing power loss in the capillary tube connecting these two chambers. At this point, for a diaphragm ΔV of 3.75 in.^{3}, the aft gas spring stiffness was 2.0×10^3 lb_f/m (3.5×10^5 N/m). The power loss of the gas spring is that due to hysteresis alone, since the diaphragm prevents any leakage losses. These power losses were calculated to be 75, 22, 27, and 107 watts for the four operating points, respectively.

3.2.1.2 Engine/Compressor Matching - Once the compressor and hydraulic transmission were characterized in terms of equivalent mass, stiffness, and damping, the actual engine/compressor matching was begun. Essentially, the matching process consisted of selecting the proper displacer rod area in the engine, and diaphragm displacement in the compressor so as to minimize the required displacer forcing function while maintaining stable system operation at each of the operating points, and for 60-Hz operation. In these analyses, compressor refrigerant flow is directly related to displacer stroke; therefore, control of the compressor is achieved through control of the displacer. Increasing the permissible diaphragm volumetric displacement enables the engine to produce the required power at a lower displacer stroke; however, stress considerations provide an upper limit on diaphragm displacement.

Increasing the virtual rod area enables the engine to provide greater thermodynamic power to the displacer, thus lowering the required displacer forcing function at a given stroke; however, the displacer stroke increases in order to shuttle the same quantity of working fluid between expansion and compression spaces. Also, the stability margin decreases somewhat with increasing rod area, a factor that becomes increasingly important at the lower power points.

Actual matching was performed using a modified version of the First-Order Code FAST H. Two virtual rod areas and two diaphragm design displacements were selected for the HAHP engine/compressor design. The lower displacement, 3.75

in.^{3}, at design point was selected to maintain maximum diaphragm stress to 35,000 psi at the design point (95°F). At 17°F (maximum stroke), the diaphragm stress is 51,000 psi, considerably lower than the yield stress of 71,000 psi. The 4.0 in.^{3} displacement was selected to increase the thermodynamic displacer drive power. At 95 and 17°F, corresponding diaphragm stresses are 39,500 and 56,000 psi. Tests must be performed to determine diaphragm life at these higher stress conditions.

For these two diaphragm displacements, system performance at the design point was calculated for virtual rod areas of 1.38, 1.5, and 2.0 in.^{2}. A detailed code was developed and used to calculate displacer gas spring leakage and hysteresis loss for the various virtual rod areas. Preliminary designs for the gas spring indicated a required increase in the length of the engine/compressor transition section (also called adapter plate) from 3.25 to 5.5 in. for displacer rod areas of 1.5 and 2.0 in.^{2}, resulting in a significant increase in control power and a reduction in engine indicated efficiency. The EM engine was not specifically designed for use with the HAHP compressor; hence, in an optimized redesign, lower input power and higher efficiency operation is expected.

The two rod areas selected for the design (1.5 and 2.0 in.^{2}) were chosen to provide an adequate safety factor on input power. While it was physically possible to incorporate a rod area greater than 2.0 in.^{2}, this was selected as the maximum for the design because at this point the displacer stroke was 10.82 mm (.426 in.) and 10.42 mm (.410 in.) for diaphragm displacements of 3.75 and 4.0 in.^{3}, respectively. For the above rod areas, diaphragm displacements, and gas spring sizes, the system was tuned at the 95°F design point by varying the effective compressor mass.

At the off-design point of 17°F, retuning the system was necessary to obtain acceptable input, power, and displacer stroke. This was done by varying the gas spring stiffness so as to maximize indicated efficiency. Although it was not necessary to retune the system at the 80 to 47°F points due to the low power levels, this was done for consistency. The results of the matching are shown in Tables 3-4 to 3-7. The discrepancy of Q_{IN} not being equal to P-V to Q_{REJ} is due to iteration accuracy of the computer code.

TABLE 3-4

MATCHING ANALYSIS RESULTS FOR PRELIMINARY CONTROL SCHEME

Frequency = 60 Hz

Displacer Rod Area = 1.5 in.^{2}

Diaphragm Displacement = 3.75 in.^{3} @ 95°F

Outdoor Temp. (°F)		95	80	47	17
X_p	(mm)	9.525	5.118	5.753	11.379
X_d	(mm)	9.725	3.642	2.736	8.641
ϕ_d	(deg)	70.9	61.9	65.4	52.7
P_c	(Bar)	5.55	2.73	3.18	5.61
θ_c	(deg)	-97.8	-83.4	-78.8	-73.3
P-V	(watts)	2907*	624	507	2712
η_c		.354	.338	.331	.412
Q_{in}	(watts)	7965	2180	1913	7343
Q_{rej}	(watts)	5143	1443	1280	4317
σ	(1/sec)	-20.7	-12.0	-4.6	-10.7
Q_{loss}	(watts)	505	92.7	80	326

Nomenclature

X_p = piston amplitude (motion)

ϕ_d = piston/displacer phase angle

η_c = engine thermodynamic efficiency

X_d = displacer amplitude (motion)

P-V = piston P-V work (shaft)

P_c = compression-space pressure amplitude

θ_c = compression-space pressure phase angle

σ = stability margin

Q_{loss} = heat loss to the surroundings

Q_{in} = heater head heat input

Q_{rej} = cooler heat output

*Computed in Table 3-10

TABLE 3-5

MATCHING ANALYSIS RESULTS FOR PRELIMINARY CONTROL SCHEME

Frequency = 60 Hz

Displacer Rod Area = 2.0 in.^{2}

Diaphragm Displacement = 3.75 in.^{3} @ 95°F

Outdoor Temp. (°F)		95	80	47	17
X_p	(mm)	9.525	5.118	5.753	11.379
X_d	(mm)	10.82	4.001	3.007	9.568
ϕ_d	(deg)	70.0	61.3	64.6	52.1
P_c	(Bar)	5.55	2.73	3.18	5.61
θ_c	(deg)	-96.9	-82.8	-77.8	-72.6
P-V	(watts)	2907	624	507	2712
η_c		.342	.344	.341	.406
Q_{in}	(watts)	8678	2341	2041	7990
Q_{rej}	(watts)	5710	1537	1345	4748
σ	(1/sec)	-19.4	-9.6	-3.0	-9.2
Q_{loss}	(watts)	573	109.9	141.9	465.1

Nomenclature

X_p = piston amplitude (motion)

ϕ_d = piston/displacer phase angle

η_c = engine thermodynamic efficiency

X_d = displacer amplitude (motion)

P-V = piston P-V work (shaft)

P_c = compression-space pressure amplitude

θ_c = compression-space pressure phase angle

σ = stability margin

Q_{loss} = heat loss to the surroundings

Q_{in} = heater head heat input

Q_{rej} = cooler heat output

TABLE 3-6

MATCHING ANALYSIS RESULTS FOR PRELIMINARY CONTROL SCHEME

Frequency = 60 Hz

Displacer Rod Area = 1.5 in.^{2}

Diaphragm Displacement = 4.0 in.^{3} @ 95°F

Outdoor Temp. (°F)		95	80	47	17
X_p	(mm)	9.525	5.118	5.753	11.379
X_d	(mm)	9.355	3.521	2.681	8.409
ϕ_d	(deg)	70.2	60.5	63.3	51.9
P_c	(Bar)	5.76	2.87	3.35	5.96
θ_c	(deg)	-94.2	-79.6	-75.0	-69.9
P-V	(watts)	2907	624	507	2712
η_c		.366	.343	.333	.417
Q_{in}	(watts)	8087	2185	1923	7475
Q_{rej}	(watts)	5127	1435	1282	4361
σ	(1/sec)	-19.4	-10.0	-4.8	-9.7
Q_{loss}	(watts)	500	73.3	97.6	374.5

Nomenclature

X_p = piston amplitude (motion)

ϕ_d = piston/displacer phase angle

η_c = engine thermodynamic efficiency

X_d = displacer amplitude (motion)

P-V = piston P-V work (shaft)

P_c = compression-space pressure amplitude

θ_c = compression-space pressure phase angle

σ = stability margin

Q_{loss} = heat loss to the surroundings

Q_{in} = heater head heat input

Q_{rej} = cooler heat output

TABLE 3-7

MATCHING ANALYSIS RESULTS FOR PRELIMINARY CONTROL SCHEME

Frequency = 60 Hz

Displacer Rod Area = 2.0 in.^{2}

Diaphragm Displacement = 4.0 in.^{3} @ 95°F

Outdoor Temp. (°F)		95	80	47	17
X_p	(mm)	9.525	5.118	5.753	11.379
X_d	(mm)	10.42	3.872	2.951	9.322
ϕ_d	(deg)	69.3	59.9	62.4	51.3
P_c	(Bar)	5.77	2.88	3.36	5.97
θ_c	(deg)	-93.4	-78.9	-74.1	-69.3
P-V	(watts)	2907	624	507	2712
η_c		.356	.349	.343	.413
Q_{in}	(watts)	8813	2339	2051	7121
Q_{rej}	(watts)	5671	1522	1347	4771
σ	(1/sec)	-17.9	-7.5	-2.7	-8.2
Q_{loss}	(watts)	543	114.6	158.1	454.4

Nomenclature

X_p = piston amplitude (motion)

ϕ_d = piston/displacer phase angle

η_c = engine thermodynamic efficiency

X_d = displacer amplitude (motion)

P-V = piston P-V work (shaft)

P_c = compression-space pressure amplitude

θ_c = compression-space pressure phase angle

σ = stability margin

Q_{loss} = heat loss to the surroundings

Q_{in} = heater head heat input

Q_{rej} = cooler heat output

3.2.1.3 Gas Spring Sizing - In order to tune the system at the 17°F point, total stiffness on the compressor ("bottom-end" stiffness) must be increased by 4.5%. From the sensitivity studies on the interim engine, it was found that a 10% variation in stiffness caused a significant detuning of the engine. In order to supply a factor of safety, this ±10% stiffness variation was designed into the compressor (corresponds to a gas spring volume variation from 50-100 in.^{3}). Sizing the aft gas spring to accommodate this volume change will result in sufficient system tuning capability over the operating range, as this results in a gas spring stiffness variation from 1.43×10^3 lb_f/in. (2.5×10^5 N/m) to 2.79 $\times 10^3$ lb_f/in. (4.9×10^5 N/m).

3.2.1.4 Compressor Component Mass - Total equivalent dynamic compressor mass for diaphragm displacements of 3.75-4.0 in.^{3} was determined to be 19.7 lb_m (8.96 kg) and 21.3 lb_m (9.66 kg), respectively (includes effective mass of the oil, and counterweight and piston masses). Assuming an oil dynamic mass of 4.33 lb_m (1.97 kg), and equal piston/counterweight masses, the component weights are:

	3.75 in.^{3} ΔV	4.0 in.^{3} ΔV
Counterweight	7.689 lb_m (3.495 kg)	8.459 lb_m (3.845 kg)
Piston	7.689 lb_m (3.495 kg)	8.459 lb_m (3.845 kg)

3.2.1.5 Transition Section Design - For the best performance, the transition section (also known as the adapter plate) is designed with 45 passages of circular cross section. The diameter of these passages should be 3/16 in., and the total length of the transition section should be 5.5 in. This section would accommodate unit designs of 1.5- and 2.0-in.^{2} rod areas, and diaphragm displacements of 3.75 and 4.0 in.^{3}.

3.2.2 HAHP Stability Analysis

This section describes the results of the stability analysis for the HAHP EM/Resonant Compressor System. The results of the matching analysis used in the evaluation of system stability are reported in Section 3.2.1.

3.2.2.1 Linear Stability Analysis (Computer Code) - An analysis of engine/compressor stability at all four operating points was conducted, assuming a linear system, using the Computer Code. The results are given in Section

3.2.1 (Tables 3-4 to 3-7) for rod areas of 1.5 and 2.0 in.^{2}, and diaphragm displacements of 3.75 and 4.0 in.^{3} (at 95°). The stability margin, σ, is the reciprocal of the longest time constant of the system transient response to small perturbation. The slowest response occurred for the 2.0-in.^{2} rod area, 4.0-in.^{3} diaphragm ΔV, 47°F operating point (lower power point); the time constant is $\sim$1/3 second.

3.2.2.2 Nonlinear Stability Analysis - While engine power can be adequately modeled as a linear system, the compressor load is known to be nonlinear. Hence, the system may have more than one operating point which can be different than that predicted by the linear analysis; compressor nonlinearity can also affect system stability. To evaluate this possibility, the system was simulated using an MTI second-order, time-stepping code, which includes compressor nonlinearities, and permits evaluation of the system response to perturbations about an operating point. The code was used to examine system stability at the operating point. This was done for the 2.0-in.^{2} rod area, 4.0-in.^{3} diaphragm displacement case, as the linear stability analysis predicted the smallest stability margin for that particular combination.

The system was found to operate stably at all operating points. Table 3-8 shows the operating condition in terms of piston stroke, displacer stroke, and displacer phase angle as predicted by linear (1st) and nonlinear (Tr) analyses. Good agreement is seen at the 95°F condition; however, the nonlinear analysis predicts a slightly different operating point at the 80, 47, and 17°F conditions. To explain this variation, the 95 and 47°F conditions were examined in detail.

TABLE 3-8
STABILITY ANALYSIS RESULTS

	95°F			80°F			47°F			17°F		
	1st	Tr	Δ(%)	1st	Tr	Δ(%)	1st	Tr	Δ(%)	1st	Tr	Δ(%)
X_p	9.53	9.53	0	5.118	5.91	15	5.75	6.01	4.5	11.38	12.1	6.3
X_d	10.42	10.2	-2.1	3.872	4.42	14	2.95	3.26	11	9.32	9.9	7.0
ϕ_d	69.3	69.5	0.3	59.9	81.0	35	62.4	72.7	17	51.3	64.4	26

Figure 3-3 shows engine/compressor normalized power versus normalized piston stroke (normalizing values are those predicted by the linear analysis). As can be seen, these curves intersect at the nominal operating point, which is stable because the compressor curve cuts the engine curve from below, i.e., for a small perturbation that reduces the piston stroke, the engine produces more power than the compressor consumes. This excess power increases the system's energy by increasing stroke back to the stable operating point. Similarly, for a small increase in stroke, the compressor draws more power than the engine produces, resulting in a stroke reduction back to the stable operating point.

Figure 3-4 shows the engine/compressor normalized power versus normalized stroke for the 47°F point. The nonlinearity of the compressor causes two solutions, as indicated by the double intersection - the lower point is unstable, while the upper is stable, for the same reasons as described above.

Conclusions - Stability of the engine/compressor system was evaluated using both linear and nonlinear system models. Both analyses indicate stable system operation at each of the four operating points. The nonlinear analysis predicted a slightly different dynamic operating condition than did the linear analysis for the 80, 47, and 17°F operating conditions.

3.3 Component Development and Breadboard Demonstration

Component development has dealt primarily with the development of the compressor and hydraulic transmission. No engine development has been conducted under this program; however, one exception is an interface analysis that was performed on the primary EM engine heater head to ensure that it met or exceeded the HAHP requirements. Component development tasks have included:

- Interface Analysis of the EM Engine Heater Head
  - Performance
  - Manufacturability
- Compressor Development
  - Valve Analyses
  - Compressor Seal Development
  - Cylinder Head Thermal/Structural Analyses

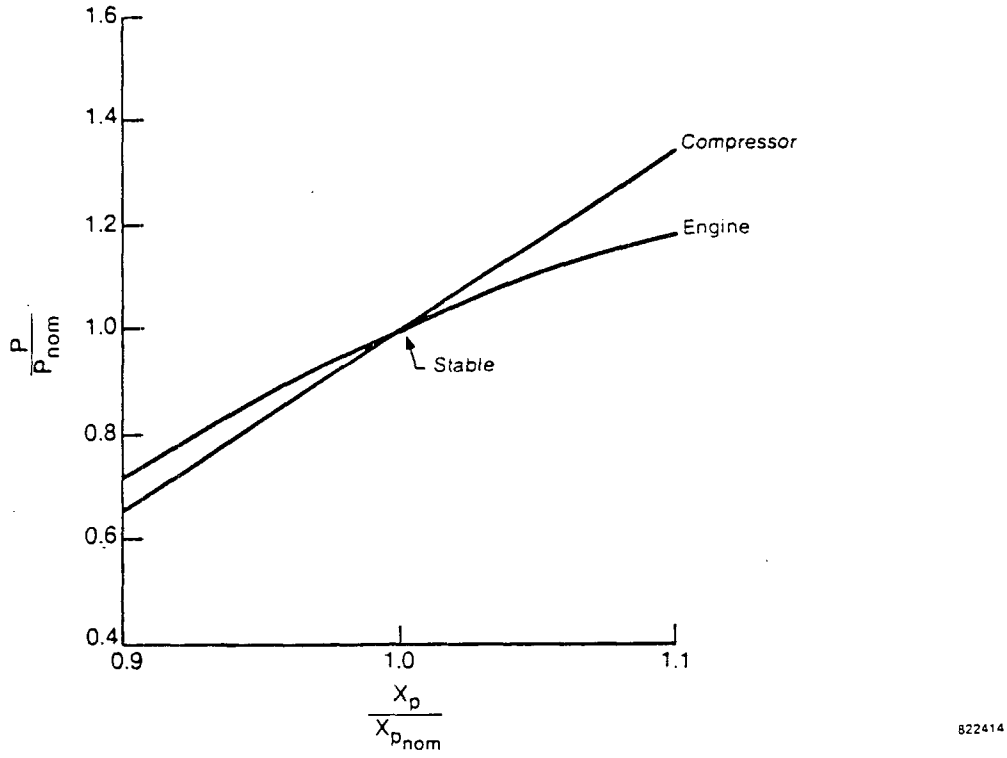

Figure 3-3 Engine/Compressor Power Versus Piston Stroke (95°F)

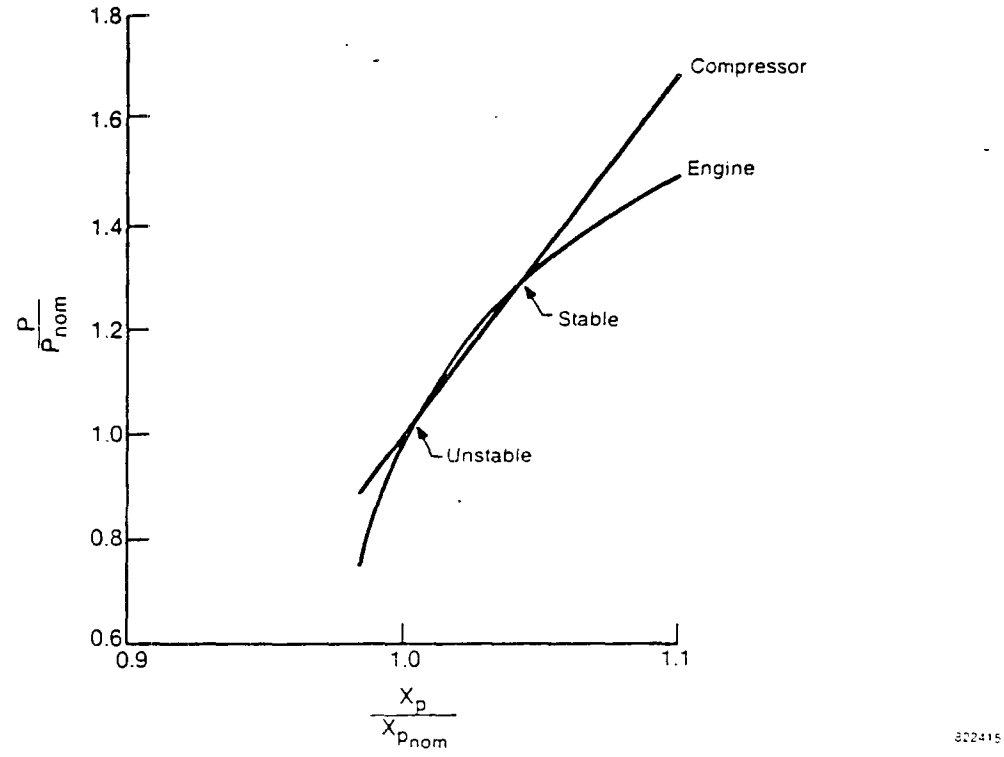

Figure 3-4 Engine/Compressor Power Versus Piston Stroke (47°F)

- Hydraulic Transmission Development
  - Diaphragm Life Characteristics
  - Hydraulic Loss Characterization
  - Freon in Oil Solubility Effects
  - Oil Management Techniques
  - Gas Spring Thermal Losses

3.3.1 Heater Head Analysis

The primary EM engine heater head (shown in Figure 2-3) is defined as a monolithic design of Inconel 713LC. The computed heater head efficiency for the head at the 95°F operating point is 93%, leading to an overall external heat system efficiency (combustor and heater head) of 86% based on lower heating value of the fuel.

Discussions on the manufacturability of the heater head have been held with Gray-Syracuse (prime casting vendor) as to the castability and cost of the head. These discussions allowed Gray-Syracuse to comment on the manufacturability of the head and make suggestions for improving delivery time. As a result of these discussions, a castable head is now possible for the HAHP engine, saving both time and money on the program.

3.3.2 Interim Engineering Model Engine Verification Testing

A critical milestone of this program successfully achieved during the first year was verification testing of the interim EM FPSE. The purpose of this testing was to:

- establish the functionality of the EM engine with the new displacer control feature; and,
- verify the accuracy of the MTI first-order design codes.

The engine was designated "interim" because it consisted of the heater head from a previously designed FPSE, and a 1-kW electric alternator load. The head and load limit the interim engine's operation to 45 Hz and 1-kW electrical power output; specifications for the EM are 60 Hz and 3.0-kW electrical power output.

The results of the verification testing are given in Table 3-9. The procedure for verification was to provide the ORNL Technical Program Manager (TPM) with calculated engine operating characteristics at the design point and three off-design points. The columns labeled "calculated" represent the data given to the TPM prior to engine testing. After testing, the data labeled "measured" was added to the table, and the comparison was made between measured and predicted data. Figures 3-5 and 3-6 present the same data in graphical form. This testing verified the validity of the MTI Stirling-engine computer codes.

TABLE 3-9

HAHP VERIFICATION TEST POINTS

(Nominal Design Points)

Gas: Helium

	Test Pt. 1		Test Pt. 2		Test Pt. 3		Test Pt. 4		Base Test Pt.	
	Meas.	Calc.	Meas.	Calc.	Meas.	Calc.	Meas.	Calc.	Meas.	Calc.
Pressure (Bar)	40	40	40	40	40	40	40	40	40	-
Frequency (Hz)	50	50	50	50	50	50	50	50	50.12	-
Piston Amp. (mm)	12.78	12.7	7.047	7.0	8.498	8.5	10.07	10.0	8.108	-
Heater Temp (°C)	640	600	588	600	625	600	614	600	390	-
Displacer Amp. (mm)	7.34	7.953	4.36	3.97	4.98	4.92	5.99	5.93	6.53	6.45
Displacer Phase (°)	61.76	65.10	49.54	59.45	53.9	60.72	52.3	62.34	79.76	79.81
Net Piston Power (W)	1724	1751.0	533	531.8	810	784.2	1049	1085.4	808.5	807.0
Data File I.D. #	2153		2142		2144		2146		2149	

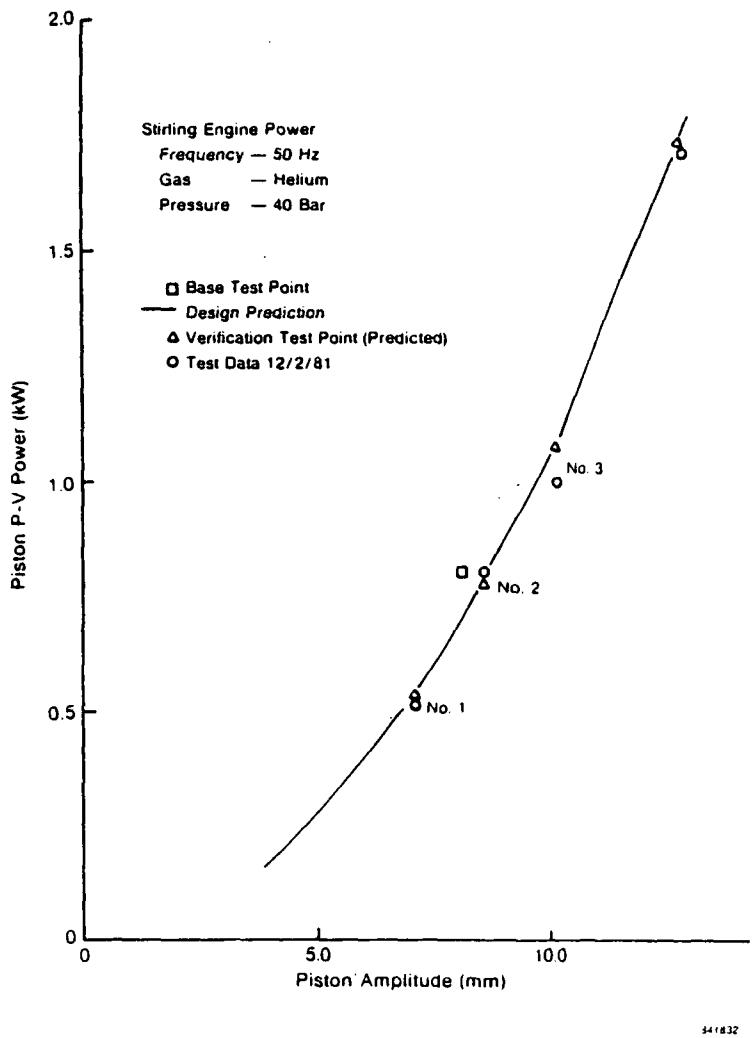

Figure 3-5 HAHP Verification Test - Power Versus Piston Stroke

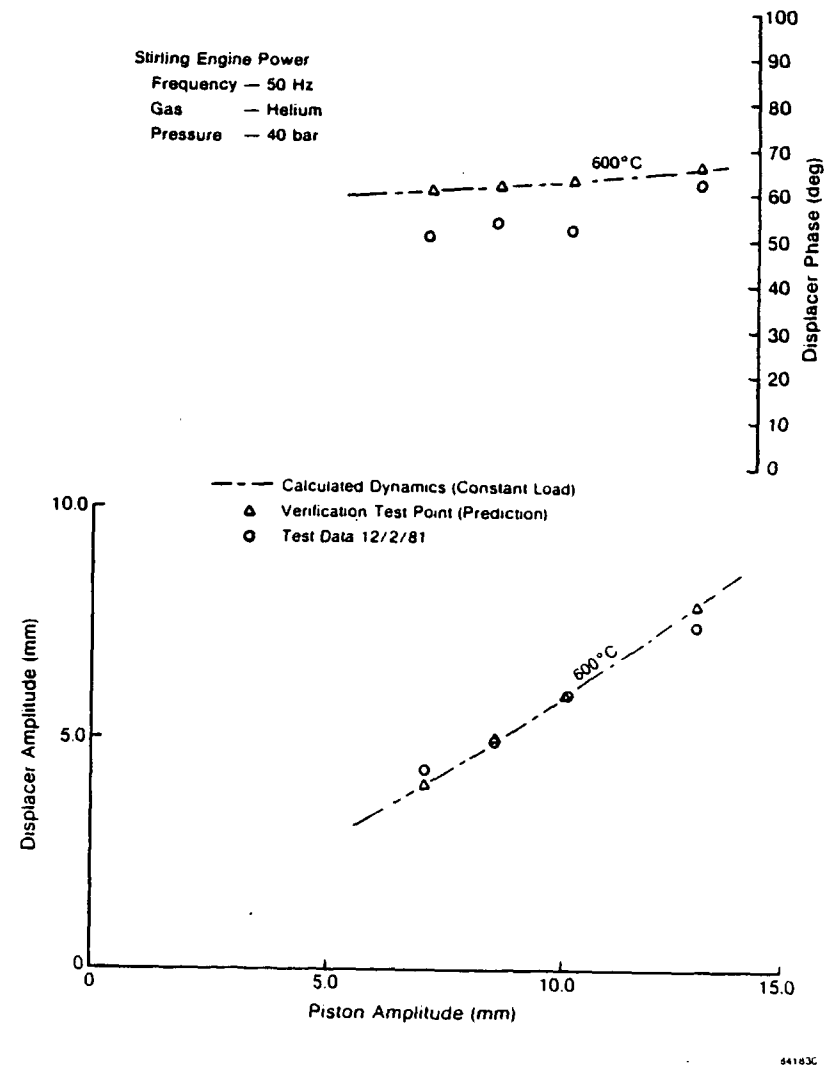

Figure 3-6 HAHP Verification Test - Dynamic Response Versus Piston Stroke

3.3.3 Compressor Development

The refrigerant compressor was designed to meet the HAHP operating requirements at the four designated ARI operating points. Table 3-10 defines the four operating points and gives the compressor characteristics at each of these points.

TABLE 3-10

BREADBOARD COMPRESSOR SPECIFICATIONS

(Based on R-22, 20°F S.H., 15°F S.C.) and He Stirling Fluid

Description	95°F	80°F	47°F	17°F
Heating/Cooling Load (Btu/hr)	-36,000	-18,000	+14,000	+38,000
Suction Pressure (psia)	90.7	111.3	83.4	42.2
Discharge Pressure (psia)	277.4	193.6	188.8	264.4
Evaporator Temperature (F)	45.0	57.3	40.1	4.2
Condensor Temperature (F)	120.8	93.9	92.2	117.0
Refrigerant Flow Rate (lb/hr)	570	230.6	110.4	290.6
Compressor Adiabatic Power (kW)	2.001	0.391	0.280	1.725
Actual Compressor Power (kW)	2.405	0.473	0.318	2.020
Operating Frequency (Hz)	60.00	60.00	60.00	60.00
Compressor Efficiency (%)*	83.20	82.70	88.00	85.40
Hydraulic Transmission Efficiency (%)	82.70	75.80	62.70	74.50
Engine Power (kW)	2.907	0.624	0.507	2.712

*Isentropic

The compressor design (shown in Figure 2-6) refers to the compressor piston, the piston cylinders, the valve assemblies, the cylinder heads, and the main piston shaft seals. Comprehensive analayses were conducted to optimize the most critical of these components; a discussion of the results follows.

3.3.3.1 Valve Design and Analysis - Valve analyses were performed for both ring- and reed-type compressor valves using the MTI valve dynamic computer codes. In each design, the valves were designed for optimum performance over the full HAHP operating range; this means trading off the valve dynamics and performance at each operating point to achieve best operation over the full

range. (Figures 2-7 and 2-8 illustrate the configuration arrived at for the reed and ring valves, respectively.) Because of their annular shape, the ring valves better utilize the available compressor head area, providing greater flow area and, hence, lower pressure drop. The greater flow area also leads to a reduction in gas and valve tip velocities, and less delay in closing of the valve, which translates into a significant reduction in compressor backflow. A discussion of the valve analysis and results follows.

MTI has engaged in the task of performing parametric studies for dynamic performance of compressor valves, and using these to generate designs of reed and ring valves for the proposed HAHP compressor. Since that time, the nominal design stroke of the compressor was reduced (with a corresponding increase in piston area in order to maintain flow), requiring that the valves be redesigned. Drawing from the body of knowledge acquired earlier, a new valve design appropriate to current HAHP compressor requirements was developed.

Approach - The first aproach to producing a new design was to take the better of the two existing ones, in this case the ring valves, and scale it up to fit the new cylinder bore. This was found to be a satisfactory starting point; refinement was carried on from there.

Design Considerations - In producing a design for compressor valves, the engineer must consider many aspects such as valve tip velocity or late closing, and a compromise must be struck within the limitations of physical constraints such as material stress limits and geometry. A listing of the variables taken into consideration appears in Table 3-11. Since the number of variables is large, and functions are often far from linear, an exhaustive study to find the optimum combination of design elements would be impractical even with modern computer techniques; therefore, by using the parametric studies as a guide, and using engineering judgment, a satisfactory design expected to closely approach the optimum can be produced.

Table 3-12 lists the undesirable and desirable traits that would not have been possible, or as great, without the tradeoff. As can be seen from the table, the 95 and 47°F conditions have been favored. The 95°F condition represents the design point, and is also the high-power point, while of the other three conditions, the 47°F condition comprises the greatest percentage of operating time

TABLE 3-11

VARIABLES EXAMINED FOR PARAMETRIC ANALYSES FOR HAHP COMPRESSOR VALVES

INDEPENDENT VARIABLES

Clearance Volume Ratio
Ratio of Suction Port Area to Discharge Port Area
Suction Plenum Volume
Discharge Plenum Volume
Suction Supply Pipe Diameter
Discharge Pipe Diameter

For Reed Valves:	For Ring Valves:
Valve Preload	Valve Preload
Valve Thickness	Valve Stiffness
Valve Length	Valve Mass
Valve Lift Limit	Valve Lift Limit
Valve Port Area	Valve Port Area
Number of Valves	Natural Frequency
Natural Frequency	

DEPENDENT VARIABLES

Peak Gas Velocity through Valve
Peak Valve Tip or Edge Velocity at Closure
Valve Closure Time Delay After Dead Center
Mass Flow Capacity
Backflow Rate
Pressure Loss
Volumetric Efficiency
Power Loss

TABLE 3-12

HAHP COMPRESSOR VALVE DESIGN TRADEOFFS AT CONDITIONS REPRESENTING HEAT PUMP AMBIENTS (°F)

Undesirable Traits	which were taken with these	Desirable Traits
High Valve Tip Velocities (Suction, 47°) (Disch, 80°)		Low Valve Tip Velocities (Suction, 95°, 80°, '7°) (Disch, 47°)
High Backflow (Suction, 80°, 17°) (Disch, 80°)		Zero Backflow (Suction, 95°) (Disch, 95°, 47°, 17°)
Late Valve Closure (Suction, 80°, 17°) (Disch, 80°)		Small Valve Closure Delay (Suction, 95°) (Disch, 95°, 47°, 17°)
High Average ΔP (Suction, None) (Disch. 17°)		Low Average ΔP (Suction, 47°, 17°) (Disch, 47°)
Multiple Openings/Closings (Suction, 80°, 17°) (Disch, 80°)		One Opening/Closing (Suction, 95°, 47°) (Disch, 95°, 47°, 17°)

over the seasons. It should be noted that backflow and valve ΔP have a direct bearing on the efficiency of the heat pump, while the other aspects generally concern longevity of the valves, which is not absolutely critical to the operation of the breadboard system for which these valves have been designed. Therefore, some degree of preference was given to maximizing efficiency at some loss in valve longevity; however, the calculated stresses in the valves and springs fall well below that required for so-called infinite life.

Summary - An optimized valve design has been arrived at using a sound engineering approach. The valves will be quite suitable for the breadboard system application, and preference has been given to good efficiency at the design point without causing unmanageable problems at other operating conditions. A layout of the valve and valve plate assembly is given in Figure 3-7.

3.3.3.2 Compressor Seal Development - Both chevron and pumping ring seal designs were analyzed for the main shaft seal on the compressor. This seal is important because it must isolate the high-pressure oil in volumes C and D (Figure 2-7) from the freon at suction pressure in volume F. A chevron seal was considered because it is a commonly used seal for this application, and its characteristics are well understood. The pumping ring seal was also considered because it has the potential for reducing oil leakage and power dissipation by the seal. Figure 3-8 is a layout drawing of the pumping ring seal. The operation of the seal is such that as the compressor piston shaft moves to the right, oil under the seal relief area is compressed, and once it exceeds the pressure on the o-ring (P_{ring}), the pumping ring lifts, and oil flows into the high-pressure cavities. As the piston moves to the left, pressure reduces in the ring clearance, and the ring seals back against the shaft, allowing a fresh supply of oil to fill the clearance. The pumping characteristic of the seal is shown in Figure 3-9, where the pumping ring was measured to pump up to a pressure differential of 850 psi, with flows of the order of 3 or 4 g/min. across a pressure differential of 800 psi.

Results of the seal analyses, given in Tables 3-13 and 3-14 for the chevron and pumping ring seals, respectively, show that these seals have the potential of providing an effective seal with low power losses. The cold-start analysis for 17°F, however, indicates that considerable power is required to overcome the

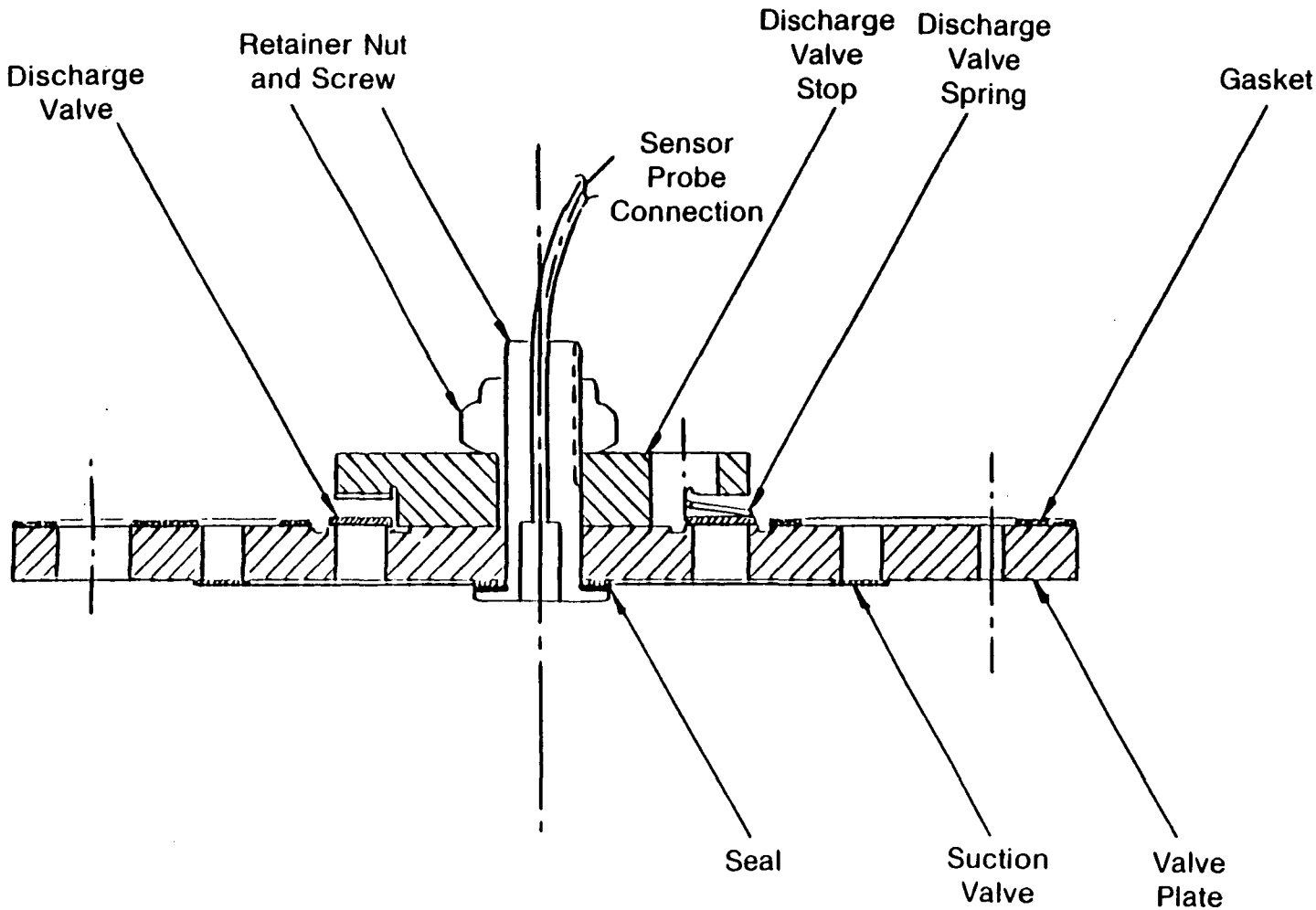

Figure 3-7 Suction/Discharge Valve Plate Assembly

841839

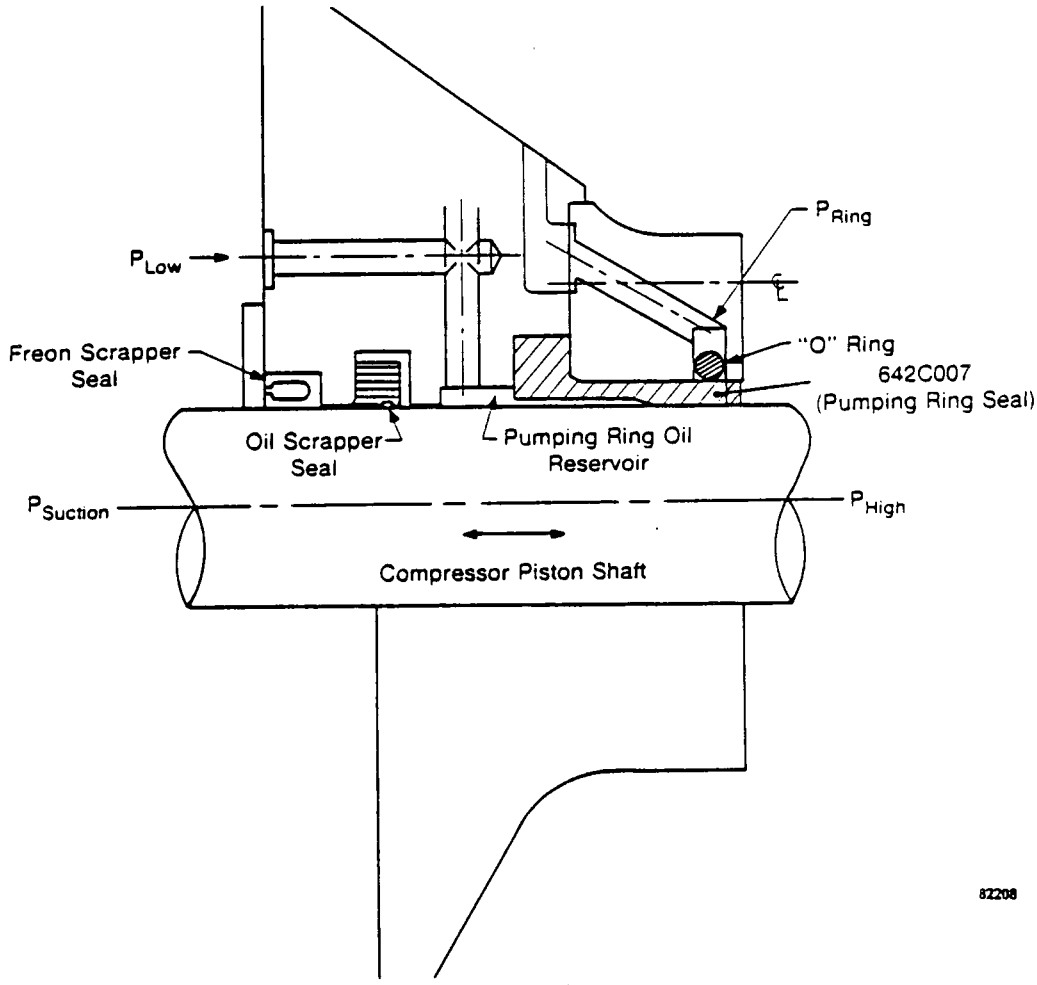

Figure 3-8 Pumping Ring Seal Layout

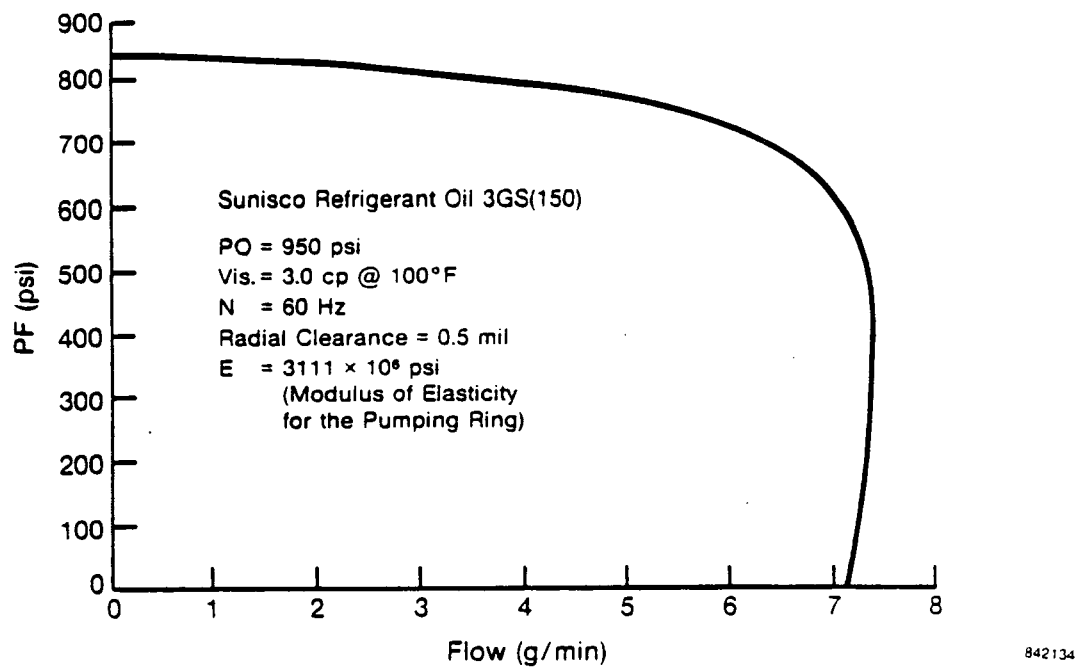

Figure 3-9 Pumping Seal Flow and Pressure Relation

TABLE 3-13

CALCULATED CHEVRON SEAL PERFORMANCE - SUMMARY

°F	CHEVRONS															PISTON RING							TOTALS		
	lbs.			in./s		lbs/s	in.	lbs.	Watts			cc/min.				lbs.		Watts			cc/min.		Watts	cc/min.	
Cond. Day	F_{f1}	F_{f2}	ΣF_f	V	f	μ	h	F_s	W_f	W_s	ΣW	Q_s *	Q_{p1} †	Q_{p2} †	ΣQ	F_f	F_s	W_f	W_s	ΣW	Q_s *	Q_p	ΣW**	ΣQ_{p1}	ΣQ_{p2}
95 (140°Oil)	205	59.7	265	90.0	.017	4.35	50	0.69	46.0	7.0	92.0	5.2	.20	.06	N/A	27.33	0.23	5.00	2.30	10	5.2	-	102	.40	.120
47 (90° Oil)	219	36.0	255	51.8	.017	11.60	50	0.90	25.9	5.1	50.8	3.0	.10	.02	N/A	15.6	0.30	1.55	1.70	3.4	3.0	-	54.2	.20	.020
17 (Normal 100° Oil)	212	70.0	282	104	.017	7.80	50	1.40	56.0	16.9	112	6.0	.11	.03	N/A	32.7	0.48	6.50	5.60	13	6.0	-	125	.22	.040
17 (Cold-Start 17° Oil)	212	70.0	282	104	.017	58.00	50	10.70	56.0	125	250	6.0	.01	.004	N/A	32.7	3.55	6.50	42.0	84	6.0	-	334	.02	.008

*Shear flow shuttles in both directions - net effect should be zero, providing no "pumping ring" phenomenon is present.
†Pressure-induced leakage - always from oil chamber to intermediate vent between chevrons; thus, $\Sigma Q_p = 2 Q_{p1} - Q_{p2}$ is the leakage from the intermediate chamber to vent area.
**Based on larger of the shear or pressure load losses.

NOMENCLATURE

F_{f1} - First chevron seal normal force
F_{f2} - Second chevron seal normal force
V - Shaft velocity
f - Seal coefficient of friction
μ - Oil viscosity
h - Radial clearance
F_s - Total seal friction force
W_f - Seal friction power dissipation
W_s - Seal shear power dissipation
Q_s - Shear leakage
Q_p - Pressure leakage

TABLE 3-14

CALCULATED PUMPING RING SEAL PERFORMANCE - SUMMARY

°F Cond. Day	PUMPING RING											PISTON RING								BALANCE SEAL			TOTALS		
	mils	lbs/s	in.	in/s		lbs.		Watts		cc/min.		lbs.			Watts			cc/min.		lbs.	Watts		Watts	cc/min.	
	C	μ	δ	V	f	F_f	F_s	W_f	W_s	Q_p †	Q_s †	F_p	F_s	f	W_p	W_s	ΣW_{p1R}	Q_p	Q_s	F_p	W	ΣW	ΣW††	ΣQ_p *	ΣQ_p **
95 (140° Oil)	0.5	4.35	0.1	90	.05	2.40	0.25	24	2.50	0 - 6.4	5.2	4.70	.040	.017	.46	--	0.92	10.5	5.2	1.0	10.0	20.0	69.5	0 - 6.4	10.5
47 (90° Oil)	0.5 0.4	11.6 11.6	130 184	51.8 51.8	.05 .05	3.08 5.86	0.42 0.53	18 34	5.85 7.32	0 - 3	5.2 4.2	6.25 6.25	.060 .070	.017 .017	.62 .78	--	1.20 1.60	5.5 2.8	5.2 4.2	1.0 1.0	6.0 6.0	12.0 12.0	37.0 55.0	0 - 3	5.5 2.8
17 (100° Oil)	0.5 0.4	7.8 7.8	130 184	104 104	.05 .05	3.08 5.86	0.57 0.71	36 69	6.7 8.4	0 - 9	6.0 4.8	16.0 16.0	.076 .095	.017 .017	3.2 4.0	-- --	6.40 8.00	19.7 38.7	6.0 4.8	1.0 1.0	12.7 12.7	25.4 25.4	74.5 110.8	0 - 9	19.7 38.7
17 (17° Oil)	0.5 0.4	58.0 58.0	130 184	104 104	.05 .05	3.08 5.86	4.26 5.32	36 69	86.1 131.5	30-35	6.0 4.8	16.0 16.0	.570 .710	.017 .017	3.2 4.0	-- --	6.40 8.00	2.8 1.4	6.0 4.8	1.0 1.0	12.7 12.7	25.4 25.4	154.0 234.0	30-35	2.8 1.4

*Discharge into balance piston cavity.
**Discharge into vent.
†Shuttles back and forth across piston ring and balance seal.
††Total watts - both sides.

NOMENCLATURE

F_{f1} - First chevron seal normal force
F_{f2} - Second chevron seal normal force
V - Shaft velocity
f - Seal coefficient of friction
μ - Oil viscosity
h - Radial clearance
F_s - Total seal friction force
W_f - Seal friction power dissipation
W_s - Seal shear power dissipation
Q_s - Shear leakage
Q_p - Pressure leakage

seal drag and viscous losses in the hydraulic transmission under cold-start conditions.

3.3.3.3 Cylinder Head Thermal and Structural Analysis - Both stress and heat transfer characteristics of the compressor cylinder heads were considered. Stress characteristics were based on the maximum discharge and minimum suction pressure the head would see, and the maximum thermal gradient that might exist between the suction and discharge plenums. A sketch of the head is given in Figure 3-10. The gas center plenum contains the hot, high-pressure discharge gas; the outer plenum (positioned circumferentially around the head) contains the cool suction vapor. The three areas of stress concern were located at points "A," "B," and "C." The results of the stress analysis are as follows (ref. attached sketch for dims. and location at chambers A, B, and C):

1. Hoop stress: $\sigma_h = pd/2t$;

   A $\sigma_h = 277(2.38)/2(.19) = 1735$ psi*;

   B $\sigma_h = (277 - 42)(1.70)/(1.95 - 1.70) = 1598$ psi; and,

   C $\sigma_h = 111(3.59)/(3.97 - 3.59) = 1049$ psi;

   where, p = pressure, d = diameter, and t = wall thickness.

2. Approximate discontinuity stress at head-cylinder junction of chamber A (ref. Timoshenke, Theory of Plates & Sheels, p. 410):

   Axial stress (assume head is ~ an ellipse with a/b = 2):

   $$(\sigma_x)_{max} = 2.172\ pa/2t \simeq 2.172\ 277(1.19)/2(.19) = 1884 \text{ psi.}$$

   Tangential stress (bending and membrane):

   $$(\sigma_t)_{max} = 1.128\ pa/t = 1.128\ 277(1.19)/.19 = 1957 \text{ psi.}$$

3. Shear in bolt boss web (section W-W):

---

*277 psi is used for laboratory operation.

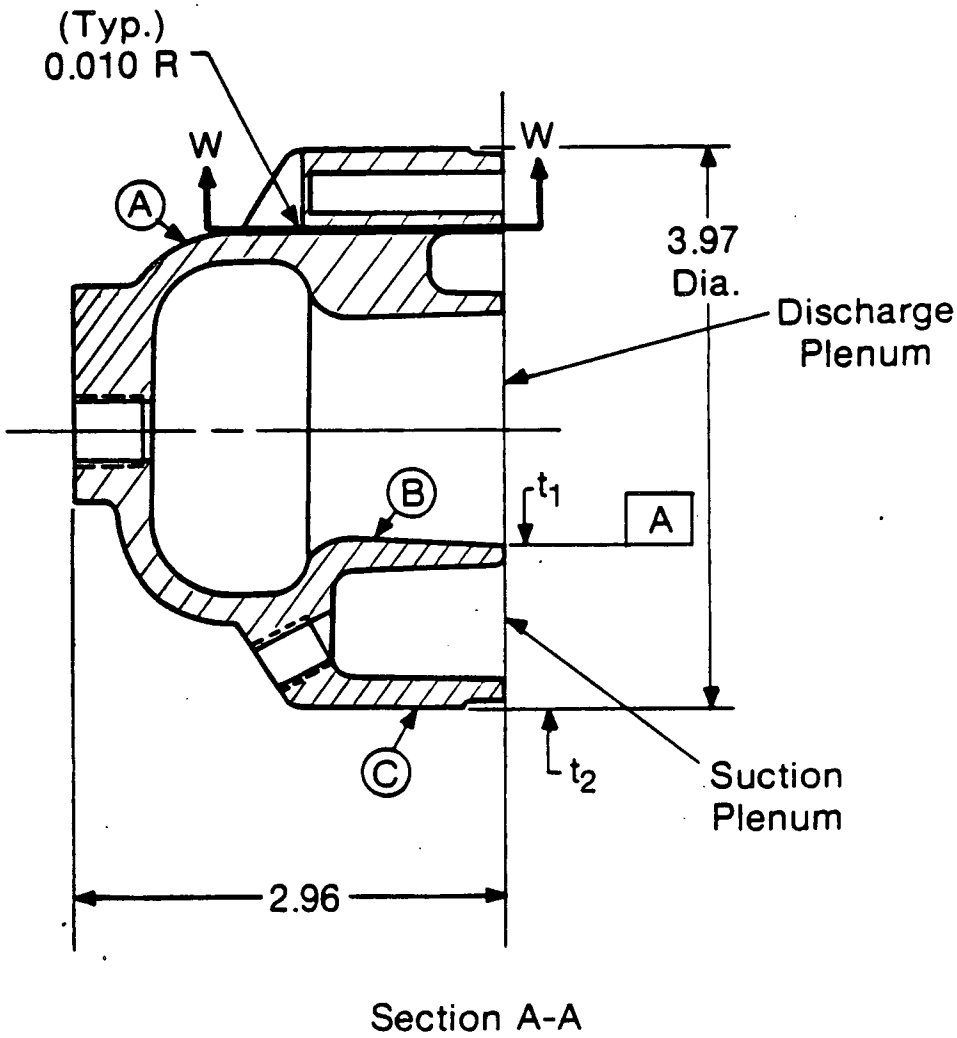

Figure 3-10 Compressor Cylinder Head

842131

Web area = .88 x .12 = .1056 in.^{2}.

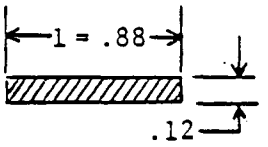

Blowoff load:

$$F = (1.70)^2(277) + \pi/4\ (3.59^2 - 1.95^2)(111) = 1420 \text{ lbs.}$$

Assuming blowoff force is carried entirely in shear in bolt boss webs, web shear stress is (8 webs):

$$\tau = F/8A = 1420/8(.1056) = 1681 \text{ psi.}$$

4. Thermal Stress at (B): A thermal stress will exist in any wall that sees suction gas on one side and discharge gas on the other. An upper limit of stress can be calculated by assuming that the wall sustains the full ΔT between inlet and discharge (ignores film drops on both sides). By assuming also that thermal distortion of the wall is fully restrained, which is probable for the geometries we are dealing with, maximum thermal stress is given by:

$$(\sigma_{th})_{max} = E\ \alpha\ \Delta T/2(1 - \nu);$$

where, E = elastic modules, 25×10^6 psi;
α = coefficient of thermal expansion, 10×10^{-6} in./in./°F;
ν = Poisson's ratio, 0.3; and,
ΔT = temperature difference between inlet and discharge, 155°.

$$(\sigma_{th})_{max} = (25 \times 10^6)(10 \times 10^{-6})(155)/2(1 - 0.3) = 27{,}700 \text{ psi.}$$

5. Fatigue Analysis - Material: Ductile Iron, Type 65-45-12 (ASTM A 536-80):

Minimum Tensile Strength	65 ksi
Minumum Yield Strength	45 ksi
Estimated Endurance Limit E.L. = .40 x Tensile	26 ksi

Alternating stress (S_a): As an approximate check on fatigue at (A), assume full pressure cycling and apply stress concentration factor of 2.5 to account for casting defects or discontinuities:

at (A), S_a = 2.5 x 1957 x 1/2 = 2450 psi;
at (B), S_a = 2.5 x 1598 x 1/2 = 2000 psi.

Mean stress (S_m): At (A), mean stress equals S_a (one half of zero-to-peak pressure stress):

at (A), S_m = 2450 psi;
at (B), mean stress is $S_a + \sigma_{th}$;
at (B), S_m = 2000 + 27,700 = 29,700 psi.

Plotting these on a Goodman Diagram:

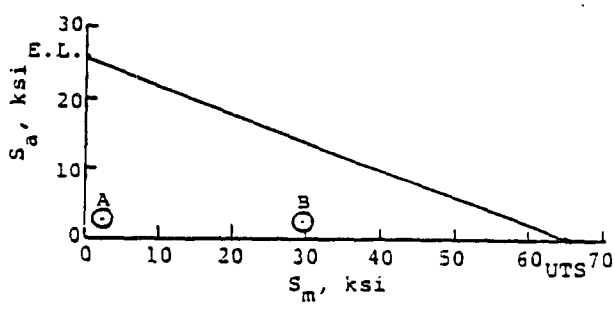

The diagram shows that both points have adequate fatigue margin even with the conservative estimate of thermal stress at (B). Thermal analysis for the head was performed to determine the amount of superheating of the suction gas that would occur from heat transfer between the suction and discharge plenums in the heads. The results indicate that even under the severest conditions of 17°F ambient, superheat increase will be limited to less than 5°F.

3.3.4 Hydraulic Transmission Development

Use of a hydraulic coupling between the engine and compressor has greatly decreased the complexity of a FPSE-driven heat pump; however, its use has introduced other unknowns into the system (diaphragm life and hydraulic power losses) that must be evaluated. A tool, the hydraulic simulator, has been developed at MTI to study hydraulic transmission. This rig (see Figure 3-11) consists of a linear motor mounted between two diaphragms, with the space between the motor plunger and diaphragms filled with a hydraulic oil which, being incompressible, transmits the motor plunger motion to the diaphragm. Gas springs on the outer

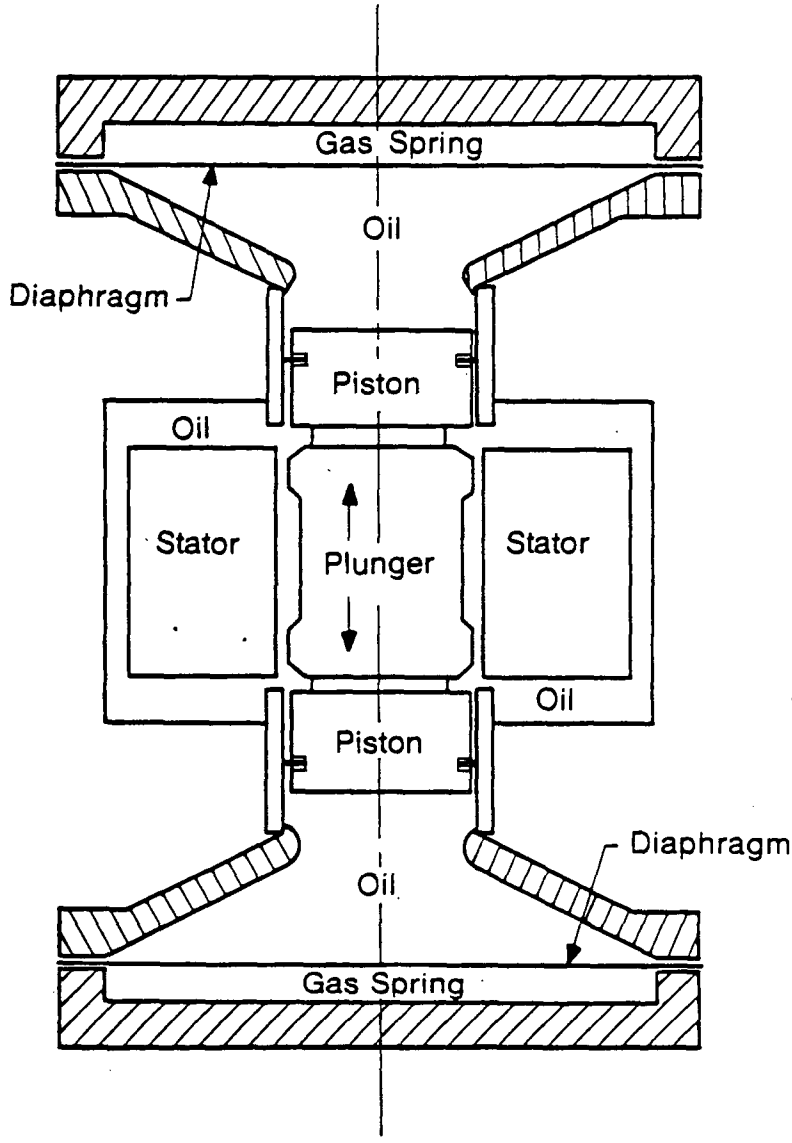

Figure 3-11 Diaphragm-Type Hydraulic Simulator Test Rig

813002

side of each diaphragm produce the resonant dynamics for the system. The purpose of the simulator is to determine the practicability of hydraulically driving a compressor, as well as to evaluate power losses associated with this type of transmission. Test objectives of the rig are to:

- demonstrate continuous, long-term operation of system and diaphragms;
- evaluate the hydraulic transmission losses (oil viscous loss, seal friction, and gas spring thermal hysteresis);
- determine the freon in oil solubility effects; and,
- develop and test an oil management system.

3.3.4.1 Diaphragm Life Testing - A contoured diaphragm (shown in Figure 3-12) was developed with the Bendix Corporation. This configuration was chosen to minimize stress concentrations at the clamped boundary of the diaphragm, and to more uniformily distribute the stress radially across the diaphragm. The Bendix Corporation was helpful in suggesting this configuration from past experience with diaphragm transmission couplings, and has been instrumental in developing the manufacturing techniques to fabricate a pair of diaphragms.

Life tests of the Bendix diaphragms were performed on the hydraulic simulator by simulating heat pump operating conditions. Table 3-15 presents the operating data for a pair of diaphragms. Two tests were run. The first was at a plunger stroke of 8.0 mm (corresponds to $\sim$86°F operating point (cooling service)), and 10.0 mm (corresponds to $\sim$93°F operating point (cooling service)). To date, more than 3×10^7 cycles have been accumulated on each diaphragm with no apparent failure; however, an accident did occur during disassembly of the machine after the 34×10^6 cycles were recorded. The diaphragms were accidently over-pressurized during a shutdown of the simulator, producing a permanent distortion in the diaphragms. The diaphragms were subsequently examined to determine if any signs of fatigue failure were present, or if the failure was due entirely to the accidental over-pressurization.

Careful examination of the diaphragms has not produced any evidence of an apparent fatigue failure or signs of initiation of a fatigue failure. In addition, no fatigue failures have occurred in over 50-million cycles of Breadboard System testing.

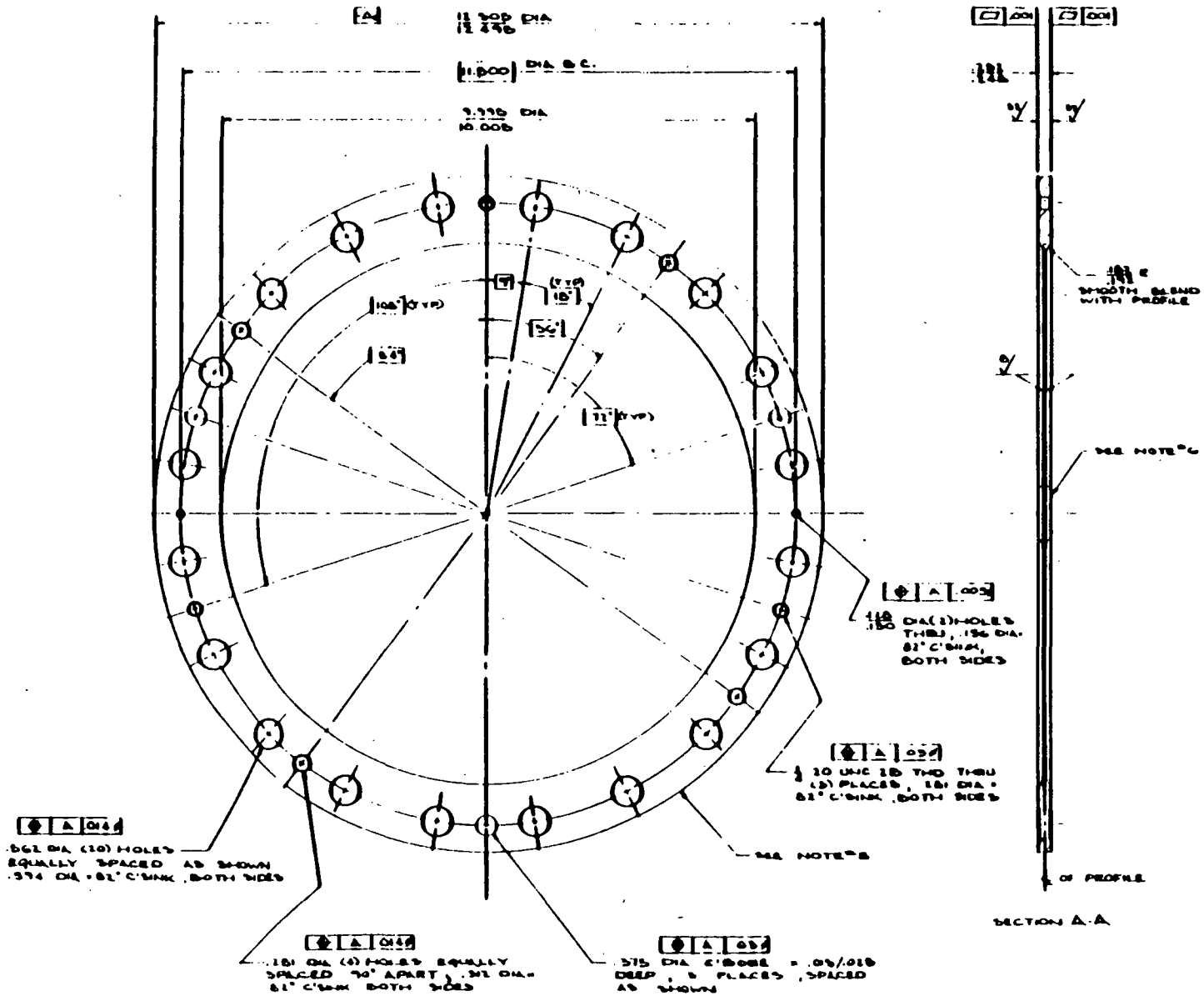

Figure 3-12 Contoured Engine and Gas Spring Diaphragm

TABLE 3-15

DIAPHRAGM LIFE TEST RESULTS

	Heat Pump Operating Data			Hydraulic Simulator Test Data		
Operating Point (°7)	Diaphragm Swept Volume (in^3)	Equivalent Hydraulic Simulator Plunger Stroke (mm)	Diaphragm Stress (psi)	Plunger Stroke (mm)	Run Time (hrs)	Number of Cycles
86.10	2.70	8.00	22,500	8.00	56.50	1.22×10^7
93.00	3.30	10.00	30,000	10.00*	100.90	2.18×10^7
Hydraulic Simulator with Limit Overstroke	3.70 (95°F)	11.10	35,000	-	-	-

*Run 20% of time at overstroke condition.

3.3.4.2 Hydraulic Transmission Losses - The hydraulic transmission losses were characterized by describing a "lower-end" efficiency for the power module. The coupled lower-end efficiency is defined as: $\eta_c = W_{adiabatic}/W_{shaft}$. Hence, η_c is the ratio of the compressor adiabatic, or ideal power (W_{ad}), to the actual engine shaft power requirement (W_{shaft}). The loss analysis included:

- all seal shear and leakage loss (includes the viscous or frictional drag on the seal, the pressure drop leakage loss, and the pumping power to return the leakage to the high-pressure supply plenum);

- oil flow (viscous) loss (includes the power required to overcome the viscous (shear) loss in the oil);

- gas spring thermal hysteresis loss (accounts for the irreversible heat transfer effects in the compressor gas spring);

- compressor, compression piston, seal loss (includes the friction drag loss on the compressor piston sealing rings); and,

- compressor plenum/valve pressure drop losses (includes flow losses in refrigerant circuit resulting from pressure drop across the suction/discharge valves and compressor cylinder head plenums).

A representative drawing of the lower end (shown in Figure 3-13) defines each of the seals contained in the unit, and Table 3-15 gives the operating specifications for each of the seals at the four designated operating points. A description of each of the seals defined in Figure 3-13 follows.

Balance Drive Seal - This seal, located on the outside diameter of the balance-weight, is a close-tolerance seal that prevents oil leakage between volumes A and B. The seal sees the pressure differential ΔP_d given in Table 3-16.

Sleeve Seal - This seal, located on the inside diameter of the four balance-weight arms, is a close-tolerance seal that seals between volumes A and C, and B and D. The seal sees the pressure differential ΔP_{sleeve} given in Table 3-16.

Balance/Piston Seal - This seal, located between the balanceweight and compressor piston, is a close-tolerance seal that prevents leakage between volumes C and D. The seal sees the pressure differential ΔP_o given in Table 3-16.

TABLE 3-16
COMPRESSOR OPERATING CHARACTERISTICS

Design Point (Ambient T)	s (Stroke Amplitude) m (in)	v (Velocity Amplitude) m/s (in/s)	Pvent MPa (psia)	Pdis MPa (psia)	ΔP_o MPa (psi)	ΔP_{sleeve} MPa (psi)	ΔP_d MPa (psi)
95°F	0.019 (0.750)	3.58 (140.9)	0.63 (90.7)	1.91 (277.4)	0.74 (107.3)	0.84 (121.8)	0.94 (13.4)
80°F	0.010 (0.380)	1.84 (72.4)	0.77 (111.3)	1.33 (193.6)	0.42 (60.9)	0.48 (69.6)	0.54 (78.3)
47 °F	0.011 (0.430)	2.07 (81.5)	0.58 (83.4)	1.30 (188.8)	0.48 (69.6)	0.50 (72.5)	0.61 (88.4)
17 °F	0.022 (0.880)	4.15 (163.4)	0.29 (42.2)	1.82 (264.4)	0.95 (137.7)	1.08 (156.6)	1.61 (175.4)

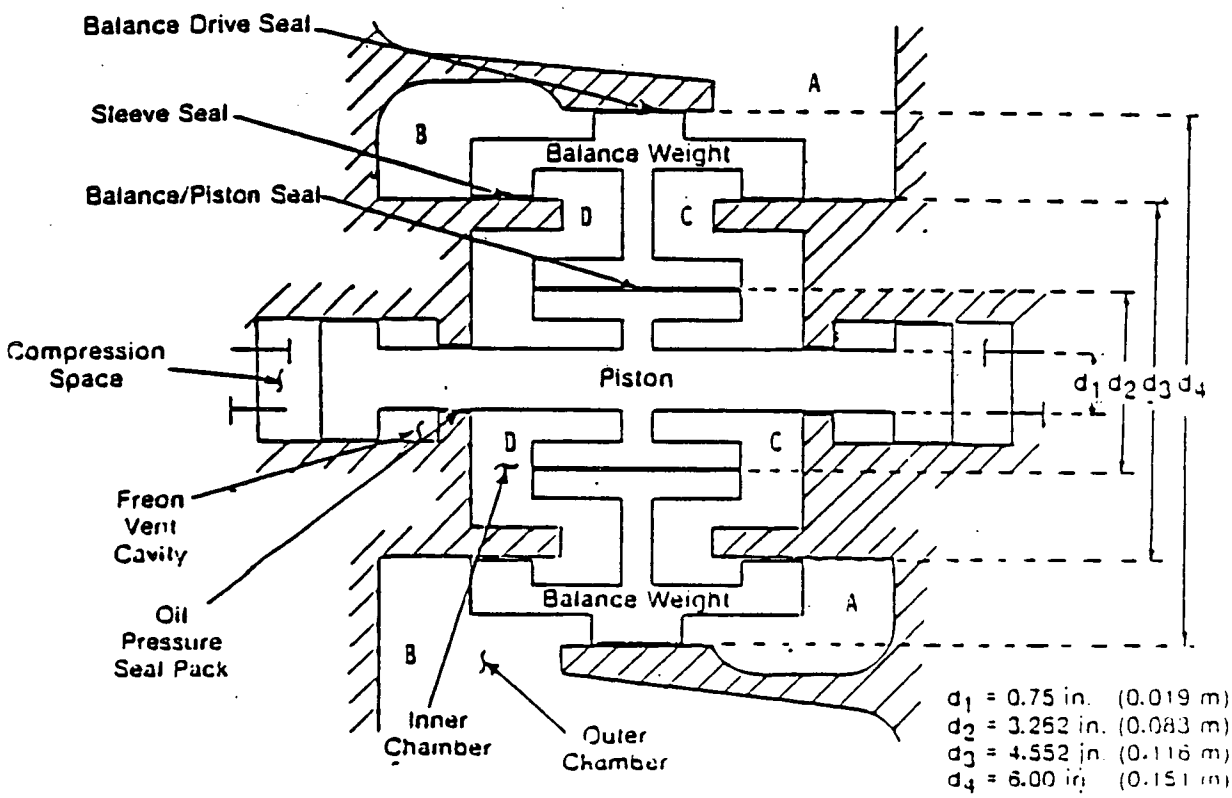

Figure 3-13 Compressor Schematic - HAHP

Nomenclature: p_{vent} = compressor suction pressure contained in refrigerant vent cavity.

p_{dis} = compressor discharge pressure.

Δp_o = pressure swing (twice the amplitude) of oil in two cavities between counterweight and piston.

Δp_{sleeve} = oil pressure amplitude across sleeve seal located at diameter d_3.

Δp_d = oil pressure amplitude across balance weight drive seal located at diameter d_4.

Oil Pressure Seal Pack - This seal, located between the compressor housing and compressor piston, is the major high-pressure seal in the hydraulic transmission, and seals the oil in the transmission from the refrigerant in the Freon vent cavity. The freon vent cavity is maintained at the compressor suction pressure from the suction plenum, and oil leakage past this seal into the vent cavity must be replenished in the transmission, requiring an oil management system.

The procedure used to evaluate the magnitude of these seal losses was to use the hydraulic simulator to provide basic loss data on the oil viscous, seal friction, and gas spring losses in a harmonic system. Referring to Figure 3-11, these three losses are seen to exist in the hydraulic simulator; therefore, by measuring electrical power input to the linear motor (stator/plunger assembly), total system loss is obtained.

Testing to date on the hydraulic simulator has been encouraging in that the total power loss measured is less than originally predicted. Figure 3-14 shows the comparison between the predicted and measured losses. The significance of this is that hydraulic transmission efficiency may exceed 80%, and total "lower-end" efficiency, hydraulic transmission, and compressor (less suction gas superheating) may exceed 70%. An illustration of the calculation for the "lower-end" efficiency is given in Figure 3-15.

A summary of seal and viscous losses calculated for hydraulic transmission is given in Table 3-17. The two numbers given for the oil pressure seal pack and scrapper seals represent losses for the chevron and pumping ring seals, respectively. The scraper seals are also part of the oil pressure seal pack (shown in

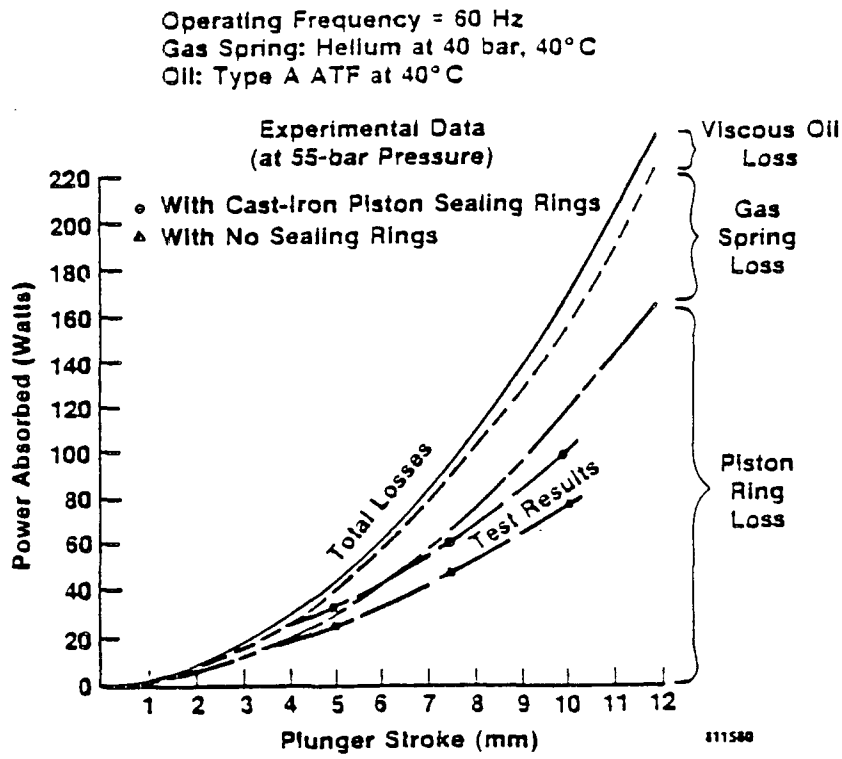

Figure 3-14 Comparison of Predicted and Measured Losses (Results of Testing on Hydraulic Simulator)

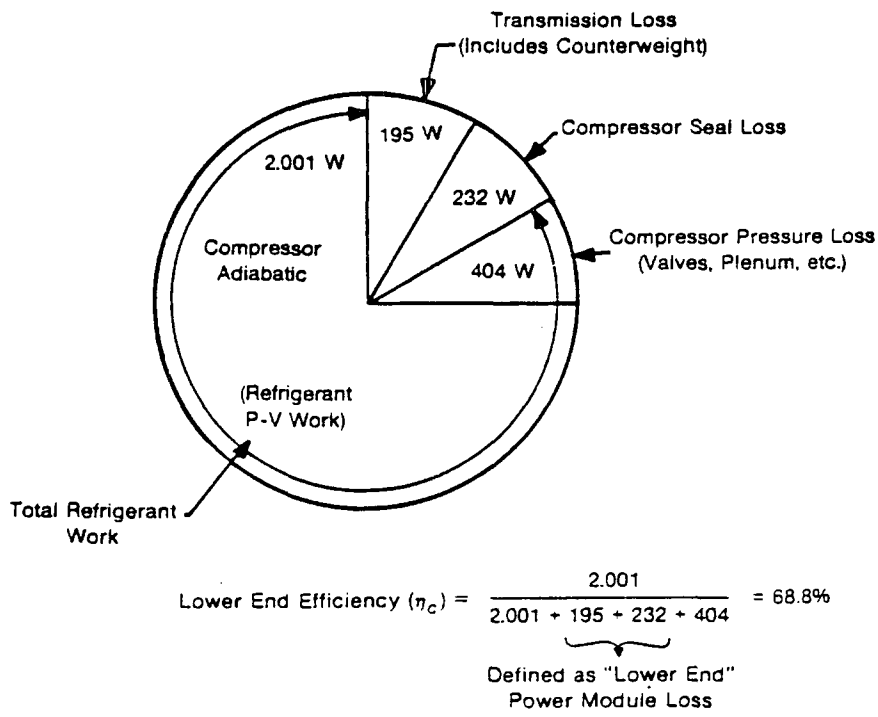

Figure 3-15 Compressor Energy Balance for 95°F Ambient

Figure 3-8). Considering the 95°F values in Table 3-17 and the shaft power required at 95°F (2907 watts) in Table 3-10, hydraulic transmission efficiency with gas spring loss is 82.7%. Total "lower-end" efficiency will be developed in the following material after a discussion of gas spring loss is presented.

TABLE 3-17
HAHP COMPRESSOR DRIVE HYDRAULIC EFFICIENCY SUMMARY
(Predicted Results)

Loss	95° Ambient	80° Ambient	47° Ambient	17° Ambient
Bal/Drive Seal (watts)	42.0	11.0	14.0	72.0
Bal/Piston Seal	32.0	7.7	9.8	59.0
Bal/Sleeve Seals	46.0	13.0	17.0	76.0
Oil Pressure Seal Pack	92.0 (50.0)*	40.0	50.8	112.0
Scrapper Seals	10.0 (20.0)*	2.6	3.4	13.0
Oil Viscous	2.2	0.5	0.7	3.2
Total	224.2 W (192.2)*	74.8 W	95.7 W	335.2 W

*Defines loss for pumping ring seals.

Gas spring loss measurements were performed by comparing total hydraulic simulator input power with N_2 and He in the gas springs. Gas spring configurations on the hydraulic simulator are shown in Figure 3-11. Because the gas springs are hermetically sealed, they may be run with either N_2 or He; the only system thermodynamic change will occur in the resulting thermal hysteresis loss, which will manifest itself in a change in required input drive power.

Tests were run for the following conditions:

Operating Parameter		N_2	He
• Frequency	Hz	60	60
• Gas Spring Pressure	Bar (psia)	58 (870)	52 (780)
• Temperature	°C (°F)	25 (77)	25 (77)
• Piston Strokes	mm	5,7.5,10	5,7.5,10
	(in)	(.2,.3,.4)	(.2,.3,.4)
• $\Delta V/V_o$ @ 10-mm Stroke		0.054	0.054
• A_o, Wetted Surface Area	cm^2 (in^2)	0.77 (0.12)	0.77 (0.12)
• Calculated Hysteresis Loss @ 10 mm	watts	18.3	68.1

The test procedure used was to measure the electrical input power to drive the hydraulic simulator at piston strokes of 5, 7.5, and 10 mm (corresponds to ($\Delta V/V_o$'s of .027, .036, and .054). The procedure was followed for both N_2 and He gas springs. Tests were run over a two-week period in November, 1981; over 125 data points were taken. Measured results were then compared to predictions made by MTI's gas spring thermal hysteresis model. The comparison was made by completing the loss ratio Q_{He}/Q_{N2} = Thermal Loss with Helium/Thermal Loss with Nitrogen = 3.66, and comparing it to the measured ratio. The results, shown in Figure 3-16 and Table 3-18, indicate that a difference exists between the predicted and measured results; for this type of gas spring, the loss is ~70% of the predicted value.

Total lower-end efficiency (including gas spring loss calculated from the MTI expression), compressor seal loss, hydraulic transmission losses with Chevron seals, and compressor adiabatic efficiency (which accounts for refrigerant flow losses in the compressor) are given in Table 3-19. Lower-end overall efficiency ranges from a maximum of 68.1% at 95°F ambient to 55.2% at 47°F ambient. Comparing lower-end efficiency to a conventional electric-driven refrigerant compressor's can efficiency* demonstrates the potential for high efficiency that this approach affords.

---

*Can efficiency is defined as the refrigerant mass flow times the enthalpy change of the refrigerant during the compressor process divided by the electric power into the motor.

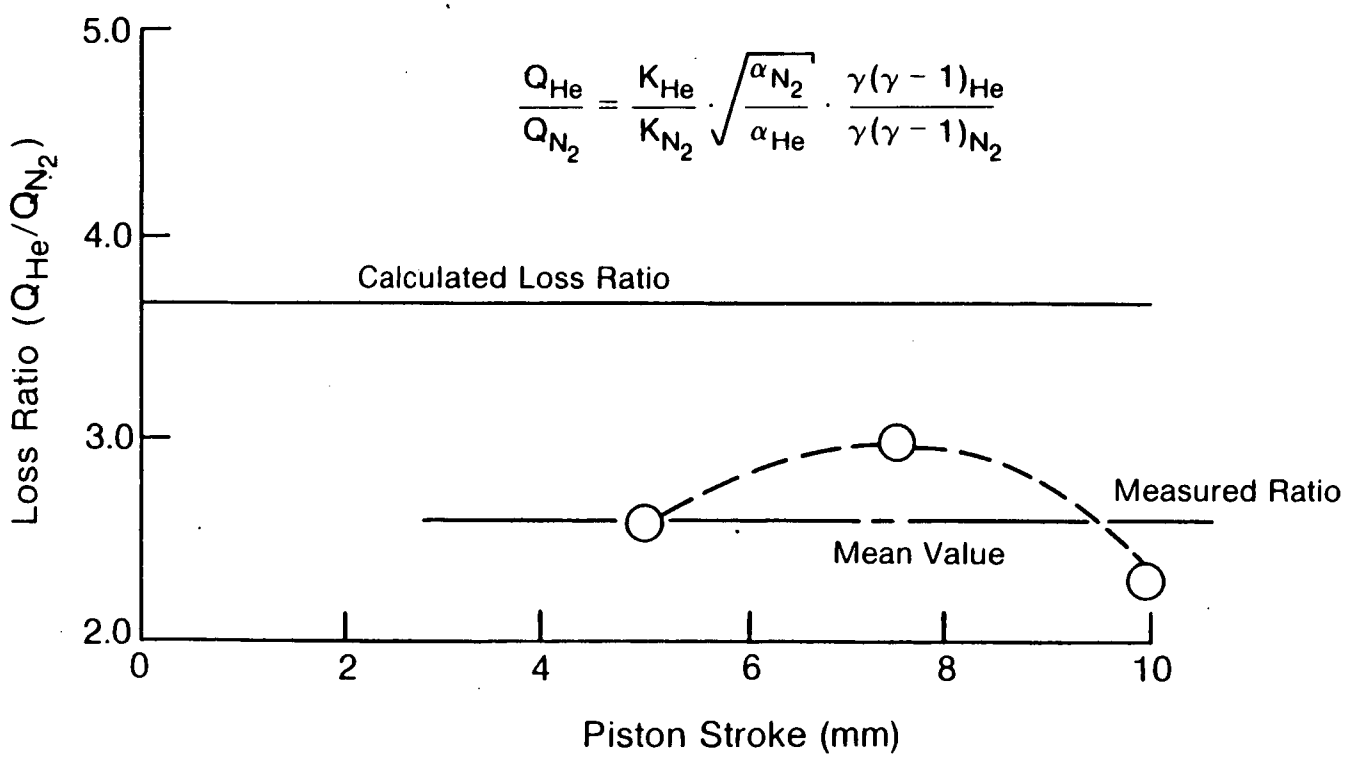

Figure 3-16 Comparison of Predicted and Measured Gas Spring Thermal Hysteresis Losses for Nitrogen and Helium on the Hydraulic Simulator

82207

TABLE 3-18
MEASURED GAS SPRING RESULTS

Stroke	5.0 mm		7.5 mm		10.0 mm	
$\Delta V/V_o$	0.027		0.036		0.054	
	N_2	He	N_2	He	N_2	He
Mean Input Power (Watts)	55.21	62.40	106.63	122.77	172.76	196.19
Standard Deviation (Watts)	6.51	7.47	7.68	13.32	10.10	15.02
$(P_{He} - P_{N2})$ (Watts)[1]	7.19		16.14		23.43	
(Q_{He}/Q_{N2}) (Watts)[2]	2.57		2.98		2.28	

[1]Denotes total input power.

[2]Denotes thermal hysteresis loss.

$$\text{Where: } (P_{He} - P_{N2}) = (Q_{He} - Q_{N2}) = Q_{N2}(Q_{He}/Q_{N2} - 1)$$
$$\bullet\ Q_{He}/Q_{N2} = (P_{He} - P_{N2})/Q_{N2} + 1$$

TABLE 3-19
ENGINE/COMPRESSOR POWER AND EFFICIENCY SUMMARY
(Predicted Values)

Loss	95° Day	80° Day	47° Day	17° Day
Hydraulic (W)	224.2 (193)	74.8	95.7	335.2
Compressor Seal	232	57	73	320
Gas Spring*	77	10.2	21	37
Total Loss Lower End (W)	533 (502)	142	189	692
Adiabatic Compressor Power (kW)	2.001	0.40	0.28	1.73
Total Engine Power (kW)	2.94 (2.907)	.624	0.507	2.712
Compressor Adiabatic Efficiency (%)	83.2	82.7	88.0	85.40
Engine/Compressor Lower-End Effic. (%)	68.1 (68.8)	62.7	55.2	63.8

*without adjustable gas spring bellows

3.3.4.3 Effect of Refrigerant (R-22) Solubility in Oil - Tests to determine the affects of Refrigerant-22 solubility in oil on the operation of the hydraulic simulator and dynamics of the diaphragms were conducted by introducing controlled amounts of Refrigerant-22 (measured as a percent by weight) into Suniso 3GS refrigerant oil. The affects were measured by comparing the change

in input power and diaphragm displacements with and without the Freon. The results for the change in required power and loss in diaphragm stroke are shown in Figure 3-17 as a function of percent by weight-dissolved refrigerant. Piston stroke was held constant at 10 mm for these tests. Figure 3-18 gives the change in solution viscosity of Refrigerant-12 dissolved in Suniso 3GS oil at 100°F*. The shape of the viscosity curve in Figure 3-18 is the cause of the saddle-shaped power curve in Figure 3-17. As more refrigerant is dissolved into the oil, the viscosity of the solution falls, decreasing the seal leakage pumping loss. At the same time, however, the lubricity of the solution falls, increasing seal friction losses. The solubility limit of R-22 in Suniso 3GS at 100°F and 125 psi is 20% by weight.

The data for diaphragm deflection attenuation is too scattered to draw a truly definitive conclusion; however, the increased seal leakage occurring at reduced solution viscosity does appear to produce a measurable reduction in displaced oil volume, thereby reducing diaphragm stroke.

3.3.4.4 Oil Management System - The oil management system for the hydraulic simulator encompasses all aspects of maintaining correct oil inventory in each of the volumes and the replenishing of oil in the hydraulic transmission that leaks past the oil pressure seal pack. The concept for this system is described in Figure 3-13, which defines the various oil volumes in the hydraulic transmission. In volumes A, B, C, and D, the oil will be at high pressure, equivalent to the pressure in the Stirling engine driver. In the intermediate cavity, volume E (Figure 2-7), a constant pressure will be maintained between the high pressure and the compressor suction pressure, which will be used to reduce the pressure differential across the seals in order to reduce seal friction and leakage. The final volume, F (Figure 2-7), will be maintained at compressor suction pressure, and will provide the drain for leakage from the other oil volumes. The internal hydraulic connection between volumes is shown in Figure 3-19. The resistive elements shown in that figure represent the oil-leakage paths across the seals; the parallel, arrowed paths represent the mid-stroke

---

*This assumes that refrigerants R-22 and R-12 behave similarily in solution with Suniso 3GS. A literature search performed seems to support the validity of this assumption.

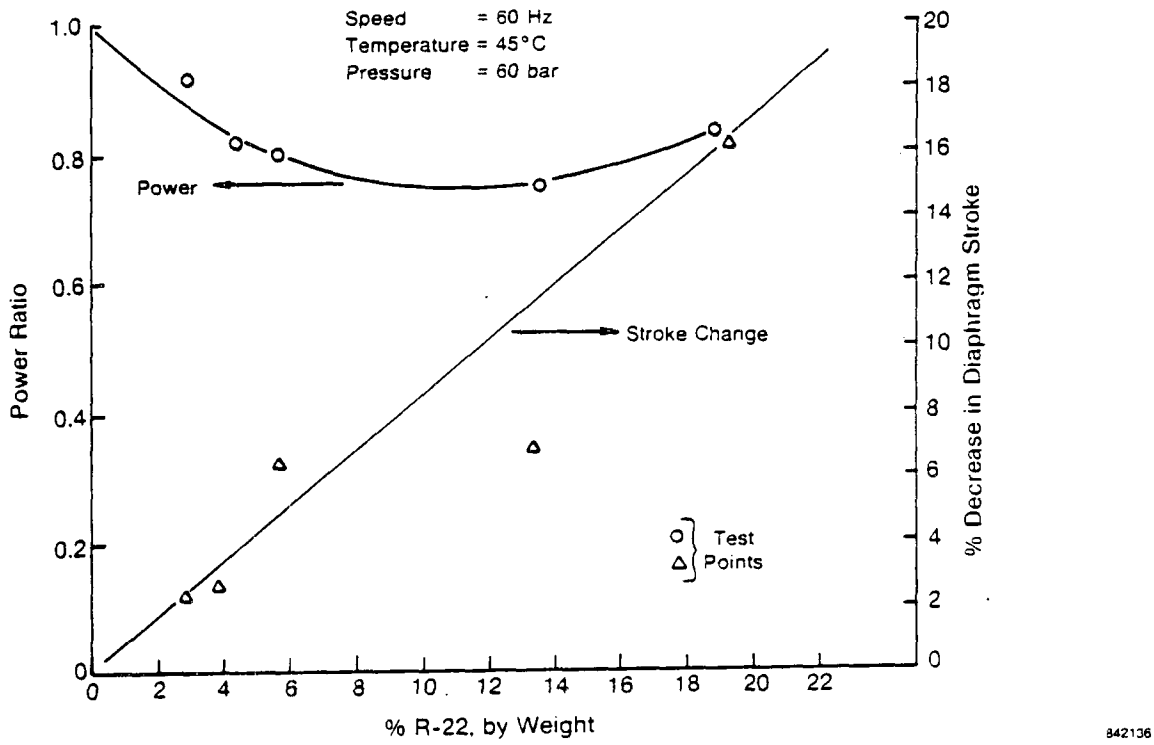

Figure 3-17 Effect of R-22 Solubility in Suniso 3GS Refrigeration Oil on Hydraulic Transmission Losses and Diaphragm Stroke for 10-mm Piston Stroke and 60 Hz

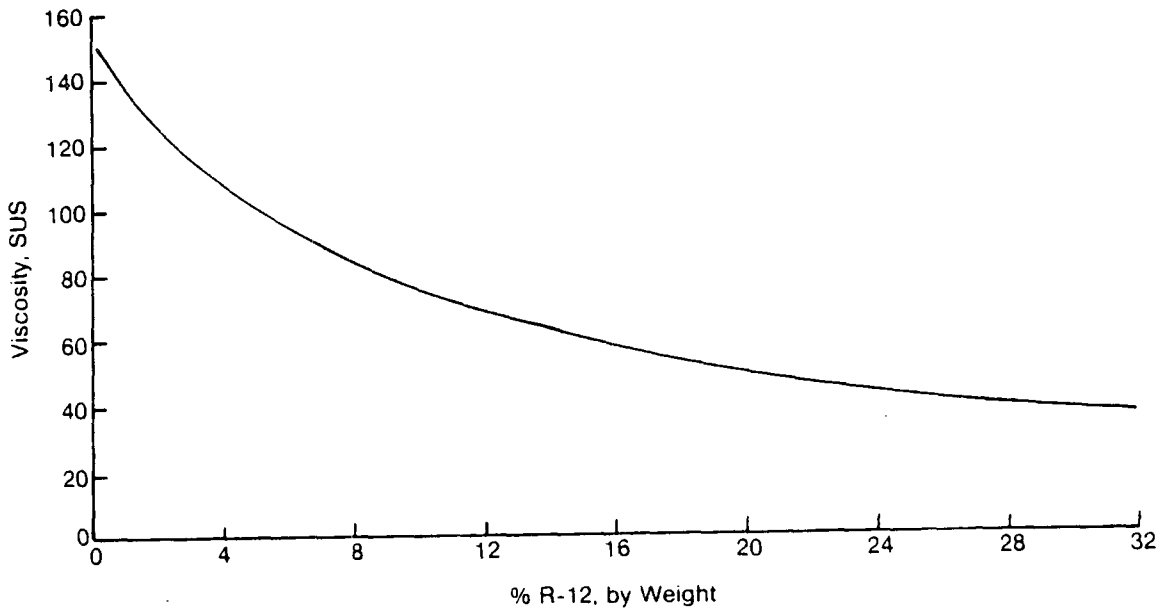

Figure 3-18 Viscosity of Solutions of R-12 in Suniso 3GS Refrigeration Oil at 100°F

porting connecting each volume. Thus, at mid-stroke, each of the high-pressure volumes A, B, C, and D are interconnected through the mid-stroke porting.

An oil management test loop was fabricated for the hydraulic simulator, and testing began shortly thereafter to evaluate the proposed scheme. During those tests, oil was drained from the upper oil cavity of the simulator (Figure 3-11) expanded to 1 atm, and returned to the simulator at high pressure (50 Bar) through the lower oil volume. The tests were conducted to determine the:

- effectiveness of centerporting to return the oil to the upper oil volume;
- ability to measure and transport small amounts of oil around the system; and,
- ability to control diaphragm offset deflections due to oil inventory changes in each volume.

From this testing, it was concluded that oil could be put back into the system during operation with no discernable diaphragm offsets, and that the mid-stroke porting would effectively return the oil to the upper oil volume.

3.3.4.5 Compressor Oil Management System - The basic concept of the oil management system is one of maintaining the correct oil inventory in each of the volumes by controlling the oil level in the separator to a range (ΔL) consistent with the deflection limits of the diaphragm. The following description of a proposed system's operation illustrates the principle of operation.

1. As the oil leaks out of volume A (see Figure 3-19) by P_A, the diaphragm will assume an offset due to the expansion of the Stirling engine working fluid (helium) against the top side of the diaphragm and the relative incompressibility of the oil in volume A. Because of the flexibility of the diaphragm and the matching of pressure between the engine and oil at all diaphragm positions, it was concluded that an oil inventory system based on pressure control would not work; a control based on inventory (level) or diaphragm offset was required.

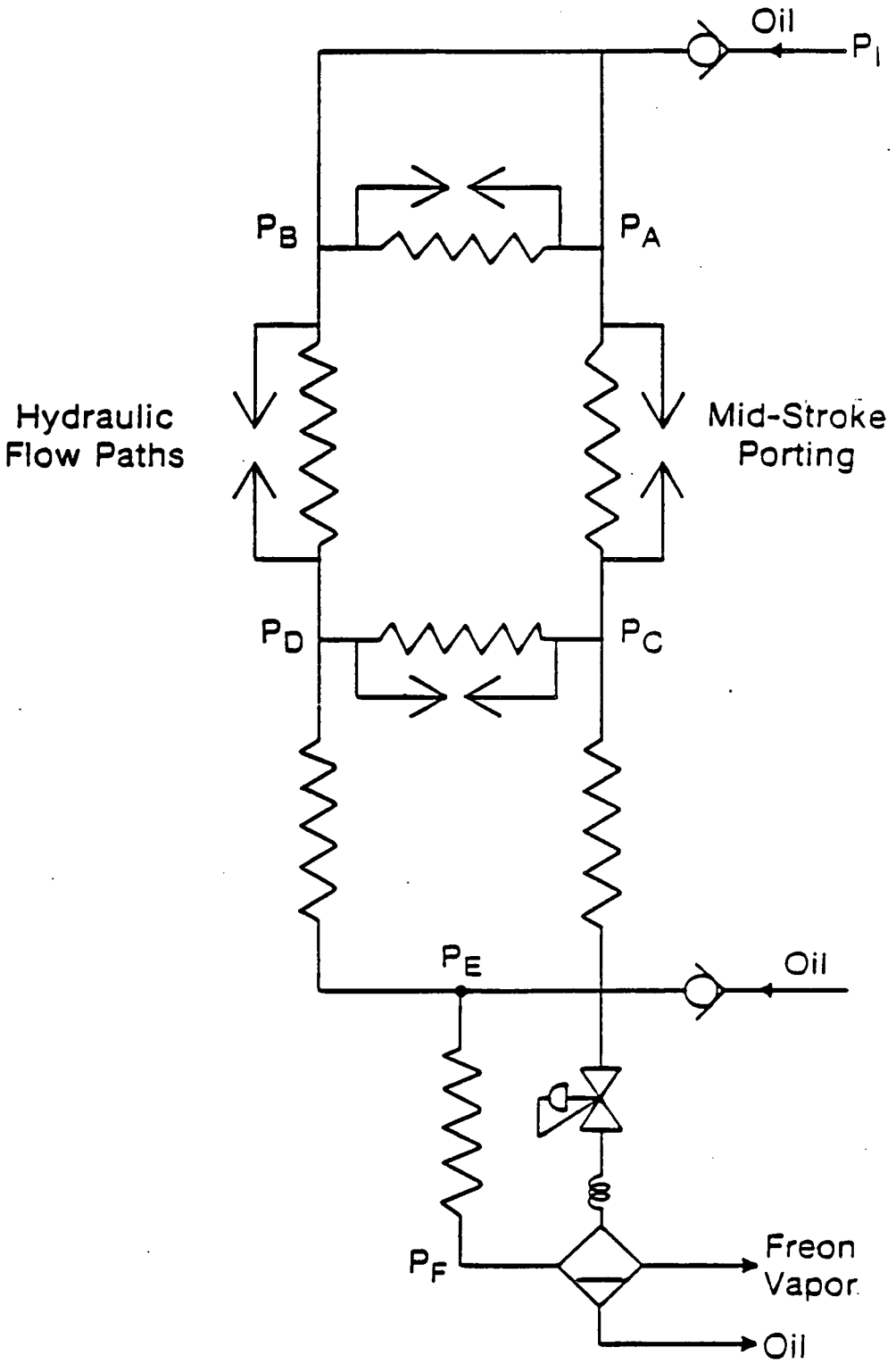

Figure 3-19 Hydraulic Flow Diagram

812980

2. The oil level in the separator will be controlled between the two limits (ΔL) by running the oil pump as required, and pumping the oil into a high-pressure accumulator.

3. From the accumulator, pressure-regulating valves will be used to set the injection pressures to volumes A and E (see Figure 3-20). For volume A, the injection pressure P_I will be set slightly above the minimum cycle pressure in A. Thus, whenever P_I becomes greater than P_A, and the accumulator contains oil, oil will flow into A. Volume E has both a forward and backward regulator to control its pressure at a constant P_E.

The use of a pumping ring seal was also considered for the high-to-low oil pressure seal. The advantage of this seal would be that it provides an internal pumping action that would pump oil from a low-pressure reservoir to high-pressure hydraulic cavities; thus, the oil management system would be simplified, and a much smaller oil pump could be used in the external circuit.

Although the pumping ring design concept has been proven to work well in the MTI automotive Stirling engine project, the concept has not yet been characterized in terms of efficiency and efficacy in the compressor. Because of its potential advantages, the pumping ring seal will be evaluated in future development work.

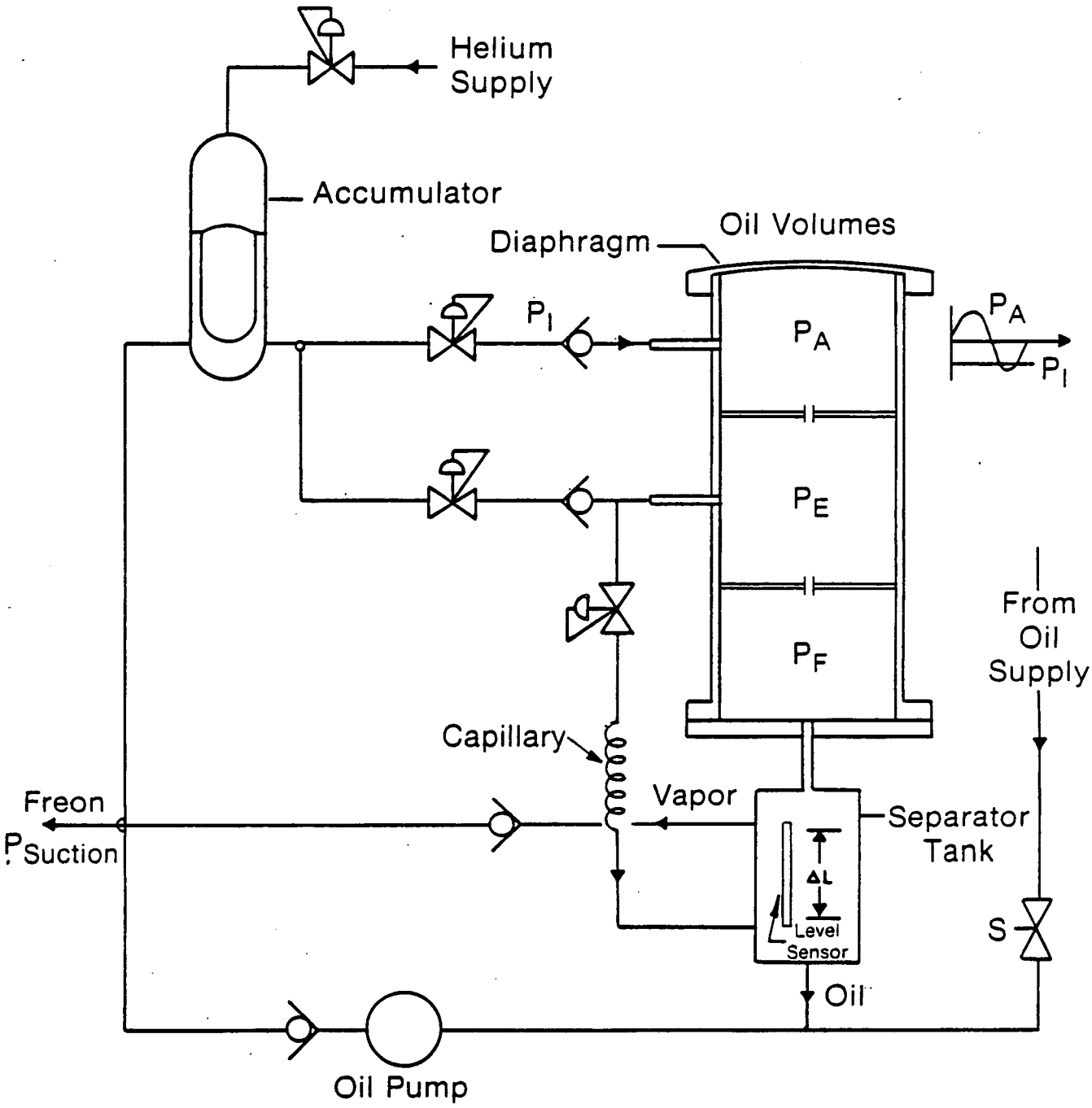

Figure 3-20 Preliminary Compressor Oil Management Circuit Concept

812977-1

4.0 SYSTEM PERFORMANCE

Based on the matching analyses performed and the hydraulic simulator loss analyses conducted for the total lower-end efficiency, performance estimates have been prepared for laboratory testing of both the breadboard power module and an advanced prototype system. The performance figures are based on calculating the coefficient of performance (C.O.P.) at the four designated operating points.

4.1 Breadboard Performance

An estimate of the achievable performance of the Breadboard System is given in Table 4-1. In addition to the losses discussed previously, additional losses were added to account for superheating of the refrigerant suction flow, refrigerant leakage past the compressor piston compression seals, and displacer gas bearing losses. None of these losses are accounted for in the analytical models used to compute the engine heater head input. Also, the calculations are based on heat input to the head, and do not include combustor inefficiencies.

4.2 Advanced Prototype System Performance

Performance values for an advanced prototype system were also computed based on projected performance for an advanced EM FPSE. The C.O.P. calculation, defined as:

$$\text{C.O.P.} = \text{Thermal Load/Total Energy Input}$$

was conducted from an energy flow diagram (as shown in Figure 4-1) for a 17°F ambient. The diagram defines input energy as the fuel to the Stirling engine and the electric parasitics:

- condenser, evaporator, and combustor fan power;
- coolant pump power; and,
- power module control power.

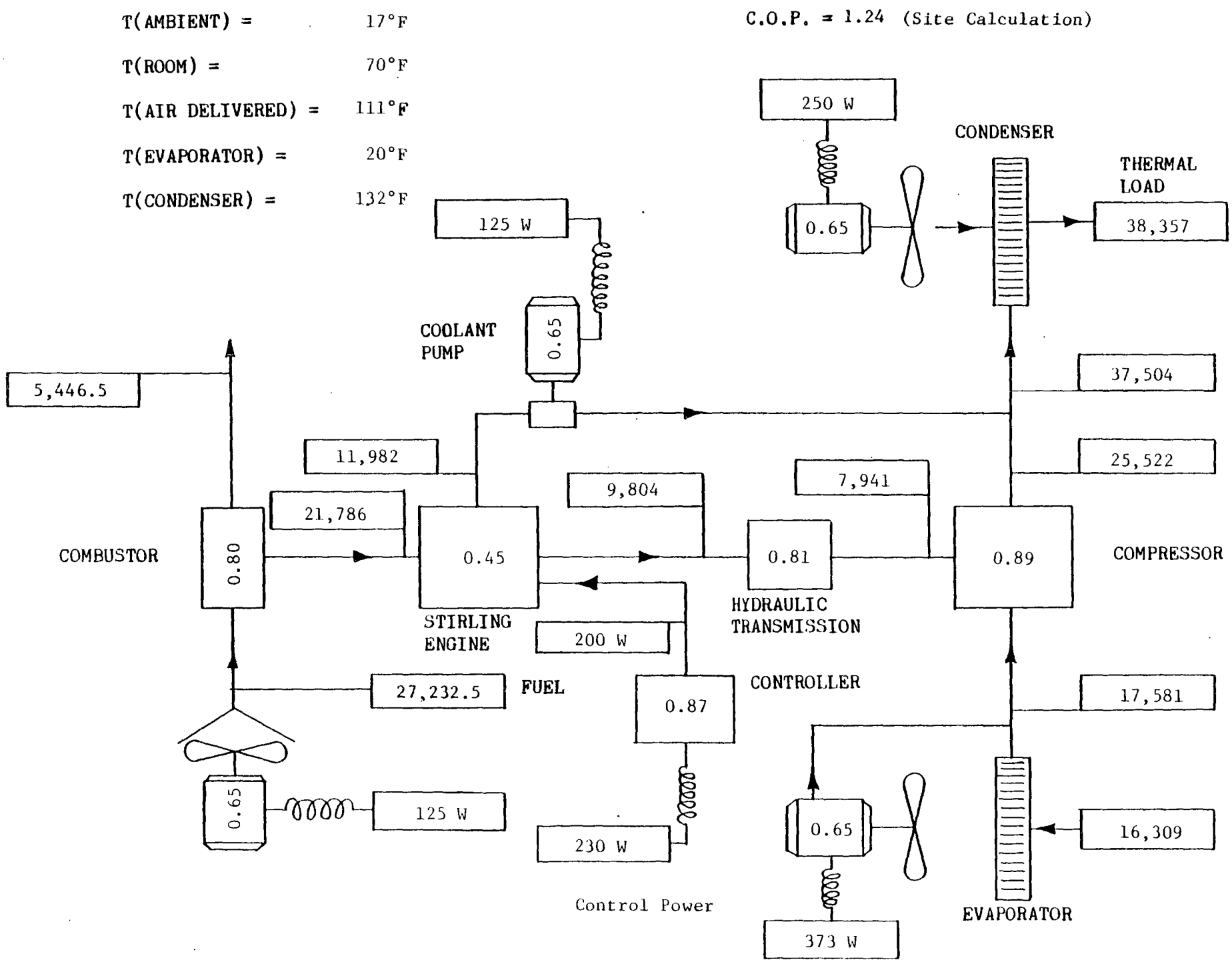

Figure 4-1 HAHP Power Flow Diagram (Advanced Prototype)

TABLE 4-1

STEADY-STATE C.O.P. ESTIMATION FOR THE BREADBOARD POWER MODULE

(Laboratory Testing)

Power Description	Power (Btu/hr) 95°F	80°F	47°F	17°F
Heating/Cooling Load	-36,000	-18,000	+14,000	+38,000
Engine, Heater Head, Heat Input	27,577	7,451	6,557	25,490
Control Power	1,906	500	350	1,200
Equivalent Superheat (10°F)	375	85	85	256
Total Input Power	29,858	8,036	6,992	26,946
C.O.P.	1.21	2.24	2.00	1.41

The steady-state parasitic electric power requirement for the system at the four designated operating points is given in Table 4-2. The condenser and evaporator fan powers for heating and cooling, respectively, are determined from the ARI standard air source unitary heat pump equipment. The C.O.P.'s calculated for an advanced diaphragm-coupled HAHP are given in Table 4-3. These are steady-state C.O.P.'s that do not account for cycling transients or defrost debits; however, the values do project the competitiveness of an advanced FPSE HAHP with conventional equipment when compared on a similar basis.

An interesting phenomenon that shows up in Table 4-3 is that for this system, with the system efficiencies stated and conditions selected, the C.O.P.'s in the heating/cooling modes are similar. This is easily explained by considering the evaporator and condenser temperatures at each of the operating points, and the pressure ratio over which the compressor must operate. Table 3-10 presented this data, showing that in order to achieve the same thermal load for heating and cooling, the same engine shaft power output is required. Thus, heat input to the Stirling engine is the same for both cases, even though in the case of heating (17°F ambient), roughly 30% of the thermal load comes from the rejected engine heat, and in the air-conditioning (AC) mode (95°F ambient), no value is recouped from the rejected heat. This phenomenon is a unique characteristic of an efficient Stirling engine, which minimizes rejected heat in the AC mode.

TABLE 4-2
ESTIMATED HAHP EXTERNAL POWER REQUIREMENTS

Parasitic Power	Power (watts) 95°F	80°F	47°F	17°F
Fan Power				
• Condenser	373	250	250	250
• Evaporator	373	250	186	373
• Combustor	125	98	98	125
Total Fan Power	871	598	534	748
Cooling Water Pump	125	75	75	125
Control Power (Advanced EM)	250	27	5	200
Controller Power Supply	38	5	1	30
Total Parasitic Power (watts)	1,284	705	615	1,103
Total Parasitic Power (Btu/hr)	4,378	2,404	2,09	3,761

TABLE 4-3
ADVANCED DIAPHRAGM-COUPLED HAHP
(Site Steady-State Calculation)

Input Power	Power (Btu/hr) 95°F	80°F	47°F	17°F
Heating/Cooling Load	-36,000	-18,000	+14,000	+38,000
System Efficiencies				
• Engine Efficiency (%)	46	36	35	45
• Combustor Efficiency (%)	85**	82	82	85
• Lower-End Efficiency (%)	79	68	60	72
Compressor Power	7,698	1,650	1,035	7,059
Engine Power	9,744	2,426	1,725	9,804
Total Heat Input	24,921	8,218	6,010	25,631
Total Parasitic Power*	4,378	2,404	2,097	3,761
Total Input Power	29,299	10,622	8,107	29,392
C.O.P.	1.23	1.69	1.73	1.29

*taken from Table 4-2
**based on higher heating value

5.0 EM 1 AND EM 4 VERIFICATION TEST

5.1 Test Objectives

Objectives of the EM 1 and EM 4 verification tests were:

- to map the first private-program EM engine (EM 1) to verify that the engine would meet the power requirements of the HAHP breadboard system at the four ARI rating points (95°F, 80°F, 47°F, and 17°F), and to establish a set of baseline performance criteria from which repeatability and performance of the fourth EM engine (EM 4) could be judged; and,

- to determine the repeatability of EM 4's performance when tested in the EM 1 configuration with an alternator load by matching or exceeding the performance obtained by EM 1 at the four equivalent ARI ambient points within the HAHP acceptance criteria outlined below in Section 5.1.1.

5.1.1 HAHP Verification Acceptance Criteria

This section specifies the acceptance criteria for the HAHP verification test. MTI's first-order code has an estimated uncertainty band of ±10% due to accumulated deviations in the input parameters, and simplifying assumptions made in the analysis. Further, most measurements can be expected to fall in a ±5% uncertainty band; therefore, the measured results are expected to fall within 15% of the calculated performance. The acceptance criteria applied to the HAHP verification test results are:

Displacer Stroke	±15%
Displacer Phase	±9°
Total Cycle Power	±15%
Net Piston Power	±15%

5.2 Test Procedures

The following subsections outline the background and test procedures followed in order to comply with and meet the test objectives of the EM 1 and 4 verification tests. Differences do exist between the EM engines coupled with the linear alternator and the EM engines coupled with the compressor in the final HAHP configuration. The differences between EM 1 and HAHP engines are given in Table 5-1. A comparison of the HAHP and EM 1 design specifications are given in Table 5-2, and outlined in the following paragraphs.

5.2.1 Rod Area

The cross-sectional area of the displacer rod is sized to provide the necessary driving force to the displacer for shuttling the gas between the expansion and compression spaces. The rod size accounts for the heat exchanger pressure drop loads imposed by those components connecting the expansion and compression spaces, and any displacer gas spring losses. In the heat pump configuration, the displacer must shuttle more gas than in the alternator configuration because of the shorter equivalent piston stroke imposed by the diaphragm deflection (stress) limits. To accomplish the sizing of the larger required displacer rod area in the HAHP configuration and still maintain the necessary displacer spring rate, the virtual rod arrangement shown in Figure 6-6 is used. The virtual rod area comes from the difference in piston areas between seal diameters 3 and 1 in Figure 6-6. Seal diameters 3 and 2 and 5 and 4 are maintained in the engine. This arrangement allows an increased area rod over the EM configuration while maintaining the EM stiffness by the addition of a third gas spring volume (volume A in Figure 6-6).

To overcome the shorter piston stroke, the rod area is increased from 3.8 cm^2 to 9.7 cm^2. Table 5-2 gives the design point operating specifications for the heat pump engine and the same engine with the alternator. Larger diaphragms can be used to reduce this; however, they are not considered an option in the breadboard demonstration because of the long lead time and development that is required. The change in rod area will have two affects on the HAHP operating characteristics. First, the displacer gas spring leakage coefficient will change, affecting both the analytical predictions and actual performance of the

TABLE 5-1
DISSIMILAR CHARACTERISTICS BETWEEN THE EM 1 AND HAHP ENGINES

Parameter	EM 1	HAHP Engine
Displacer Rod Area (cm^2)	3.80	9.70
Engine/Compressor Transition Plate	None	Yes
Load	Electric Alternator	Refrigerant Compressor
Variable-Piston Gas Spring Volume	None	10% on Bottom-End for Stiffness Control

TABLE 5-2
COMPARISON OF EM 1 AND HAHP ENGINE DESIGN SPECIFICATIONS

Parameter		HAHP at 95°F	EM 1 Nominal Operating Point
Mean Head Temperature	(°C)	760	760
Mean Pressure	Bar	60	60
Frequency	(Hz)	60	60
Displacer Rod Area	(cm^2)	9.70	3.8
Diaphragm Volume Amplitude	(cm^3)	65.55	-
Equivalent Piston Stroke	(mm)	12.7	20.6
Displacer Stroke	(mm)	18.71	16.0*
Piston-to-Displacer Phase Angle		70.2	65.0
Displacer Control Power	(watts)	447	389
Engine P-V Power	(watts)	2,907	4,300

*Maximum Displacer Stroke = 20.00 mm

HAHP engine; and second, changing the rod will alter the spring rate and hysteresis losses of the displacer gas springs.

5.2.2 Transition Plate

In the alternator configuration, the lower end of the displacer drive system is nested in the compression space, and clearance is provided in the power piston by hollowing out the center of the piston. In the HAHP System, a diaphragm replaces the power piston, and clearance for the displacer drive must be provided in a transition plate (see Figure 5-1). The addition of a transition plate changes the engine characteristics through the addition of:

- pumping loss through the passages in the transition plate;
- wetted surface area, thus increasing compression-space hysteresis loss; and,
- void volume to the engine.

5.2.3 Load

The alternator and compressor represent different spring and damping components to the engine, and will affect the engine's dynamic tuning and response to load changes. The compressor being a nonlinear load will make control more difficult.

5.2.4 Variable-Piston Gas Spring Volume

The HAHP's lower end (the diaphragm-coupled hydraulic compressor) has a variable gas spring volume* that gives a 10% adjustment to the piston gas spring stiffness. A sensitivity analyses performed for the interim engine verification testing showed that the effect of piston spring rate on displacer stroke and control power was very sensitive to spring rate. The alternator load on the EM engines does not have this characteristic; therefore, matching each HAHP operating point with the EM 1 engine/alternator system becomes difficult and costly because of the hardware changes required to tune the engine at each of the off-design

---

*incorporated into the system to enable dynamic tuning at each operating point

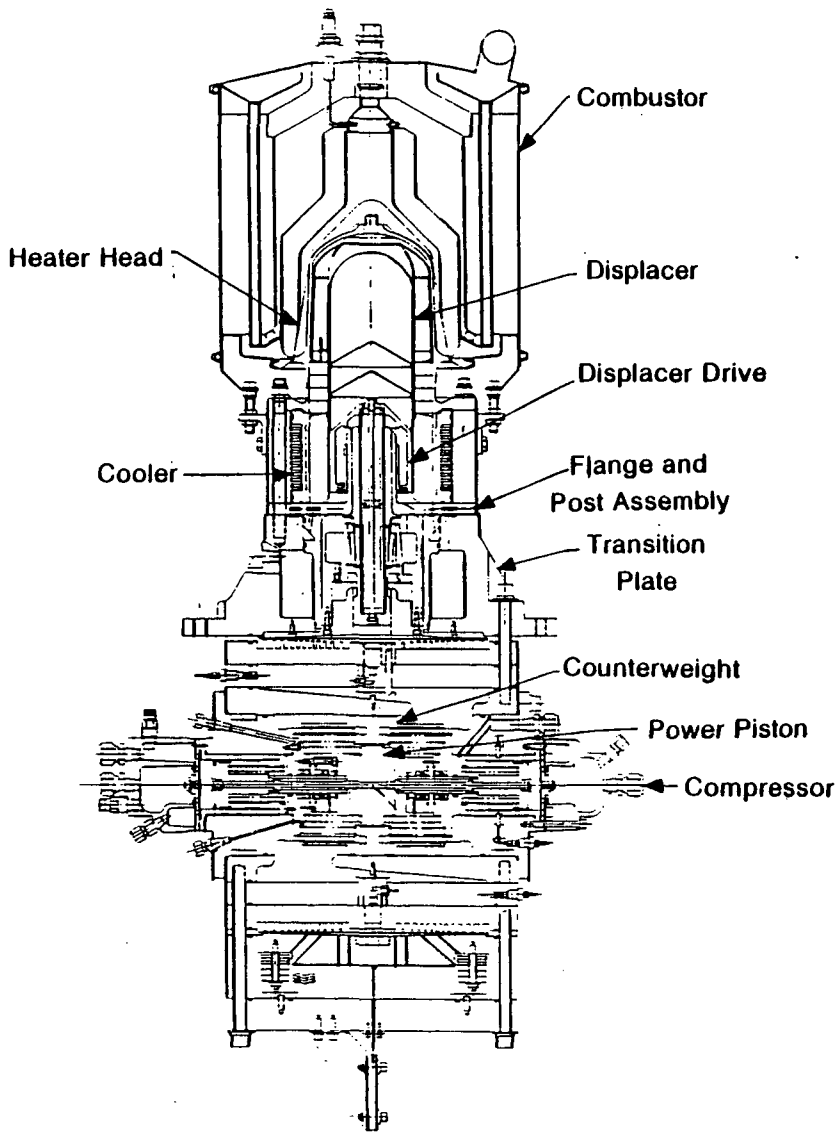

EM4 with Compressor
HAHP Breadboard
Diaphragm Displacement Amplitude
61.45 cc (3.75 in.³)

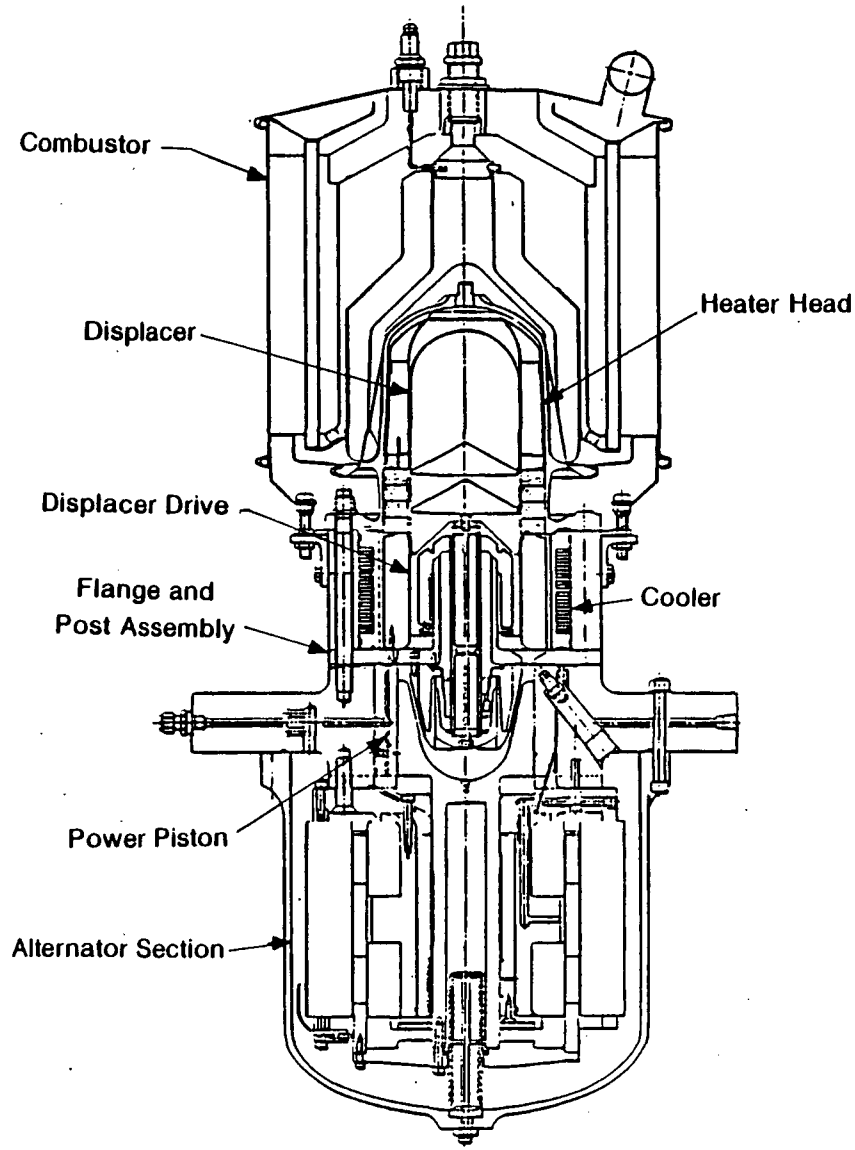

EM1–EM4 with Alternator
EM Prototype
Piston Displacement Amplitude
102.58 cc (6.26 in.³)

Figure 5-1 Comparison of the EM Engine/Alternator Configuration and the EM Engine /Compressor

83463

points. A comparison between the EM engine/alternator configuration and the EM engine/compressor is shown in Figure 5-1 to illustrate the physical differences.

To verify that the EM engine will perform as the HAHP prime mover, the characteristics of each engine were analytically mapped by assuming a fixed mean heater temperature and a compression-space seal eccentricity of 50%. The analytical maps for the breadboard engine and compressor are plotted in Figure 5-2, and in Figure 5-3 for the EM engine with an alternator load. The maps are plotted as piston P-V power delivered to the diaphragm versus counterweight stroke for the compressor configuration. The curves were calculated for a fixed displacer-to-piston matrix phase angle of 65°, and for displacer-to-piston-stroke ratios (X_d/X_p) ranging from 0.5 to 1.5.

Four points that simulate the four ARI operating points for the HAHP System were derived from the analytical maps. The four points simulated by the EM engine in the alternator configuration were found from the analytical maps by matching EM 1's piston and displacer strokes to the HAHP's compressor and displacer strokes, and deriving a representative piston P-V power. The operating characteristics for these points, and the EM 1 nominal operating points, are shown in Table 5-3.

5.3 EM 1 Mapping Procedures and Test Results

The test procedures followed during the engine mapping of EM 1 for the HAHP program are outlined below:

- engine was heated to maximum heater head control temperature;
- the piston stroke, which was determined to simulate one of the four ARI equivalent HAHP points in Table 5-3, was established;
- the alternator resistive load was modulated while maintaining piston stroke and heater control temperature until the corresponding displacer stroke outlined in Table 5-3 was attained;
- while maintaining the alternator resistive load, and with control temperature fixed, the piston stroke was varied with data points taken at each discrete value of piston stroke; and,

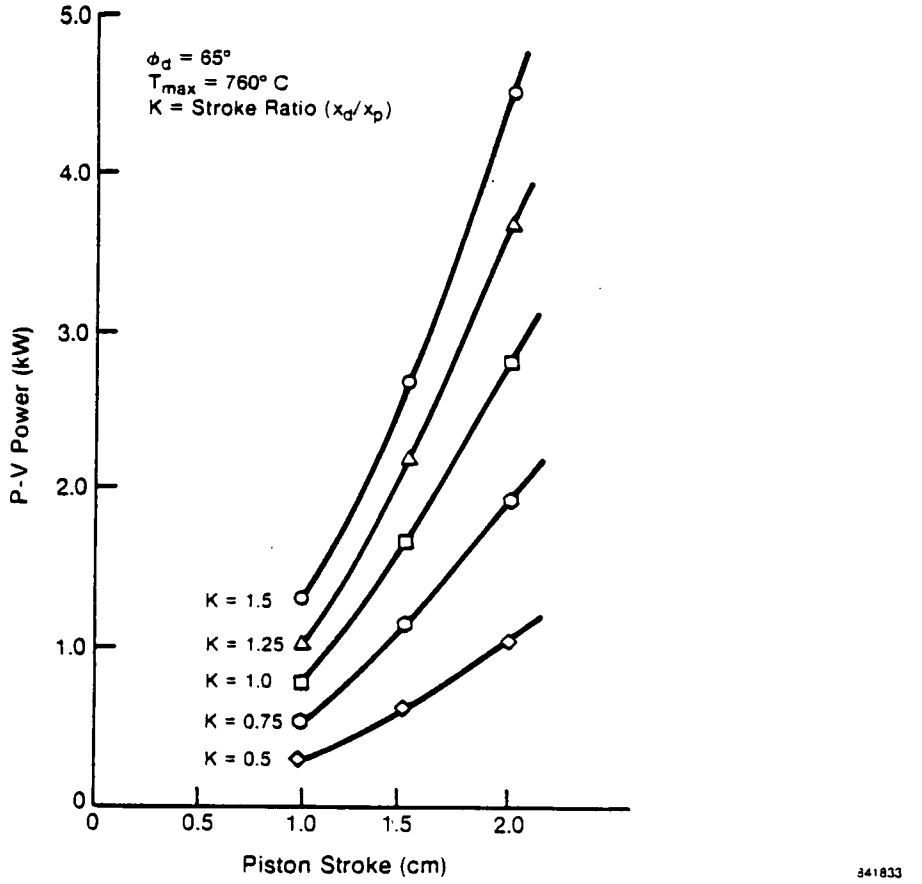

Figure 5-2 Engine Operating Characteristics for the HAHP Engine Configuration

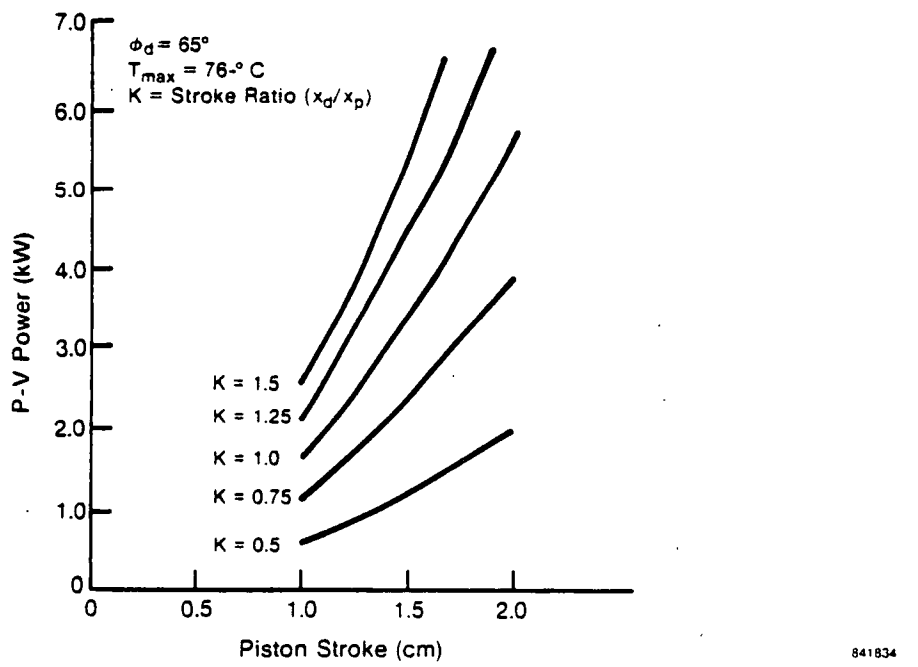

Figure 5-3 Engine Operating Characteristics for the EM 1 Engine Configuration

TABLE 5-3

HAHP VERIFICATION TEST DATA

Engine Parameter	EM 1 Nominal Operating Point		95°F Ambient			80°F Ambient			47°F Ambient			17°F Ambient			High-Power Large Displacer Stroke Test		
			HAHP	Equivalent EM 1		HAHP	Equivalent EM 1		HAHP	Equivalent EM 1		HAHP	Equivalent EM 1		HAHP	EM 1	
	P*	M**	A***	P	M	A	P	M	A	P	M	A	P	M		P	M
Mean Head Temperature (°C)	760		760	760		760	760		760	760		760	760			760	
Mean Pressure (Bar)	60		60	60		60	60		60	60		60	60			60	
Frequency (Hz)	60		60	60		60	60		60	60		60	60			60	
Piston (Compressor) Stroke (mm)	20.60		19.50	19.5		10.24	10.20		11.51	11.50		22.76	20.00			12.3	
Displacer Phase Angle (deg)	65		70.20	65		60.50	65		63.30	65		51.90	65			65	
Displacer Stroke (mm)	16.00		18.71	12.7		7.04	7.10		5.36	5.75		16.82	14.80			18.5	
Stroke Ratio	0.78		0.98	--		0.69	0.70		0.47	0.50		0.74	0.75			1.5	
Piston P-V Power (w)	4200		2907	2907		624	1000		507	750		2712	3850			3750	
Displacer Control Power (w)	389		387	--		-85.5	--		-70.8	--		-108	--			600+	
Head Heat Input (w)																	

* Predicted
** Measured
***Analytical
+Test limited to maximum displacer control power.

- the above procedure was repeated for each of the equivalent points outlined in Table 5-3 to generate the map.

The map generated by the above procedures is shown in Figure 5-4 as piston P-V power versus piston stroke with alternator load resistance as the parameter. The fixed parameters that were maintained during test while generating the map data were:

P_m - mean engine charge pressure of 60 Bar;

f - engine frequency that gave the closest operating phase as in Table 5-3 for the given builds' displacer/piston masses and displacer gas spring (rod area and g/s damping loss effects on the stiffness);

C_a - alternator tuning capacitance to maintain a zero alternator power factor and, hence, a pure resistive load;

I_f - alternator field current fixed at 2.5 amps;

A/F - air to fuel ratio (17:1); and,

$T_{control}$ - heater head temperature by which the operator maintained the required fuel flow.

Also indicated on the map in Figure 5-4 are the four engine testing limits. These are explained below.

- Facility Resistive Load - The resistive load in the facility during the mapping of EM 1 was accomplished with a motor-driven, infinitely variable resistance between the high and low limits with a low resistance limit of .92 Ω.

- 7.5-amps RMS Control Current Limit - This was the design limit that is the analytically determined current limit where the displacer control feature would begin to enter saturation. Since none of the four ARI equivalent points required higher currents than 7.5-amps

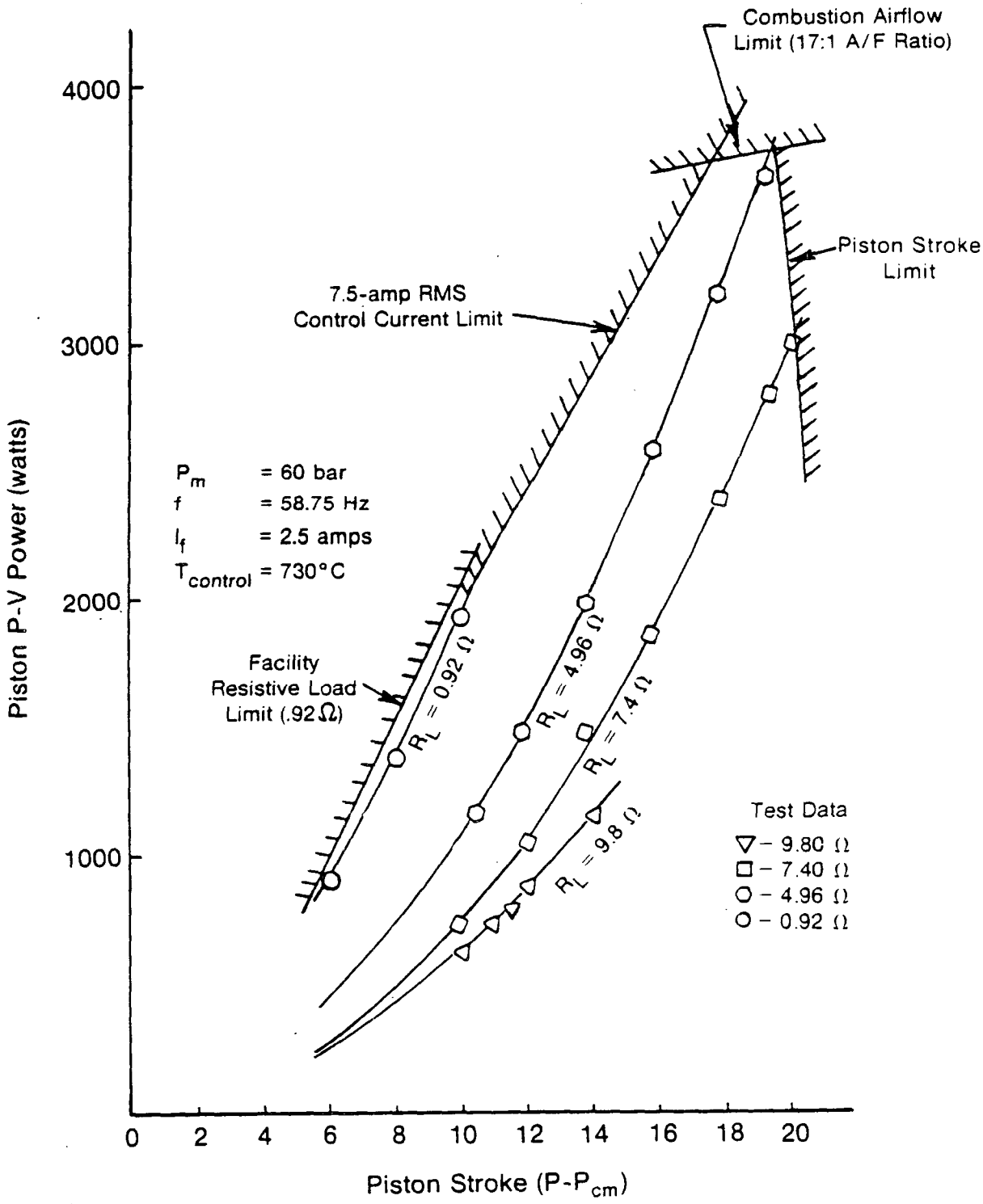

Figure 5-4 EM 1 Load Map (Piston P-V Power Versus Piston Stroke)

8418

RMS, the .92 Ω load line test was terminated when this limit was reached. The slope of the limit line shown in Figure 5-4 was established by extrapolating the control current from the 4.96 test data for the high point, and the actual test data point for the .92 Ω load line for the low point.

- Combustion Airflow Limit - This limit, not necessarily a rigid point, could move up or down depending on the blower bypass valve setting, instrumentation in the air supply plumbing, air/fuel ratio, and, as later determined, combustor air leakage.

- Piston Stroke Limit - Maximum design stroke of the EM 1 piston is 20.6 mm, which is defined by the geometric clearance in the piston cylinder from stop to stop, and would be theoretically achieved if the piston were to oscillate about the geometric center. As during the mapping test, the piston center of oscillation was biased off this center, limiting the amplitude of the piston stroke.

Figure 5-5 shows the remaining thermocouple (T/C) readings of the original 54 T/C's when the 95° ARI equivalent point in Table 5-3 was run. The control T/C reading is indicated on the curve and is shown to be a representative indication of the mean heater head temperature.

Figure 5-6 shows displacer stroke versus piston stroke for the EM 1 load map shown in Figure 5-4. Indicated on the curves in Figure 5-6 are the EM 1 equivalent ambient-day HAHP operating points outlined in Table 5-3. The predicted piston P-V powers for each of the four ARI points in Table 5-3 are shown on the completed EM 1 load map in Figure 5-7. Reviewing the points in Figure 5-7, the following is demonstrated:

- EM 1 can provide required power at the HAHP operating characteristics; and,
- the anlaytical model predicted EM 1 power to within a small deviation.

Table 5-4, a completed tabulation of EM 1 mapping results, shows a point-for-point comparison between engine characteristics obtained from EM 1

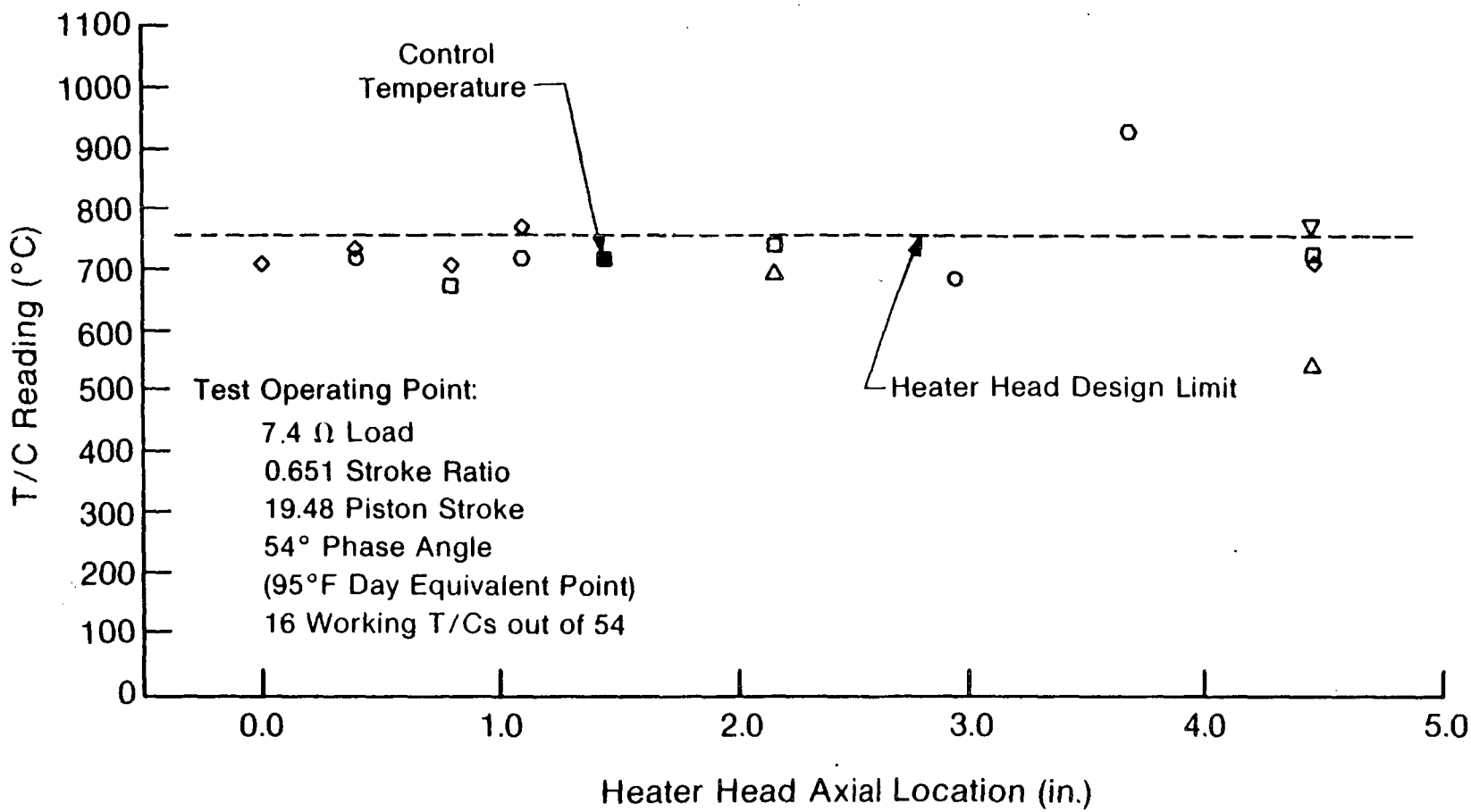

Figure 5-5 T/C Reading Versus Heater Head Axial Location

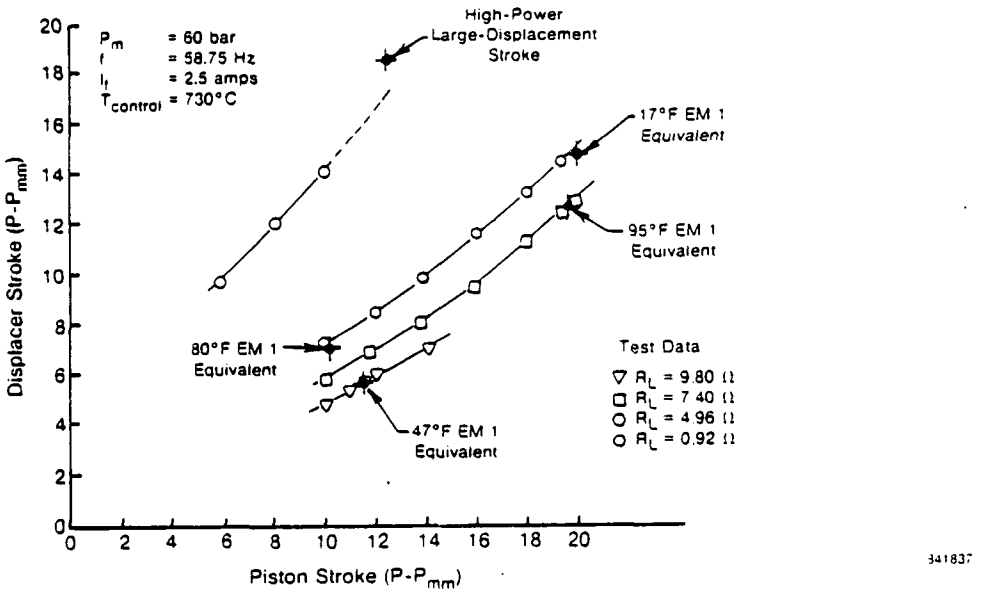

Figure 5-6 Displacer Stroke Versus Piston Stroke for EM 1

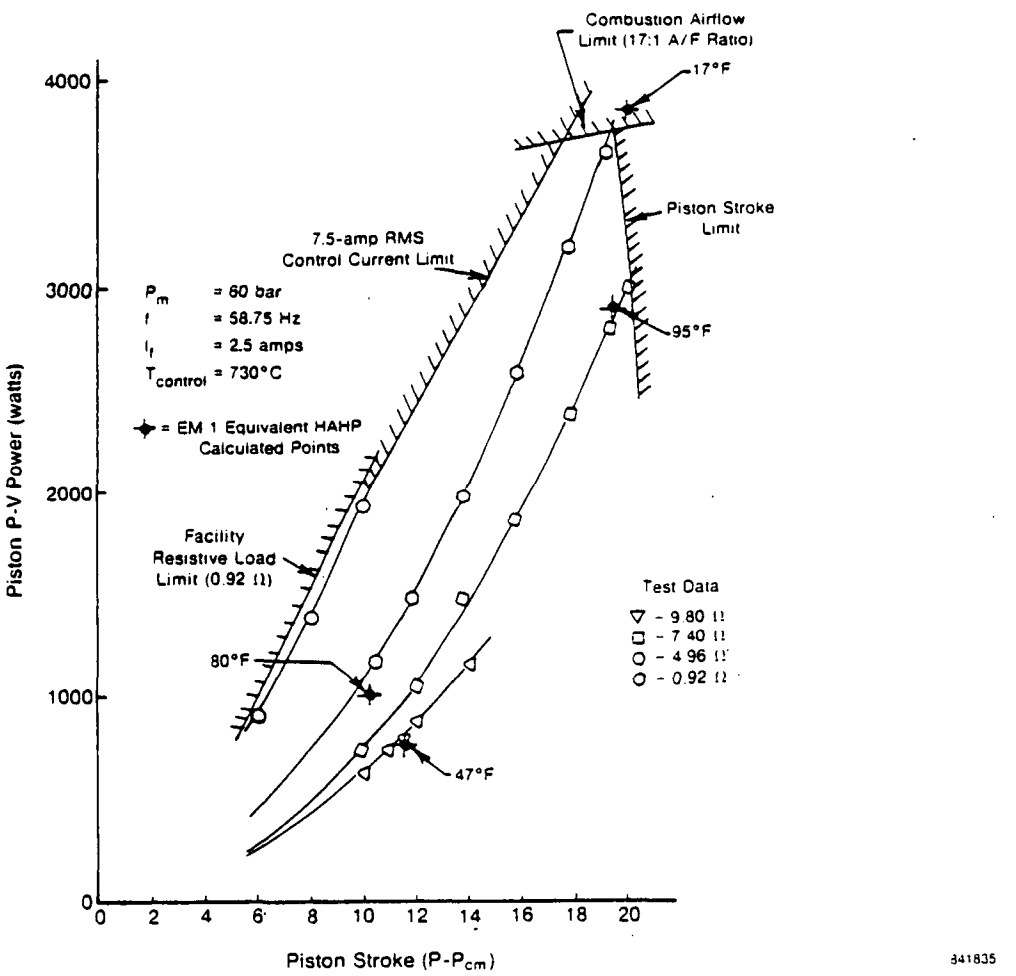

Figure 5-7 P-V Power Versus Piston Stroke for EM 1

TABLE 5-4

HAHP VERIFICATION TEST DATA
(EM 1 ENGINE)

Engine Parameter	EM 1 Nominal Operating Point		95°F Ambient			80°F Ambient			47°F Ambient			17°F Ambient			High-Power Large Displacer Stroke Test		
			HAHP	Equivalent EM 1		HAHP	Equivalent EM 1		HAHP	Equivalent EM 1		HAHP	Equivalent EM 1		HAHP	EM 1	
	P*	M**	A+	P	M	A	P	M	A	P	M	A	P	M		P	M
Mean Head Temperature (°C)	760	743	760	760	722	760	760	732	760	760	725	760	760	736		760	729
Mean Pressure (Bar)	60	60.12	60	60	59.97	60	60	59.70	60	60	59.50	60	60	60.24		60	59.90
Frequency (Hz)	60	58.26	60	60	58.12	60	60	58.70	60	60	58.09	60	60	58.67		60	58.10
Piston (Compressor) Stroke (mm)	20.60	18.55	19.50	19.50	19.48	10.24	10.20	10.48	11.51	11.50	11.52	22.76	20.00	19.20		12.3	10.15
Displacer Phase Angle (deg)	65	59.35	70.20	65	54.21	60.50	65	66.20	63.30	65	60.87	51.90	65	59.80		65	50.76
Displacer Stroke (mm)	16.00	16.00	18.71	12.70	12.69	7.04	7.10	7.22	5.36	5.75	5.66	16.82	14.80	14.10		18.5	14.08
Stroke Ratio (mm)	0.78	0.863	.098	0.65	.652	0.69	0.70	0.689	0.47	0.50	0.491	0.74	0.75	0.734		1.5	1.39
Piston P-V Power (w)	4200	4204.7	2907	2907	2822	624	1000	1167	507	750	791.4	2712	3850	3647		3750	1970
Displacer Control Power (Current amps) (w)	389	1246.0 (10.2)	387	--	98.4 (2.07)	-85.5	--	17.40 (2.09)	-70.80	--	21.50 (1.58)	-108	--	397.2 (4.8)		600++	788 (7.3)
Head Heat Input HADC = 0.0 (kW)	12.61	11.31		9.55	8.63		3.49	3.85		3.02	3.17		11.40	9.84		10.0	5.52

* Predicted
** Measured
\+ HAHP design conditions
++ Test limited to maximum displacer control power.

mapping, and the analytical characteristics for each of the HAHP equivalent ambient-day ARI points and the EM 1 nominal operating points.

5.4 EM 4 Verification Test Procedures (Alternator Load)

Upon completion of the EM 1 mapping phase, EM 4 was assembled with newly fabricated hardware that included:

- displacer dome and body assembly;
- displacer end cover;
- flange and post assembly;
- load-side gas spring piston and cylinder resulting in a 3.5-cm^2 rod area (EM 1 rod area was 3.0 cm^2);
- engine heater head;
- engine cooler; and,
- regenerator liner and expansion-space stuffer assembly.

The newly fabricated EM 4 engine was operated along the same 5.4 Ω load line as EM 1 to demonstrate the P-V power and engine efficiency repeatability shown in Figure 5-8. Conditions for each of the four selected ARI equivalent points in Table 5-3 were then established and data taken to demonstrate and verify that EM 4 could provide the power characteristics required to drive the HAHP in the same manner as demonstrated during the EM 1 verification tests.

5.5 EM 4 Test Results (Alternator Load)

The EM system assembly consists of two mated subassemblies - the combustor assembly and the engine assembly. The combustor system converts the chemical energy of natural gas to heat energy used to provide the heat source to the engine assembly. The engine assembly then converts the heat energy crossing the heater head control volume boundary to produce an oscillating pressure wave which can then produce work by moving a piston or pistons. The ability of the EM 1 hardware, as compared to EM 4 hardware, to convert heat energy to available work is an evaluation of the differences in internal engine clearances and heat exchangers from one engine to another of the same design. The differences are due to individual internal engine component tolerances that make up the engine assemblies. The potential of the engine pressure wave to do work is lessened

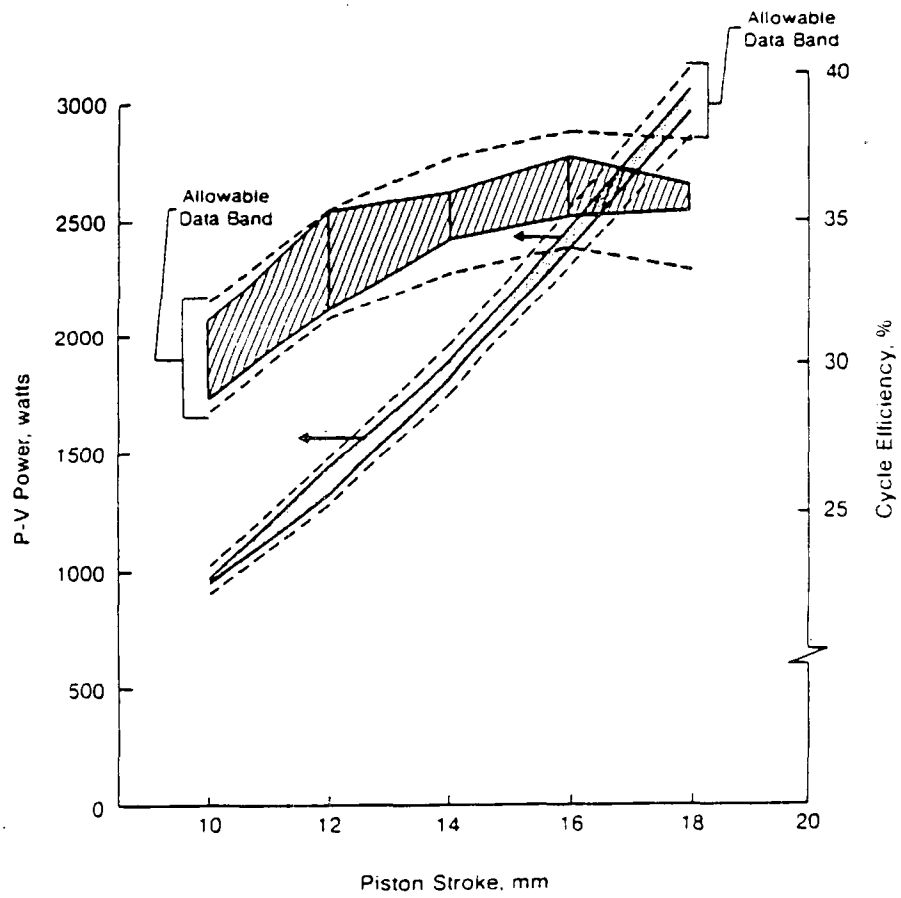

Figure 5-8 Engine-to-Engine Repeatability Data (EM 1 Versus EM 4)

83572-1

due to the various losses within the engine, and dominantly appears as a reduction in the compression-space pressure amplitude and phase angle. Available work from the engine pressure wave in the compression space is used to drive the piston as piston P-V power, and to aid in driving the overdamped displacer. The load on the displacer is the heat exchanger pumping and displacer gas/spring losses. The power required to overcome the pumping losses is required for engine operation and must be considered as part of the engine-to-engine performance evaluation. Any amount of the available engine P-V work used to drive the displacer reduces the power available at the piston. To evaluate how well the EM 1 engine assembly converts heat energy to power as compared to the EM 4 engine assembly, the engine cycle efficiency (the total engine power available to do work divided by the heat input to the heater head) was used. The total amount of internal engine power available to do work is the piston P-V power (useful work) plus that amount of cycle power used to drive the displacer minus the heat exchanger pumping power, which is equal to the displacer gas spring power loss minus the input displacer control power.

Test results comparing EM 4 and EM 1 are plotted in Figure 5-9 as the cycle efficiency defined above and P-V power versus piston stroke. Tabulated on Figure 5-9 are the operating conditions from the EM 1/EM 4 engine tests at the 16-mm piston stroke, showing that the set points between the two tests were within a 5-6% margin.

Figure 5-10, a plot of displacer control current versus piston stroke for the engine-to-engine repeatability test, shows that a lower control current was required for EM 4 during this test than for EM 1. EM 4 was then operated at the ARI operating points outlined in Table 5-3.

Figures 5-11 and 5-12 are the EM 1 plots of displacer stroke and piston P-V power versus piston stroke (generated during EM 1 mapping) with the corresponding EM 4 data points indicated on the curves. The P-V powers obtained with EM 4 are seen to be slightly different (two lower, one higher, and one exact) than the EM 1 P-V powers. Prior to running the EM 4 verification tests, the infinitely variable alternator load resistance (autotransformer) that was in the EM 1 test cell facility was changed out with a step-wise, finite load resistance for future testing under the private program. The installed finite steps in resistance did not match exactly with the load resistance values obtained during the EM 1

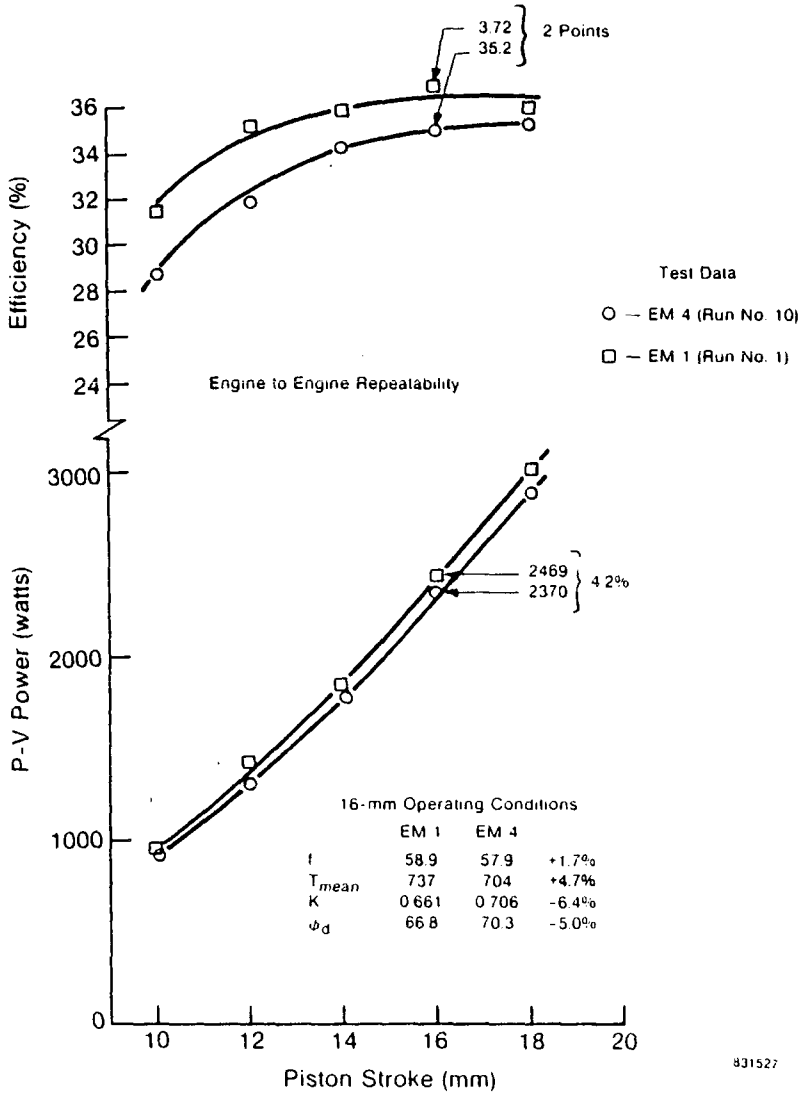

Figure 5-9 P-V Power/Efficiency Versus Piston Stroke

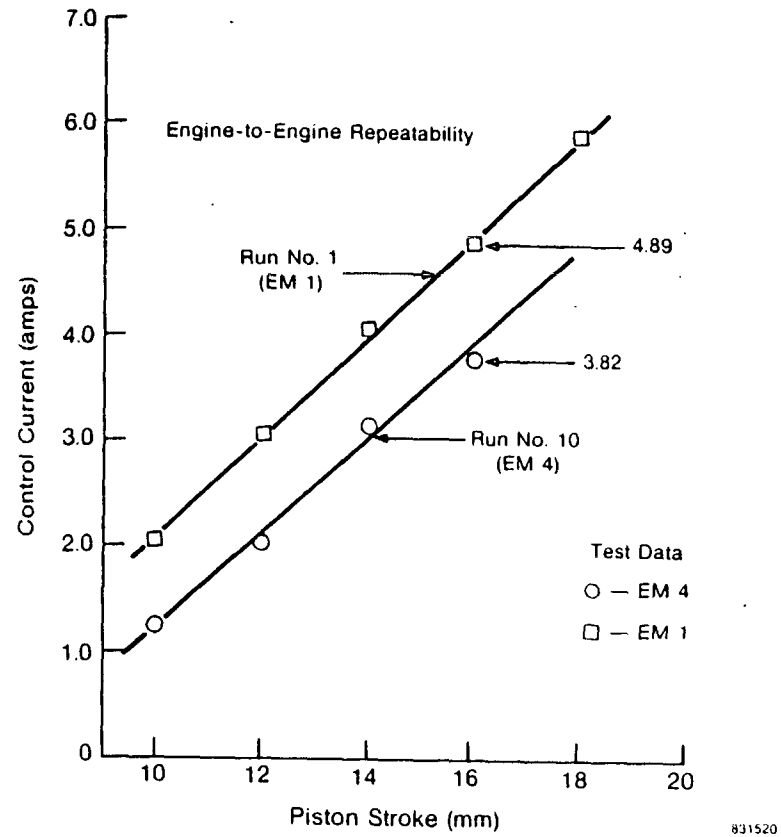

Figure 5-10 Displacer Motor Current Versus Piston Stroke

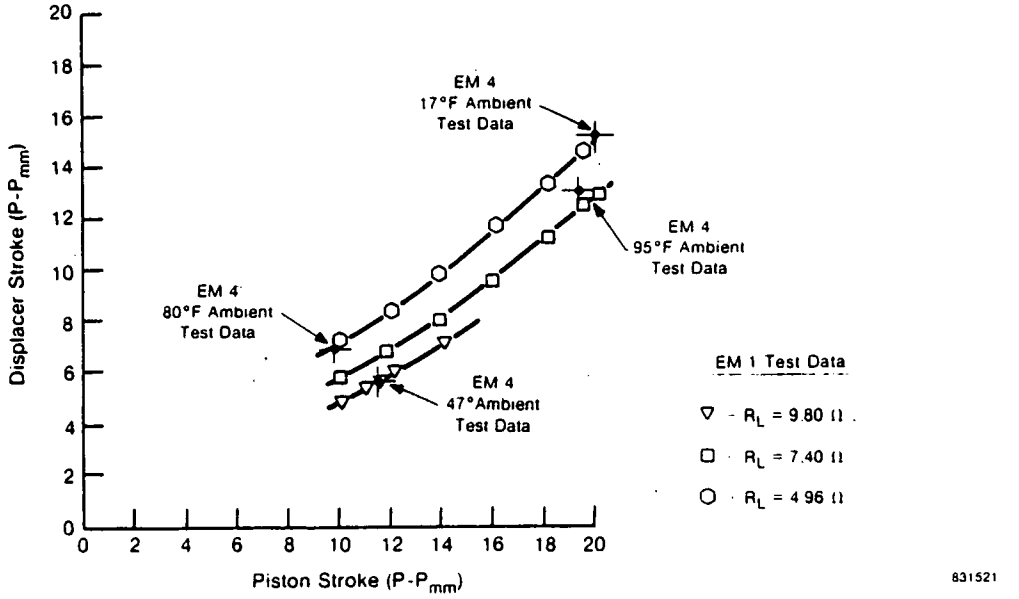

Figure 5-11 EM Load Map - Displacer Stroke Versus Piston Stroke

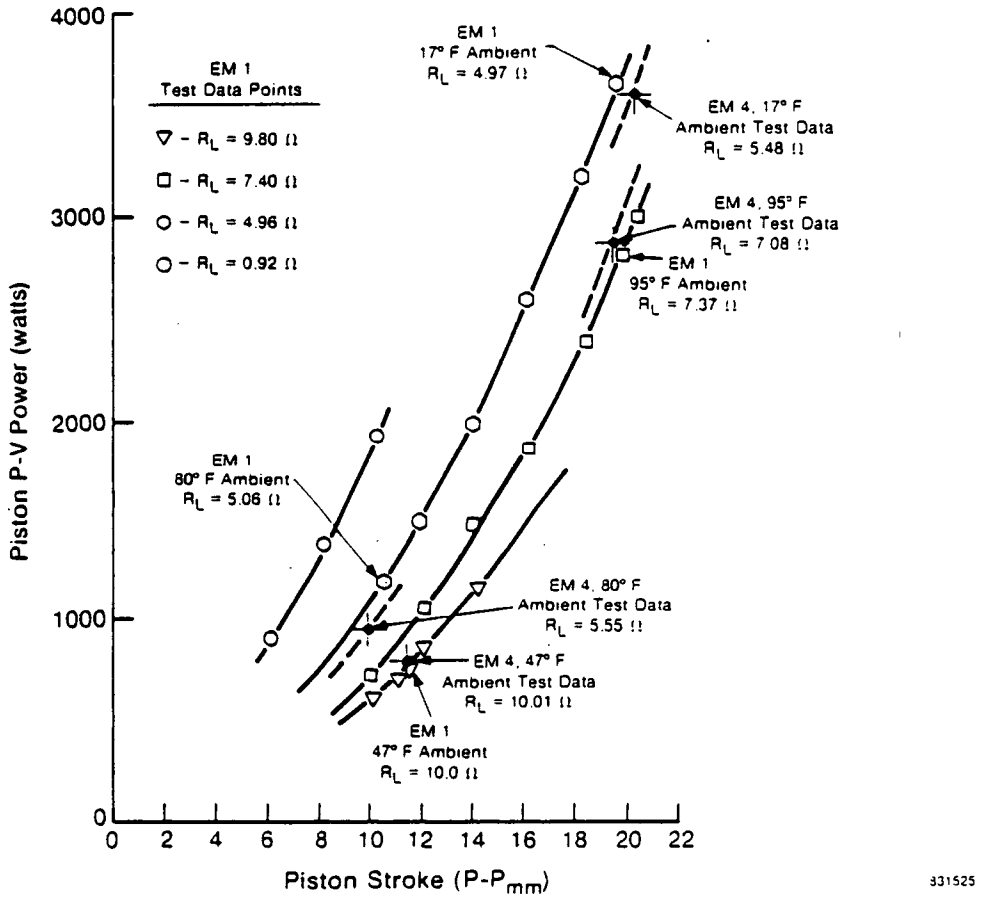

Figure 5-12 EM Load Map - Piston P-V Power Versus Piston Stroke

mapping tests, and the closest values to each of the EM 1 load lines were selected to set the equivalent ARI points during EM 4 testing.

Figure 5-12 shows that EM 4 P-V power points are consistent with those of EM 1, deviating only because of the difference in load resistance values between the comparable points. To illustrate this, EM 1 P-V power is first shown cross-plotted against load resistance in Figure 5-13 for constant piston strokes. Extrapolation of the 9.8 Ω load line was employed for strokes greater than 14 mm, rendering plot accuracy questionable at the higher strokes. EM 4 piston strokes at the ARI equivalent points were then plotted on the same type of plot, resulting in the curves in Figure 5-14. These show EM 1 P-V power versus load resistance for EM 4 piston strokes. Also indicated on the curves are the four EM 4 piston P-V powers at the EM 4 load resistance, demonstrating that within an accuracy of the cross plot, EM 4 matched EM 1 P-V power almost exactly. A point-for-point comparison between the EM 1 and 4 tests at the equivalent ARI test points is tabulated in Table 5-5. The differences in operating characteristics between EM 1 and 4 at the four ARI operating points were due to:

- Load Resistance - As previously mentioned, EM 4 load resistance could not exactly match EM 1 because of a facility change, thus affecting the stroke ratio.

- Heater Head Temperature - The combustor at the EM 4 high power points (95° and 17°) would not maintain temperature because of excessive leaks, primarily affecting P-V power, control current, and displacer phase (higher phase at lower temperatures).

- Rod Area Change - There was only one set of 3.0-cm^2 rod hardware (EM #1 and the change to 3.5 cm^2 (EM-4)) that primarily affected displacer phase.

At a later date, EM 1 hardware was reassembled, and the HAHP 95° equivalent point was repeated with emphasis on a better match for heater head temperature. Table 5-6 summarizes the comparison between EM 4 and a rerun of the EM 1 point. EM 1 control current is shown to be higher than EM 4 in Table 5-6, which is consistent with the engine-to-engine repeatability tests. Also, plotting the

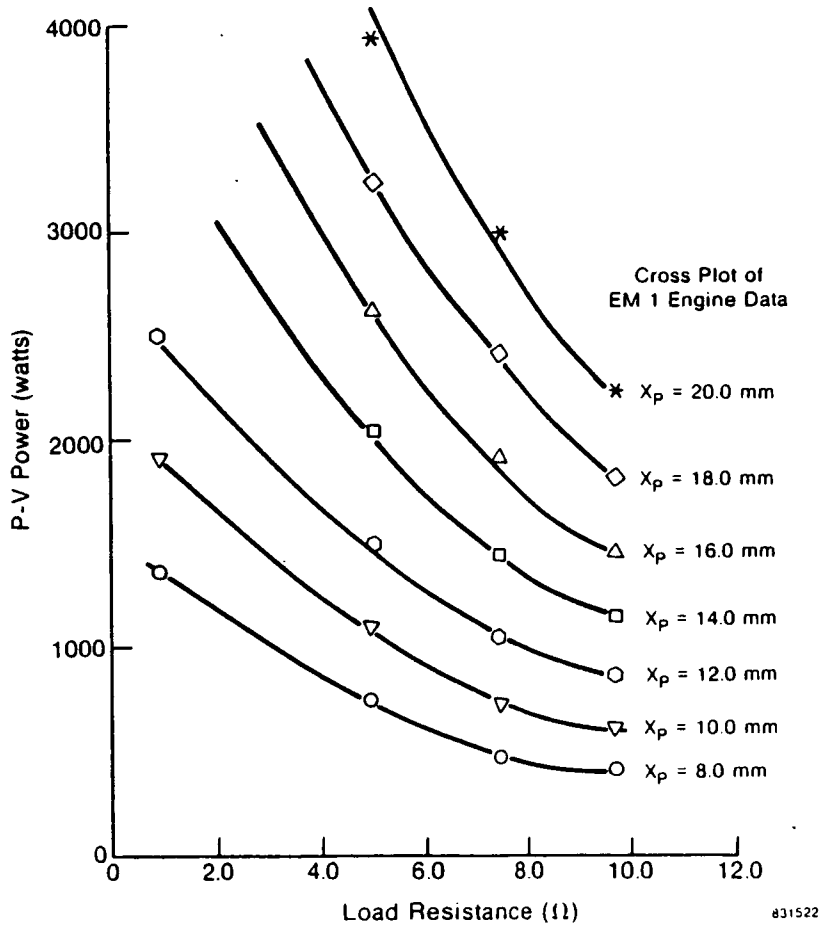

Figure 5-13 P-V Power Versus Load Resistance

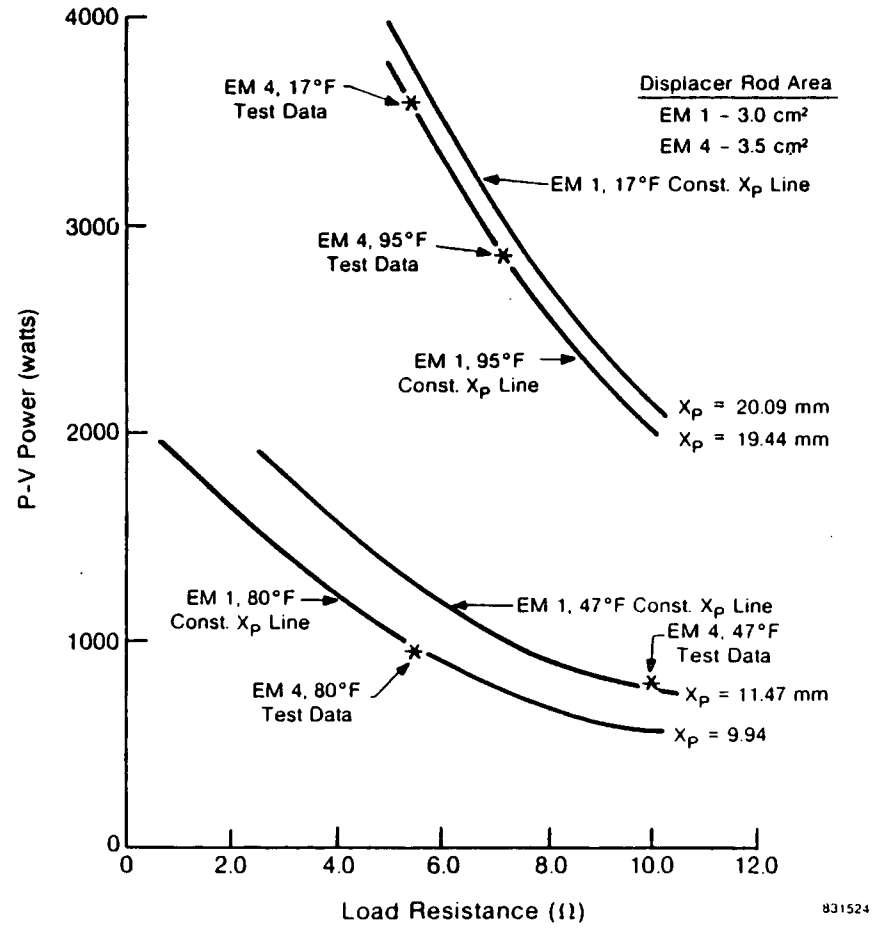

Figure 5-14 P-V Power Versus Load Resistance

TABLE 5-5

HAHP VERIFICATION TEST DATA
(EM 4 ENGINE)

	95°F Ambient				80°F Ambient				47°F Ambient				17°F Ambient			
		Equivalent EM				Equivalent EM				Equivalent EM				Equivalent EM		
ENGINE PARAMETER	HAHP	P*	EM 1	EM 4	HAHP	P	EM 1	EM 4	HAHP	P	EM 1	EM 4	HAHP	P	EM 1	EM 4
Mean Head Temperature (°C)	760	760	720	676	760	760	729	703	760	760	725	746	760	760	708	663
Mean Pressure (Bar)	60	60	59.97	59.63	60	60	59.70	59.80	60	60	59.50	59.3	60	60	60.24	59.56
Frequency (Hz)	60	60	58.12	57.94	60	60	58.70	57.80	60	60	58.04	57.95	60	60	58.67	57.98
Piston (Compressor) Stroke (mm)	19.50	19.50	19.48	19.44	10.24	10.20	10.48	9.94	11.51	11.50	11.52	11.47	22.76	20.00	19.20	20.09
Displacer Phase Angle (deg)	70.20	65	54.21	73.89	60.50	65	66.20	71.67	63.30	65	60.87	65.82	51.90	65	59.80	73.01
Displacer Stroke (mm)	18.71	12.70	12.69	13.03	7.04	7.10	7.22	6.94	5.36	5.75	5.66	5.73	16.82	14.80	14.10	15.25
Stroke Ratio	0.98	0.65	0.652	0.671	0.69	0.70	0.689	0.698	0.47	0.50	0.491	0.499	0.74	0.75	0.734	0.759
Piston P-V Power (w)	2907	2907	2822	2886	624	1000	1167	948	507	750	791.40	799.2	2712	3850	3647	3616
Displacer Control Power (w)	387	--	98.40	256.4	-85.50	--	17.40	13.60	-70.80	--	21.50	-3.38	-108	--	397.20	440.10
(Current amps)	--	--	2.07	5.20	--	--	2.09	1.61	--	--	1.58	1.35	--	--	4.80	7.12
Head Heat Input	--	--	8.63	9.64	--	--	3.85	3.46	--	--	3.17	3.76	--	--	9.84	10.54
Load Resistance (Ω)	--	--	7.37	7.08	--	--	5.06	5.55	--	--	9.52	10.01	--	--	4.97	5.48

*Predicted

displacer-side gas spring losses for EM 1 and 4 in Figure 5-15 shows that the EM 4 gas spring and, hence, engine seal losses for the HAHP configuration, were significantly lower than with EM 1.

TABLE 5-6

COMPARISON BETWEEN EM 4 AND A RERUN OF THE EM 1 POINT

		95°F Ambient	
Engine Parameter		EM 4	EM 1 Rerun
Mean Head Temperature	(°C)	676	672
Mean Pressure	(Bar)	59.63	59.68
Frequency	(Hz)	57.94	59.60
X_p	$(P-P_{mm})$	19.44	19.21
ϕ_d	(°)	73.89	71.42
X_D	$(P-P_{mm})$	13.03	12.31
K	(X_d/X_p)	0.671	0.641
P-V Power	(watts)	2886	3195
Q_{head}	(kW)	9.64	9.52
$P_{control}$	(watts)	256.40	281.00
Control Current	(amps)	5.20	8.08
Load Resistance	(Ω)	7.08	7.19

5.6 EM 1 and EM 4 Verification Test Conclusions

EM 1 and 4 engine-to-engine repeatability test conclusions can be summarized as:

- within the 5-6% variance in operating conditions (dynamics and head temperature), EM 4 repeated EM 1 P-V power within 4.1%, EM 4 efficiency was two points lower than EM 1, and EM 4 required lower control current than EM 1;

- EM 4 will perform at the four HAHP equivalent operating points;

- EM 4 is equivalent to EM 1 (power is within 10% and efficiency within two points); and,

- EM 4 is suitable for breadboard demonstration.

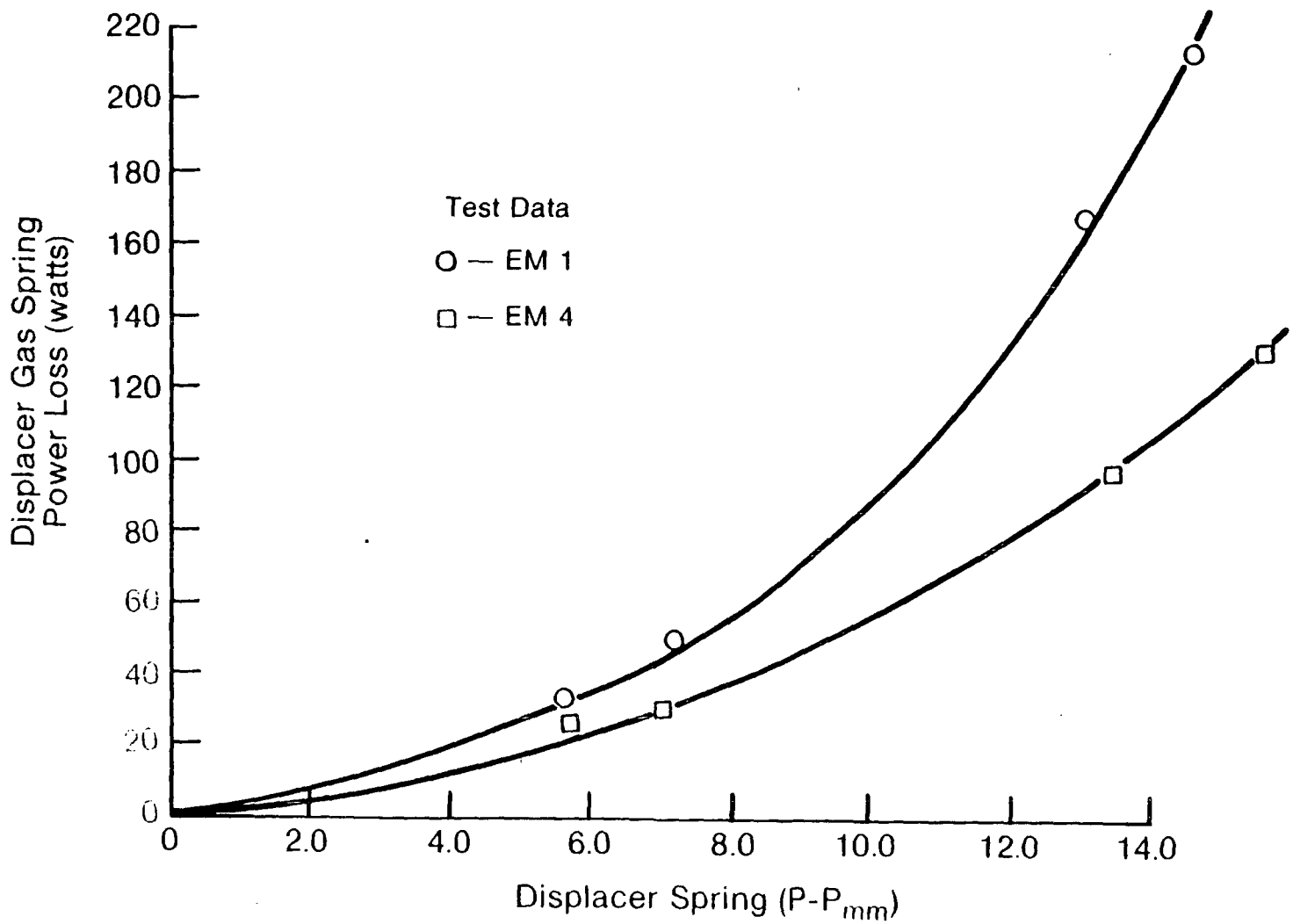

Figure 5-15 Displacer Gas Spring #2 - Loss Versus Displacer Stroke

6.0 BREADBOARD SYSTEM

6.1 System Description

The following sections describe the HAHP Breadboard System.

6.1.1 Engine Characteristics

Figure 6-1 is a layout of the HAHP Breadboard Engine/Compressor, which consists of a gas-fired FPSE prime mover powering a diaphragm-driven, resonant, free-piston compressor. The engine has a monolithic heater head (cast in Inconel 718 and final machined) designed with extended surface area fins that provide a constant temperature distribution along the surface. Internal engine heat transfer to the working gas (He) is accomplished by flow through channels formed by convoluted foil. The annular regenerator cavity between the head and cooler is filled with random wire-weave, die-formed Metex regenerator discs.

The engine cooler is a He-water heat exchanger housed in an aluminum housing. The gas path consists of rectangular channels machined in the cooler. The water path is formed by machining passages in the cooler O.D. to force the water in a counter-crossflow manner relative to working gas entering from the regenerator.

The displacer drive power split for a given displacer drive power requirement is determined by the effective displacer rod area, which is established by the proper selection of piston diameters separating the three gas spring volumes. The displacer rod bearing consists of two hydrostatic gas bearing journals - one double-plane admission and one single-plane admission. The gas feed to the HAHP Breadboard System hydrostatic bearings will be provided by an external air-actuated, positive-displacement helium boost pump (Figure 6-2).

The FPSE prime mover will be the EM 4 engine that will have been operated in the configuration of EM 1 with an alternator load. Figure 6-3 compares the alternator and compressor assemblies with the basic EM engine. As shown, the same hardware components are maintained above the flange and post assembly. As was pointed out in the "Engineering Model Engine Mapping Procedures for the Heat-Actuated Heat Pump Program," the major differences between EM 1 and 4 in

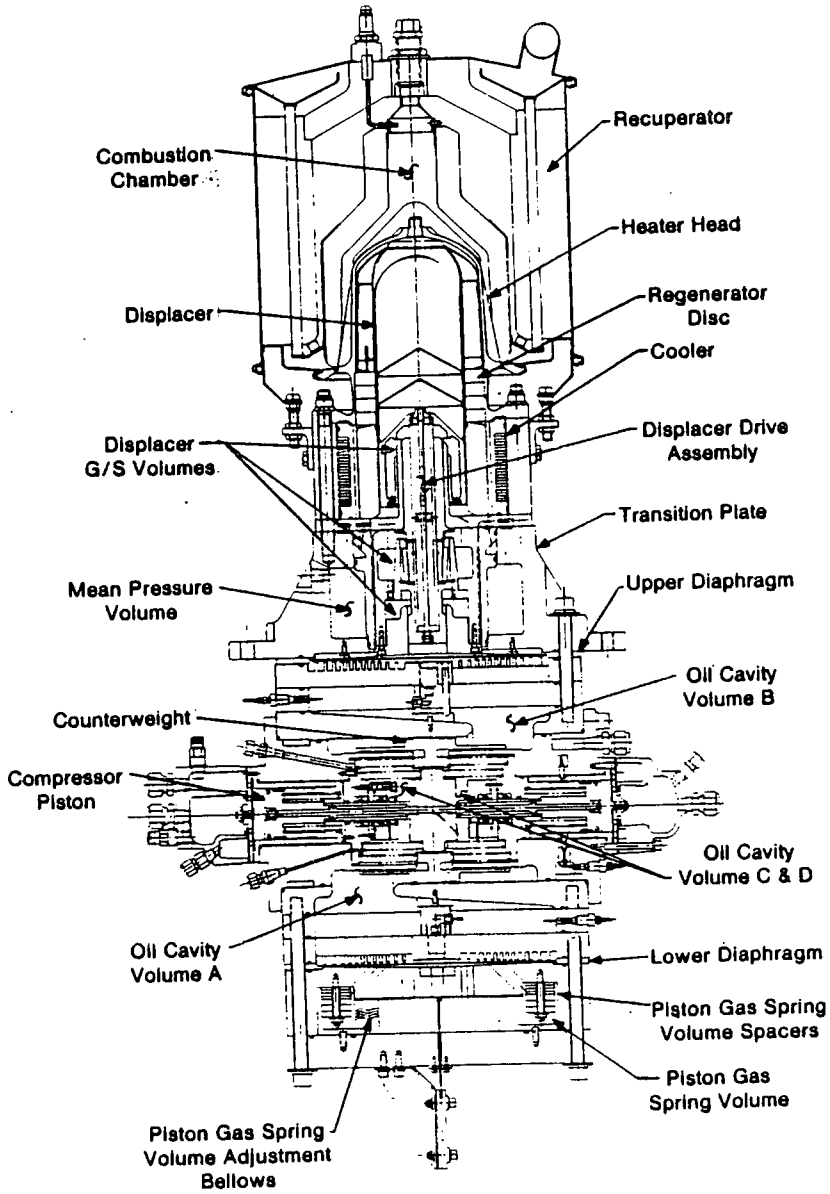

Figure 6-1 HAHP Engine/Compressor Layout

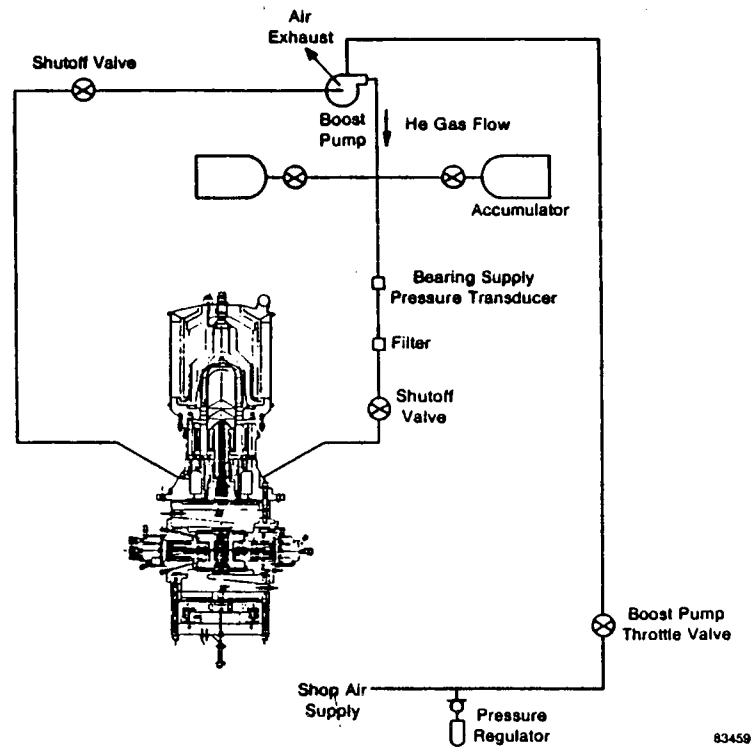

Figure 6-2 Displacer Bearing Supply

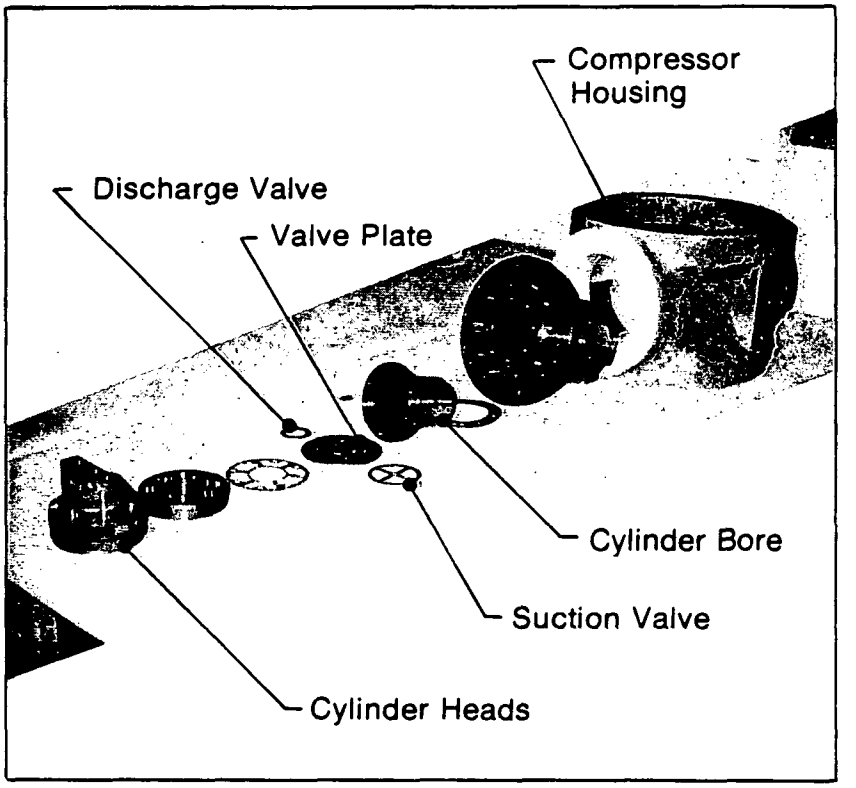

Figure 6-3a HAHP Compressor and Hydraulic-Drive Hardware

MTI-21444A

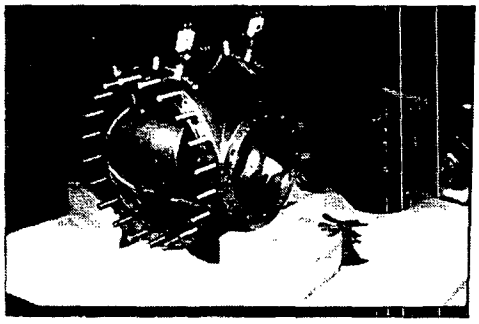

Compressor Housing

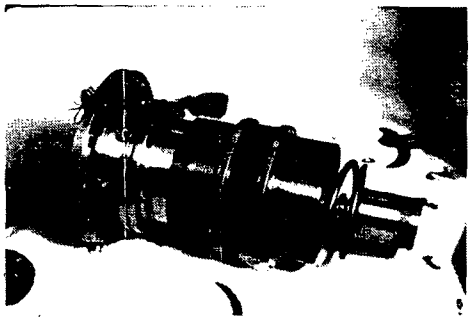

Counterweight Cylinder Sleeve Assembly

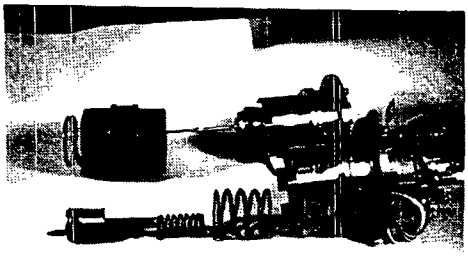

Internal Assemblies

Valve Plate and Cylinder Head Assemblies

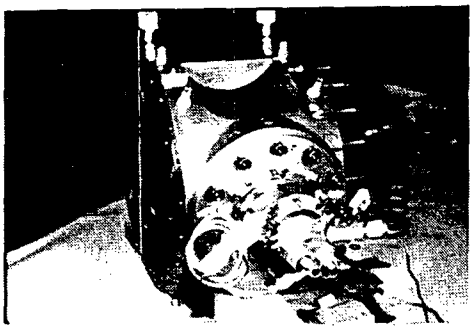

Cylinder Head Assembly

Figure 6-3b Compressor and Hydraulic Transmission Hardware

their final HAHP configurations are: 1) rod area; 2) addition of a transition plate; 3) load; and, 4) addition of variable-piston gas spring volume.

6.1.2 Compressor Description

Power generated by the engine pressure wave is transmitted to the counterweight through an oil volume separated from the engine working gas by a diaphragm. In turn, the counterweight transmits power to the compressor piston through oil volumes C and D (see Figure 2-6a). The piston restoring force comes primarily from the lower end gas spring volume which is worked by the deflection of the lower diaphragm as the counterweight oscillates. The counterweight and compressor piston with cylinder sleeves slide into the housing, and the heads and compressor plenums cap the assembly, as shown in Figure 6-3a. The HAHP breadboard compressor housing is free-standing, taking the high-pressure loads in the casing walls, thus making the cast-iron casing much heavier, but leaving the compressor components accessible for laboratory work.

The hydraulic-drive system depends on effective, close-tolerance clearance seals throughout for its function. It is possible for preferred leakage across the driving seals to occur, resulting in a net oil change in the oil volumes that will cause a drifting of the reciprocating elements from the center location. To correct this potential problem, center-port slots are machined into the bores piloting the reciprocating elements. At the mid-stroke point, the seal is short-circuited by the slots, allowing a fluid connection across the oil volumes. Should the pressure across the piston not be balanced, then corrective flow will occur through the port, balancing the pressure in the volumes on either side. Mechanical springs on the counterweight and compressor piston provide the centering force to keep these elements on center. The resonant compressor is loaded by pumping refrigerant through a water-cooled refrigerant test loop. Some photographs of the compressor and hydraulic transmission hardware is shown are Figure 6-3b.

6.1.3 Refrigerant Loop and Compressor Loading Control

The refrigerant loop (see schematic in Figure 6-4) consists of the following:

- desuperheat heat exchanger (Freon to water);

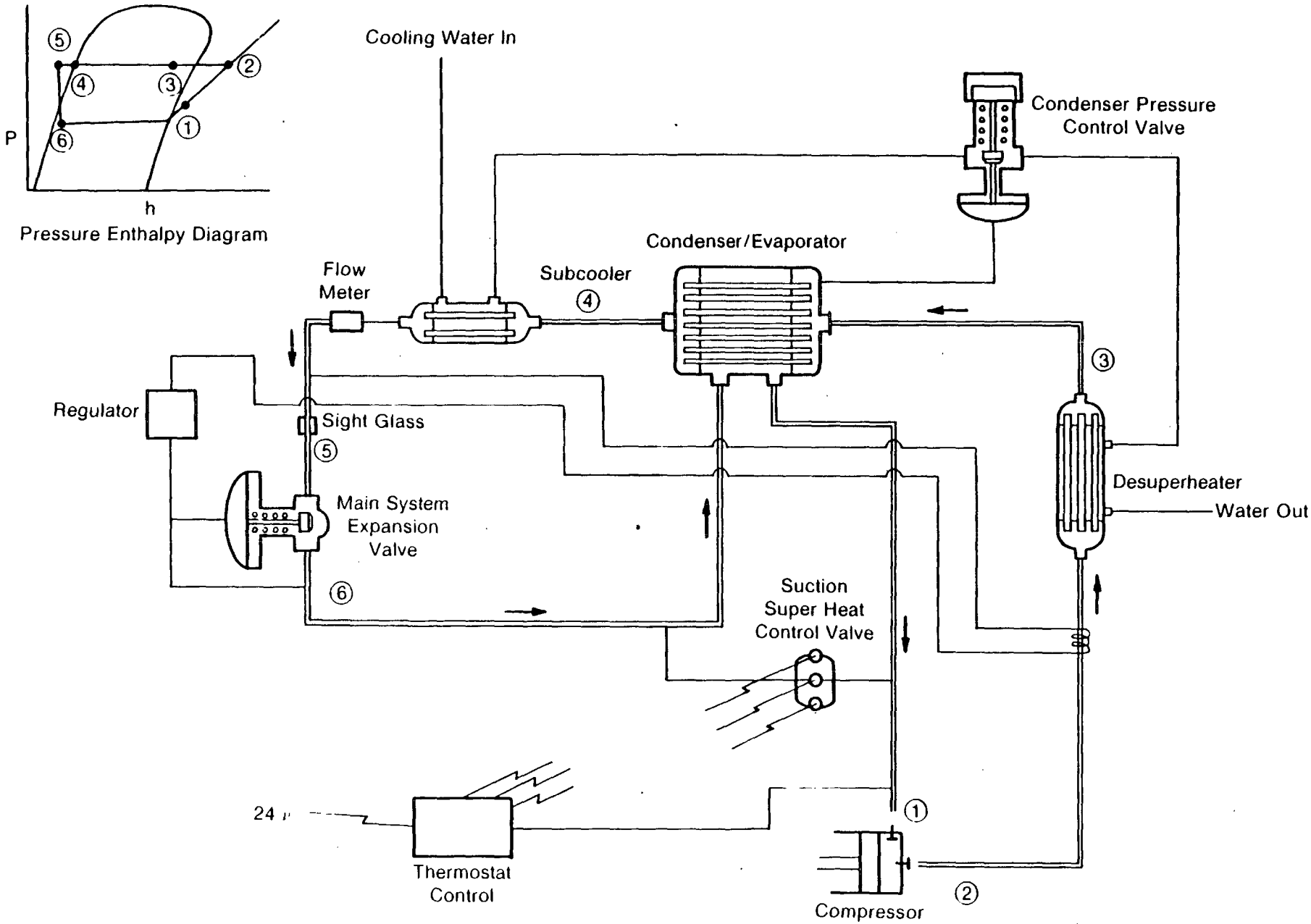

Figure 6-4 Calorimeter System Schematic

832973

- condenser-evaporator (Freon-Freon);
- subcooler/liquid receiver (Freon to water);
- line filter;
- bearingless flow meter;
- vapor quality sight glass;
- main system expansion valve; and,
- thermostatically/manually controlled desuperheat mixing valves.

Water flow is maintained by setting the manual adjustment at the water regulator, which presets the spring tension and provides the force to balance with a sealed pressure force. The sealed pressure force is generated from a temperature bulb (fluid-filled line) referenced to the condenser inlet line downstream of the desuperheater. This arrangement of manual-course adjustment plus constant-temperature fine control will maintain a constant preselected condenser pressure.

The evaporator pressure (temperature) is maintained by the main system expansion valve by way of a through-flow regulator (Grove valve). The driving potential for the Grove valve is a refrigerant loop tap from the upstream liquid side of the valve being flashed to a vapor by a small heat exchanger at the compressor discharge line, venting finally to the low-pressure side of the main expansion valve passing through the Grove valve. The Grove valve is manually set to provide the required evaporator pressure for a given mass flow rate, and the interaction of the regulator and main system expansion valve provide a constant evaporator pressure for varying mass flows.

Compressor suction desuperheat is controlled by mixing wet vapor of low quality from the evaporator inlet to the dry gas at the compressor suction inlet line. Control of the desuperheat valves is accomplished by the action of three thermostatic valves of varying orifice size that can be selected from the control console. The thermal bulb reference to the thermostat controller is located in the suction line. As the suction temperature rises (rising superheat temperature), the thermostat opens the selected desuperheat valve to allow more wet vapor to mix with the superheat vapor cooling the vapor.

The operating range and control characteristics of the three basic controls as a function of mass flow rate for given condenser/evaporator pressures will have to

be determined. It is assumed that the condenser-to-evaporator heat exchanger is of sufficient size so as not to be limiting. The compressor load (for controlled condenser/evaporator pressures) can then be made a function of mass flow rate and compressor mechanical efficiency:

$$\dot{W} = \dot{m}\, n/(n - 1)P_b\nu_b[(P_c/P_b)^{n - 1/n} - 1]\eta_m;$$

where, P_b = compressor suction pressure;
P_c = compressor discharge pressure;
ν_b = specific volume at inlet;
η_m = mechanical efficiency;
η = polytropic gas constant (1.173); and,
$\dot{m}$ = refrigerant mass flow rate.

The compressor mass flow rate for a given geometry and operating frequency is a function of the volumetric efficiency:

$$\dot{m} = \eta_v\, VD/\nu_3;$$

where, η_v = volumetric efficiency;
VD = total swept volume per time; and,
ν_3 = compression volume inlet specific volume (valve pressure drop).

The volumetric efficiency is related to the clearance volume factor:

$$\eta_v = [1 + C - C\,(P_c/P_b)^{1/n}]\nu_3/\nu_b;$$

where, C = clearance volume factor.

Finally, the clearance volume factor can be related to stroke:

$$C = V_d/V_b - V_d;$$

where, V_d = $V_{cl} + X_{p-p}A_p - X_{pL}A_p$;
V_b = $X_{p-p}\, A_p$;
A_p = piston area;
X_{pL} = operating stroke;

X_{p-p} = maximum stroke; and,
V_{cl} = clearance volume.

In summary, within the limitations of the test loop controls, to maintain fixed condenser/evaporator pressures and suction superheat temperature, the compressor load and, hence, engine load can be maintained as a function of stroke once refrigerant flow is established.

6.1.4 HAHP Breadboard System Instrumentation

The HAHP Breadboard System is instrumented to provide 17 time-dependent measurements that yield amplitude, phase, DC offset, and an optional Fourier harmonic analysis. In addition to time-dependent measurements, the system is instrumented to include 12 steady-state measurements and 52 channels of T/C's. These measurements and probe types are outlined in Tables 6-1 and 6-2. Figure 6-5 is a schematic of the HAHP Breadboard System instrumentation. The anticipated calculated output is outlined in Table 6-3, and Table 6-4 is a definition of terms.

6.2 HAHP Breadboard System Test Plan

6.2.1 Introduction

This test plan describes the testing that will be conducted on the HAHP Breadboard System. An overview of the engine and compressor characteristics, and the system interaction with the Refrigerant calorimeter that is used to load the compressor can be found in Section 6.1, which also constains a description of the breadboard system hardware. This section describes the test procedures and test sequencing that will be followed. The objectives of this test program are to:

- achieve steady-state operation at the four simulated ambient operating points of 95°F, 80°F, 47°F, and 17°F;

- map the system steady-state performance over the full HAHP operating conditions with the refrigerant calorimeter; and,

TABLE 6-1
HAHP SYSTEM MEASUREMENT POINTS

Time-Dependent Measurements*:

Parameter	Probe Type
1. Displacer Stroke	Eddy Current
2. Counterweight Stroke	Eddy Current
3. Piston Stroke	Eddy Current
4. Compression-Space Pressure - Displacer Side	Strain Gage and Bridge
5. Compression-Space Pressure - Diaphragm Gas Side	Strain Gage and Bridge
6. Heater-Side Displacer Gas Spring Cavity Pressure	Strain Gage and Bridge
7. Upper Virtual Rod Cavity Pressure	Strain Gage and Bridge
8. Lower Virtual Rod Cavity Pressure	Strain Gage and Bridge
9. Upper Oil Cavity Pressure	Piezoresistive
10. Lower Oil Cavity Pressure	Piezoresistive
11. Compressor LH Valve Plate Pressure	Strain Gage and Bridge
12. Compressor RH Valve Plate Pressure	Strain Gage and Bridge
13. Piston Gas Spring Pressure	Piezoresistive
14. Upper Diaphragm Position	Eddy Current
15. Lower Diaphragm Position	Eddy Current

TABLE 6-2
HAHP SYSTEM MEASUREMENT POINTS

Steady-State Measurements:

Parameter	Probe Type
1. Combustion Airflow	Laminar-Flow Element
2. Fuel Flow	ΔP Transducer, ABS. Pressure/Temperature
3. Temperatures - Air, Gas, and Liquid other than noted below (52 channels)	Type-K Thermocouples
4. Engine Cooling Water Flow	Bearingless Turbine
5. Engine Coolant Temperature Difference	RTD
6. Refrigerant Flow	Bearingless Turbine
7. Compressor Suction Pressure	Piezoresistive
8. Compressor Suction Temperature	Thermistor
9. Compressor Discharge Pressure	Piezoresistive
10. Compressor Discharge Temperature	Thermistor
11. Piston Gas Spring Bellows Position	LVDT
12. Engine Mean Pressure	Piezoresistive

*Amplitude, Phase, DC Offset, Optional Fourier Analysis

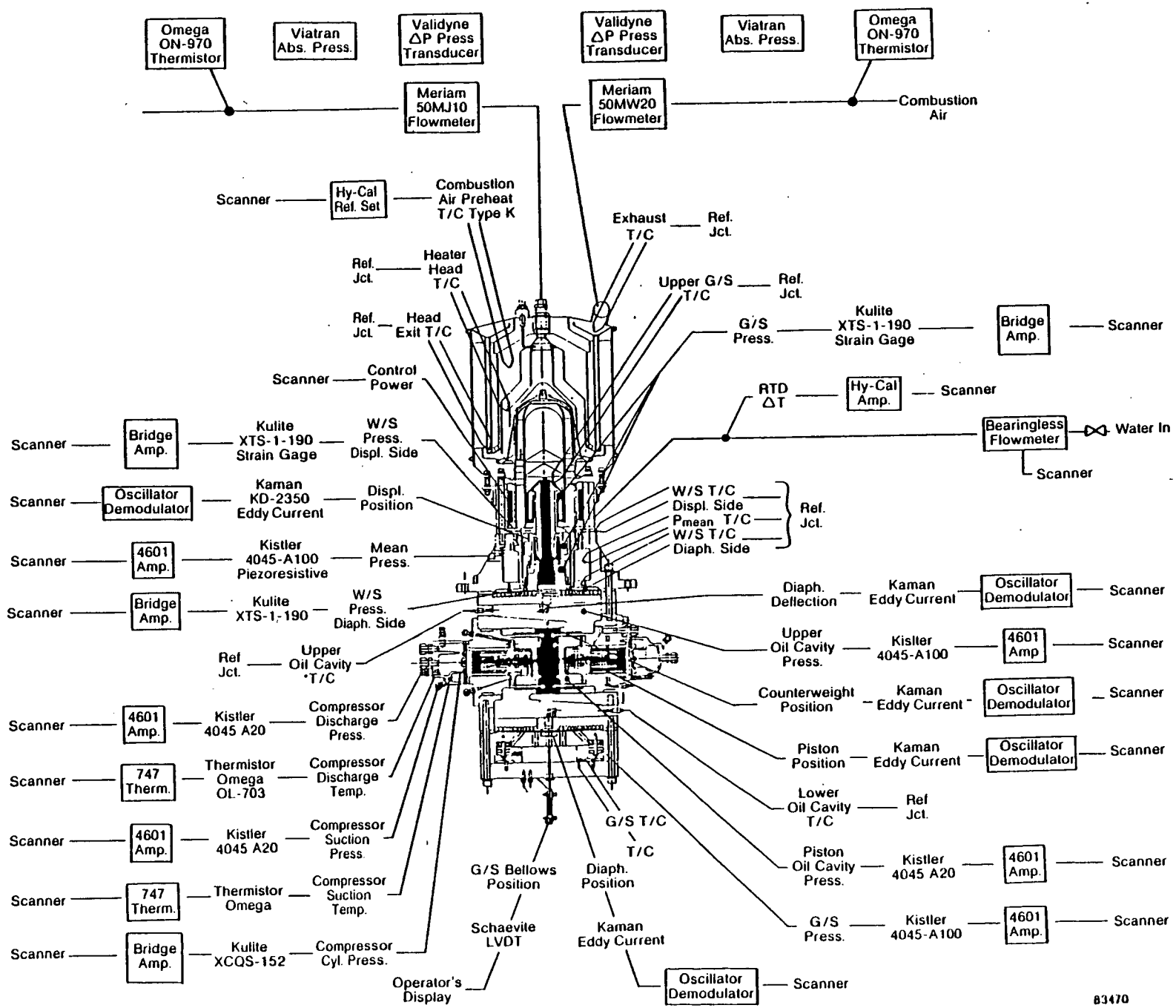

Figure 6-5 HAHP Instrumentation Schematic

TABLE 6-3

HAHP DATA REDUCTION PARAMETERS

System Dynamics

XP	XCW	XD	XUD	XLD
POFFSET	CWOFFSET	DOFFSET	UDOFFSET	LDOFFSET
FREQ	AUD/UD	AXD/LD	AXD/CW	PHID
ACW/XP	ACW/UD	ACW/LD	XD/XP	XCW/XP

Combustor Energy Flow

FUEL FLO	AIRFLOW	A/F	Q RATE	Hair In
HPREHT	HHEADEX	HEXHST	ETA RECP	QHEADC
QHEADE	ENG. BAL	ETA COMB	RAD & CONV	

Displacer Control Power

ALPAM	IRMS	VRMS	MPWRIN	ALPAS
KMS	CMS	FMS	K/KOS	C/COS
ETAMS	SAT			

Displacer G/S Calculations

PGSE	PGSB	PGSA	AGSE	AGSB
AGSA	PWGSE	PWGSB	PWGSA	PWGST
PLGSE	PLGSB	PLGSAS	DHLC	PHGSE
PHGSB	PHGSA	KGSE	KGSB	KGSA
KGST	CGSE	CGSB	CGSA	CGST

System Operating Conditions

KAPPA	PHID	PMEAN	THEAD	XP

Displacer Force Balance

PUCAR	PLCAR	PCAR	APCAR	KDXD
AKDXD	MDXDO	FMS	FRES	AFRES

Displacer Power Balance

PTHER	PGST	PFMS	PRESIDL	DPTRANS
ADPTRANS				

Engine Performance

P-V POWER	ENG QREJ	ETAC	PFAC

Lower-End Drive Performance

PVCW	PVCOMPLH	PVG/S	CWLOSS	PISLOSS
ETACW	ETAPST	PUOC	PLOC	PPG/S
AUOC	ALOC	AG/S	PVCOMRH	ETALEND

Lower-End Dynamics

KUDC	KLDC	KCW	KCOMLH	KPG/S
KT	CC/W	CP	CCOMP	CG/S
CTOT	MOIL	DP/PGS	KCOMRH	CCOMPLH
CCOMPRH	KCOMT			

Compressor Performance

FLO WORK	PCUMPRH	APCOMPRH	FLO-PVP	PDIS
APCOMPLH	TDIS	PSUC	TSUC	PCOMPLH
TSH	ETAVOL			

Engine Pressure

PUCS	APUCS	PLCS	APLCS	PFP
PFD	PFD/PFP			

Heater Head Temperature Distribution

TD 5.32	TD 4.92	TD 4.52	TD 4.22	TD 3.84
TF 3.15	TF 2.40	TF 1.65	TF .895	TF .625

TABLE 6-4

DEFINITION OF TERMS

System Dynamics

XP	Piston Stroke (cm)
XCW	Counterweight Stroke (cm)
XD	Displacer Stroke (cm)
XUD	Upper Diaphragm Displacement (cm)
XLD	Lower Diaphragm Displacement (cm)
POFFSET	Piston Offset (cm)
CWOFFSET	Counterweight Offset (cm)
DOFFSET	Displacer Offset (cm)
UDOFFSET	Upper Diaphragm Offset (cm)
LDOFFSET	Lower Diaphragm Offset (cm)
FRE	System Frequency (H_e)
AXD/UD	Phase Angle - Displacer for Upper Diaphragm (°)
AXD/LD	Phase Angle - Displacer to Lower Diaphragm (°)
PHID	Phase Angle - Displacer to Piston (°)
ACW/XP	Phase Angle - Counterweight to Piston (°)
ACW/UD	Phase Angle - Counterweight to Upper Diaphragm (°)
ACW/XP	Engine Stroke Ratio - Displacer to Piston
XCW/XP	Stroke Ratio - Counterweight to Piston

Combustor Energy Flow

FUEL FLO	Fuel Flow (SCFH)
AIR FLO	Airflow (SCFH)
A/F	AIr Fuel Volume Flow Ratio
Q RATE	Combustor Firing Rate (kW)
HAIR IN	Combustion Air Entrance Enthalpy (kW)
HPREHT	Combustor Preheat Enthalpy (kW)
HHEADEX	Heater Head Gas Exit Enthalpy (kW)
ETARFCP	Recuperator Effectiveness (%)
QHEADC	Heater Head Flux From Combustor Energy Balance (kW)
QHEADE	Heater Head Flux From Engine Energy Balance (kW)
ENG BAL	Engine Energy Balance (kW)
ETACOMB	Combustor Efficiency (%)
RAD & CONV	Calculated Free Convection Loss (kW)

Displacer G/S Calculations

PGSE	Cavity E Pressure Amplitude (Bar)
PGSB	Cavity B Pressure Amplitude (Bar)
PGSA	Cavity A Pressure Amplitude (Bar)
AGSE	Cavity E Pressure Phase (°)
AGSB	Cavity B Pressure Phase (°)
AGSA	Cavity A Pressure Phase (°)
PWGSE	Cavity E Power Loss (watts)
PWGSB	Cavity B Power Loss (watts)
PWGSA	Cavity A Power Loss (watts)
PWGST	Total Displacer Gas Spring Power Loss (watts)
PLGSE	Calculated Cavity E Leakage Loss (watts)
PLGSB	Calculated Cavity B Leakage Loss (watts)

TABLE 6-4 CONTINUED

PLGSA	Calculated Cavity A Leakage Loss (watts)
DHLC	Calculated Effective Compression-Space Leakage Coefficient (m^3)
PHGSE	Calculated Cavity E Hysteresis Loss (watts)
PHGSB	Calculated Cavity B Hysteresis Loss (watts)
PHGSA	Calculated Cavity A Hysteresis Loss (watts)
KGSE	Cavity E Spring Component (N/m)
KGSB	Cavity B Spring Component (N/m)
KGSA	Cavity A Spring Component (N/m)
KGST	Total Gas Spring Stiffness (N/m)
CGSE	Cavity E Damping (N sec/m)
CGSB	Cavity B Damping (N sec/m)
CGSA	Cavity A Damping (N sec/m)
CGST	Total Gas Spring Damping (N sec/m)

System Operating Conditions

KAPPA	Engine Stroke Ratio (XD/XP)
PHID	Engine Phase Angle (°)
PMEAN	Engine Change Pressure (Bar)
THEAD	Mean Heater Temperature (°C)
XP	Piston Stroke (cm)

Displacer Force Balance

PUCAR	Upper Compression-Space Pressure Force (N)
PLCAR	Lower Compression-Space Pressure Force (N)
PCAR	Displacer Engine Force (N)
APCAR	Angle of the Displacer Engine Force (°)
KDXD	Displacer Resultant Spring Pressure Force (N)
AKDXD	Angle of the Spring Pressure Force (°)
MDXDD	Displacer Inertia Force (N)
FMS	Calculated Displacer Control Force (N)
FRES	Residual Displacer Force Magnitude (N)
AFRES	Angle of the Residual Displacer Force (°)

Displacer Power Balance

PTHER	Thermodynamic Displacer Drive (watts)
PGST	Total Gas Spring Loss (watts)
PFMS	Calculated Resultant Control Power (watts)
PRESIDL	Residual Displacer Power (Pumping Power) (watts)
DPTRANS	Transition Section ΔP Magnitude (Bar)
ADDTRANS	Transition Section ΔP Phase (°)

Engine Power Performance

PV POWER	Engine P-V Power (kW)
ENG QREJ	Engine Heat Rejection (kW)
ETAC	Engine Thermodynamic Efficiency (%)
PFAC	Engine Power Factor (1/m)

TABLE 6-4 CONTINUED

Lower-End Drive Performance

PVCW	Counterweight P-V Power (kW)
PVCMLH	Left-Hand Compressor P-V Power (kW)
PVG/S	Piston Gas Spring Power Loss (watts)
CWLOSS	P-V Power - Counterweight Power - G/S Loss (watts)
PISLOSS	CW Power - Compressor Power - G/S Loss (watts)
ETACW	Counterweight Drive Efficiency (%)
ETAPST	Piston Drive Efficiency (%)
PUOC	Upper Oil Cavity Pressure Amplitude (Bar)
PLOC	Lower Oil Cavity Pressure Amplitude (Bar)
PPG/S	Piston Gas Spring Pressure Amplitude (Bar)
AUOC	Upper Oil Cavity Pressure Phase (°)
ALOC	Lower Oil Cavity Pressure Phase (°)
AG/S	Piston Gas Spring Pressure Phase (°)
PVCOMRH	Right-Hand Compressor P-V Power (kW)
ETALEND	Lower-End Drive Efficiency (%)

Lower-End Dynamics

KUDC	Calculated Upper Diaphragm Spring Stiffness (N/m)
KLDC	Calculated Lower Diaphragm Spring Stiffness (N/m)
KCN	Counterweight Spring Component (N/m)
KCOMLH	Compressor Left-Hand Spring Component (N/m)
KRG/S	Piston Gas Spring Component (N/m)
KT	Total Lower-End Spring Stiffness (N/m)
CC/W	Counterweight Damping (N sec/m)
CP	Piston Gas Spring Damping (N sec/m)
CCOMPLH	Left-Hand Compressor Damping (N sec/m)
CCOMPRH	Right-Hand Compressor Damping (N sec/m)
CCOMP	Total Compressor Damping (N sec/m)
CG/S	Piston Gas Spring Damping (N sec/m)
CTOT	Total Lower-End Damping (N sec/m)
MOIL	Equivalent Oil Mass (KG)
DP/PGS	dP/P of Piston Gas Spring
KCOMT	Total Compressor Spring Stiffness (N/m)

Compressor Performance

FLO WORK	in Δh of Compressor (kW)
PCOMPRH	Right-Hand Compressor Chamber Pressure Amplitude (Bar)
APCOMPRH	Right-Hand Compressor Chamber Pressure Angle to Piston (°)
FLO-PVP	m Δh - P-V Compressor (watts)
PDIS	Compressor Manifold Discharge Pressure (psia)
PCOMPLH	Left-Hand Compressor Chamber Pressure Amplitude (Bar)
TDIS	Compressor Manifold Discharge Temperature (°F)
PSUC	Compressor Manifold Suction Pressure (psia)
TSUE	Compressor Manifold Section Temperature (°F)
APCOMPLH	Left-Hand Compressor Chamber Pressure Phase to Piston (°)
TSH	Superheat (°F)
ETAVOL	Volumetric Efficiency

TABLE 6-4 CONTINUED

Engine Pressure Wave

PUCS	Upper Compression-Space Pressure Amplitude (Bar)
APUCS	Upper Compression-Space Pressure Amplitude Phase to Piston (P)
PLCS	Lower Compression-Space Pressure Amplitude (Bar)
APLCS	Lower Compression-Space Pressure Amplitude Phase to Piston (°)
PFP	Piston Pressure Factor (Bar)
PFD	Displacer Pressure Factor (Bar)
PFD/PFP	Pressure Factor Ratio

Heater Head Temperature Distribution

TD 5.32	Average Dome Temperature at Station 5.32 (°C)
TD 4.92	Average Dome Temperature at Station 4.92 (°C)
TD 4.22	Average Dome Temperature at Station 4.22 (°C)
TD 3.87	Average Dome TEmperature at Station 3.87 (°C)
TD 3.15	Average Head Temperature at Station 3.15 (°C)
TF 2.40	Average Head Temperature at Station 2.40 (°C)
TF 1.65	Average Head Temperature at Station 1.65 (°C)
TF .895	Average Head Temperature at Station .895 (°C)
TF .625	Average Head Temperature at Station .625 (°C)

- determine system transient characteristics, and establish the necessary control parameters for a completely automated system.

Individual Test Directives, which will outline the build hardware components, and detail the corresponding test procedures for the major testing task, will be issued commensurate with each major testing task.

Outlined below are systematic procedures encompassing a series of operating tests designed to characterize the dynamic/mechanical behavior and control of the engine/compressor system through the start-up transients in order to achieve the steady-state operating points at the four ARI ambient load conditions. The predicted HAHP engine operating conditions are shown in Tables 6-5 through 6-8. Tables 6-5 and 6-6 compared the operating conditions for a 61.45-cc displacement and 9.68/12.90-cm^2 virtual rod areas. A definition of the virtual rod configuration is given in Section 5.2. Tables 6-7 and 6-8 compare the operating conditions for a 65.5-cc displacement and 9.68/12.90-cm^2 virtual rod areas. Hardware for both the 9.68/12.90-cm^2 virtual rod areas, and the 61.45/65.5-cc diaphragm displacements are available. Having two displacer gas spring rod areas available in hardware allows the flexibility of increasing the displacer thermodynamic drive power by hardware interchange in the event assembly clearances and eccentricities result in higher-than-anticipated gas spring losses. The following tests will establish the:

- displacer gas spring losses;
- engine tuning sensitivity and control;
- design point piston stroke;
- design point condenser/evaporator pressures at intermediate piston strokes; and,
- four ARI operating points.

6.2.2 Test Procedures

6.2.2.1 Displacer Gas Spring Characterization - Figure 6-6 is a sketch of the HAHP displacer gas spring (G/S) geometry. The principle gas spring volumes have been given the nomenclature of Volumes A, B, and E (Volumes C and D have been reserved for the compression space and drain volumes). This nomenclature has been maintained in the computer code and data reduction logic. Also indicated

TABLE 6-5
PREDICTED HAHP ENGINE OPERATING CONDITIONS

Virtual Rod Area: 9.6774 cc
Diaphragm Displacement: 61.45 cc @ 95°F

Outdoor Temperature (°F)		95	80	47	17
Xp	(mm)	9.525	5.118	5.753	11.379
Xd	(mm)	9.725	3.642	2.736	8.641
ϕd	(deg)	70.9	61.9	65.4	52.7
Pc	(Bar)	5.55	2.73	3.18	5.61
θc	(deg)	-97.8	-83.4	-78.8	-73.3
Ps	(w)	497	-32.1	-101	-51.9
cm	(deg)	-0.8	118.9	160.4	98.2
P-V	(watts)	2907	624	507	2712
ηc		.354	.338	.331	.412
Qin	(watts)	7965	2180	1913	7343
Qrej	(watts)	5143	1443	1280	4317
σ	(1/s)	-20.7	-12.0	-4.6	-10.7

TABLE 6-6
PREDICTED HAHP ENGINE OPERATING CONDITIONS

Virtual Rod Area: 12.903 cc
Diaphragm Displacement: 61.45 cc @ 95°F

Outdoor Temperature (°F)		95	80	47	17
Xp	(mm)	9.525	5.118	5.753	11.379
Xd	(mm)	10.82	4.001	3.007	9.568
ϕd	(deg)	70.0	61.3	64.6	52.1
Pc	(Bar)	5.55	2.73	3.18	5.61
θc	(deg)	-96.9	-82.8	-77.8	-72.6
Ps	(w)	450	-114	-151	-201
cm	(deg)	-3.9	114.2	158.5	109.9
P-V	(watts)	2907	624	507	2712
ηc		.342	.344	.341	.406
Qin	(watts)	5710	1537	1345	4748

TABLE 6-7
PREDICTED HAHP ENGINE OPERATING CONDITIONS

Virtual Rod Area: 9.6774 cc
Diaphragm Displacement: 65.55 cc @ 95°F

Outdoor Temperature (°F)		95	80	47	17
Xp	(mm)	9.525	5.118	5.753	11.379
Xd	(mm)	9.355	3.521	2.681	8.409
ϕd	(deg)	70.2	60.5	63.3	51.9
Pc	(Bar)	5.76	2.87	3.35	5.96
θc	(deg)	-94.2	-79.6	-75.0	-69.9
Ps	(w)	387	-85.5	-70.8	-108
cm	(deg)	1.6	143.1	148.3	105.7
P-V	(watts)	2907	624	507	2712
ηc		.366	.343	.333	.417
Qin	(watts)	8087	2185	1923	7475
Qrej	(watts)	5127	1435	1282	4361
σ	(1/s)	-19.4	-10.0	-4.8	-9.7

TABLE 6-8
PREDICTED HAHP ENGINE OPERATING CONDITIONS

Virtual Rod Area: 12.903 cc
Diaphragm Displacement: 65.55 cc @ 95°F

Outdoor Temperature (°F)		95	80	47	17
Xp	(mm)	9.525	5.118	5.753	11.379
Xd	(mm)	10.42	3.872	2.951	9.322
ϕd	(deg)	69.3	59.9	62.4	51.3
Pc	(Bar)	5.77	2.88	3.36	5.97
θc	(deg)	-93.4	-78.9	-74.1	-69.3
Ps	(w)	285	-161	-136	-272
cm	(deg)	12.1	149.7	151.9	114.3
P-V	(watts)	2907	624	507	2712
ηc		.356	.349	.343	.413
Qin	(watts)	8813	2339	2051	8121
Qrej	(watts)	5671	1522	1347	4771
σ	(1/s)	-17.9	-7.5	-2.7	-8.2

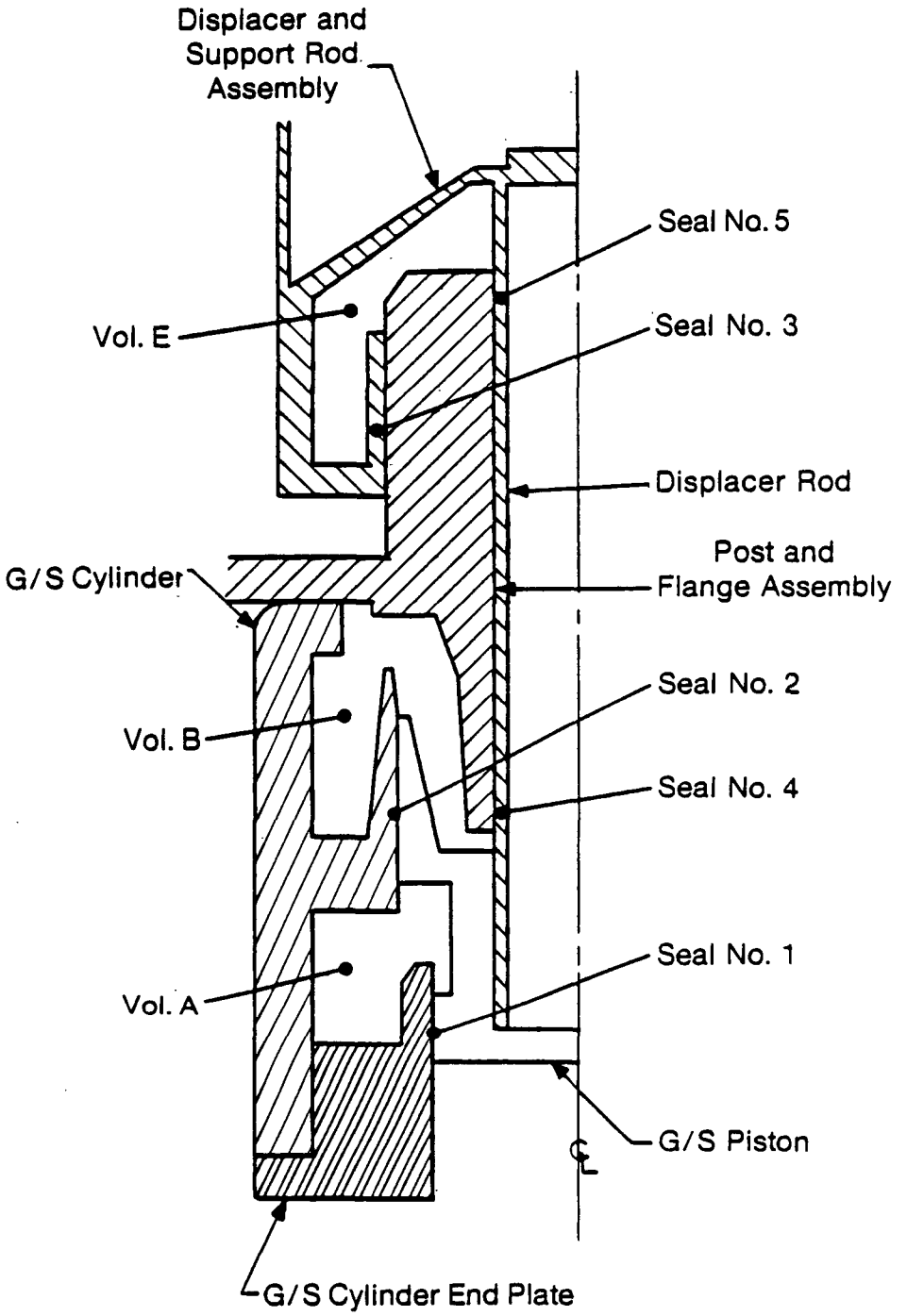

Figure 6-6 HAHP Displacer Gas Spring Volumes

83460

in Figure 6-6 are the five gas spring clearance seals (1 through 5) numbered in a manner similar to the volumes to maintain commonality between hardware and software. The baseline hardware procured allows for 9.677-cm2 and 12.903-cm2 rod areas. By changing out the G/S piston and G/S end plate to change the virtual rod diameter at Seal 1, the rod area can be changed. Gas spring Volumes A and B constitute the virtual rod packaging that was required to allow flexibility in rod area changes for the HAHP configuration. Volume E remains unchanged from the basic geometry of the EM engine.

Figure 6-7 is a plot of the calculated gas spring loss as a function of displacer stroke for the worst case clearances, an assumed eccentricity of 80%, and a virtual rod area of 9.677 cc. Instrumentation of the gas spring volumes consists of pressure transducers in each volume and the displacer position probe. Section 3.1.4 listed the parameters to be calculated as part of the gas spring data reduction. Data reduction calculations will then allow plots of predicted gas spring performance for given geometry and operating conditions.

Method of Execution

1. Prepare the system facility for engine operation.

2. Center the oscillating masses, and unload the piston.

3. Set the design frequency of 60 Hz at the oscillator; set maximum gain at the oscillator with zero gain at the Elgar AC power supply.

4. Begin to stroke the displacer, adding heat as required to achieve the design displacer stroke with a minimum of power transferred to the piston.

5. Take engine data at discrete displacer stroke values to generate a map of displacer gas spring behavior versus displacer stroke.

6. Repeat the procedure by modulating the frequency to maintain zero alpha angle while the displacer is stroked, transferring minimum power to the piston.

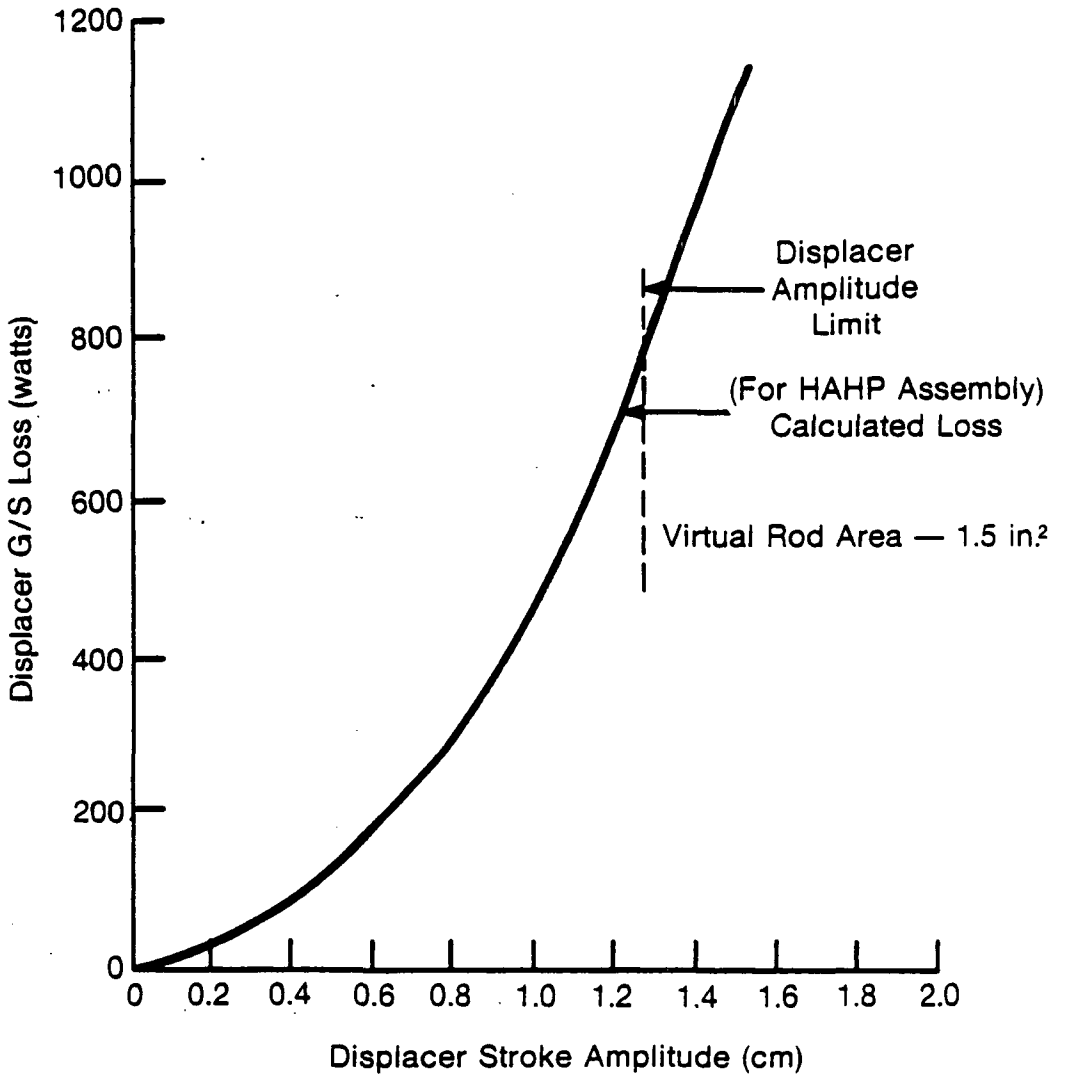

Figure 6-7 Calculated Displacer Gas Spring Losses Versus Displacer Stroke

83418

6.2.3 Engine Tuning Sensitivity and Control

The HAHP Engine/Compressor Breadboard System has two external, direct-tuning controls - the variable-volume piston gas spring and variable-frequency displacer control. Deviations in compressor load conditions will affect the reactive power component of the compressor and, hence, the bottom-end stiffness. Depending on stroke, and due to nonlinearities, bottom-end stiffness is expected to vary with operating conditions, thus affecting system tuning. The object of this test series is to gain system operation experience, and experimentally determine optimum control settings through start-up transients.

Method of Execution

1. Start the system and heat the heater head to 500°C, driving the system at 60 Hz.

2. Establish a piston operating stroke of 1.2 cm and displacer stroke ratio of .959 by loading the piston with closure of the loop expansion valve if necessary. Maintain a loop condenser pressure of 19.1 Bar by modulating the desuperheat water flow valve. Set up the loop desuperheat control for a 10-15° suction superheat.

3. While maintaining the 1.2-cm piston stroke and.959 stroke ratio, change the frequency +2 Hz from 60 Hz in 0.5-Hz increments; continue to sweep frequency until minimum control is established.

4. Reestablish the 60-Hz operating point and sweep the piston gas spring volume control, taking discrete data points until the minimum motor current point is established.

5. Reestablish the optimum system operation frequency; at that frequency, sweep the gas spring volume control to find the optimum setting.

6. Repeat the above procedures at piston strokes of 1.4, 1.6, 1.8, and 2.0 cm.

7. Heat the system to 600°C and 700°C, and repeat the above.

8. The above procedures will allow mapping the system for optimum frequency and gas spring volume at the design stroke ratio and condenser pressure.

6.2.4 Design Point Piston Stroke

The purpose of this test sequence is to gain experience in engine/compressor operation through the start-up transient to design piston stroke, providing shakedown evaluation of the mechanical operation of the engine. It is not intended to establish design point operation during this test, but to provide sufficient compressor loading to allow control of the piston stroke so that lower-end drive losses and dynamics may be evaluated.

Method of Execution

1. Prepare the system facility for engine operation.

2. Unload the piston by opening the loop expansion bypass valve; operate the displacer, adding heat to start piston oscillation.

3. Operate the displacer, and add heat to the engine to start piston oscillation.

4. Heat the engine and continue to operate the displacer with the piston unloaded until the design piston stroke is attained.

5. Take data points at discrete piston strokes to allow evaluation of lower-end losses as a function of piston stroke.

6.2.5 Design Point Condenser/Evaporator Conditions at Intermediate Piston Strokes

The purpose of this test is to establish load control experience for lower system mass flows and compressor volumetric efficiencies at the design point condenser/evaporator temperature (pressure) conditions.

Method of Execution

1. Prepare the system facility for engine operation.

2. Unload the piston by opening the loop expansion bypass valve; operate the displacer, adding heat to start piston oscillation.

3. Continue to drive the piston until a stroke of 1.4 cm is achieved.

4. Maintain the 1.4-cm stroke and design point stroke ratio while powering the engine by adding heat and closing down the loop expansion valve.

5. Continue to allow condenser pressure to build up and evaporator pressure to drop until design pressures are attained. Steady the condenser pressure by selecting the proper desuperheat water flow and evaporator pressure with the proper setting of the loop expansion Grove valve.

6. Select the proper degree of suction superheat (10-15°), and steady the system.

7. Select the optimum engine tuning by modulating frequency and gas spring volume to establish the minimum control current.

8. Heat engine to design head temperature; maintain piston stroke.

9. Stroke the engine in increments of 0.2 cm to the design stroke, and repeat the above procedures.

6.2.6 Establishing the Four ARI Operating Points

The compressor operating points, design specifications, and power requirements are tabulated in Tables 6-9 and 6-10. The object of this test is to bring together the experiences of the engine/compressor input power, tuning, and load controls to demonstrate the ARI operating points outlined in Table 6-9. It is

TABLE 6-9

COMPRESSOR POWER AND EFFICIENCY

Predicted (or Calculated)

Outdoor Temperature	°F	95	80	47	17
Stroke	mm (in)	19.1 (0.750)	10.2 (0.403)	11.5 (0.453)	22.8 (0.896)
Evaporator Pressure	Bar (psia)	6.25 (90.7)	7.67 (111.3)	5.75 (83.4)	2.91 (42.2)
Suction Valve ΔP	Bar (psi)	0.52 (7.5)	0.30 (4.3)	0.19 (2.7)	0.33 (4.8)
Suction Pressure	Bar (psia)	5.74 (83.2)	7.38 (107.0)	5.56 (80.7)	2.58 (37.4)
Condenser Pressure	Bar (psia)	19.13 (277.4)	13.35 (193.6)	13.02 (188.8)	18.23 (264.4)
Discharge Valve ΔP	Bar (psi)	0.90 (13.1)	0.45 (6.5)	0.26 (3.8)	0.70 (10.2)
Discharge Pressure	Bar (psia)	20.03 (290.5)	13.80 (200.1)	13.28 (192.6)	18.93 (274.6)
Work w/o ΔP/Work w/ΔP		0.885	0.880	0.936	0.909
Compressor η	(.94 x above)	0.832	0.827	0.880	0.854
Adiabatic Power	(watts)	2001	391	280	1725
Actual Power	(watts)	2405	473	318	2020
Compressor Damping	(N-S/m)	373.0	254.1	135.2	219.5
Compressor Stiffness	(N/m)	3.256×10^5	3.133×10^5	3.226×10^5	2.577×10^5
Suction Gas Superheat	°C (°F)	6-8 (10-15)	6-8 (10-15)	6-8 (10-15)	6-8 (10-15)

TABLE 6-10

COMPRESSOR SEAL LOSS

Predicted

Outdoor Temperature	°F	95	80	47	17
Oil Temperature	(°C)	38	27	27	47
Total Seal Loss	(watts)	427	129	162	599
Itemized Losses	(∿watts)				
Balance Drive Seal	(2)	42	11	14	72
Balance Piston Seal		32	7.7	9.8	59
Balance Sleeve Seal	(2)	46	13	17	76
Pumping Ring	(2)	70	38	42	84
Compression Suction Seal	(2)	3.8	2.0	2.4	4.4
Oil Viscous Loss		2.2	0.5	0.7	3.2
Piston Rings	(2)	234	56	76	320

intended at this time to demonstrate the ARI operating points in the following order: 80°F ambient day, 47°F, 95°F, and 17°F. The following procedures outline the approach to establish the 80°F ambient-day operating point. Establishing the remaining operating points will be accomplished in a similar manner.

Method of Execution

1. Prepare the system facility for engine operation.

2. Unload compressor piston by opening loop expansion bypass valve; operate the displacer, adding heat to start piston oscillation.

3. Continue to drive piston until a stroke of 1.024 cm is attained.

4. Maintain piston stroke by closing down the loop expansion valve, and allowing condenser pressure to rise while operating the displacer as the system heats up.

5. Maintain system tuning by modulating the system drive frequency and variable-piston gas spring volume as previously determined.

6. Once a discharge pressure of 13.35 Bar is achieved, open the manual adjust, compressor discharge desuperheat water valve to set the condenser pressure of 13.35 Bar.

7. Continue to close the loop regulator expansion valve to set a suction pressure of 7.674 Bar.

8. Adjust the suction superheat control to set 10-15° of suction superheat, and allow the system to stabilize.

7.0 COMPRESSOR DEVELOPMENT

7.1 Compressor Description

Figure 7-1 shows the HAHP compressor assembly, which consists of a plunger and counterweight that are hydraulically coupled to each other, compression pistons and cylinders, and a gas spring. A compressor piston is located at each end of the plunger and valve plates, and plenum chambers are outboard of the pistons. The engine and gas spring diaphragms hermetically seal the hydraulic oil in the transmission (Volumes A, B, C, and D) from the working fluids in the engine and gas spring. The diaphragms also provide the force transfer link from the engine to the transmission fluid. The high-pressure oil in the transmission is sealed from the refrigerant by oil seals located along the piston shafts. The compressor is double-acting with valve assemblies and flow plenums (cylinder heads) located on either side of the housing. An integral ring-type reed valve is used for the suction valves, and a spring-backed ring valve is used for the discharge valves. The cylinder heads have common suction and discharge manifolds that connect to the refrigerant test loop described in Section 6.1.3. Tables 7-1 through 7-4 list design specifications for the compressor.

7.2 Compressor Development Objectives

The purpose of HAHP compressor development testing is to provide an optimized compressor as a whole component for the HAHP breadboard system, and to develop subcomponents of the compressor itself. These subcomponents include:

- Chevron seals;
- pumping ring seals;
- suction and discharge valves and plenums;
- clearance seals and mid-stroke ports;
- diaphragms and diaphragm support plates;
- oil-level sensors; and,
- bellows-actuated spool valves.

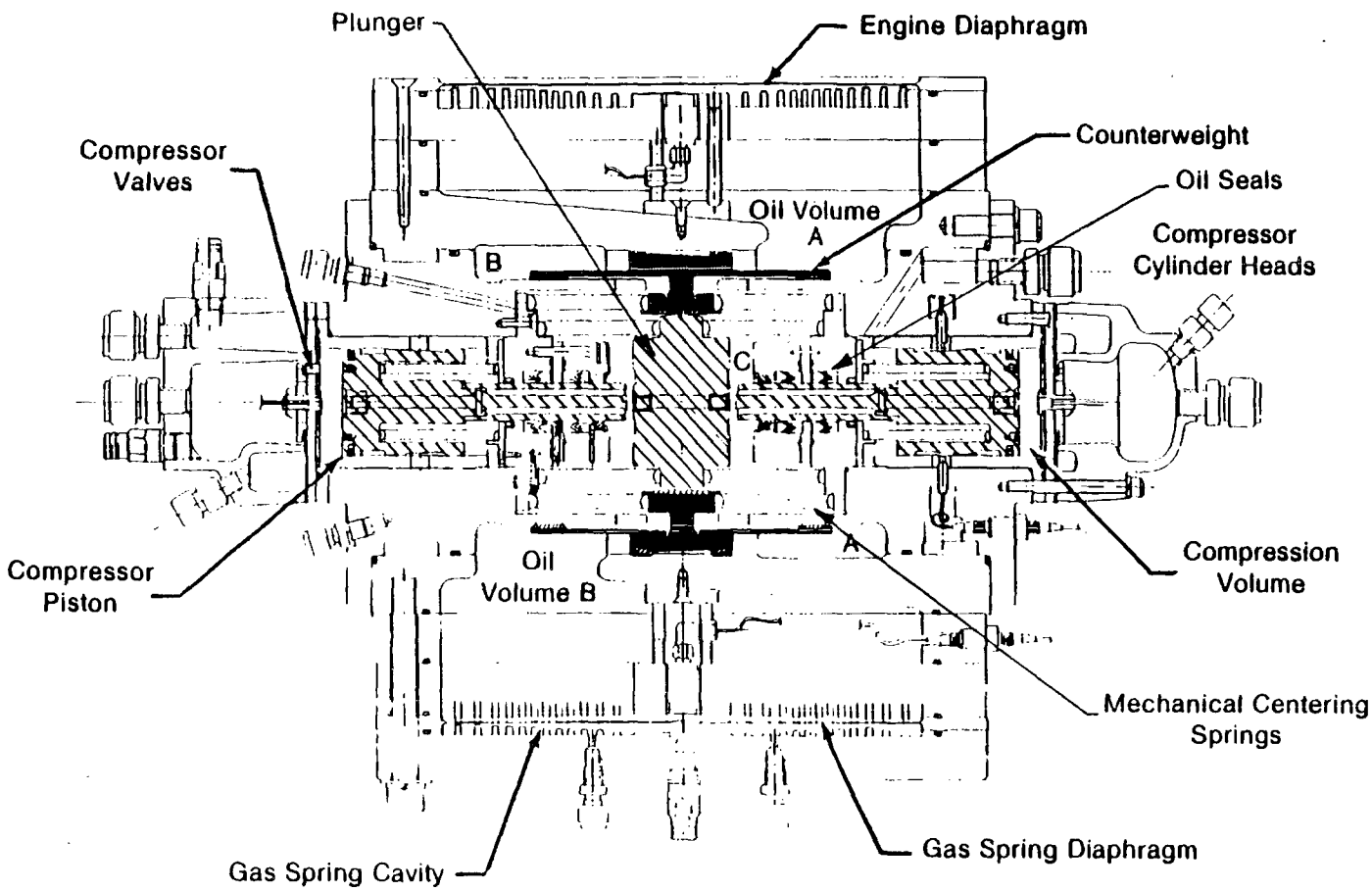

Figure 7-1 HAHP Compressor Assembly

TABLE 7-1
HAHP OPERATING POINTS

Outdoor Temperature	°F	95		80		47		17	
Heating/Cooling Load	Joule/s (Btu/hr)	-10,551	(-36,000)	-5275	(-18,000)	+4103	(+14,000)	+11,137	(+38,000)
Evaporator Pressure	Bar (psia)	6.25	(90.6)	7.67	(111.30)	5.75	(83.40)	2.91	(42.2)
Condenser Pressure	Bar (psia)	19.13	(277.4)	13.35	(193.60)	13.02	(188.8)	18.23	(264.4)
Evaporator Temperature	°C (°F)	7.2	(45.0)	14.1	(57.30)	4.5	(40.1)	-15.4	(4.20)
Condenser Temperature	°C (°F)	49.3	(120.8)	34.4	(93.90)	33.4	(92.2)	47.2	(117.0)
Refrigerant Flow Rate	kg/hr (lbm/hr)	258.6	(570.0)	104.6	(230.60)	50.1	(110.4)	131.8	(290.6)

TABLE 7-2
COMPRESSOR DESIGN SPECIFICATIONS

Outdoor Temperature	°F	95		80		47		17	
Piston Area	cm^2 (in^2)	23.9	(3.70)	23.9	(3.70)	23.9	(3.70)	23.9	(3.70)
Piston Stroke	mm (in)	19.1	(0.750)	10.2	(0.403)	11.5	(0.453)	22.8	(0.896)
Suction Volume	mℓ (in^3)	25.2	(1.54)	8.6	(0.52)	6.2	(0.38)	27.7	(1.69)
Swept Volume	mℓ (in^3)	45.4	(2.77)	24.4	(1.49)	27.5	(1.68)	54.2	(3.31)
Clearance Volume	mℓ (in^3)	10.5	(0.64)	21.1	(1.28)	19.5	(1.19)	6.1	(0.37)

TABLE 7-3

COMPRESSOR POWER AND EFFICIENCY

Outdoor Temperature	°F	95	80	47	17
Stroke	mm (in)	19.1 (0.750)	10.2 (0.403)	11.5 (0.453)	22.8 (0.896)
Evaporator Pressure	Bar (psia)	6.25 (90.7)	7.67 (111.3)	5.75 (83.4)	2.91 (42.2)
Suction Valve ΔP	Bar (psi)	0.52 (7.5)	0.30 (4.3)	0.19 (2.7)	0.33 (4.8)
Suction Pressure	Bar (psia)	5.74 (83.2)	7.38 (107.0)	5.56 (80.7)	2.58 (37.4)
Condenser Pressure	Bar (psia)	19.13 (277.4)	13.35 (193.6)	13.02 (188.8)	18.23 (264.4)
Discharge Valve ΔP	Bar (psi)	0.90 (13.1)	0.45 (6.5)	0.26 (3.8)	0.70 (10.2)
Discharge Pressure	Bar (psia)	20.03 (290.5)	13.80 (200.1)	13.28 (192.6)	18.93 (274.6)
Work w/o ΔP/Work w/ΔP		0.885	0.880	0.936	0.909
Compressor η	(.94 × above)	0.832	0.827	0.880	0.854
Adiabatic Power	(watts)	2001	391	280	1725
Actual Power	(watts)	2405	473	318	2020
Compressor Damping	(N-S/m)	373.0	254.1	135.2	219.5
Compressor Stiffness	(N/m)	3.256×10^5	3.133×10^5	3.226×10^5	2.577×10^5
Suction Gas Superheat	C (°F)	6-8 (10-15)	6-8 (10-15)	6-8 (10-15)	6-8 (10-15)

TABLE 7-4

COMPRESSOR SEAL LOSS

Outdoor Temperature	°F	95	80	47	17
Oil Temperature	(°C)	38	27	27	47
Total Seal Loss	(watts)	427	129	162	599
Itemized Losses	(~watts)				
Balance Drive Seal	(2)	42	11	14	72
Balance Piston Seal		32	7.7	9.8	59
Balance Sleeve Seal	(2)	46	13	17	76
Pumping Ring	(2)	70	38	42	84
Compression Suction Seal	(2)	3.8	2.0	2.4	4.4
Oil Viscous Loss		2.2	0.5	0.7	3.2
Piston Rings	(2)	234	56	76	320

The test plan includes procedures for testing all of these components except for the pumping rings, the bellows-actuated spool valve, and the diaphragms; these will be covered in a separate test plan.

7.3 Test Objectives

Objectives of this test are to optimize and characterize the operation of the hydraulic drive system, observe and optimize compressor valve performance, map compressor performance, and demonstrate steady-state operation at the 95°F ambient-day design point and operation over the range of desired conditions. To characterize the compressor independent of the engine, the hydraulic simulator described in Section 3.3.4 will be used as the driver, thus enabling a straight electric-drive system to be used that will eliminate the dynamic interaction between engine and compressor that occurs in the Breadboard System.

7.4 Test Plan Procedures

7.4.1 Establish Tuning of the System

Any linear-oscillating device, or system of devices, require that total effective mass and spring rate must be in such a relationship so that natural frequency matches that which is desired (and at which the driver power supply operates). In the HAHP Breadboard System, the compressor is designed to operate at 60 Hz with a 60-Bar charge pressure; however, when the compressor is coupled to the hydraulic simulator, the total effective mass of the system is greater than for the breadboard, so a greater spring rate is required to operate at 60 Hz. Spring rate for the gas springs can be varied proportionally to charge pressure. For the volume of gas springs provided, it has been calculated that ∿70-Bar pressure will be required to operate at 60 Hz.

To establish tuning (which is determined by the phase angle between motor current and plunger position)*, the following execution was followed:

---

*while 90° is theoretically ideal tuning, maximum power occurs when the phase angle is ∿110°.

- vacuum and charge the system to 40 Bar;
- keep oil management circuitry deactivated;
- provide power to the motor; observe operating characteristics of system; and,
- increase charge pressure in 2.5-Bar increments until tuning is optimized.

7.4.2 Reinjection of Hydraulic Fluid

High-pressure oil will leak past the piston journal seals, so it must be collected and periodically reinjected to maintain centering of the diaphragms.

Initial testing will be conducted with Chevron seals. The test procedure is to observe operation of the reinjection system while the compressor is running to see how it affects the operation of the compressor both with and without freon load, to make necessary adjustments, and determine leakage rates. The seal leakage rate is measured by timing how long it takes to fill the oil-level sensor tank, which has a capacity of $\sim$30 mℓ ($\sim$2 in.^{3}).

7.4.3 Evaluation of Clearance Seals and Mid-Stroke Ports

Proper functioning of sliding seals and mid-stroke ports is necessary for operation of the compressor at large strokes. Excessive leakage of oil around the clearance seals will result in an inability to reach full compressor piston stroke. Ineffective mid-stroke ports will fail to keep the moving components centered, which will result in them striking the bump stops before full stroke is reached; therefore, the seals and ports must be tested and optimized before long-stroke operation can be demonstrated. To evaluate seal leakage, the following execution will be followed:

- operate system to 12 mm in compressor piston stroke increments of 1 mm;
- record stroke ratios between the three moving components; and,
- if total compressor piston stroke attenuation exceeds 10%, adjustment of seal clearances may be necessary.

To evaluate mid-stroke porting, the following execution will be followed:

- operate system to 12 mm in compressor piston stroke increments of 1 mm;

- at each stroke, allow the oil management system to go through at least one cycle with only one injection port opened to one of the cavities A, B, C, or D (as shown in Figure 7-1), and observe the mean positions of the moving components during this operation;

- produce an external biasing force on the compressor piston by isolating and pressurizing the vent chamber behind one piston, record the net force applied versus mean offset of the piston for each stroke increment, and observe the ability of the mid-stroke ports to allow the piston to move back to center after the force is removed; and,

- if the moving components fail to return to within 1 mm of mid-stroke, or if the compressor piston moves too readily off center when a biasing force is applied, adjustment of mid-stroke ports may be necessary.

When the above tests have been completed, and the seals and ports are performing satisfactorily, the same tests should be performed at compressor piston strokes of 15 and 19 mm.

7.4.4 Quantify Parasitic Losses

Since the compressor will be running at greater pressure amplitudes in development testing than in the breadboard system, parasitic losses measured in this test can be expected to be greater than that experienced by the breadboard. Instrumentation into the compressor allows measurement of power at several points in the compressor and, by comparing these, certain groups of parasitic losses can be quantified; these are:

- counterweight clearance seals (friction and leakage combined) plus a portion of hydraulic fluid losses; and,

- high-pressure seal friction (Chevron seals or pumping rings) plus balance seals, piston journal bearings, and piston compression rings.

The compressor will be operated in compressor piston stroke increments of 2 mm up to 19 mm for recording of data, and the loss measurements made by calculating the dot product of piston motions with the force due to the pressure difference acting on the area.

The general equation power calculation is:

$$W = \pi \text{ frequency} \times \text{area} \times Po \times Xo \times \sin \alpha_{p,x};$$

where, Po is the amplitude of the pressure wave, Xo is the amplitude of the piston position, and $\alpha_{p,x}$ is the phase angle between them.

7.4.5 Optimize Compressor Valve Performance

Several assembly options are available to adjust valve performance. Suction and discharge valves have been fabricated from a selection of material thicknesses that allow variation of valve mass and spring rate. Cylinder head spacers enable adjustment of plenum volumes from a minimum of 75 mℓ to 300 mℓ (5 in.^{3} to 20 in.^{3}) per cylinder.

Initial operation will be from rest with equal suction and dicharge pressures, slowly building up the pressure ratio while observing P-V traces for indications of valve characteristics. Suction pressures should be kept in the 6 Bar (90 psia) range to simulate high ambient-temperature heat pump operating conditions. Low-suction-pressure (winter conditions) testing will be performed after satisfactory operation has been achieved with summer conditions.

Overall compression performance data and P-V diagrams will be recorded for stroke increments of 2 mm to 19 mm. This will be repeated for several hardware combinations to determine the best combination from the selection available.

Inspection of parts after test will also help in the evaluation of valves. Any evidence of fatigue cracking, fretting, or extrusion is indicative of unsatisfactory valve characteristics.

7.4.6 Mapping of Compressor Performance

After optimization of the valves, performance of the compressor can be mapped. All testing will be done in stroke increments of 2 mm up to 19 mm, and evaporator temperatures between 0°C and 15°C in 3°C increments, with compressor suction temperature at 3° superheat in all cases.

In addition, compressor performance data, including P-V diaphragms, should be recorded for operating conditions that approximate the four HAHP specification operating points. Note that this test plan does not call for operation at strokes exceeding 19 mm because of drive limitations. For this reason, the 17°F day conditions will not be reproduced during compressor development testing.

7.5 Test Results

Testing during this report period covered the last of the hydraulic simulator testing (including demonstration of principles that are critical to the oil management system), and shakedown of the HAHP compressor.

7.5.1 Hydraulic Simulator Tests

Modifications to the hydraulic simulator*, made in preparation for compressor testing, have been completed, and the simulator has successfully operated up to its full design stroke of 25 mm. From the results obtained, it was noted that:

- Initial runs agreed with predictions (see Figure 7-3). A later run where parts wore in, was much better than the prediction. The drop in power above 15-mm strokes appears to have occurred from a wearing in or seating of the piston bearing pads. This reduction remained

*see Figure 7-2 for a schematic of the hydraulic simulator

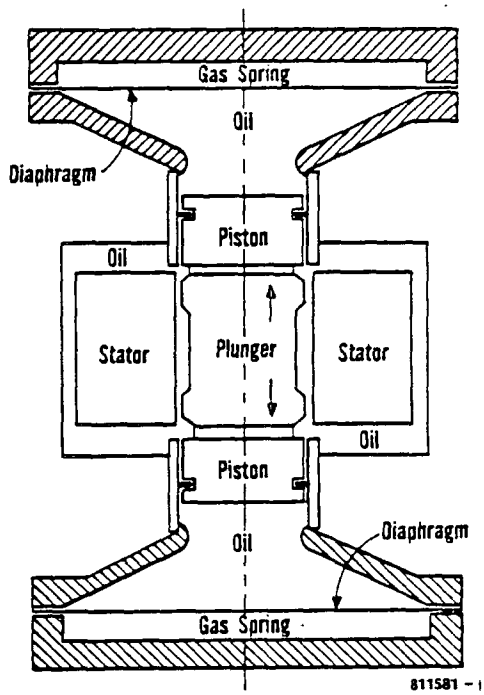

Figure 7-2 Hydraulic Simulator Test Rig

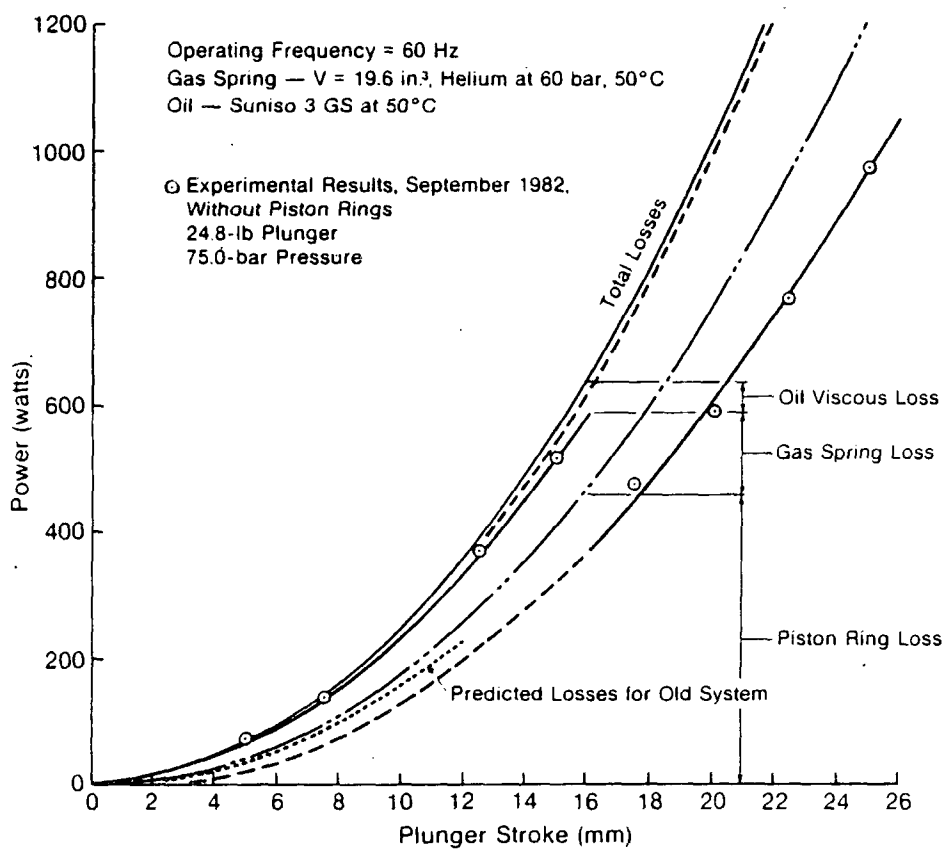

Figure 7-3 Hydraulic Simulator, 3.250" ϕ Pistons - Predicted Losses

constant at the higher strokes, and was repeatable; time prevented retaking data at the lower strokes.

- When the simulator was first run after the modifications, input power was very high - ~1.5 kW at 12-mm stroke. It was reasoned that the high power was caused by the large pressure amplitudes that were required to resonate the new piston. By reducing piston mass, the losses decreased dramatically (shown in Figure 7-4 for the two cases of running with cast-iron piston rings and without). The significance of this data to the actual pressure amplitude in the compressor is shown by the point representing the "Equivalent HAHP Compressor Operating Condition." This provides some additional verification for the low transmission losses projected for the heat pump system.

- No surging of centering springs was noticed at the 25-mm stroke. The centering springs had the following characteristics.

Maximum Stroke	30.5 mm (1.20 in.)
Surge Frequency	189 CPS
Maximum Stress @ 25 mm	503.3 MPa (73,000 psi)
Prestress	100.8 MPa (14,630 psi)
Material	AISI-6150 A232

From past experience in a helium environment, these springs could have caused difficulties. The oil must provide sufficient damping to eliminate surging.

7.5.2 Oil Management System Testing (No Refrigerant)

The simulated oil management system shown in Figure 7-5 was run on the hydraulic simulator. Testing results revealed that:

- the amount of oil in each of the volumes could be controlled within safe working limits of diaphragm offset deflections;

- the center porting was effective in distributing the oil uniformly between all volumes; and,

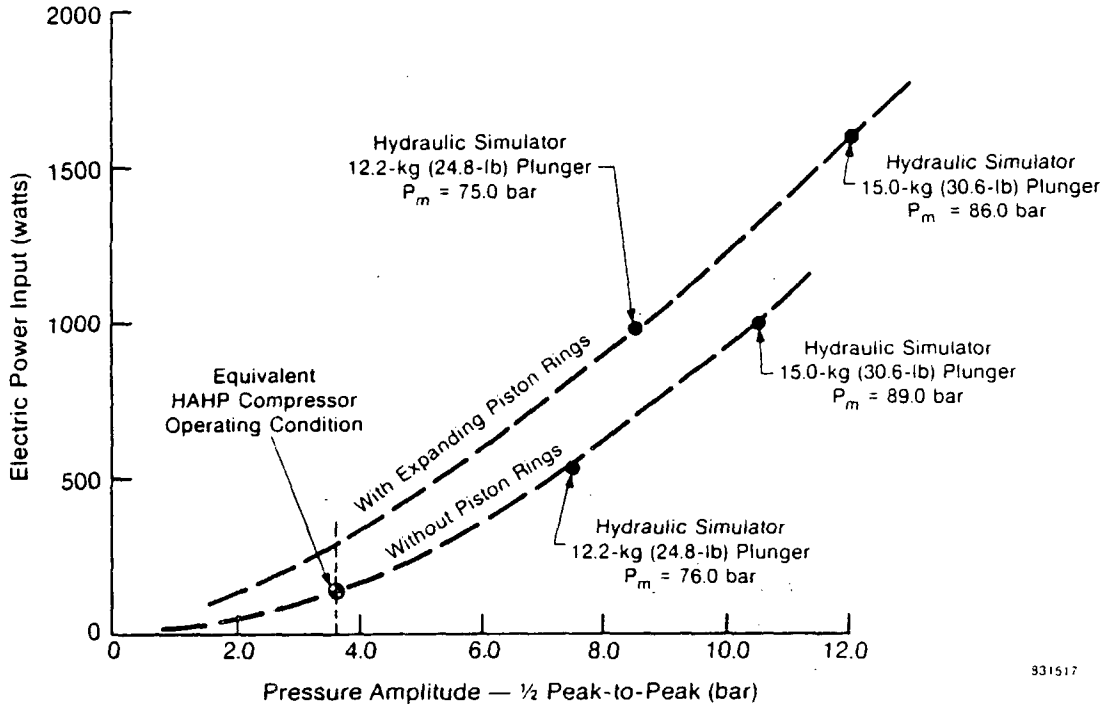

Figure 7-4 HAHP Hydraulic Simulator, Parasitic Losses Versus Pressure Amplitude

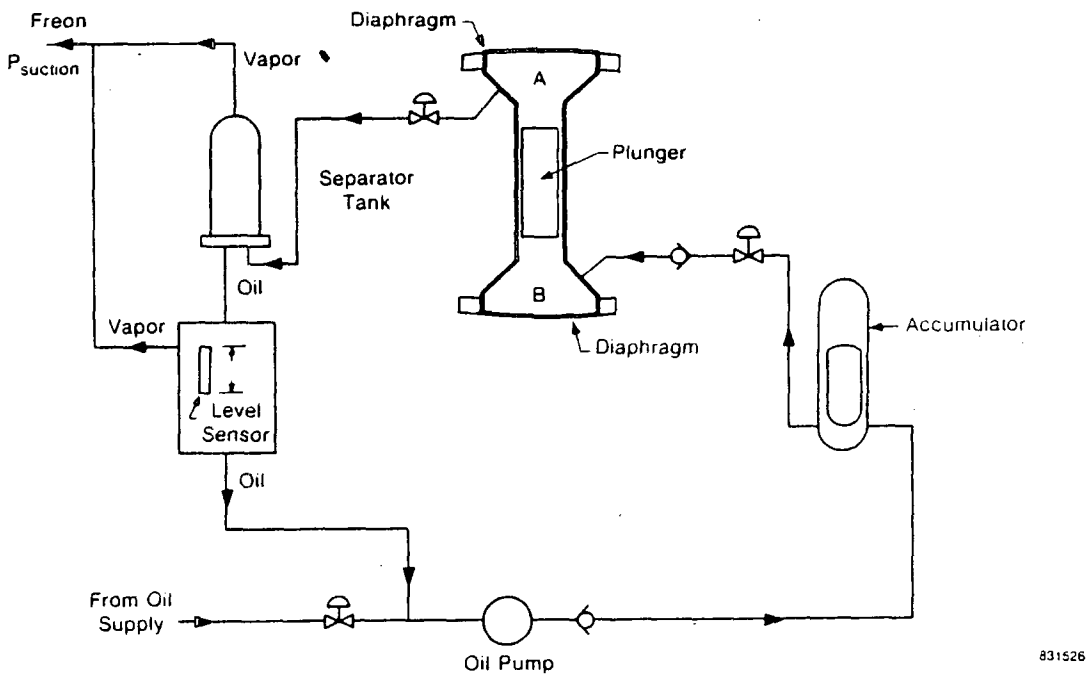

Figure 7-5 Oil Management System with Hydraulic Simulator

- each of the individual components performed well; thus, the system can be used for compressor component and breadboard system testing.

7.5.3 Compressor Testing

7.5.3.1 Early Testing (with no cylinder heads) - Shakedown testing of the HAHP Compressor Drive System (Configuration MC-010), which began in early October, 1982, demonstrated that hydraulically shuttling the plunger and counterweight did not introduce any difficulties when compared to operation of the hydraulic simulator by itself. Particularly satisfying was the low leakage rate of oil past the Chevron seals (leakage did not appear erratic or affected by changes in plunger stroke), with full oil charge pressure (up to ~62 Bar) inside, and atmospheric pressure outside.

Initial operation of the test rig was at 60 Hz with ~62-Bar charge pressure. As noted (see Section 7.4.1), the system was not tuned under these conditions, and the pressure was not raised because the Chevron seals were not designed for higher pressure; nevertheless, strokes as high as 5.5 mm were achieved. During these runs, the plunger could not be centered, even with corrective locating forces applied (by pressurizing vent chambers). Several hypotheses were put forth to explain this, including incorrect center-port locations, insufficient center-port flow capacity, and poorly matched mechanical springs; subsequently, all of these were eliminated as possibilities. Additionally, it was found that the center bearing seal on the counterweight was too short, allowing disengagement of the seal under stroke conditions greater than the 13 mm.

For greater flexibility, the test rig was operated using an Elgar variable-frequency power supply from Test Cell #1. Running in tune at ~48 Hz, it was possible to drive the motor to a 12.5-mm stroke before encountering the power limitation of the Elgar unit. It was noted that when stroke was higher than ~7 mm, the plunger would run very near to center, but the off-center tendency would consistently return when running below a 7-mm stroke (this is believed to be a manifestation of disengagement of the center bearing seal). The counterweight was then removed and modified to correct the seal length.

Power consumption data from these early tests showed that the added mass of the compressor counterweight and pistons resulted in increased losses when compared to the hydraulic simulator (as expected) due to higher required gas spring stiffness and concomitantly large pressure wave amplitudes. Figure 7-6 shows that the power requirement was actually somewhat lower than would have been expected. Importantly, Figure 7-7 shows that parasitic losses for the combined system (hydraulic simulator and HAHP compressor) are virtually indistinguishable from losses for the simulator by itself (for similar reciprocating mass), indicating that hydraulic fluid, clearance seals, and the high-pressure Chevron seals are absorbing very small amounts of power.

The next configuration tested featured several improvements that benefitted from the power consumption as it related to dynamic considerations. The motor plunger mass was reduced from 11.3 to 9.1 kg (24.8 to 20.1 lbs.), and the counterweight from 4.9 to 4.5 kg (10.7 to 9.9 lbs), thus reducing the equivalent reciprocating mass from 18.3 to 15.9 kg (40.3 to 35.0 lbs.). In addition, one gas spring was reduced in volume from 330 mℓ to 245 mℓ (20 in.^{3} to 15 in.^{3}), which made it equal to the other.

In this configuration, it was found that operation at 60 Hz was possible with charge pressures of 68-72 Bar. No damage to the Chevron seals was experienced at these pressures. At 60 Hz, the machine did not achieve its design stroke of 18 mm because of a high power draw on the power supply. Inspection of the hardware after 20 hours showed that some galling had occurred on the compressor piston shaft in the vicinity of the Chevron seals. Run marks were also found on the compressor drive piston where it ran against the counterweight. These problems were corrected before testing with the cylinder heads in place was started.

Due to the considerable problems encountered in the debugging of the Data Acquisition System (DAS), which was going on during this period, little significant data was taken; however, testing showed that the test rig modifications allowed the system to operate stably at 60 Hz, with power consumption comparable to what was previously experienced.

7.5.3.2 Testing With Freon Load - The compressor was tested with a Freon load for the first time near the end of this report period; only preliminary results are presented at this time. Testing was conducted as part of compressor shake-

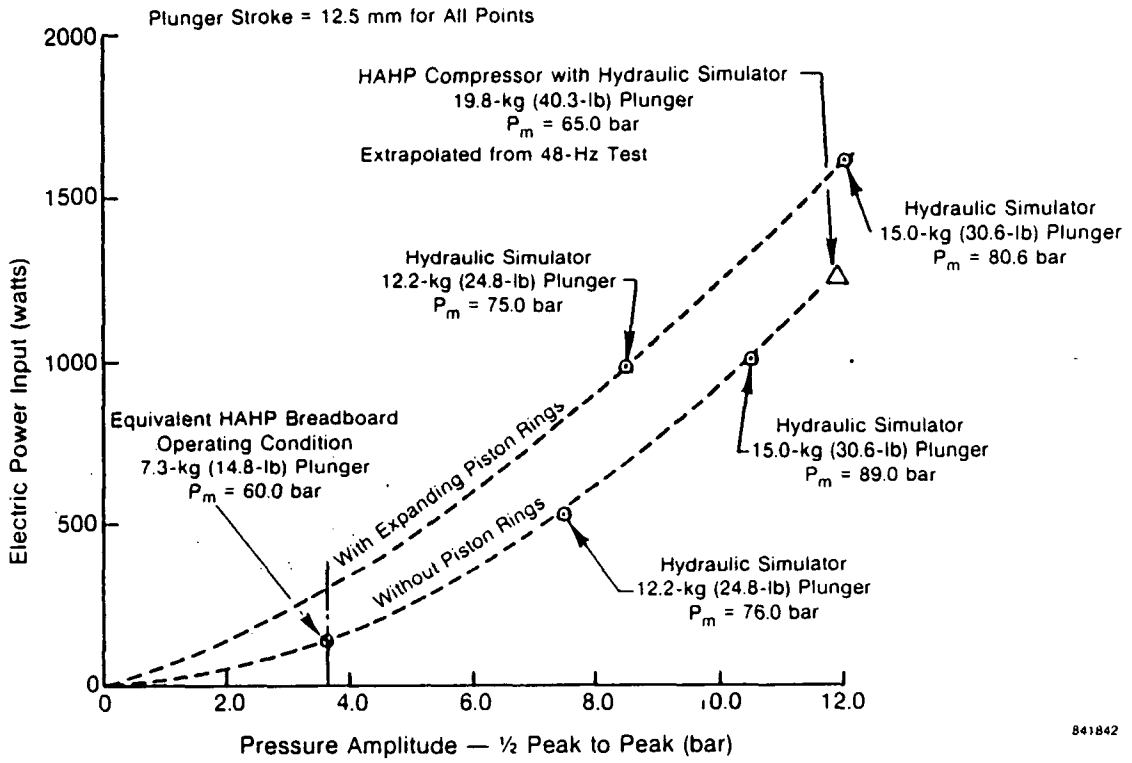

Figure 7-6 HAHP Hydraulic Simulator - Parasitic Losses Versus Pressure Amplitude

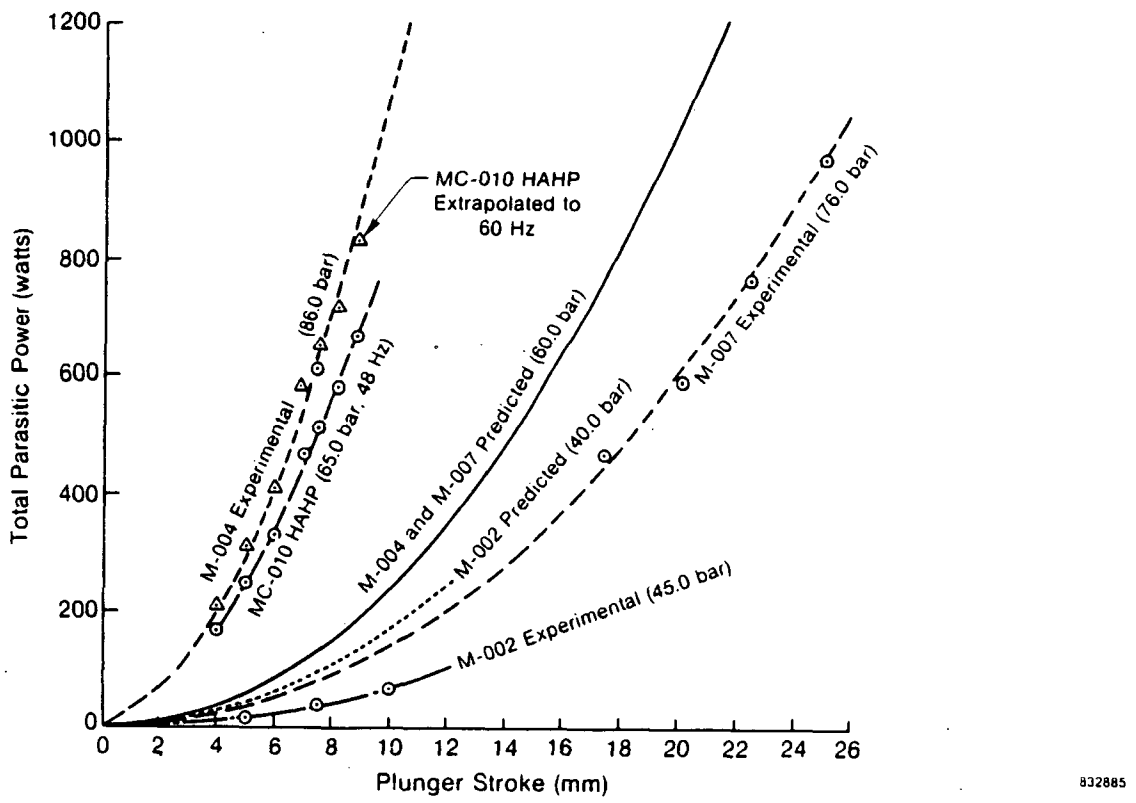

Figure 7-7 HAHP Hydraulic Simulator - Predicted and Experimental Parasitic Losses

down testing to gain operating experience and perform debugging*; however, the system performed exceptionally well, and proved to be very stable, allowing some data to be collected. Table 7-5 is a comparison of this data to a 47°F day. It should be understood that no particular attempt was made to duplicate the 47°F conditions during the test - the similarity was purely coincidental.

TABLE 7-5
INITIAL COMPRESSOR TEST DATA

Parameter		Compressor Test Data	47°F Ambient
Simulator Charge Pressure	(Bar)	78.80	-
Frequency	(Hz)	60.00	60.000
Compressor Stroke	(mm)	12.00	11.500
	(in.)	00.47	00.453
Suction Pressure	(psia)	95.00	83.400
Discharge Pressure	(psia)	165.00	188.000

*Debugging of the DAS continued during this testing. Questionable displacement and Freon mass flow signals were being fed to the computer so that power calculations could not be performed. A complete checkout of the DAS will be performed before additional testing is performed.

8.0 BREADBOARD SYSTEM TESTING

8.1 Shakedown Testing

Shakedown testing of the Breadboard System was started in February, 1983. The purpose of this testing was to gain a familiarity with the hardware, and determine the resonant/stability operating conditions for the machine. From this testing it was concluded that:

- the two control parameters:
  - compressor gas spring volume; and,
  - displacer control frequency,

  would effectively tune the system for resonant operation at each of the designated operating points (17°F, 47°F, 80°F and 95°F ambient temperatures).

- the system operated stably, and is easily controlled with the displacer power control; and,

- either high losses in the lower end (transmission and compressor) or poor engine performance were limiting the compressor stroke. The operating conditions achieved compared to predicted conditions at the 40°F operating point are shown in Table 8-1.

The problem with the Breadboard System at this time is shown in Figure 8-1, where the stroke ratio (Displacer Stroke/Piston Stroke) is shown as a function of the piston stroke for several refrigerant discharge pressures and a 90-psia suction pessure. The limit achieved on the piston stroke is set by the physical limit of the displacer stroke (20 mm); thus, for the 95°F ambient conditions:

$$P\ (\text{suction}) = 90\ \text{psia; and,}$$
$$P\ (\text{discharge}) = 277\ \text{psia.}$$

A piston stroke of 19 mm and a stroke ratio of 0.98 were predicted; a piston stroke of only 10.8 mm was achieved. Similarly, the effect this had on engine

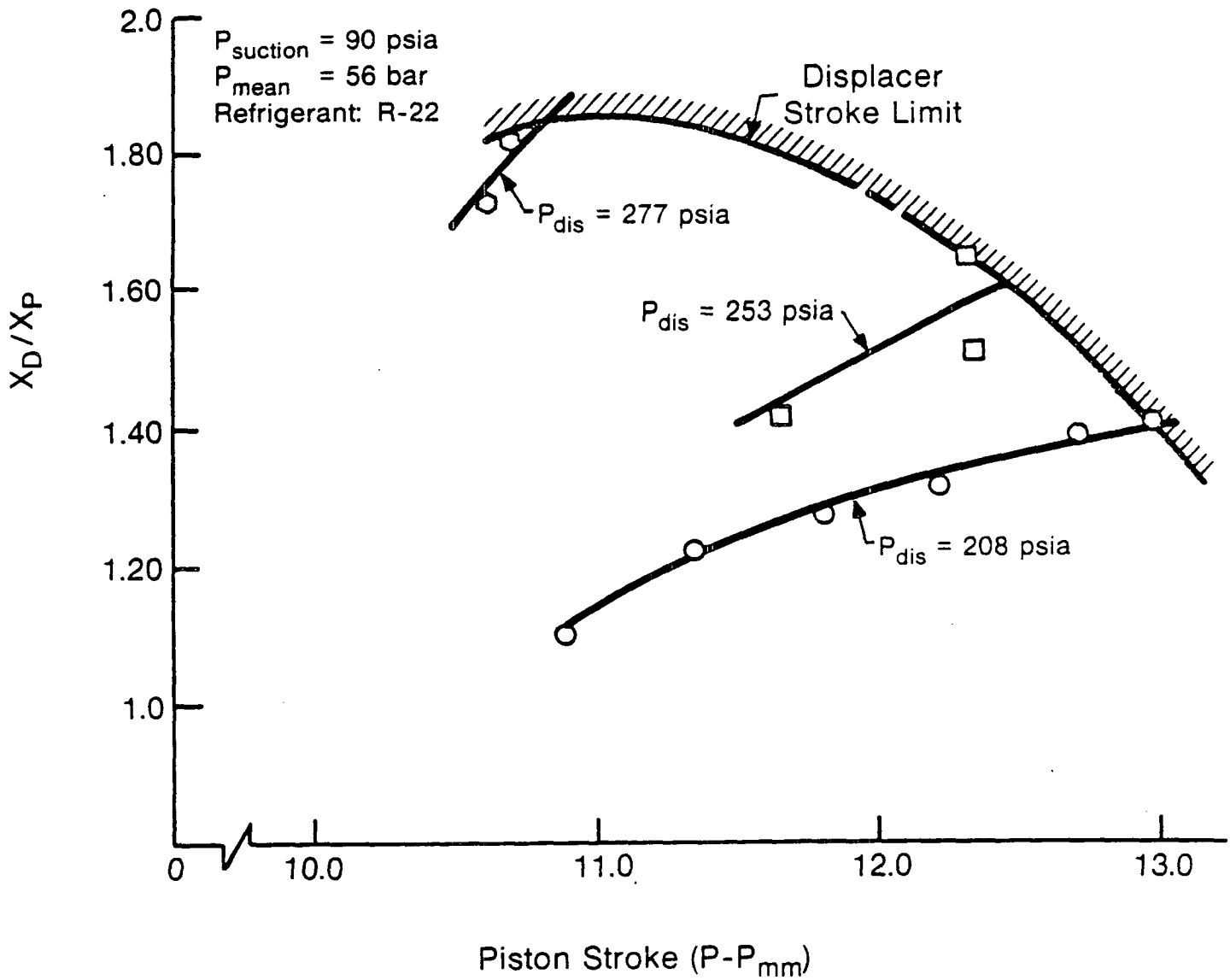

Figure 8-1 Displacer/Piston Stroke Ratio Versus Piston Stroke for the Breadboard System

P-V power is shown in Figure 8-2 for each of the ambient operating conditions. The results determined from these curves indicate that either higher-than-predicted lower end losses are limiting the piston stroke and preventing the engine from developing the rated P-V power, or higher-than-predicted losses are occurring in the engine. Recalling the verification testing performed on the heat pump engine (EM 4) (refer to Table 5-6), it was concluded that EM 4, when coupled to an alternator load, performed as well as the standard MTI engine (EM 1). Therefore, it is postulated that the hydraulic transmission and compressor at this stage in their development have higher losses than predicted.

TABLE 8-1

BREADBOARD SYSTEM SHAKEDOWN TEST RESULTS

		Test Results	Predicted 47°F Conditions
Charge Pressure	(Bar)	62.2	60
Frequency	(Hz)	51.6	60
Heater Head Temperature	(°C)	61.7	750
Firing Rate	(kW)	6.0	1.5
Displacer Motor Current	(amp)	6.5[1]	3.1
Displacer Stroke	(mm)	12.7	5.4
Counterweight Stroke	(mm)	9.8	11.6
Compressor Piston Stroke	(mm)	10.1	11.6
Refrigerant Suction Pressure	(psia)	96.6	83.4
Refrigerant Discharge Pressure	(psia)	157.0	188.8

[1]Limiting test condition was high control current.

The result of higher losses on the breadboard system's performance is shown in Figure 8-3 where the predicted operating load lines for the system and the load lines measured during shakedown testing are plotted. These curves represent the engine operating characteristics as measured for EM 4 operating with an alternator load at a different stroke ratio (K). Superimposed are the load lines for the lower end as predicted and measured for 95°F ambient conditions. These curves show that because the load is stiffer than predicted, i.e., the hydraulic transmission losses appear greater than predicted, the machine at its present

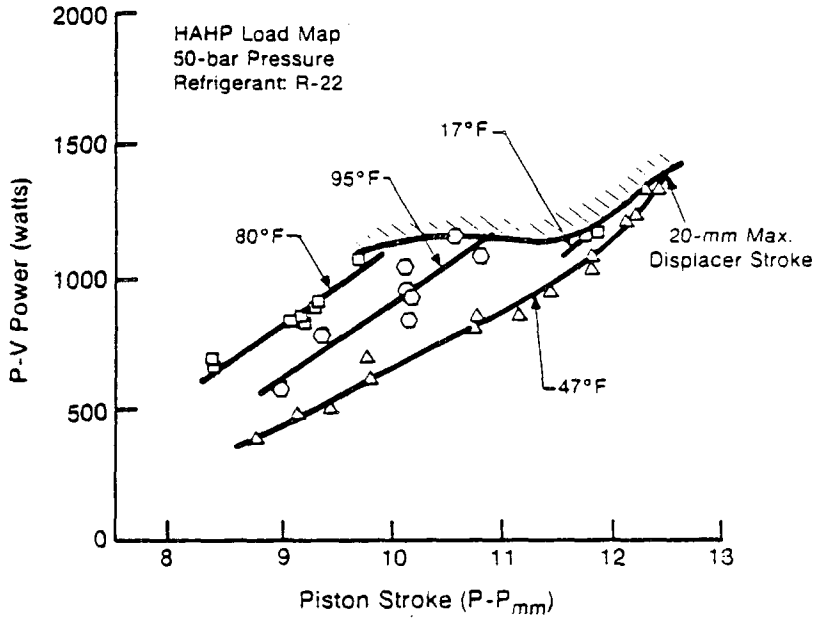

Figure 8-2 P-V Power Versus Piston Stroke for the Breadboard System

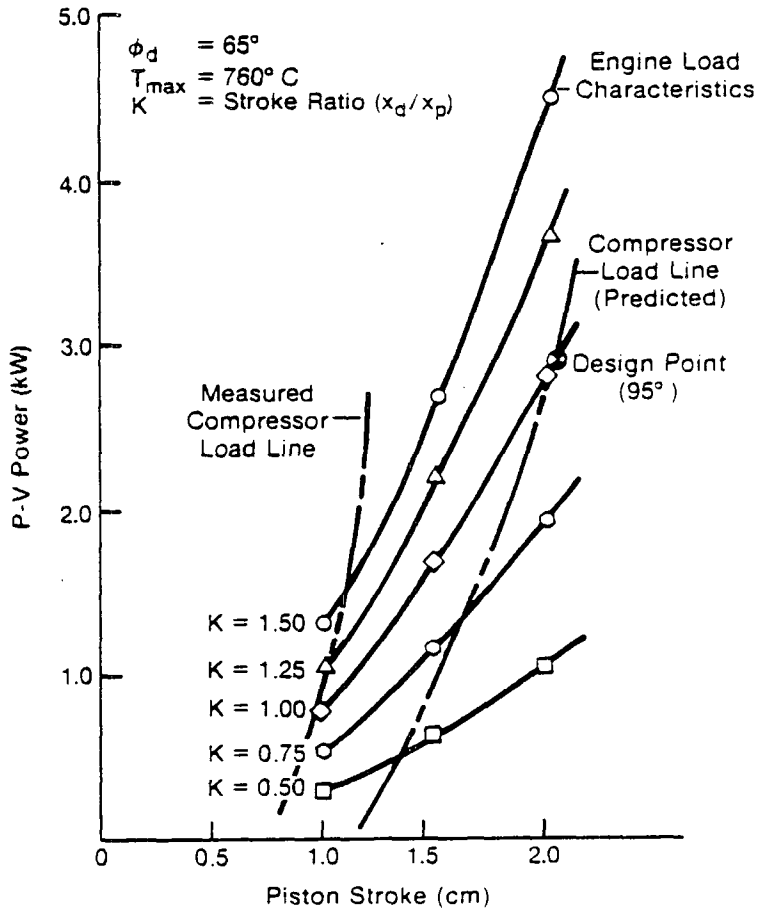

Figure 8-3 Engine Operating Characteristics for the HAHP Engine Configuration

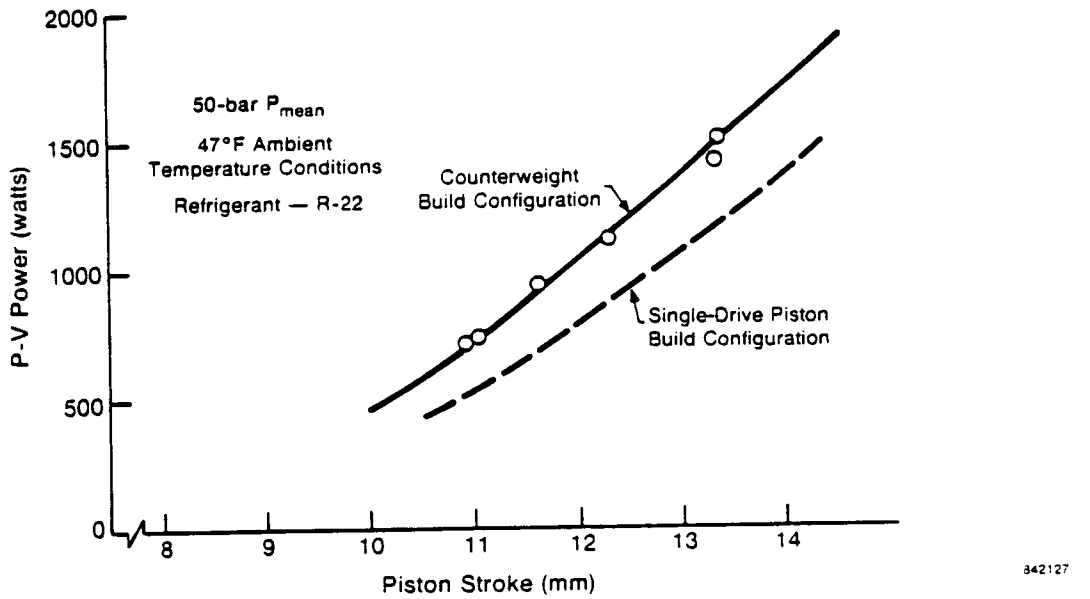

Figure 8-4 P-V Power Versus Piston Stroke for the Breadboard System With and Without the Counterweight

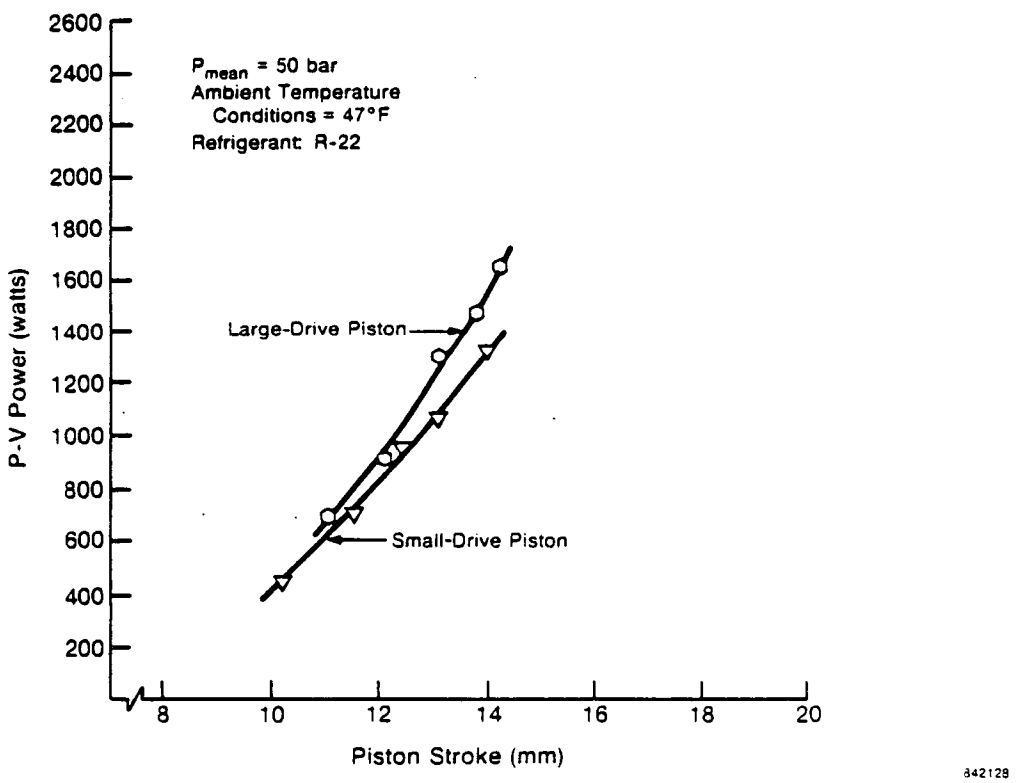

Figure 8-5 P-V Power Versus Piston Stroke for the Breadboard System for Two Different Drive Piston Diameters (No Counterweight)

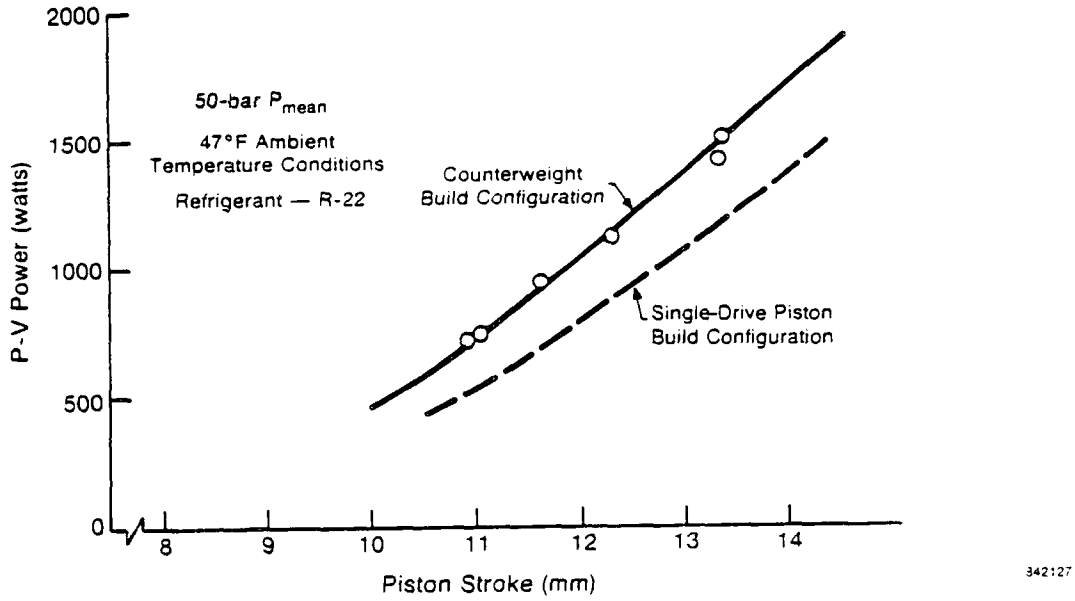

Figure 8-4 P-V Power Versus Piston Stroke for the Breadboard System With and Without the Counterweight

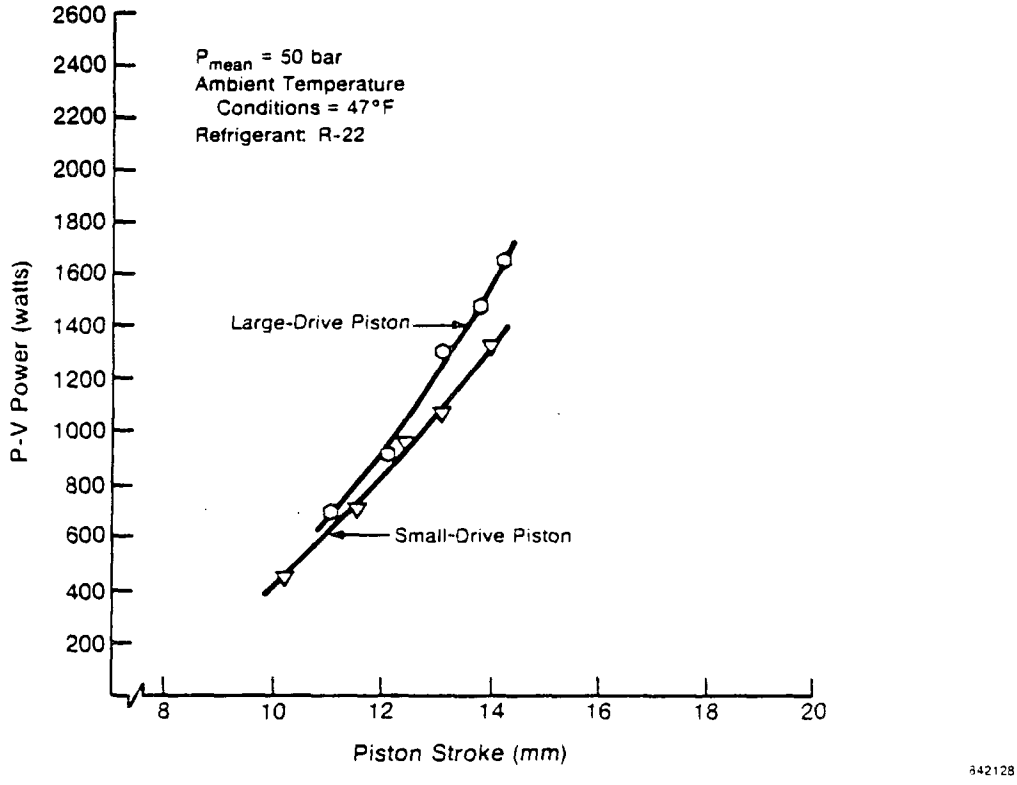

Figure 8-5 P-V Power Versus Piston Stroke for the Breadboard System for Two Different Drive Piston Diameters (No Counterweight)

TABLE 8-2

OAK RIDGE NATIONAL LABORATORY HIGH-EFFICIENCY HEAT PUMP TEST

Ambient Temperature (°F)	Test Conditions		HAHP Measured Conditions	
	$P_{suction}$ (psia)	$P_{discharge}$ (psia)	$P_{suction}$ (psia)	$P_{discharge}$ (psia)
95	84.8	231	82.2	234.2
90	83.5	223.5	80.26	228.4
80	80.	198.5	75.9	204.6
47	80.5	210.0	76.41	217.3
35	68.5	195.5	71.88	197.3
17	44.5	195	45.33	195.97

The capacity and performance measured are given in Figure 8-6. These curves are typical for a mid-Alantic residence requiring three tons of refrigeration at a 95°F ambient temperature. The performance data presented in Figure 8-6 was obtained from

$$\text{C.O.P.} = \frac{\text{Heating/Cooling Capacity}}{\text{Heat Input to the Heater Head} + \text{Control Power}}$$

The cooling capacity was computed from the enthalpy difference between the refrigerant entering the evaporator and that entering the compressor. The heating capacity was computed from the heat removed from the refrigerant in the condenser plus the heat rejected by the engine. The state points for cooling 4 and 1, and for heating 4 and 2, are shown on the refrigerant loop schematic (Figure 6-4). Because the breadboard system is low in capacity, the C.O.P.'s are also low. Further development is required to reach the full potential of the breadboard system. The C.O.P. goals for laboratory testing are given in Table 4-1.

A comparison between measured and predicted performance at the 47 and 95°F operating conditions is given in Table 8-3. The condition to once again note is the difference in stroke ratio (displacer stroke/piston stroke) between the

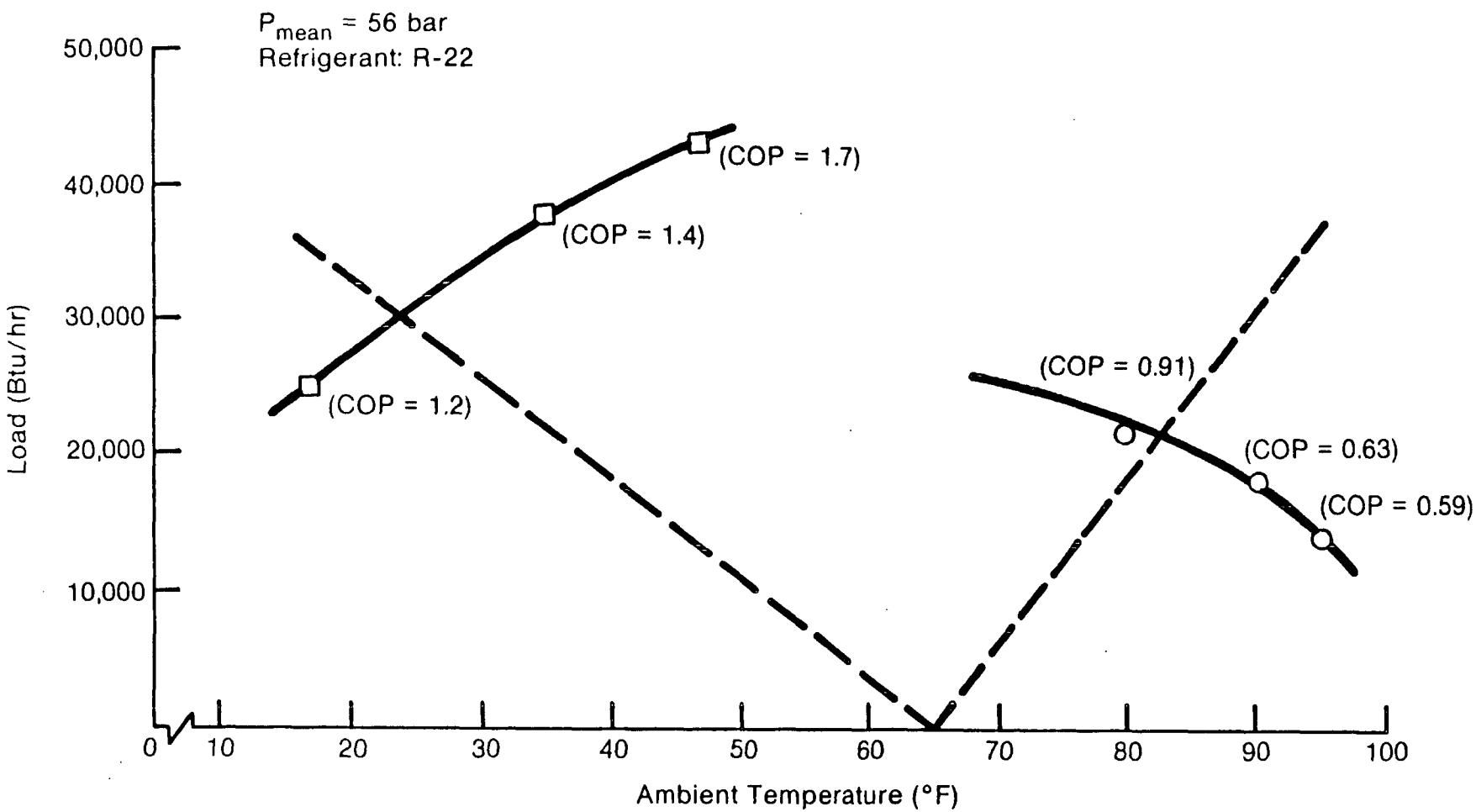

Figure 8-6 Breadboard System Preliminary Heating and Cooling Capacity for the Westinghouse Test Points (Results prior to 9/30/83)

TABLE 8-3

HAHP BREADBOARD SYSTEM DATA

		47°F Ambient		95°F Ambient	
		Predicted	Measured	Predicted	Measured
Operating Conditions					
Ambient Temperature	(°F)	47	47	95	95
Heating/Cooling Load, R-22	(Btu/hr)	14,000	25,987	36,000	16,238
Suction Pressure	(psia)	80.5	80.97	84.8	91.7
Suction Temperature	(°F)	38.2	55.5	41.1	104.4
Discharge Pressure	(psia)	210.0	202.5	231.0	279.9
Freon Mass Flow Rate	(lbm/hr)	110.4	166.8	570.0	216.8
Engine Conditions					
Mean Pressure	(Bar)	60.0	51.27	60.0	56.3
Frequency	(Hz)	60.0	53.0	60.0	57.1
Piston Stroke	(mm)	11.51	10.0	19.05	10.68
Displacer Stroke	(mm)	5.90	13.7	20.84	19.51
Piston/Displacer Phase	(deg)	62.4	64.6	69.3	56.71
Head Temperature, Mean	(°C)	760	634	760	730.0
Compression-Space Pressure	(psia)	48.7	42.9	83.7	70.42
Pressure/Piston Phase	(deg)	-74.1	-25.1	-93.4	-17.98
Thermodynamics	(watts)				
Heat Input		2,051.0	4,160.6	8,813.0	7,072.0
Heat Rejected		1,347.0	3,561.0	5,671.0	5,353.9
Motor Input Power		-38.9	121.8	313.0	527.1
P-V Power		507.0	721.0	2907.0	1,191.0
Displacer Gas Spring Loss		--	--	290.0	631.4
Piston Gas Spring Loss		21.0*	3.4**	114.0*	77.2**
Hydraulic Transmission Loss		205.9	340.0	539.0	520.9

*Using Helium Gas with adjustable gas spring
**Using Nitrogen Gas

predicted and measured conditions. The large stroke ratio (1.37 and 1.83 at the 47 and 95°F conditions) is representative of the capacity shortfall.

8.3 Future Developments

Testing as of the end of this program has shown that the shortfall in capacity is manifested in the high stroke ratio. Future development must address whether the cause for this lies in the engine, hydraulic transmission, or compressor. To evaluate this, the following three-step effort is required:

- perform an analytical evaluation using existing data to see if the engine performance matches predictions under the given operating conditions;

- measure the hydraulic transmission losses, and characterize the transmission over the full stroke range;

- evaluate compressor performance by measuring the compression cylinder P-V diagrams; and,

- calibrate the refrigerant test loop with a known three-ton commercial compressor.

A follow-on to this program, Phase IA, has been initiated to address these questions. Results of this work will appear as a supplement to this text.

ATTACHMENT

THE PHASE IA PROGRAM

BACKGROUND AND OBJECTIVE

By the completion of the HAHP Phase I program, the FPSE Breadboard System had demonstrated certain minimum levels of performance which proved the mechanical feasibility of the diaphragm-coupled, compression-design concept. This performance included stable, controllable operation over the entire ambient temperature range, good efficiency measurement, and the capability to modulate capacity. The Breadboard had one critical shortcoming - a deficiency in the design point capacity. Figure 1 shows the measured capacity and the shortcoming, which becomes apparent at ambient temperatures above 87°F. The reason for the capacity shortfall was not known at the completion of the Phase I contract; furthermore, the source of the deficiency could have been in the engine, the compressor, or due to a mismatch between the engine and compressor.

To address the capacity shortfall problem, a Phase IA effort was initiated, the purpose of which was to experimentally and analytically identify the reason for the capacity decrement. The project was scheduled for a three-month period from November, 1983 through January, 1984. The project was structured with two technical tasks: 1) Breadboard Design Studies and Performance Analysis; and, 2) Component Development and Breadboard System Test.

RESULTS AND CONCLUSIONS

Analyses of test data and computer simulation confirmed that the compressor losses were significantly larger than the design values. This resulted in a load stiffness that exercised the engine to its mechanical limits before full refrigeration capacity could be established.

A subsequent matching analysis was conducted to correlate test data with computer model predictions. This analysis identified some major differences between the test hardware/conditions and the originally designed hardware/operating conditions. The analysis also showed that the Breadboard System was performing as expected at the measured operating conditions and load characteristics. Further, the analysis showed that if the compressor losses could be reduced, the existing set of engine/compressor hardware would be capable of producing the original design capacity of three tons at the 95°F ambient condition.

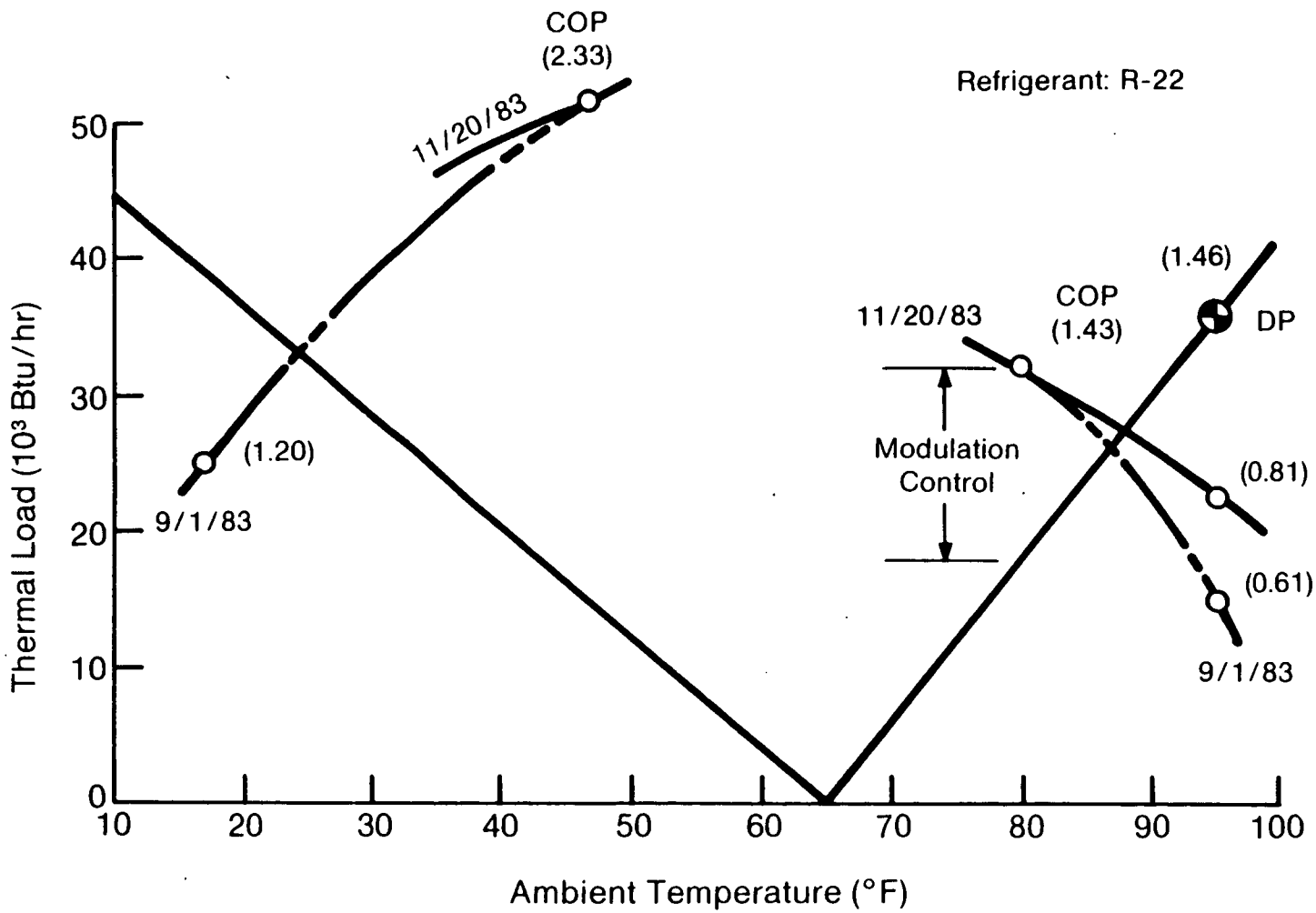

Figure 1 Residential Heating and Cooling Load Lines

841840

The remainder of this program effort was directed toward identifying and quantifying loss mechanisms in the compressor. Several significant areas were investigated, and areas for improving the compressor performance were identified.

DISCUSSION

BREADBOARD DESIGN STUDIES AND PERFORMANCE ANALYSIS

As mentioned above, the major technical issue left unresolved at the end of the Phase I program was the lack of a full understanding as to why the Breadboard power module could not be made to produce its design capacity of three tons of refrigeration at the 95°F ambient condition; i.e., at freon suction and discharge pressures of 90 psia and 270 psia, respectively. Developing an analytical and experimental understanding of the performance decrement was the main focus of the Phase IA effort.

Initial insight into the problem is provided by the engine/compressor load map shown in Figure 2. The figure shows a family of engine load characteristics for various stroke ratios (displacer stroke divided by compressor piston stroke) and two compressor load lines which represent the 95°F day load characteristics. From the figure, it can be seen that the measured compressor load is much stiffer than the predicted compressor load line, thus implying that more and more displacer stroke is required to provide increased compressor piston, i.e., increased capacity. The measured compressor load is so 'stiff,' however, that the physical stroke limit of the engine displacer is reached before the required piston stroke can be developed. It is important to recognize that the 'Engine Load Characteristics' shown in Figure 1 were determined by computer simulation, as was the predicted compressor load line. The questions that arose regarding the problem at hand were several.

- Is the computer code accurately modeling the Breadboard system?
- Is the engine strong enough to drive the compressor?
- Is the compressor capable of providing three tons of refrigeration?
- Is there a basic mismatch between the EM and the diaphragm-coupled compressor?

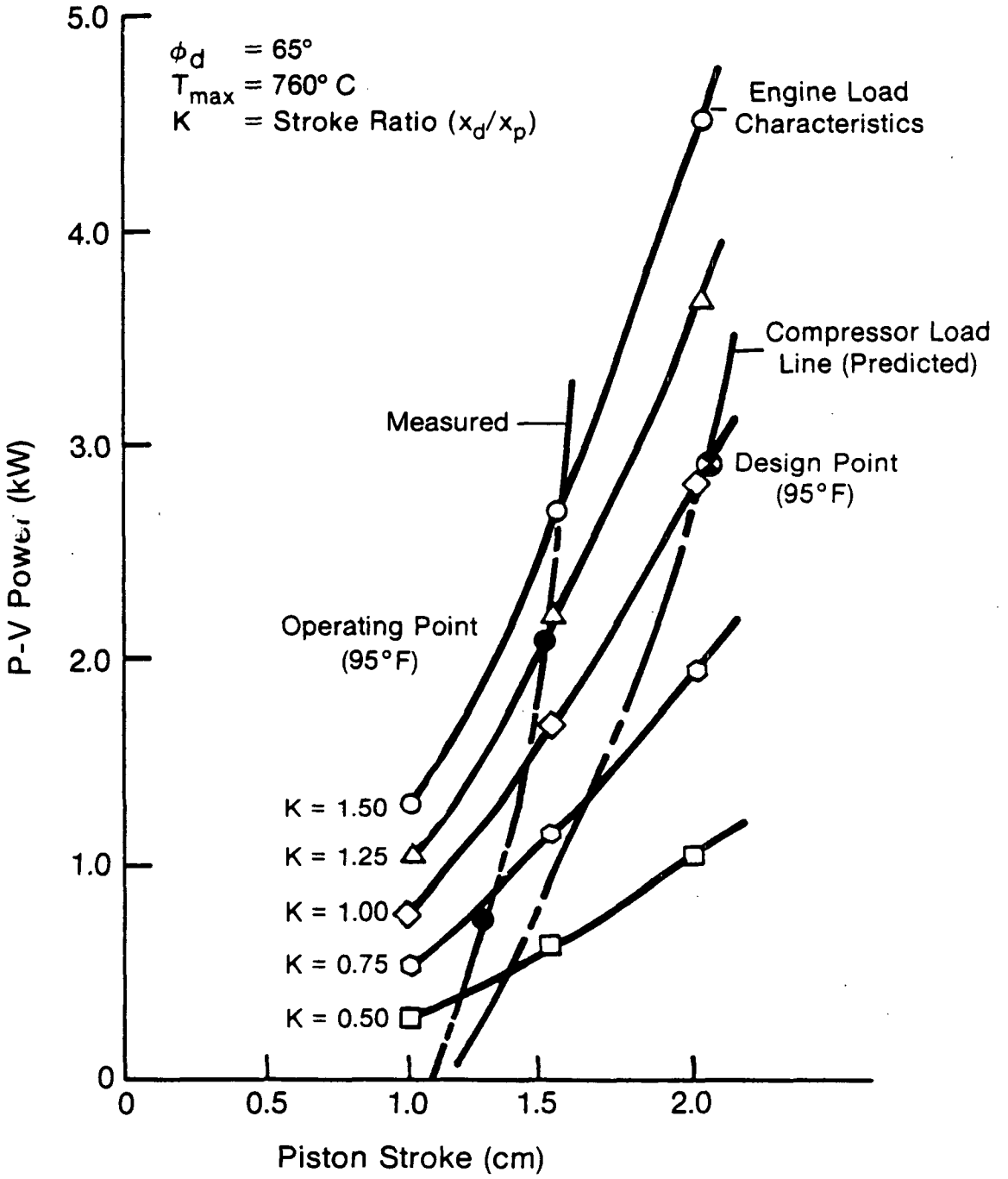

Figure 2 Engine Operating Characteristics for the HAHP Engine Configuration

841855

These are the issues that were addressed as part of the Phase IA Breadboard Design Study and Performance Analysis Task.

As a first step, the computer model was examined in terms of its capability to predict and correlate with test data. Figure 3, which depicts the result of this effort, shows engine test data, along with a first- and second-pass analysis. At first, the computer code was predicting significantly higher-than-measured power output from the engine to the compressor; however, at closer inspection several significant differences were seen to exist between the breadboard computer model and the actual hardware (Table 1 itemizes these differences).

TABLE 1

PHYSICAL DIFFERENCES BETWEEN COMPUTER MODEL AND BREADBOARD SYSTEM

Model	Breadboard System	Expected Engine Thermodynamic Efficiency Improvement
Insulated Displacer	Uninsulated Displacer	3% (EM - 2.6 kW)
Screen Regenerator Matrix (80% Porosity) (3.5-mil wire size)	Matrix Regenerator Matrix (75% Porosity) (3.5-mil wire size)	3% (EM - 2.6 kW)
760°C Average Heater Head Temperature	675°C Average Heater Head Temperature	2% (HAHP - 2.2 kW)
60-Bar Mean Pressure	<60-Bar Mean Pressure (Typically)	-----
60-Hz Operating Frequency	<60-Hz Operating Frequency (Typically)	-----

Specifically, the engine operates with an uninsulated displacer and with metex woven-wire regenerator matrices, while the computer model simulates an insulated displacer and a screen-mesh regenerator matrix. Also, the heater head temperature, mean pressure, and operating frequency are lower than originally

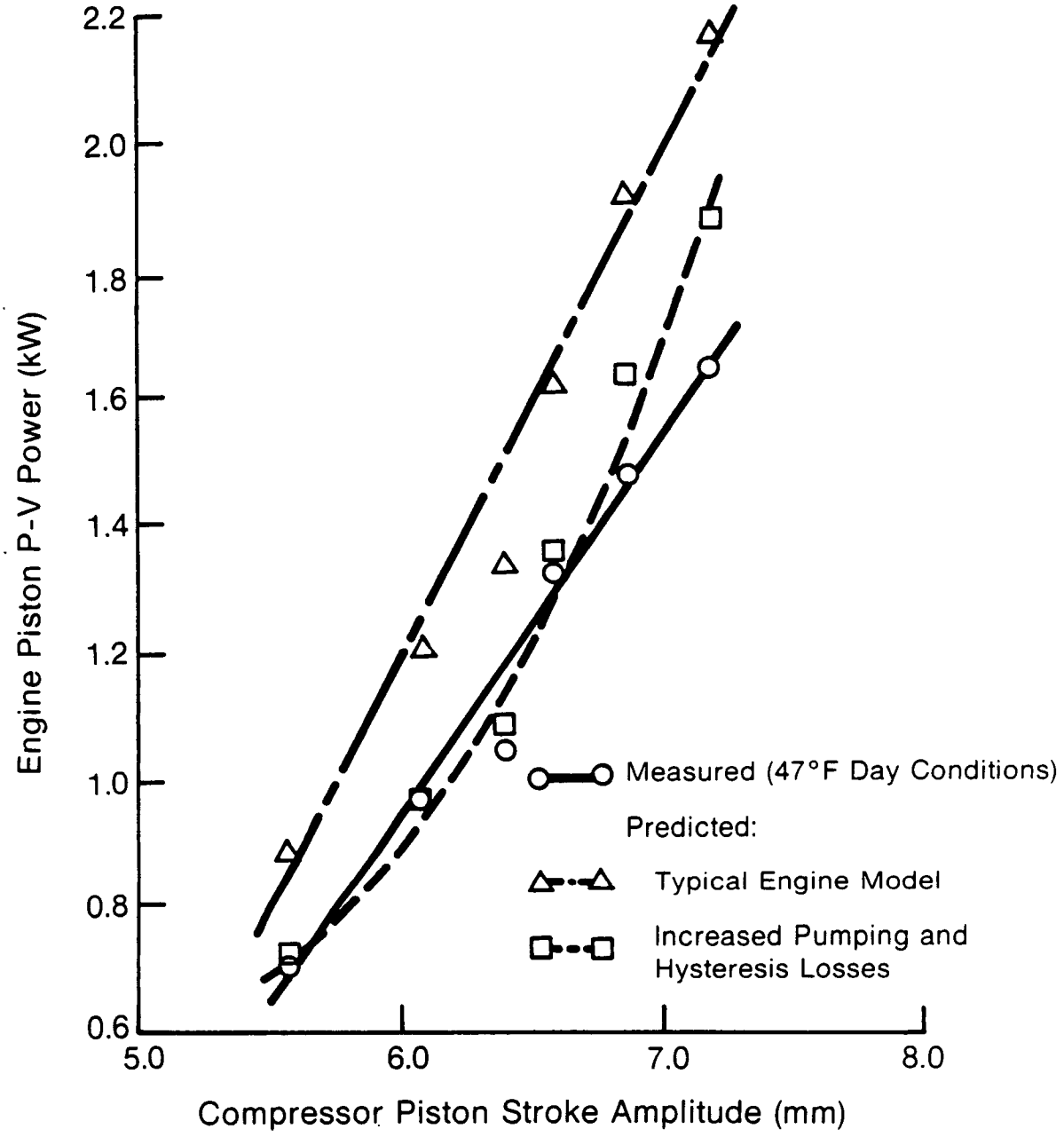

Figure 3 Measured and Predicted Engine Power Versus Piston Stroke

modeled. Furthermore, inspection of the test data revealed that pumping losses through the transition plate between the engine and upper diaphragm were measured to be greater than predicted.

The model of this engine loss mechanism was modified to reflect the increased power loss. Also, engine displacer clearance seals were determined to be larger than originally designed and modeled into the computer code. The final difference was to include measured compressor losses into the breadboard dynamic model that were substantially higher than the originally predicted values.

The result of this effort was the good agreement achieved between test data and code prediction, as indicated in Figure 3, the data of which is representative of a 47°F ambient day operation. The next step was to use the computer code to predict the 95°F day operating condition, and compare the predicted results with test data (the results are displayed in Table 2). As shown, input parameters to the code were taken directly from test data. The result was a predicted engine power that closely agreed with the measured engine power. So far, and analytical effort affirmatively answered the first question under evaluation: the computer code does accurately model the actual engine/compressor operation.

TABLE 2

HAHP - MEASURED VERSUS PREDICTED ENGINE PERFORMANCE

95°F Ambient Condition

Engine Parameter		Test Measurement	Code Prediction*
Mean Head Temperature	(°C)	653	653
Mean Pressure	(Bar)	59	59
Frequency	(Hz)	58.6	58.6
Piston Stroke (Compressor)	(mm)	16.34	16.34
Displacer Phase Angle	(deg.)	65.1	65.1
Displacer Stroke	(mm)	19.22	19.22
Stroke Ratio	(mm)	1.18	1.18
Piston P-V Power	(w)	2155	2186

*Code matched at 47°F ambient conditions.

With a well-verified analytical tool in place, the next step of the analysis involved identifying the source of the capacity shortfall: the compressor, the engine, or a mismatch between the two. The approach to resolving this question was to take the original design point model for the breadboard, and modify the model in parametric fashion to describe each known variance between design conditions and actual operating conditions to determine whether both the dynamic and thermodynamic conditions could be matched with actual test conditions, and to evaluate the sensitivities to these step-by-step changes. Table 3 shows the results of this effort.

The first row of Table 3 specifies the design parameters for an 80°F ambient day condition, the second row specifies the test parameters, and the remainder of the table steps through the changes made to the analytical model. The objective of this approach was to determine whether a set of parameters existed that would yield the design point P-V power at substantially reduced displacer stroke, i.e., at displacer stroke approaching the design value. The major single change to displacer stroke occurred in Row 5. To achieve this change, it was assumed that the compressor load losses could be reduced to their design level so that the overall power consumed by the compressor would be 624 watts. Other changes were made to reflect implementation of the design prediction. The final row shows that, indeed, the model predicts that the design level of power output can be achieved at a displacer stroke relatively close to the original prediction.

Table 4 lists a summary of engine performance predictions and measurements for several ambient conditions. By applying the same modeling logic that was developed for the 80°F day condition discussed above, a similar conclusion can be drawn for the 95°F condition, i.e., for the most part, the excessive compressor losses are the cause of the capacity decrement, and that through compressor development and minor modification of engine hardware, the Breadboard System should be capable of meeting its full design capacity objective.

COMPONENT DEVELOPMENT AND BREADBOARD SYSTEM TEST

This task was established with the objective of characterizing the compressor losses and improving the Breadboard capacity output. As described in the previous section, the compressor exhibited a much stiffer load level than originally

TABLE 3

PREDICTION ADJUSTMENTS FOR DESIGN-TEST DIFFERENCES

80°F Ambient Conditions
Compressor Piston Stroke = 10.2 mm
Displacer Phase Angle = 60.2°

Engine Parameter	Piston P-V Power (w)	Displacer Stroke (mm)	Mean Head Temperature (°C)	Mean Pressure (Bar)	Frequency (Hz)	Drive-Piston Area (in2)	Disp. Insulation I = Insulated U = Uninsulated	Regen. Matrix S = Screen M = Metex
Design Prediction	624	7.04	760	60	60	10.67	I	S
Test Measurement	892.5	14.57	674	53	54	12.11	U	M
Revised Prediction Baseline	1022	14.57						
Increased Leakage Loss	893	14.57						
Match Design Power	624	11.2						
Increase Head Temperature		10.2	760					
Match Design Pressure, Frequency		9.35		60	60			
Insulate Displacer		9.23					I	
Screen Regenerator		9.05						S
Match Design Piston Area		9.18				10.67		S

TABLE 4

HAHP VERIFICATION TEST DATA

Engine Parameter	95°F Ambient					80°F Ambient					47°F Ambient				
	HAHP	Equivalent EM				HAHP	Equivalent EM				HAHP	Equivalent EM			
	M	HAHP	P	EM 1	EM 4	M	HAHP	P	EM 1	EM 4	M	HAHP	P	EM 1	EM 4
Mean Head Temp. (°C)	659	760	760	720	676	674	760	760	729	703	675	760	760	725	746
Mean Pressure (Bar)	57	60	60	59.97	59.63	52	60	60	59.70	59.80	57	60	60	59.50	59.3
Frequency (Hz)	56	60	60	58.12	57.94	54	60	60	58.70	57.80	57	60	60	58.04	57.95
Piston Comp. Stroke (mm)	16.34	19.50	19.50	19.48	19.44	10.11	10.24	10.20	10.48	9.94	11.80	11.51	11.50	11.52	11.47
Displ. Phase Angle (deg)	65.9	70.20	65	54.21	73.89	60.2	60.50	65	66.20	71.67	75	63.30	65	60.87	65.82
Displacer Stroke (mm)	19.22	18.71	12.70	12.69	13.03	14.57	7.04	7.10	7.22	6.94	8.13	5.36	5.75	5.66	5.73
Stroke Ratio	1.18	0.98	0.65	0.652	0.671	1.44	0.69	0.70	0.689	0.698	0.69	0.47	0.50	0.491	0.499
Piston P-V Power (W)	2155	2907	2907	2822	2886	892.5	624	1000	1167	948	740.9	507	750	791.40	799.2
Displ. Control Power (W)	275	387	--	98.40	256.4	125	-85.50	--	17.40	13.60	96.8	-70.80	--	21.50	-3.38
(Current amps)	(5.22)	--	--	2.07	5.20	(1.76)	--	--	2.09	1.61	(3.49)	--	--	1.58	1.35
Head Heat Input (kW)	7.84	--	--	8.63	9.64	4.92	--	--	3.85	3.46	3.53	--	--	3.17	3.76
Resistance Load (Ω)	--	--	--	7.37	7.08	--	--	--	5.06	5.55	--	--	--	9.52	10.01
Compressor Loss ?? (W)	450					250					297				

P = Predicted
M = Measured

predicted (refer to Figure 1). Because of the steepness of the compressor load line, the compressor piston could not be made to operate much above 70 percent of its design capability. As a result, compressor loss data could not be secured in the longer stroke operating regimes, i.e., beyond a 14-mm stroke. The ORNL Program Manager suggested that the compressor could be unloaded, i.e., made less stiff, by replacing the R-22 refrigerant with a lower-density fluid. For experimental purposes, R-500 refrigerant was selected as the replacement fluid.

As predicted, the R-500 refrigerant unloaded the compressor sufficiently to enable operation at strokes up to 19 mm, thus enabling the compressor losses to be characterized over the entire dynamic operating range. Figure 4 illustrates the results of the testing. As indicated, test data taken with R-500 extends to the full limit of the compressor stroke, whereas the data taken with R-22 covers a limited stroke range. Furthermore, Figure 4 shows that the measured hydraulic transmission losses were twice that predicted.

To investigate whether the hydraulic losses were stroke- or pressure-ratio-dependent (assuming a constant frequency), tests were performed to measure the losses at various strokes and pressure ratios. The results of these tests are indicated in Figure 5. Although the figure shows only a few data points, the curves represent the results achieved at dozens of other test conditions. These tests concluded that the compressor losses were primarily stroke-dependent and insensitive to the freon pressure ratio.

Having established that the compressor losses were higher than predicted, and primarily stroke-dependent, the next step was to identify the individual loss components, and quantify the relative magnitude of each. Figure 6 schematically illustrates the compressor energy flows. From the figure, three loss regions can be identified for investigation:

1. losses within the oil volume (OIL LOSSES);
2. losses associated with the piston and seals (PISTON LOSSES); and,
3. GAS SPRING losses.

The aggregate of losses in each of these regions were deduced from power measurements taken in each of the compressor's critical volumes. Dynamic pressure

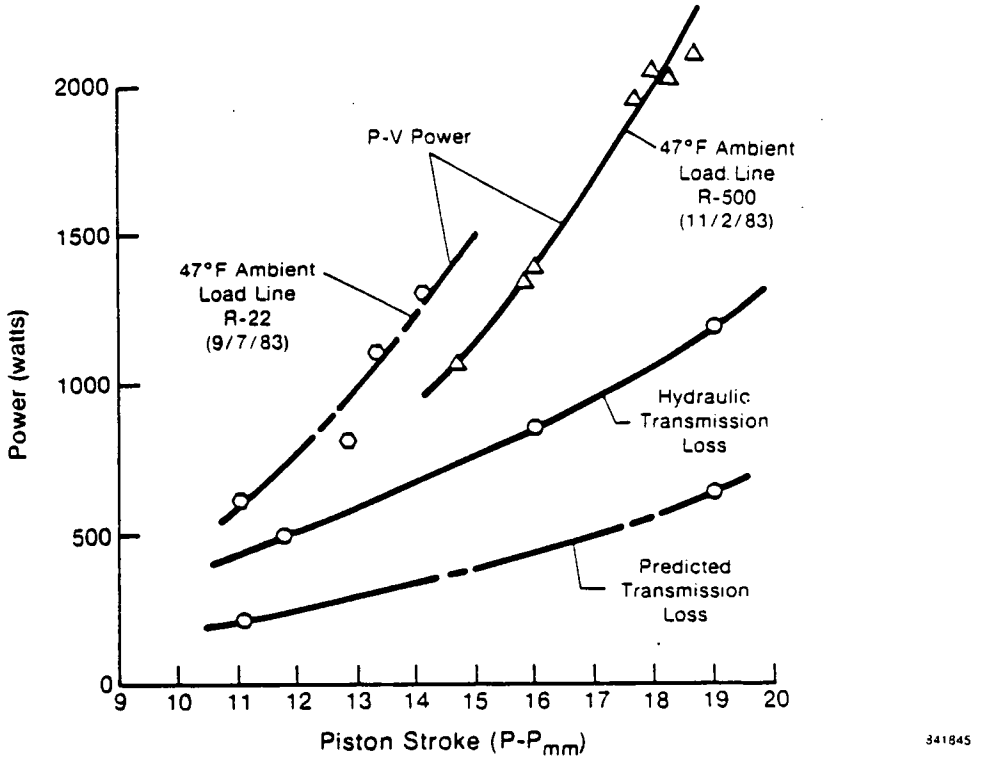

Figure 4 Breadboard Characteristics

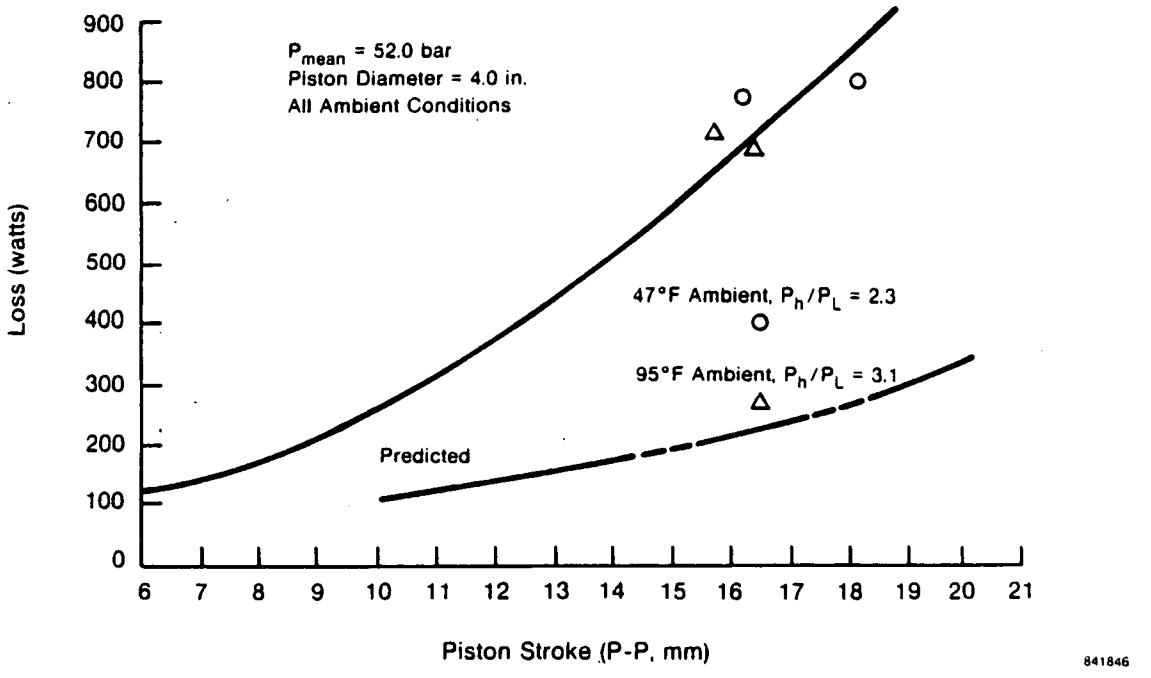

Figure 5 Drive Losses for HAHP Compressor

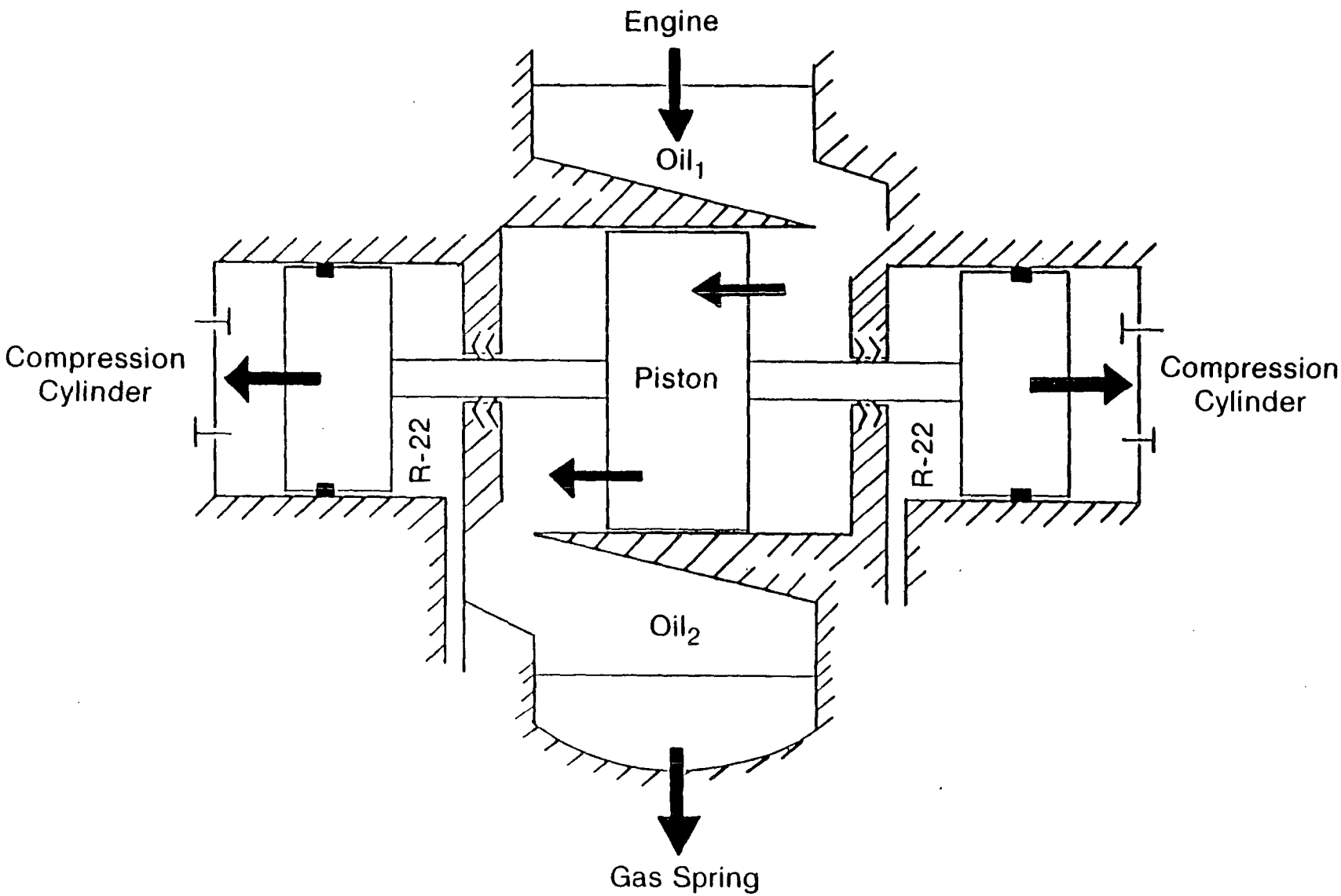

Figure 6 Compressor Measured Energy Flow

transducers and position probes were installed so that P-V power calculations could be made for each of the regions of interest. The measured losses are compared with predicted losses for each of these regions in Table 5. At the time the data was taken, individual component loss predictions could not be verified; as a result, only the cumulative losses were measured. Nonetheless, in each loss category the measured loss was significantly higher than that predicted (this was especially true for the hydraulic viscous losses).

TABLE 5
COMPARISON OF LOWER-END LOSSES WITH PREDICTIONS FOR DIRECT ACTING COMPRESSOR

	47°F Ambient		95°F Ambient	
Loss (watts)	Predicted	Measured	Predicted	Measured
Piston				
• Chevron Seal	54.2	-	102.0	-
• Comp Piston Seal	73.0	-	234.0	-
• Clearance Seal	17.0	-	46.0	-
• Pumping	61.0*	-	176.0*	-
Subtotal	205.2	340.0	558.0	775.0
Hydraulic				
• Viscous	0.7	-	2.1	-
• Porting	-	-	-	-
Subtotal	0.7	100	2.1	295.0
Gas Spring	21.0*	60.0	114.0*	175.0
Total	226.9	500.0	674.1	1245.0

*computed from actual hardware implementation

To investigate the loss contribution from each of the mechanisms, a series of independent tests were scheduled. The first effort was devoted to measuring the Chevron seal power drain. Tests were conducted on the breadboard unit, which was operated with refrigerant R-500. The operating conditions were:

Refrigerant	R-500
Suction Pressure	45 psia
Discharge Pressure	150 psia
Displacer Strokes	5 to 18 mm
Piston Strokes	10 to 18 mm
P(mean)	55 Bar

The purpose of the testing was to determine if the compressor losses were strongly affected by the Chevron seal friction. By eliminating one seal pack, the effective friction rubbing area would be cut in half. The tests showed a reduction of 30% in the piston power loss at an 18-mm stroke, and a reduction of 43% in the stroke ratio (displacer stroke/piston stroke). These results are shown in Figures 7 and 8.

In addition to the seal test, modifications to the Breadboard System were made to reduce or eliminate other compressor losses. Extraneous hydraulic lines were removed from the compressor. The lines introduced possible oil leak paths between the upper and lower oil cavities; however, significant change in system performance was noted. A more significant item was uncovered when a .305-inch ID refrigerant transfer line connecting the two variable volumes behind the compressor pistons was replaced with a larger (.5-inch ID) line. During this change, an unsuccessful attempt was made to pressurize the aft piston freon volumes. Subsequent inspection of the piston rings showed that the backer rings that support the Rulon rider ring were severely out-of-round, causing significant blow-by of freon around the compressor piston.

Additional test evidence points to piston seal leakage as a most likely cause of compressor inefficiency and capacity decrement. Figure 9 shows a measured P-V diagram for one of the freon cylinders. Superimposed on this diagram are the ideal adiabatic compression and expansion curves. As indicated, the measured data shows that only 50 percent of the adiabatic compression rate was achieved with the hardware. Leakage past the compression seal could readily account for the nonideal compression rate. To investigate this hypothesis, a set of improved ring seals was designed and scheduled for future testing.

Other items that have been scheduled for investigation include:

- evaluation of fluid viscosity effects and clearance seal losses;
- gas spring characterization;
- clearance volume effects; and,
- discharge plenum sizing.

These items, identified as potentially significant, have been recommended for examination during subsequent development phases of the program.

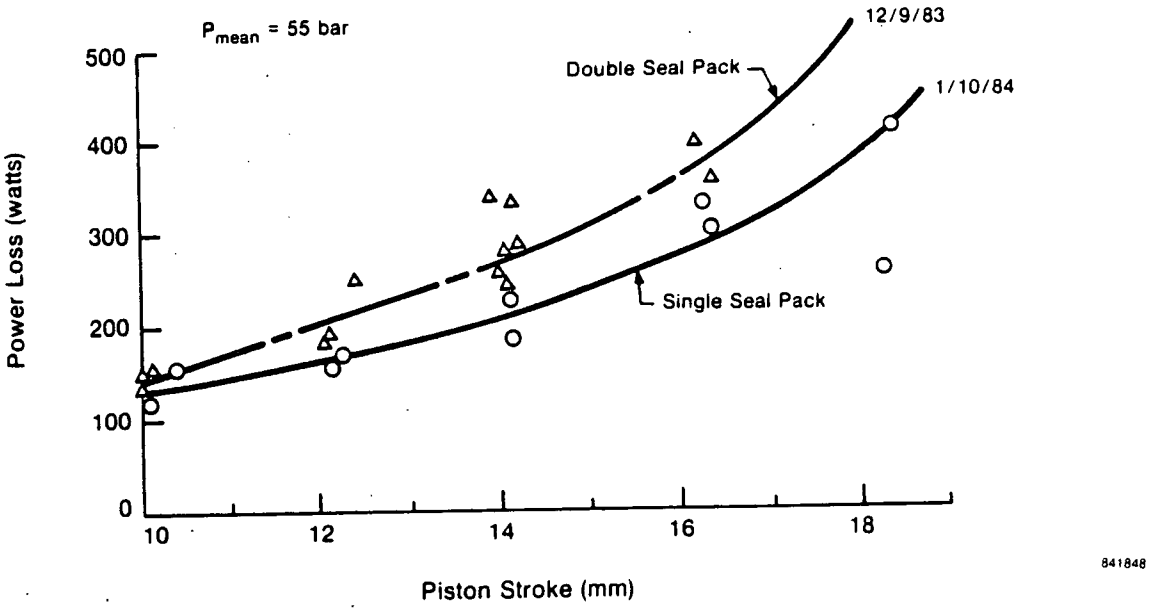

Figure 7 Compressor Power Piston Loss

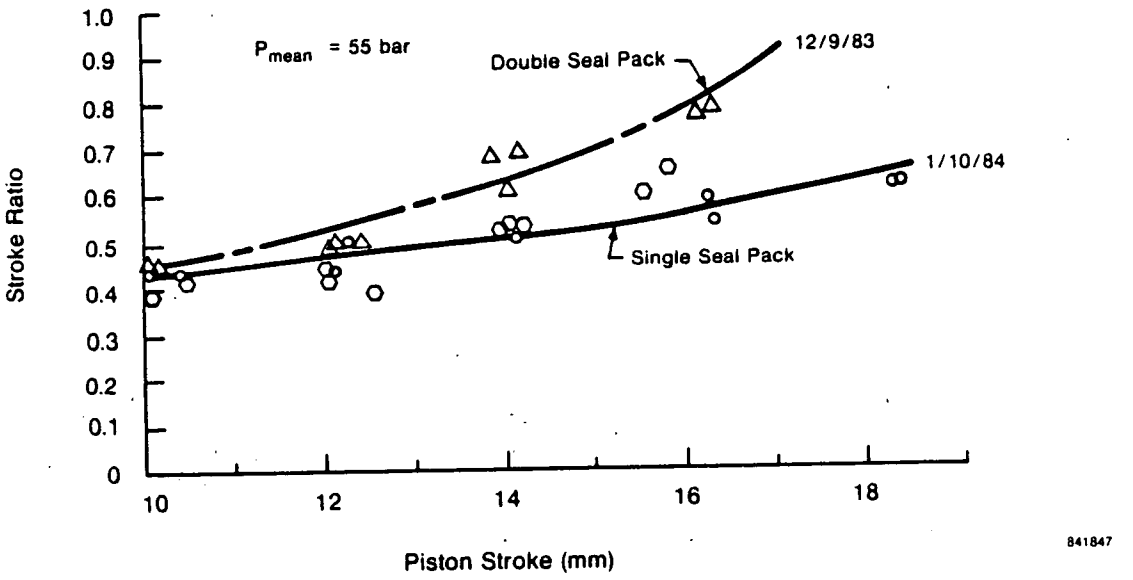

Figure 8 Change in Stroke Ratio

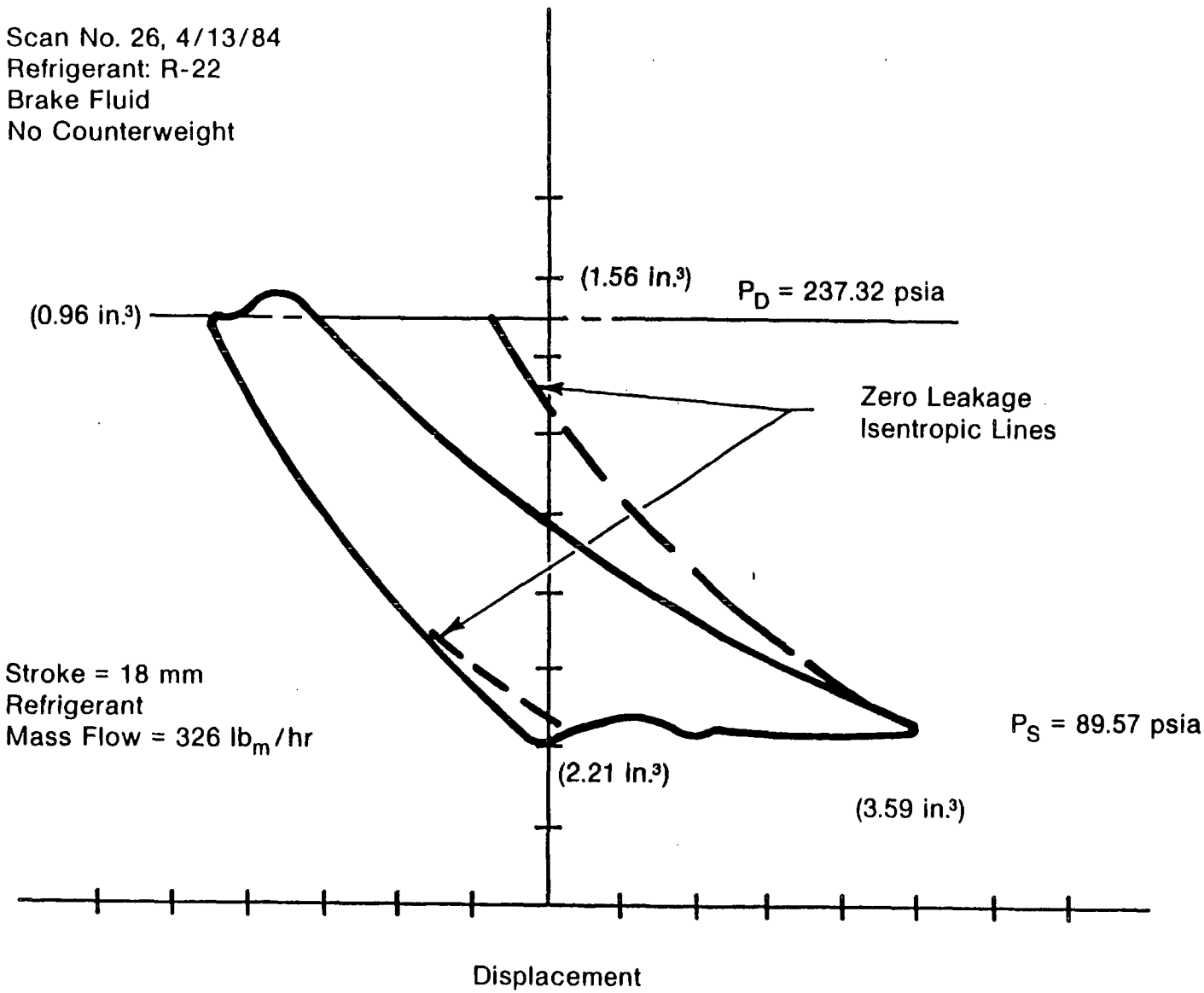

Figure 9 Compressor P-V Diagram